Earth Pressures of Overconsolidated Collapsible Soil Subjected to Inundation

Phuoc Huy Nhut Nguyen

A Thesis

in the Department

of

Building, Civil and Environmental Engineering

Presented in Partial Fulfilment of the Requirements

for the Degree of

Doctor of Philosophy (Civil Engineering) at

Concordia University

Montreal, Quebec, CANADA

February 2018

CONCORDIA UNIVERSITY

School of Graduate Studies

This is to certify that the thesis prepared

By: **Phuoc Huy Nhut Nguyen**

Entitled**:** **Earth Pressures of Overconsolidated Collapsible Soil Subjected to Inundation**

and submitted in Partial Fulfillment of the Requirements for the degree of

Doctor of Philosophy (Civil Engineering)

complies with the regulations of the University and meets with the accepted standards with respect to originality and quality.

Signed by the final examining committee:

_____ Chair
Dr. S. Bergler

_____ External Examiner
Dr. A. Foriero

_____ External to program
Dr. C. Y. Su

_____ Examiner
Dr. L. Lin

_____ Examiner
Dr. A. Zsaki

_____ Supervisor
Dr. A. M. Hanna

Approved by _____
Dr. A. Bagchi, Chair, Department of Building, Civil & Environmental Engineering

April 6, 2018 _____
Dr. A. Asif
Dean, Faculty of Engineering and Computer Science

ABSTRACT

Earth Pressures of Overconsolidated Collapsible Soil Subjected to Inundation

Phuoc Huy Nhut Nguyen, Ph.D.

Concordia University, 2018

Collapsible soils are known as problematic soils, which can be found in many regions around the world. Collapsible soils possess considerable strength when they are dry; however, when they are inundated, they lose their strength and exhibit excessive settlement. The amount of soil collapse increases with the increase of the so-called collapse potential "C_p", the wetting zone, and the degree of saturation (S). Accordingly, maximum collapse will take place due to full saturation. Collapsible soils can be inundated by heavy and continuous rainfall, excessive irrigation, broken water/sewer lines, or by rising the ground water. Furthermore, collapsible soils can be also found in construction site, in compacted fine soils at low water content (less than the optimum water content). Consequently, it is impossible to avoid construction on collapsible soils, which are potential for excessive settlement, differential settlement, landslides and falls, earth cracks. This type of soil has been responsible for damaging variety of civil engineering structures, loss of lives. Construction on such kind of soil shows extraordinary geotechnical problems, retaining walls are not an exception. With civilization, backfills behind retaining walls made of collapsible soils are widely used in practice. The earth pressures acting on these walls experience radical changes when the backfills of collapsible soils are wetted.

In the literature, there are lack of theories/methods for estimating the earth pressures acting on walls retaining collapsible soils. In this study, experimental investigations on at-rest and passive earth pressures of overconsolidated collapsible soil on retaining walls were

conducted. A prototype model of a vertical wall, retaining horizontal backfill of collapsible soil, was developed in the laboratory. Collapsible soil was prepared in the laboratory by mixing kaolin clay with fine sand. The model was instrumented to measure the earth pressure at strategic points on the wall, the total earth pressure acting on the wall, and the overconsolidation ratio (OCR) of the soil. Tests were conducted on the wall retaining collapsible soil at the dry and at fully saturated conditions for both the at-rest and passive earth pressures. The test results showed that both the at-rest and passive earth pressures increased with the increase of the collapse potential (C_p) and overconsolidation ratio (OCR) for the dry soil. At full saturation, the at-rest and passive earth pressures reduced considerably. Generally, the higher the collapse potential of the collapsible soil, the larger the decrease in the at-rest and passive earth pressures of the soil when the soil gets inundated.

In this investigation, for the case of at-rest earth pressure, empirical formulae were developed to determine the coefficient of at-rest earth pressure (K_0) of the dry and saturated overconsolidated collapsible soil. For the case of passive earth pressure, analytical model was developed. Accordingly, design theory was presented for estimating the coefficient of passive earth pressure (K_p) of overconsolidated collapsible soil at the dry and saturated conditions. Moreover, considering for the case of presence of unsaturated states of collapsible soil in practice, design charts were developed to assist designers in approximating the coefficient of at-rest (K_0) and passive (K_p) earth pressures of this soil at different degree of saturation.

ACKNOWLEDGEMENTS

I would like to express my deepest gratitude to my supervisor, Prof. Adel Hanna, for his abiding encouragement, constant interest, talented support, suggestions, and ideas during the preparation of this dissertation. I want to express my heartfelt gratitude for the patience and support he gave when I was a novice researcher. Without his vast knowledge, great experience, and remarkable insights, this dissertation would have never been successful.

I also would like to thank all professors and the staff in the Building, Civil, and Environmental Engineering department for their collaboration, advice, and information. I have been blessed to receive unconditional consultation and technical assistance from technical staff at Concordia University including Mr. Mark Elie, Mr. Luc Demers, Mr. Joseph Hrib, and Mr. Jaime Yeargans.

I extend my most gratefulness to my parents and my dear wife for their constant support and encouragement throughout my studies.

Special thanks to the Natural Sciences and Engineering Research Council (NSERC) of Canada and Concordia University for providing financial support for this research.

TABLE OF CONTENTS

LIST OF FIGURES ix

LIST OF TABLES xvii

LIST OF SYMBOLS xix

Chapter 1. INTRODUCTION 1

1.1. General 1

1.2. Statement of the Problem 5

1.3. Research Objectives 5

Chapter 2. LITERATURE REVIEW 7

2.1. General 7

2.2. Literature Pertinent to Collapsible Soil 7

2.3. Literature Pertinent to At-rest and Passive Earth Pressures 26

2.3.1. General 26

2.3.2. At-rest Earth Pressure 30

2.3.3. Passive Earth Pressure 37

2.4. Discussion 49

Chapter 3. EXPERIMENTAL INVESTIGATION 50

3.1. General 50

3.2. Experimental Setup 50

3.3. Collapsible Soil Preparation 56

3.4. Test Procedure 61

3.5. Test Program 63

3.6. Validation of the Experimental Setup 66

Chapter 4. TEST RESULTS AND ANALYSIS FOR THE CASE OF AT-REST PRESSURE 71

4.1. General 71

4.2. Results and Analysis 71

4.3. Developing Empirical Formulae 93

4.3.1. Proposed Formula for Estimating Coefficient of At-Rest Earth Pressure K_0 for Collapsible Soils at the Dry State 95

4.3.2. Proposed Formula for Estimating Coefficient of At-Rest Earth Pressure K_0 for Collapsible Soils for the Case after Full Inundation 98

4.3.3. Proposed Design Charts for Predicting Coefficient of At-Rest Earth Pressure K_0 for Unsaturated Collapsible Soils at Different Degree of Saturation 101

Chapter 5. TEST RESULTS AND ANALYSIS FOR THE CASE OF PASSIVE PRESSURE 105

5.1. General 105

5.2. Results and Analysis 105

5.3. Parametric study 145

5.4. Analytical Model 152

5.5. Proposed Design Charts for Predicting Coefficient of Passive Earth Pressure K_p for Unsaturated Collapsible Soils at Different Degree of Saturation 172

Chapter 6. CONCLUSIONS AND RECOMMENDATIONS.....177

6.1. Conclusions.....177

6.2. Recommendations for Future Work.....180

REFERENCES 181

LIST OF FIGURES

Fig. 1.1. World distribution of collapsible soil (Loess) (Catt, 1986) 1

Fig. 1.2. (a) Sinkholes developed nearby the railway line; (b) Filling the voids by grouting as soil treatment (Sakr et al., 2008) 3

Fig. 1.3. Three different types of wall movement (Bowles, 1968) 4

Fig. 2.1. A family of collapsible soils (Rogers, 1995) 8

Fig. 2.2. Schematic view of key characteristics of collapsible soils (Howayek et al., 2011/12) .. 9

Fig. 2.3. Different inter-particle bonds in collapsible soil (Clemence and Finbarr, 1981) 10

Fig. 2.4. A chart of bulk unit weight against unit weight of soil constituents (Ayadat and Hanna, 2012) 13

Fig. 2.5. Design chart for identification of soil collapse behavior (Ayadat and Hanna, 2013) 14

Fig. 2.6. Typical collapse potential test result (Jennings and Knight, 1975) 15

Fig. 2.7. Predicted and tested values of P_c' with matric suction (Ψ) (Ali, 2015) 23

Fig. 2.8. At-rest earth pressure (Das, 2009) 27

Fig. 2.9. Passive earth pressure (Das, 2009) 27

Fig. 2.10. Variation in lateral earth pressure with wall movement (Das, 2009) 28

Fig. 2.11. Typical values of earth pressure coefficient (K) of cohesionless soils with wall movement (Barnes, 2010) 29

Fig. 2.12. Mohr's circles at rest, active, and passive states (Budhu, 2008) 29

Fig. 2.13. Assumed failure plane for Rankine theory: Passive state (Liu and Evett, 2008) 38

Fig. 2.14. Rankine's passive earth pressure distribution against a retaining wall with backfill cohesive soils (Das, 2009) 39

Fig. 2.15. Passive wall movement: (a) RTT mode; (b) RBT mode (Fang et al., 1994) 41

Fig. 3.1. Layout of experimental setup 51

Fig. 3.2. Location of transducers on the mode retaining wall..... 53

Fig. 3.3. Pressure transducers and its special box..... 53

Fig. 3.4. Water tank..... 54

Fig. 3.5. Water distribution system..... 54

Fig. 3.6. Photograph of the experimental setup 55

Fig. 3.7. Data acquisition system and measuring equipment..... 56

Fig. 3.8. Particle size distribution for the collapsible soil mixtures..... 60

Fig. 3.9. Photograph of the application of the surcharge Ps 62

Fig. 3.10. Test results: (a) Horizontal pressure measured by wall transducers versus time; (b) Vertical pressure in the sand mass measured by transducers versus time 67

Fig. 3.11. Test results: (a) Load-displacement curve (load cell reading); (b) Load-displacement curves for each transducer mounted on the wall; (c) Vertical pressure in the sand mass versus the wall displacement..... 69

Fig. 4.1. Results from test no. 1 & 4 for soil - A (C_p = 4.2%): (a) Horizontal pressure measured by wall transducers versus time; (b) Vertical pressure in the soil mass measured by transducers versus time 72

Fig. 4.2. Results from test no. 2 & 5 for soil - C (C_p = 12.5%): (a) Horizontal pressure measured by wall transducers versus time; (b) Vertical pressure in the soil mass measured by transducers versus time 74

Fig. 4.3. Results from test no. 3 & 6 for soil - D (C_p = 18%): (a) Horizontal pressure measured by wall transducers versus time; (b) Vertical pressure in the soil mass measured by transducers versus time 75

Fig. 4.4. Results from test no. 7 & 10 for soil - A (C_p = 4.2%): (a) Horizontal pressure measured by wall transducers versus time; (b) Vertical pressure in the soil mass measured by transducers versus time 77

Fig. 4.5. Results from test no. 8 & 11 for soil - C (C_p = 12.5%): (a) Horizontal pressure measured by wall transducers versus time; (b) Vertical pressure in the soil mass measured by transducers versus time 78

Fig. 4.6. Results from test no. 9 & 12 for soil - D (C_p = 18%): (a) Horizontal pressure measured by wall transducers versus time; (b) Vertical pressure in the soil mass measured by transducers versus time 80

Fig. 4.7. Results from test no. 13 & 16 for soil - A (C_p = 4.2%): (a) Horizontal pressure measured by wall transducers versus time; (b) Vertical pressure in the soil mass measured by transducers versus time 81

Fig. 4.8. Results from test no. 14 & 17 for soil - C (C_p = 12.5%): (a) Horizontal pressure measured by wall transducers versus time; (b) Vertical pressure in the soil mass measured by transducers versus time 83

Fig. 4.9. Results from test no. 15 & 18 for soil - D (C_p = 18%): (a) Horizontal pressure measured by wall transducers versus time; (b) Vertical pressure in the soil mass measured by transducers versus time 84

Fig. 4.10. Results from test no. 19 & 22 for soil - B (C_p = 9.0%): (a) Horizontal pressure measured by wall transducers versus time; (b) Vertical pressure in the soil mass measured by transducers versus time 86

Fig. 4.11. Results from test no. 20 & 23 for soil - B (C_p = 9.0%): (a) Horizontal pressure measured by wall transducers versus time; (b) Vertical pressure in the soil mass measured by transducers versus time 87

Fig. 4.12. Results from test no. 21 & 24 for soil - B (C_p = 9.0%): (a) Horizontal pressure measured by wall transducers versus time; (b) Vertical pressure in the soil mass measured by transducers versus time 89

Fig. 4.13. Results from test no.3 and test no. 3*(2^{ND}) performed on dry soil - D (C_p =18%): (a) Horizontal pressure measured by wall transducers versus time; (b) Vertical pressure in the soil mass measured by transducers versus time 90

Fig. 4.14. Results from test no.6 and test no. 6*(2^{ND}) performed on saturated soil - D (C_p =18%): (a) Horizontal pressure measured by wall transducers versus time; (b) Vertical pressure in the soil mass measured by transducers versus time 91

Fig. 4.15. Test result: collapse settlement due to inundation versus time 92

Fig. 4.16. The theoretical values of K_0 obtained from the proposed formula [Eq. (4.3)] for the dry state 96

Fig. 4.17. The theoretical values of K_0 obtained from the proposed formula [Eq. (4.4)] for the case after full inundation 99

Fig. 4.18. Design charts: the theoretical values of K_0 for unsaturated collapsible soils: (a) OCR = 1; (b) OCR = 3; (c) OCR = 5; (d) OCR = 7. 104

Fig. 5.1. Results for test no.1 (Se1) for Soil A – C_p = 4.2%: (a) Load – displacement curve (load cell reading); (b) Load – displacement curves for each transducer; (c) Vertical pressure in the soil mass versus the horizontal wall displacement 107

Fig. 5.2. Results for test no.2 (Se1) for Soil B – C_p = 9.0%: (a) Load – displacement curve (load cell reading); (b) Load – displacement curves for each transducer; (c) Vertical pressure in the soil mass versus the horizontal wall displacement 108

Fig. 5.3. Results for test no.3 (Se1) for Soil C – C_p = 12.5%: (a) Load – displacement curve (load cell reading); (b) Load – displacement curves for each transducer; (c) Vertical pressure in the soil mass versus the horizontal wall displacement 110

Fig. 5.4. Results for test no.4 (Se1) for Soil D – C_p = 18%: (a) Load – displacement curve (load cell reading); (b) Load – displacement curves for each transducer; (c) Vertical pressure in the soil mass versus the horizontal wall displacement 111

Fig. 5.5. Results for test no.5 (Se2) for Soil A – C_p = 4.2%: (a) Load – displacement curve (load cell reading); (b) Load – displacement curves for each transducer; (c) Vertical pressure in the soil mass versus the horizontal wall displacement 113

Fig. 5.6. Results for test no.6 (Se2) for Soil B – C_p = 9.0%: (a) Load – displacement curve (load cell reading); (b) Load – displacement curves for each transducer; (c) Vertical pressure in the soil mass versus the horizontal wall displacement 114

Fig. 5.7. Results for test no.7 (Se2) for Soil C – C_p = 12.5%: (a) Load – displacement curve (load cell reading); (b) Load – displacement curves for each transducer; (c) Vertical pressure in the soil mass versus the horizontal wall displacement 116

Fig. 5.8. Results for test no.8 (Se2) for Soil D – C_p = 18%: (a) Load – displacement curve (load cell reading); (b) Load – displacement curves for each transducer; (c) Vertical pressure in the soil mass versus the horizontal wall displacement 117

Fig. 5.9. Results for test no.9 (Se3) for Soil A – C_p = 4.2%: (a) Load – displacement curve (load cell reading); (b) Load – displacement curves for each transducer; (c) Vertical pressure in the soil mass versus the horizontal wall displacement 119

Fig. 5.10. Results for test no.10 (Se3) for Soil B – C_p = 9.0%: (a) Load – displacement curve (load cell reading); (b) Load – displacement curves for each transducer; (c) Vertical pressure in the soil mass versus the horizontal wall displacement.....120

Fig. 5.11. Results for test no.11 (Se3) for Soil C – C_p = 12.5%: (a) Load – displacement curve (load cell reading); (b) Load – displacement curves for each transducer; (c) Vertical pressure in the soil mass versus the horizontal wall displacement.....122

Fig. 5.12. Results for test no.12 (Se3) for Soil D – C_p = 18%: (a) Load – displacement curve (load cell reading); (b) Load – displacement curves for each transducer; (c) Vertical pressure in the soil mass versus the horizontal wall displacement.....123

Fig. 5.13. Results for test no.13 (Se'1) for Soil A – C_p = 4.2%: (a) Load – displacement curve (load cell reading); (b) Load – displacement curves for each transducer; (c) Vertical pressure in the soil mass versus the horizontal wall displacement.....125

Fig. 5.14. Results for test no.14 (Se'1) for Soil B – C_p = 9.0%: (a) Load – displacement curve (load cell reading); (b) Load – displacement curves for each transducer; (c) Vertical pressure in the soil mass versus the horizontal wall displacement.....126

Fig. 5.15. Results for test no.15 (Se'1) for Soil C – C_p = 12.5%: (a) Load – displacement curve (load cell reading); (b) Load – displacement curves for each transducer; (c) Vertical pressure in the soil mass versus the horizontal wall displacement.....128

Fig. 5.16. Results for test no.16 (Se'1) for Soil D – C_p = 18%: (a) Load – displacement curve (load cell reading); (b) Load – displacement curves for each transducer; (c) Vertical pressure in the soil mass versus the horizontal wall displacement.....129

Fig. 5.17. Results for test no.17 (Se'2) for Soil A – C_p = 4.2%: (a) Load – displacement curve (load cell reading); (b) Load – displacement curves for each transducer; (c) Vertical pressure in the soil mass versus the horizontal wall displacement.....131

Fig. 5.18. Results for test no.18 (Se'2) for Soil B – C_p = 9.0%: (a) Load – displacement curve (load cell reading); (b) Load – displacement curves for each transducer; (c) Vertical pressure in the soil mass versus the horizontal wall displacement.....132

Fig. 5.19. Results for test no.19 (Se'2) for Soil C – C_p = 12.5%: (a) Load – displacement curve (load cell reading); (b) Load – displacement curves for each transducer; (c) Vertical pressure in the soil mass versus the horizontal wall displacement.....134

Fig. 5.20. Results for test no.20 (Se'2) for Soil D – C_p = 18%: (a) Load – displacement curve (load cell reading); (b) Load – displacement curves for each transducer; (c) Vertical pressure in the soil mass versus the horizontal wall displacement.....135

Fig. 5.21. Results for test no.21 (Se'3) for Soil A – C_p = 4.2%: (a) Load – displacement curve (load cell reading); (b) Load – displacement curves for each transducer; (c) Vertical pressure in the soil mass versus the horizontal wall displacement.....137

Fig. 5.22. Results for test no.22 (Se'3) for Soil B – C_p = 9.0%: (a) Load – displacement curve (load cell reading); (b) Load – displacement curves for each transducer; (c) Vertical pressure in the soil mass versus the horizontal wall displacement.....138

Fig. 5.23. Results for test no.23 (Se'3) for Soil C – C_p = 12.5%: (a) Load – displacement curve (load cell reading); (b) Load – displacement curves for each transducer; (c) Vertical pressure in the soil mass versus the horizontal wall displacement.....140

Fig. 5.24. Results for test no.24 (Se'3) for Soil D – C_p = 18%: (a) Load – displacement curve (load cell reading); (b) Load – displacement curves for each transducer; (c) Vertical pressure in the soil mass versus the horizontal wall displacement.....141

Fig. 5.25. Results from test no.4 and test no.4*(2^{ND}) performed on the dry soil D – C_p = 18%: (a) Load – displacement curve (load cell reading); (b) Load – displacement curve (transducers readings); (c) Vertical pressure in the soil mass versus horizontal wall displacement

.....143

Fig. 5.26. Results from test no.16 and test no.16*(2^{ND}) performed on the saturated soil D – C_p = 18%: (a) Load – displacement curve (load cell reading); (b) Load – displacement curve (transducers readings); (c) Vertical pressure in the soil mass versus horizontal wall displacement

.....145

Fig. 5.27. Load – displacement curves (Se2) for dry collapsible soils with different clay content

(Different collapse potential) 146

Fig. 5.28. Load – displacement curves (Se'2) for saturated collapsible soils with different collapse potential 147

Fig. 5.29. Load – displacement curves for dry and saturated collapsible soil A – C_p = 4.2% (test no. 5 and test no. 17).....148

Fig. 5.30. Load – displacement curves for dry and saturated collapsible soil D – C_p = 18% (test no. 8 and test no. 20).....149

Fig. 5.31. Geometry of the model used.....152

Fig. 5.32. Trial slip surfaces for soil A 154

Fig. 5.33. Trial slip surfaces for soil B 155

Fig. 5.34. Trial slip surfaces for soil C 156

Fig. 5.35. Trial slip surfaces for soil D 157

Fig. 5.36. Analytical results: the angle (α) versus the collapse potential C_p (Ps = 0) 162

Fig. 5.37. Analytical results: the angle (α) versus the OCR (Ps = 0) 163

Fig. 5.38. Failure wedge with planar surface 166

Fig. 5.39. Forces acting on typical element of failure wedge 167

Fig. 5.40. Design chart: coefficient of passive earth pressure K_p of collapsible soil at the dry state 169

Fig. 5.41. Comparison between the results obtained from the present theory and the experimental results of the present investigation for the dry state 170

Fig. 5.42. Reduction factor R_F 171

Fig. 5.43. Comparison between experimental results and those obtained from the proposed empirical formula [Eq. (5.13)] 172

Fig. 5.44. Design charts: values of K_p for collapsible soil at different degree of saturation "S" (C_p = 4.2%).....173

Fig. 5.45. Design charts: values of K_p for collapsible soil at different degree of saturation "S" (C_p = 9.0%).....174

Fig. 5.46. Design charts: values of K_p for collapsible soil at different degree of saturation "S" (C_p = 12.5%).....175

Fig. 5.47. Design charts: values of K_p for collapsible soil at different degree of saturation "S" (C_p = 18%).....176

LIST OF TABLES

Table 2.1. Classification of collapse potential (ASTM D5333-03) 16

Table 2.2. Collapse potential C_p and severity of problems of foundation (Jennings and Knight, 1975) 16

Table 3.1. Chemical analysis of the Kaoline clay ("Digitalfire.com reference library") 58

Table 3.2. Physical properties of the Kaoline clay ("Digitalfire.com reference library") 58

Table 3.3. Summary of the response to wetting Oedometer tests on these mixtures used in this investigation 58

Table 3.4. Physical properties of collapsible soil mixtures 59

Table 3.5. Mixtures classification based on collapse potential C_p 60

Table 3.6. Details of testing program for at-rest earth pressure (for the purpose of developing empirical formulae) 63

Table 3.7. Test program for at-rest earth pressure (for the purpose of validating the proposed empirical formulae) 64

Table 3.8. Details of testing program for passive earth pressure 65

Table 3.9. Test program for studying the repeatability of the test results 66

Table 4.1. Summary of test results for at-rest earth pressure 94

Table 4.2. Comparison between experimental and theoretical values of K_0 for overconsolidated collapsible soil at dry state 97

Table 4.3. Comparison between the predicted values of K_0 obtained from Eq. (4.3) and the values given by Jaky (1944) for the case of normally consolidated soils at dry state 98

Table 4.4. Comparison between experimental and theoretical values of K_0 for overconsolidated collapsible soil after full inundation 100

Table 4.5. Comparison between theoretical and experimental results from additional tests of K_0 for overconsolidated collapsible soil after full inundation 100

Table 5.1. Summary of test results for passive earth pressure.....151

Table 5.2. Summary of the trials considered for soil A (C_p = 4.2%).....158

Table 5.3. Summary of the trials considered for soil B (C_p = 9.0%).....159

Table 5.4. Summary of the trials considered for soil C (C_p = 12.5%).....160

Table 5.5. Summary of the trials considered for soil D (C_p = 18%).....161

Table 5.6. Comparison between the predicted and experimental values of the passive earth force Pp and the coefficient of passive earth pressure K_p.....168

LIST OF SYMBOLS

b = width of the retaining wall

C_p = Collapse potential

C_c = Coefficient of curvature

C_u = Coefficient of uniformity

c’ = Cohesion

DAS = Data acquisition system

e = void ratio

e_0 = initial void ratio

e_L = void ratio at liquid limit

FS = factor of safety

Gs = Specific gravity

H = height of the retaining wall

h_0 = initial specimen height

I_m = maniability index

K_0 = Coefficient of at-rest earth pressure

K_p = Coefficient of passive earth pressure

LL = Liquid limit

LVDT = Linear variable displacement transducer

OCR = overconsolidation ratio

PI = Plasticity index

PL = Plastic limit

P_p = total passive earth force

Ps = surcharge loading

S = Degree of saturation

S_c = settlement of the soil layer

α = the slope of the slip surface with the horizontal

β = the inclined backfill angle

γ = unit weight of soil

γ' = effective unit weight of soil

δ = the wall friction angle

σ_h = horizontal earth pressure

σ_v = vertical earth pressure

σ_p = passive earth pressure

ϕ = friction angle of the soil

ϕ_{cr}' = critical state friction angle

θ = angle of back side of wall and a horizontal line

μ = poisson's ratio

ω = moisture (water) content

ω_0 = initial water content

Δe = change in void ratio

Δh = change in specimen height

ΔL = horizontal wall displacement

CHAPTER 1
INTRODUCTION

1.1. General

Collapsible soils are in the group of problematic soils, and can be found in many regions around the world including America, Asia, Africa, and Europe; in which, collapsible soils distribution has occupied approximately 17% of the United States, 17% of Europe, 15% of Russia and Siberia, and the large areas of China (Ayadat and Hanna, 2013; Iranpour and Haddad, 2016). Figure 1.1 presents the world distribution of collapsible soil (loess) (Catt, 1986). Collapsible soils exhibit low compressibility and high shear strength at natural water content levels (low water content), and if wetted they collapsed under their self-weight and/or surcharge loads, and loss of strength (Jiang et al., 2012).

Fig. 1.1. World distribution of collapsible soil (Loess) (Catt, 1986)

Nowadays, industrial and urban developments have recently exposed geotechnical engineers to relatively significant challenges when collapsible soils are presented in construction fields. The rise of ground water table or water used for farming, industrial development or water from other natural or human activities can cause severe damages to structures rested on collapsible soils. Many structures built on or in collapsible soils failed due to the soil collapse upon becoming wet. Consequently, the structures resting on collapsible soils have been facing to a number of potential problems. Collapse and problems related to collapse such as differential settlement, earth cracks, landslides and falls, instability in the slope supporting the structure, failure occurrence in the side walls of the dam reservoirs, have been responsible for serious damages to the infrastructures constructed on collapsible soil, consisting of loss of human lives (Garakani et al., 2015). For example, in China, Li et al. (2016) presented that a total of about 1505 buildings damaged and about 80km long underground pipelines ruptured due to collapse of collapsible soils were recorded from 1974 to 1975. It was noted that the cost associated with collapsible ground preparation was approximately one third of the total cost of the infrastructure (Li et al., 2016). Another example, the sinkholes developed in the collapsible soil along the northern coast of Egypt, in Al-Ghrabaneyat area, damaged the railway line nearby. It was difficult and costly to keep the railway in a regular working condition (Figure 1.2). Also in that area, two more buildings suffered from large and irregular settlements, seriously damaging the structure (Sakr et al., 2008).

Generally, collapsible soils take a strong reaction to inundation, and it is not easy to predict and control in advance. Once inundated, the soil volume reduction takes place fast and suddenly and no approach can be used to stop the trouble at that time. It is difficult, time-consuming, and costly for repairing infrastructures damaged due to collapse of collapsible soils.

(a) (b)

Fig. 1.2. (a) Sinkholes developed nearby the railway line; (b) Filling the voids by grouting as soil treatment (Sakr et al., 2008)

In general, all soils including natural soil deposits or compacted soils are susceptible to collapse due to wetting. The amount of collapse or severity of collapse is depended on the so-called collapse potential "C_p" of the soil. The problems of industrial and civil structures dealing with collapsible soils are determined by the degree of collapse potential. The higher the collapse potential is, the severer the problem occurs.

Retaining walls are widely used in the United States, Asian countries, and other countries around the world. Retaining walls have being used popularly in structures including basement walls, bulkheads, abutments, tunnels, or flood walls. Retaining walls are primarily designed to counter the lateral earth forces. Lateral earth pressures acting against the retaining wall are one of the most important concerns in the design of retaining wall. Typically, three types of lateral earth pressure (Figure 1.3) can be acted on the wall, including at-rest, active, and passive earth pressures. These types of earth pressure can be developed due to the movement of the wall.

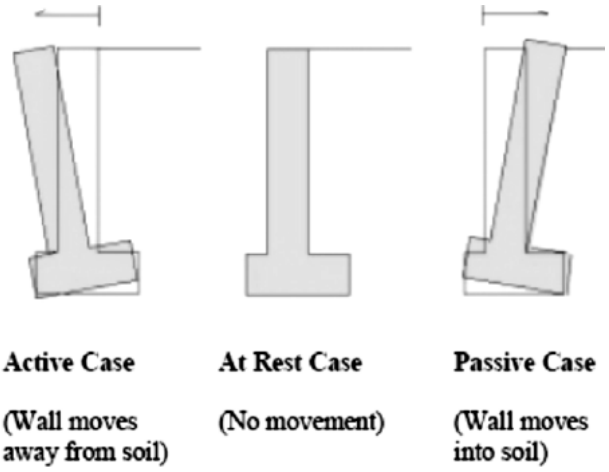

Fig. 1.3. Three different types of wall movement (Bowles, 1968)

Active and passive earth pressures are evolved on the wall when the movement of the wall are sufficient to mobilize full shear strength capacity of the soil. The active earth pressure is developed on the wall when the wall is allowed to move freely away from the retaining soil. In this case, the lateral stress in the soil mass decreases sufficiently to reach a minimum value known as the active failure state. Whereas, the passive earth pressure is developed when the wall moves toward the backfill soil, causing soil compression behind the wall. In this case, the lateral stress in the soil mass increases sufficiently to reach a maximum value known as the passive failure state. The passive earth pressure is also known as the resisting force to the active movement of the wall.

In practice, backfills behind bridge abutments or plate anchors are heavily under passive earth pressure.

At-rest earth pressure is occurred in the situation where the retaining walls have no lateral movement or the lateral movement of the wall is not adequate to develop the soil shear strength capacity. Basement walls or tunnels are typical examples of earth retaining structures facing to at-rest earth pressure.

1.2. Statement of the problem

With civilization, it is impossible to avoid construction on/in collapsible soils. Construction on such kind of soils has involved a number of potential problems, the retaining wall is not an exception. Earth pressures evaluation plays an important role in geotechnical engineering. An accurate prediction of the earth pressure acting on the retaining wall is significant to the safe design of many infrastructures.

Unfortunately, in the literature, there is lack of studies about the case of retaining wall with backfill of overconsolidated collapsible soil. Consequently, no design theory for predicting the at-rest and passive earth pressures acting on the wall retaining overconsolidated collapsible soil subjected to inundation are found. In the literature, Jaky, Coulomb, and Rankine's theories are the most common and reliable methods for calculation of lateral earth pressures acting on the wall. Besides that, numerous theories have been developed and reported. However, those methods and attempts have been limited for cases of backfills of normally and overconsolidated cohesionless soils or cohesive soils. They cannot be applied for the case of inundation of backfill collapsible soil because the soil will experience reduction in strength and excessive settlement upon inundated, which further influence the earth pressure of this soil on the walls.

It is no doubt that a remarkable decrease in the earth resistance of the soil after inundation can result in severe problems to many infrastructures.

1.3. Research Objectives

The main goal of this research is to provide methods to predict the at-rest and passive earth pressures of overconsolidated collapsible soil at the dry and saturated states. It is also to

establish the effect of the collapse potential and the overconcolidation ratio of the soil on the at-rest and passive earth pressures. Therefore, the objectives of this thesis are listed as follows:

a. To conduct a literature review and to prepare a state-of-the-art report on collapsible soils and theories / studies on the at-rest and passive earth pressures.
b. To develop a prototype model of a vertical wall retaining horizontal backfill of overconsolidated collapsible soil in the laboratory to investigate the effect of inundation due to the rise of ground water table on the at-rest and passive earth pressures. This model is instrumented to measure the at-rest and passive earth pressures at selected points on the wall, the total earth pressure acting on the wall, and the overconsolidation ratio (OCR) in the soil mass.
c. To examine the role of the soil collapse potential C_p and stress history (overconsolidation ratio - OCR) on the at-rest and passive earth pressures.
d. To develop theories to estimate the values of coefficients of at-rest (K_0) and passive (K_p) earth pressures for both dry and saturated soil conditions.
e. To develop design charts for predicting the values of K_0 and K_p of unsaturated collapsible soil at different degree of saturation.

CHAPTER 2
LITERATURE REVIEW

2.1. General

This chapter presents the state-of-the art literature review with emphasis on the background about collapsible soils and lateral earth pressure acting on the retaining wall. The theories and studies on the at-rest and passive earth pressures are also reported.

2.2. Literature Pertinent To Collapsible Soil

Collapsible soils are mostly found in form of unsaturated soil at low initial water content, which are susceptible to loss of strength due to decrease in bulk volume upon becoming wet. Generally, collapsible soil deposits share two typical features. Firstly, they are loose and cemented deposits. Secondly, they are naturally near dry. Collapsible soils own loose structure with particles joined together commonly by chemical cement or clay bond. In their natural unsaturated condition, collapsible soils are strong and stable thanks to the cemented or bonded nature. However, due to their unstable soil fabric and weak inter-particle bond strength, the unsaturated collapsible soils are susceptible to significant volumetric decrease upon wetting. Bond strength is easy to be weakened by water, which causes collapse and loss of strength. (Ali, 2015; Haeri and Garakani, 2016).

There are plenty of sources causing collapsible soils wetted, including but not limited to heavy and continuous rainfall, excessive irrigation, broken water or sewer lines, other kinds of artificial flooding from the surface, or upward water saturated from rising ground water table (Haeri, 2016; Iranpour and Haddad, 2016).

Collapsible soil is basically classified into two groups including natural occurring collapsible soils and man-made soils (Clemence and Finbarr, 1981; Mossaad et al., 2006). Natural deposits involve Aeolian deposits, water-laid deposits, and residual soils. The most substantial natural deposits of collapsible soils are Aeolian or windblown deposits –well known as loess. Loess is thick, yellowish or brown deposit of windblown dust. It is a product of past glacial activity in an area. Water laid deposits can form alluvial fans, flows, and flowslides. Resident soils are the product of weathering of rocks. The particle size of the residual materials can be various from large fragments to gravel, sand, silt, colloids, and even organic material. Other soil types such as volcanic tuff, gypsum, loose sands cemented by soluble salts, dispersive clays, or sodium-rich montmorillonite clays may exhibit collapsible behavior upon wetting. Man-made soils consisting of compacted soils, construction debris, mine tailings, and coal ash fills may also exhibit collapse. Figure 2.1 shows classification of different types of collapsible soils (Rogers, 1995).

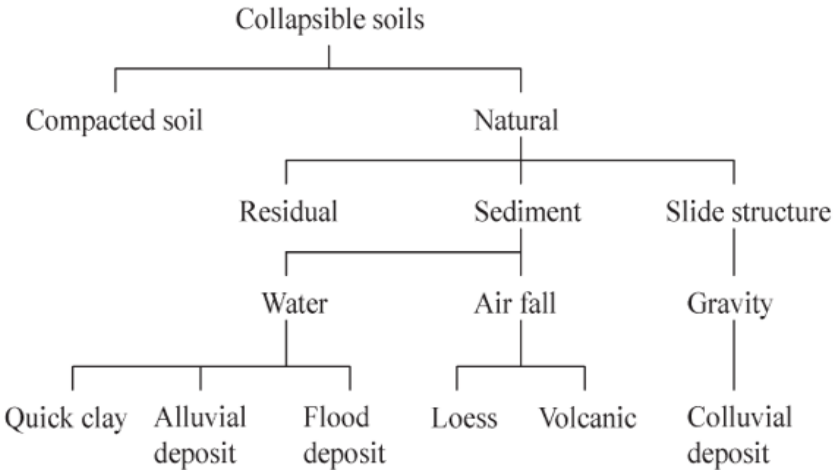

Fig. 2.1. A family of collapsible soils (Rogers, 1995)

Collapsible soils are generally characterized by some specific engineering properties including high void ratio, low natural density, low natural water content, great dry strength and stiffness, zero or slight plasticity, and high percentage of fine grained particles (Howayek et al., 2011/12; Haeri, 2016). Figure 2.2 illustrates the schematic view of main characteristics of collapsible soils.

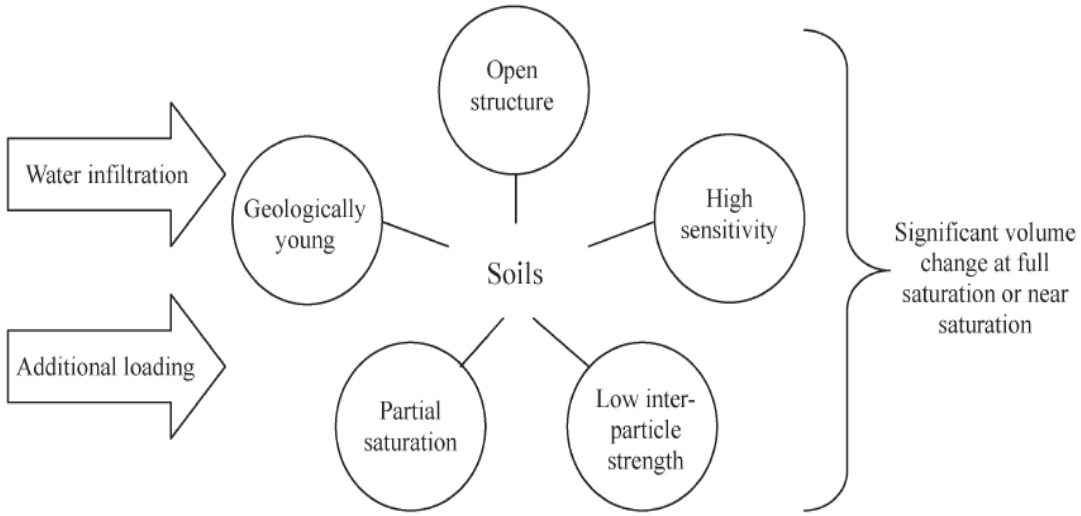

Fig. 2.2. Schematic view of key characteristics of collapsible soils (Howayek et al., 2011/12)

Collapsible soil basically possesses a honey-comb, open, and unstable structure of bulky shaped grains with the grains held in place by inter-particle bonding material such as cementation, chemical, physical attraction or soil suction (negative pore pressures) (Mossaad et al., 2006). When the support is taken off by addition of water, the grains slide over each other, moving into void spaces. In general, the greater the water content, the lower the bond strength. Physically, all collapsible soils are weakened by adding water. Immediate collapse in strength is found in the case where the grains are held together by capillary suction, slow collapse in strength in the case of chemical cementing, and much lower collapse in strength in the case of

clay buttresses (Clemence and Finbarr, 1981). Figure 2.3 presents different types of inter-particle bonds for collapsible soils that reported by Clemence and Finbarr (1981).

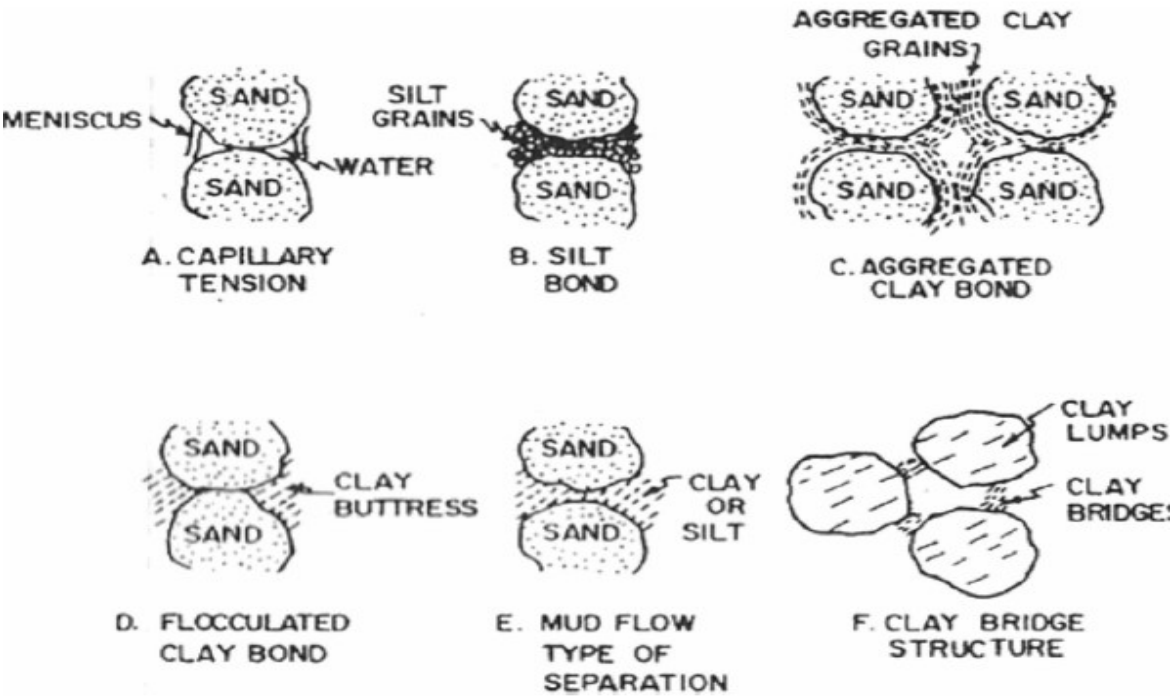

Fig. 2.3. Different inter-particle bonds in collapsible soil (Clemence and Finbarr, 1981)

The collapse mechanism accompanying wetting is based on the reduction of inter-particle bonds, followed by the collapse of the soil structure. The collapse occurs in the soil with three main phases (summarized by Li et al. 2016). The first phase (pre-collapse phase) occurs when the soil is subjected to high values of matric suction. In this phase, the soil experiences small volumetric deformations due to matric suction decrease, no slippage occurs between the particles and the structure of the soil still remains intact. The second phase (collapse phase) occurs when the soil undergoes intermediate values of matric suction. In this phase, the soil experiences a significant volume decrease due to matric suction decrease. The structure of the soil is also

adjusted due to bonding break. The third phase (post-collapse phase) occurs when the unsaturated soil reaches full saturation. In this phase, the soil is not subjected to further volume decrease due to matric suction decrease. Klukanova and Frankovska (1995) proposed the process of collapse mechanism, consisting of three phases. Phase 1: the original microstructure is demolished due to increasing humidity (soil suction reduced) and external total stress. Phase 2: it is involved the disintegration of microstructure. Phase 3: a new microstructure is formed after the collapse is completed.

Identification of collapsible soils is very important to the geotechnical field. The practical engineers often require a fast approach of indicating the collapsible soils. Geotechnical zonation maps can be used for identifying the collapsible soils preliminarily. These zonation maps have been established and developed based on actual boreholes, laboratory tests, and field tests. The maps may provide helpful information about the location and depth of collapsible deposits. (Ayadat and Hanna, 2013)

Collapse criteria based on soil parameters

The methods available in the literature can be grouped into four categories (Ayadat and Hanna, 2012) as follows:

- Methods based on void ratio, density, and water content relationship
- Methods based on water content and Atterberg limits relationship
- Methods based on density and Atterberg limits
- Methods based on particle size distribution of soils

1. Methods based on void ratio, density, and water content relationship

Denisov (1951) introduced a coefficient of collapse K as: $K = \frac{e_L}{e_0}$ (2.1)

Where: e_0 = void ratio at nature, and e_L= void ratio at liquid limit

The degree of soil collapsibility could be determined as follows:

K=0.5-0.75: highly collapsible soil

K=0.75-1.0: moderate collapse

K>1.0: non-collapsible loam

K=1.5-2.0 non-collapsible soil

Clevengar (1958) stated the criterion based on natural dry unit weight as follows:

$\gamma_d < 12.6$ kN/m^3 : highly collapsible

12.6 kN/m^3 $\leq \gamma_d \leq$ 14.0 kN/m^3 : may be collapsible

$\gamma_d > 12.6$ kN/m^3 : non-collapsible

2. Methods based on water content and Atterberg limits relationship

Freda (1964) introduced the criteria based on collapse index as follows: $K_L = \frac{\frac{m}{S_r} - PL}{PI}$ (2.2)

Where: m = natural moisture content

S_r = degree of saturation

PL = plastic limit

PI = plasticity index

The soil is susceptible to collapse if the collapse index $K_L > 0.85$

3. Methods based on density and Atterberg limits

Beckwith (1979) proposed use of typical index properties to identify collapsible soils. Collapsible soils could be demonstrated by a value of plasticity index PI < 10, the unit weight γ_d<14.9 kN/m^3 and moisture content ω< 4% to 8%.

4. Methods based on particle size distribution of soils.

Handy (1973) introduced the criteria for Iowa loess in terms of clay content (<0.002mm)

Clay content<16% : the probability of collapse is high

Clay content: 16-24% : the probability of collapse is moderate

Clay content: 24-32% : the probability of collapse is less than 50%

Clay content : >32% : the probability of collapse is nearly zero

Ayadat and Hanna (2012) suggested the criterion for the susceptibility of soil to collapse based on bulk unit weight of soil and unit weight of soil constituents. This criterion was presented by a chart as below:

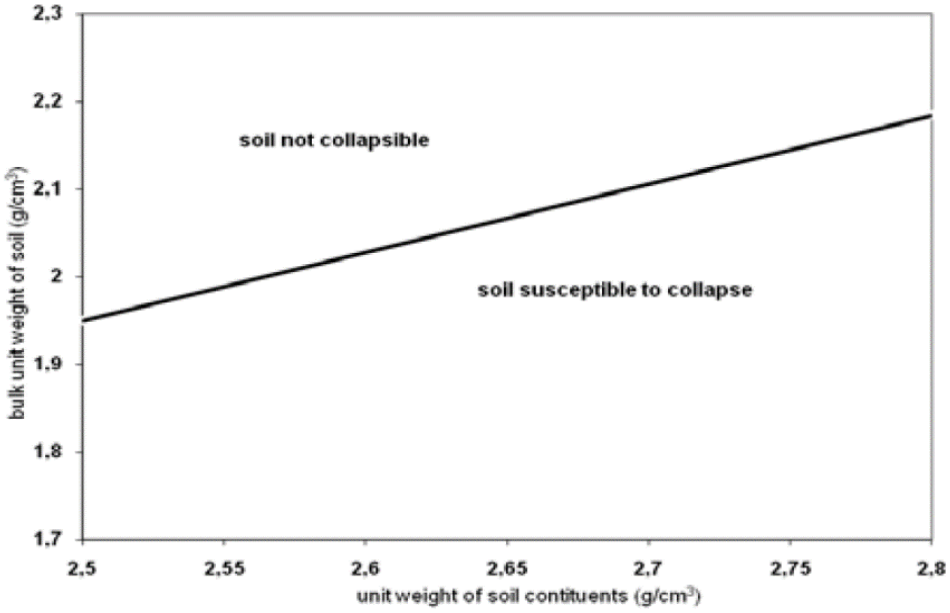

Fig. 2.4. A chart of bulk unit weight against unit weight of soil constituents (Ayadat and Hanna, 2012)

In addition, the collapse criterion based on relative density, soil equivalent diameter, and the maniability index which was defined as $I_m = \frac{w_L - w_0}{IP}$ (2.3) (IP: plasticity index, w_0: initial water content, w_L: liquid limit) was developed for practical application by Ayadat and Hanna, (2013), as shown in Figure 2.5.

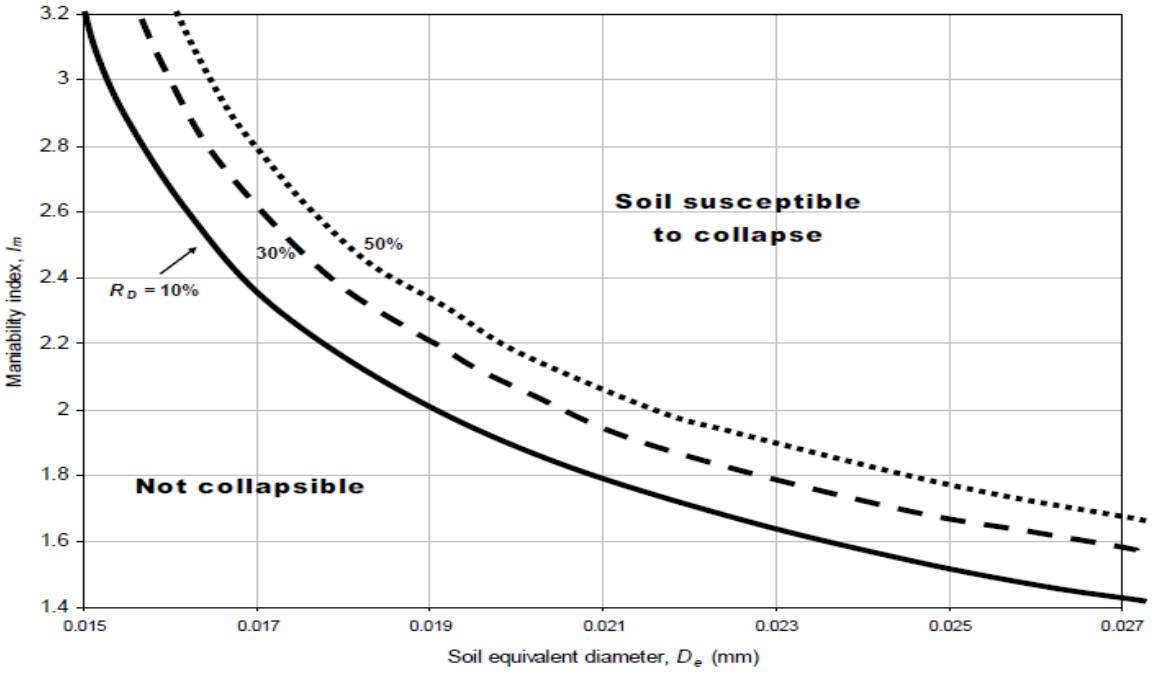

Fig. 2.5. Design chart for identification of soil collapse behavior
(Ayadat and Hanna, 2013)

Prediction methods based on laboratory tests

The most common way for measurement of collapsibility is to conduct single oedometer test (Vakili, 2013; ASTM D5333-03). The single oedometer test consists of several steps. Firstly, soil specimen (within the oedometer ring) at natural water content is placed in the oedometer apparatus. Secondly, a predetermined vertical stress is gradually applied to the soil specimen until reaching a maximum load of 200 kPa. Thirdly, the soil specimen is inundated while the load is still maintained on the soil specimen. The relative soil compression (in terms of

void ratio) is determined from the measurements of vertical settlements of the specimen. The collapse potential (C_p) is equal to the deformation of soil due to the addition of water, divided by the initial height of the specimen.

The collapse potential (C_p) is the collapse strain due to inundation of the specimen under 200 kPa pressure in oedometer apparatus: $C_p = \frac{\Delta h}{h_0} \cdot 100\% = \frac{\Delta e}{1+e_0} \cdot 100\%$ (2.4)

Where

Δh = change in specimen height due to wetting under 200 kPa pressure (mm)

h_0 = initial specimen height (mm)

Δe= change in void ratio due to wetting under 200 kPa pressure

e_0 = initial void ratio

Figure 2.6 depicted the typical collapse test result which presented by Jennings and Knight (1975).

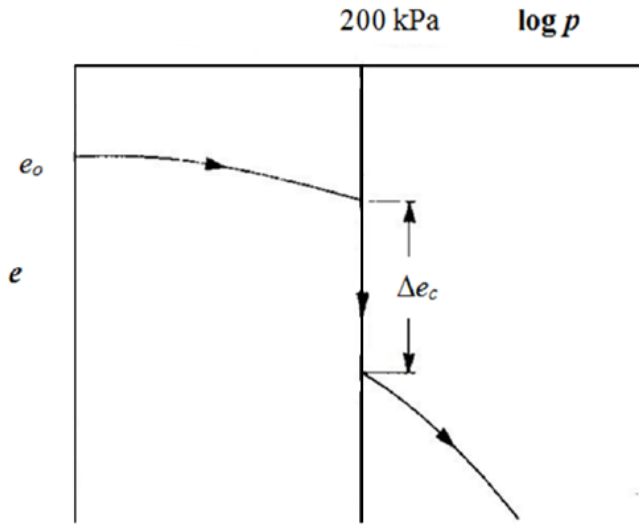

Fig. 2.6. Typical collapse potential test result (Jennings and Knight, 1975)

According to ASTM D5333-03, the classification of collapse potential is illustrated in Table 2.1.

Table 2.1. Classification of collapse potential (ASTM D5333-03)

Degree of collapse	Collapse potential (%)
None	0
Slight	0.1 to 2.0
Moderate	2.1 to 6.0
Moderately severe	6.1 to 10.0
Severe	>10

Jennings and Knight (1975) proposed a classification for severity of foundation problems with respect to collapse potential C_p as table below:

Table 2.2. Collapse potential and severity of problems of foundation (Jennings and Knight, 1975)

Collapse Potential, C_p (%)	**Severity of problem**
0-1	No problem
1-5	Moderate trouble
5-10	Trouble
10-20	Severe trouble
>20	Very severe trouble

Collapse potential (C_p) can be employed to roughly calculate settlement that may occur in a collapsible soil layer at a certain place (ASTM D5333-03). The settlement of the soil layer might be approximated as:

$$S_c = C_p \frac{H}{100} \qquad (2.5)$$

Where: S_c = settlement of the soil layer upon wetting

C_p = collapse potential

H = thickness of the soil layer.

Many treatment methods for collapsible soils have been studied and suggested by a number of scientists and researchers (Mossaad et al., 2006; Houston et at., 2001; Soliman and Hanna, 2010; Ayadat and Hanna, 2005; Jefferson et al., 2008; Mohamedzein and Al-Rawas, 2011; Abbeche et al. 2010; Mohamed and Gamal, 2012; Ali, 2015). The mitigation methods differ in both concept and methodology to go well with a certain problem. To choose which approach should be used depends on many factors including the site condition, the depth of the collapsible soil layer, and the thickness of the collapsible soil layer.

These treatment methods consist of, but not limited to, removal and replacement, removal and presume compaction, avoidance of wetting, pre-wetting, controlling wetting, preloading, stone columns, encapsulated stone columns, dynamic compaction, pile or pier foundation, chemical stabilization (e.g. cement, salts, sulfur cement, sodium silicate solution, lime, and phosphoric acid), grouting, and reinforcement using geosysthetics.

- Removal and compaction: this method can be applied before construction, with the collapsible soils are situated shallowly.

- Pre-wetting (increase in moisture content) simply means that the collapsible soils are wetted before constructing structures, so that the settlement due to soil collapse will be small. This method is often used in cases where the collapsible soils are identified prior to structures

built. This approach is not very effective in the case where collapsible soil layers are located at a great depth (more than 5m).

- Controlling wetting: the method is similar to pre-wetting, except that it is used when the structures are constructed.

- Chemical stabilization or grouting can strengthen the collapsible soils by introducing a chemical compound to add cementation that enhances inter-particle bonds. This can reduce the soil collapse upon becoming wet. This approach may not be economical if heavy structures will be constructed in the soil improvement area.

- Dynamic compaction can lessen the void ratio but it is not sufficient to eliminate the collapse problem. This technique can provide a significant improvement up to 2.5 to 3 m in the area with deep ground water level.

- Geosysthetics materials benefit in increasing bearing capacity and decreasing settlement of foundation on/in collapsible soils.

- Piles, piers, stone columns, or encapsulated stone columns have been employed as a mitigation alternative. The load is transferred through the collapsible soil layer to a good soil layer such as stiff clay, dense sand, or bedrock. The approach can be used effectively for heavy structures built on the collapsible soil area, but costly.

The choice of one or combination of these techniques depends on numerous parameters consisting of timing of mitigation, source of loading, source of wetting, nature of ground to treat, environmental conditions, and economic considerations.

Haeri, Khosravi et al. (2014) attempted to assess the effect of soil disturbance on the hydro-mechanical behavior of the highly collapsible loessial soil during wetting by conducting modified suction-controlled triaxial tests on undisturbed and reconstituted loessial soil specimens taken from Golestan province of Iran. The natural composition of the soil matrix, the non-homogenous distribution of macro or micro pores, and the weak inter-particle bonding between grains were listed as a group that was significantly influenced by the disturbance of highly collapsible loessial soils samples. The authors reported that due to differences in the soil pore size and pore size distribution, the capacity for water retention and consequently the stress state of the soil could be strongly different for tests conducted on undisturbed and reconstituted samples. An increase in volumetric strain was recorded during the wetting process due to the decrease in matric suction. They also found that for the low mean net stress testing, the deformation of measurements for undisturbed samples were lower than that for reconstituted samples. For the higher mean net stress testing, a similar wetting-induced volumetric strain behavior were found for both undisturbed and reconstituted samples. The author believed that this behavior was resulted from the effect of the mechanical stress on the natural composition of the soil matrix, which could break the cemented bonds between soil particles and decrease the effect of non-homogeneity in the distribution of pores on the deformation behavior of the loessial soils.

Zhou et al. (2014) attempted to examine the soil behavior and failure mechanism of loess slopes subjected to water infiltration in Heifangtai Plateau in Gansu province of China. They reported that landslides in the area could be triggered by water infiltration through two different processes including wetting of soil at a shallow depth to due short term rainfall or irrigation, and fully saturating due to rising of groundwater table in deep soil resulting from prolonged

irrigation. They conducted a series of laboratory tests such as undrained compression on the anisotropically consolidated saturated samples, drained shear by decreasing mean effective stress at constant axial load on saturated samples, and wetting by decreasing matric suction at constant axial load on unsaturated samples. Based on their experiments, they stated that under constant axial load condition, the saturated loess experienced two modes of failure with increasing pore water pressure. At a lower stress level, the initially drained deformation might evolve into an undrained sudden failure; whereas, at the higher stress level, progressive failure was found. They also supposed that in saturated loess, at low stress, a rapid increase in pore water pressure at constant axial load was due to the main triggering mechanism of loess landslides. They additionally suggested that the improvement of the flooding irrigation method and the construction of a vertical drainage system penetrated to the pebble stone layer could be taken as a serious consideration in remediation measures for the area.

Haeri, Garakani et al. (2014) attempted to characterize the deformation behavior of a highly collapsible undisturbed loessial soil under changing mean net stress or matric suction conditions, using a modified triaxial test device with suction and saturation controls. The soil specimens were taken from the Hezar Pich Hills area near the city of Gorgan, Iran. They found that the hydro-mechanical behavior of collapsible soil was considerably stress-path dependent. With the same mean net stress values, the deformation measurements of samples subjected to isotropic compression were frequently larger than that subjected to wetting-induced collapse. The soil specimens subjected to isotropic compression underwent a decrease in their volumetric strain as the mean effective stress increased; whereas, the soil specimens subjected to wetting-induced collapse experienced a decrease in volumetric strain when the effective stress was decreased during the wetting process. They also presented that for the isotropic compression

tests, the soil water retention curve of the loessial soil depended on the mean net stress; while less sensitivity to the mean net stress were recorded for the specimens subjected to wetting-induced collapse.

Garakani et al. (2015) investigated the hydro-mechanical behavior of loessial soil during isotropic and shear loadings using the modified triaxial test device. Tests were conducted on undisturbed specimens taken from loessial deposits in Gorgan city, Iran. The authors reported that the hydro-mechanical behavior of loess was essentially affected by the extent of applied mean net stress and the degree of suction. The magnitude and extent of collapse were different, depending on the applied state of the stress and the hydro-mechanical loading path. They also presented that the collapse phenomenon in natural loess was mostly a continuous – stepwise reduction in volume rather than a sudden reduction as water enters the voids. It was found that any increase in the magnitude of mechanical stresses (confining net stress or shear stress) or degree of saturation (wetting process) leaded to an increase in the magnitude of collapse. Generally, an increase in isotropic loads, suction, and shear loads caused an increase in the amount of collapse.

Ali (2015) presented the field plate load tests aiming to understand the behavior and performance of compacted sand replacement over treated collapsible soil by pre-wetting and compaction. The field tests were conducted on collapsible soils of Borg Al-Arab area, Egypt. The author reported that replacement soil improved the stability of collapsible soil by uniform distribution of water on surface. Increase in thickness of compacted sand replacement layer leaded to increase in the bearing capacity of inundated compacted collapsible soil. Significant settlements were found in foundations of structures on collapsible soils after being saturated, resulting in serious structure damage. It was suggested that in order to densify and stabilize

collapsible soils, the collapsible soil should be flooded before construction. The author also found that the total amount of collapsibility potential depended on initial moisture content, extent of wetting depth, duration of wetting, and the pattern of moisture migration. Finally, it was concluded that saturation and preloading of collapsible soil before construction could be helpful to stabilization of collapsible soils.

Haeri (2016) presented the studies taken place at Advance Soil Mechanics Laboratory of Sharif University of Technology, Tehran, Iran to study the intact behavior of the collapsible loessial soils taken from Hezar Pich Hill in the city of Gorgan, Iran. The author conducted tests using automatic unsaturated oedometer and fully automatic unsaturated triaxial devices. The author reported that the hydro-mechanical behavior of intact collapsible loessial soils was essentially different from that of the reconstituted samples. The water absorption and associated volume change or wetting collapse of the intact samples was stepwise and generally greater, while the wetting collapse of the reconstituted samples experienced almost linearly increasing upon becoming wet and smaller. The author also stated that the shear tests on reconstituted samples overestimated the shear strength of the natural loess. Thus, the author recommended that the reconstituted specimens of loess should not be used to predict the behavior of natural loessial soils. It was recommended to conduct undisturbed sampling and tests on intact natural loess to predict accurately the collapse potential, hydro-mechanical behavior, and shear strength of this type of collapsible soil.

Haeri and Garakani (2016) studied the hardening behavior of the collapsible loessial soil by conducting modified suction-controlled triaxial tests on undisturbed loess samples taken from Hezar Pich Hill in Gorgan city, Iran. The authors stated that collapse and reduction in volume of the specimen was due to suction decrease, and an elastic rebound happening due to the mean

effective stress decrease. Additionally, the amount of volume reduction due to pore collapse was significantly higher than the amount of dilation and elastic rebound due to the effective stress decrease. Consequently, the resultant was volume decrease while effective stress decreased at the same time. The authors also found that during the test, the soil samples could undergo hardening or softening, depending on the level of applied mean net stress or matric suction. They also provided a coupled constitutive model to show the relation between the values of mean effective yield stress, degree of saturation, and matric suction for unsaturated collapsible loessial soils (Figure 2.7).

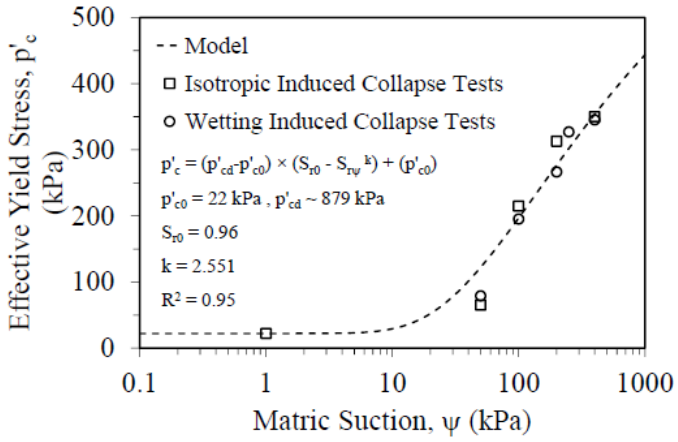

Fig. 2.7. Predicted and tested values of P_c' with matric suction (ψ) (Haeri and Garakani, 2016)

Haeri et al. (2016) attempted to study the role of sample disturbance and soil structure in the hydro-mechanical behavior of collapsible soils by conducting modified suction-controlled trixial tests on intact and reconstituted specimens of the loessial soil taken from Golestan province of Iran. The author found that the collapse phenomenon in tact loessial samples was mostly a stepwise reduction in volume rather than a continuous decrease with a constant rate or a sudden drop in volume as water added. They supposed that this behavior could be explained by the non-homogenous distribution of macrospores or microspores in intact specimens which

leaded to the presence of void spaces with different levels of collapse potential within soil matrix. They also presented that the intact samples were highly contractive and experienced mostly ductile shear strength behavior; whereas, the reconstituted samples seemed to undergo strain softening and dilatancy after failure. The authors additionally reported that the shear strength values of reconstituted samples were higher than that of intact samples when sheared at the same applied mean stresses and matric suctions. Thus, it was concluded that the specimen disturbance could result in the underestimation of volume change due to collapse and overestimation of shear strength. The authors stated that the shear strength from tests conducted on reconstituted specimens was overestimated for the natural soil, due to the different structures of the intact and reconstituted samples. Based on their experiments, the hydro-mechanical behavior of loessial soils was significantly affected by specimen disturbance and the soil structure.

Li et al. (2016) summarized a state of the art review on collapse mechanism with special reference to loess soil deposits, focusing on three different categories including traditional approaches, microstructure approaches, and soil mechanics-based approaches. The traditional approaches for interpreting the wetting-induced collapse mechanism consisted of loss of capillary tension, solution of soluble salts, shortage of clays, and under compaction. However, the traditional or conventional approaches were found to be unsatisfactory for universally explaining the collapse behavior of loess soils. These approaches were valuable to better understand collapsibility of local loess soil from simple tests. Microstructure approaches for interpreting wetting-induced collapse behavior were focused on four factors including particle pattern, contact relation, pore form, and bonding material. Among these factors, pore form and bonding material were proposed as the two dominant factors which have more influence on the

collapse behavior. It was concluded that microstructure approaches were widely acknowledged to play an important role in controlling the mechanical behavior of loessial soils. However, the microstructure approaches could not provide quantitative descriptor. The soil mechanics-based approaches for interpreting the collapse behavior provided the elastoplastic modeling for understanding collapse behavior. The elastoplastic models could define the yield surface for unsaturated soils, which obviously divided elastic and plastic deformations of unsaturated soils. Thus, these models could be a useful tool to explain the collapse phenomenon as soil yields or the stress path crosses the yield surface due to loading or wetting or both. It was found that these approaches based on concepts of elastoplastic breakage mechanics, such as the binary medium model and the block structural model, were validated to provide reasonable prediction of collapse behavior for natural loess soils. However, it was not easy to apply these models in conventional practice due to the difficulty in determining the parameters required for the models from time-consuming and resource-consuming experiments. Finally, it was recommended that future research studies should be focused on providing much simpler models with less parameters and parameters which are easy to determine from conventional tests.

Iranpour and Haddad (2016) conducted laboratory investigation aiming to understand the impacts of nanomaterials on collapsible soil behavior. The collapsible soil specimens were taken from arid and semi-arid regions of Iran. Then, the specimens were treated with four different types of nanomaterials, including nanoclay, nanocopper, nanoalumina, and nanosilica, and combined under different percentages of the total dry weight of the soil. Soil tests were carried out in natural water content and density. The authors stated that enhancing the resistance of clay and silt bridges as well as cementation factors in the structure of collapsible soils could reduce the danger likelihood of collapse because soil collapse highly depended on the structure of soil.

They presented that the dry unit weight and the water content significantly affected the soil collapse potential. Based on their experiments, they found that the combination of soil and nanomaterials was very sensitive and the amount and the type of nanomaterials added to the collapsible soil could get not only positive impact but also have negative impact on improvement of collapsible soils. It was concluded that the combination of nanomaterials with collapsible soils should be used at the most appropriate percentage to avoid negative effects resulting from adding nanomaterials more than the optimum value. The author also suggested that the negative effect could be reduced by combining nanoparticles with collapsible soil in the form of colloid solutions.

2.3. Literature Pertinent to At-Rest and Passive Earth Pressures

2.3.1. General

Earth retaining structures including, but not limited to, basement walls, bulkheads, abutment, and retaining walls are often met in foundation engineering. They are primarily designed to counter the lateral earth loads. Design of retaining structures requires knowledge and comprehension of lateral earth pressures that cause the lateral forces on the retaining structures.

At-rest earth pressure: The wall is static and it does not move toward or backward of its initial position (Figure 2.8). In this case, the earth pressure refers to the at-rest earth pressure ($K = K_0$: coefficient of at-rest earth pressure), and corresponds to a state of static equilibrium in the backfill soil mass. The resultant of at-rest earth pressure exerted on the wall is P_0.

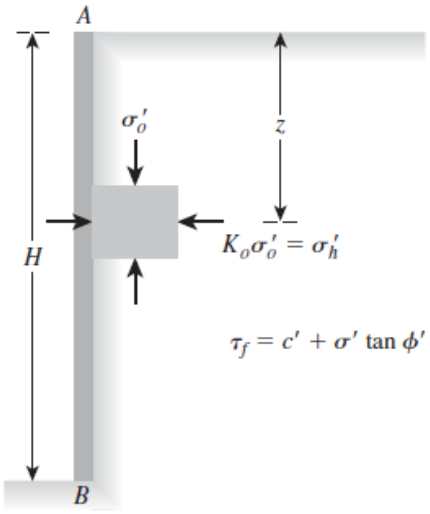

$$K = K_0 = \frac{\sigma'_h}{\sigma'_v} \quad (2.6)$$

Fig. 2.8. At-rest earth pressure (Das, 2009)

Passive earth pressure: The wall moves toward the retaining soil (Figure 2.9). The earth pressure increases from at-rest to passive earth pressure (K = K_p: coefficient of passive earth pressure) due to soil compression behind the wall. The resultant of passive earth pressure exerted on the wall is the passive thrust P_p.

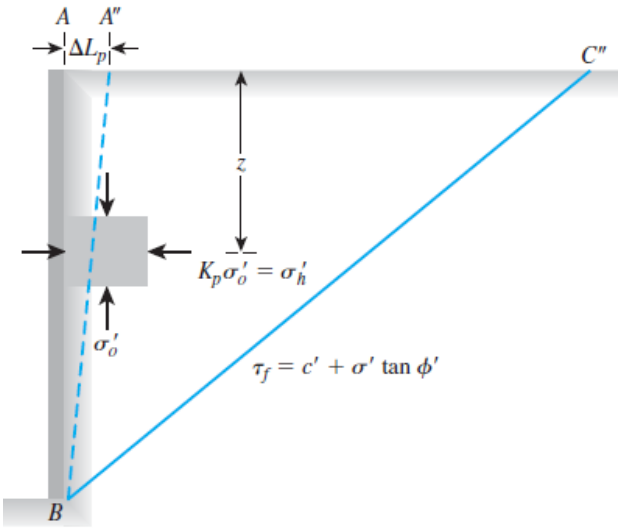

$$K = K_p = \frac{\sigma'_h}{\sigma'_v} = \frac{\sigma'_p}{\sigma'_v} \quad (2.7)$$

Fig. 2.9. Passive earth pressure (Das, 2009)

The relationship between wall movement and variation of the magnitude of lateral earth pressure is presented in Figure 2.10.

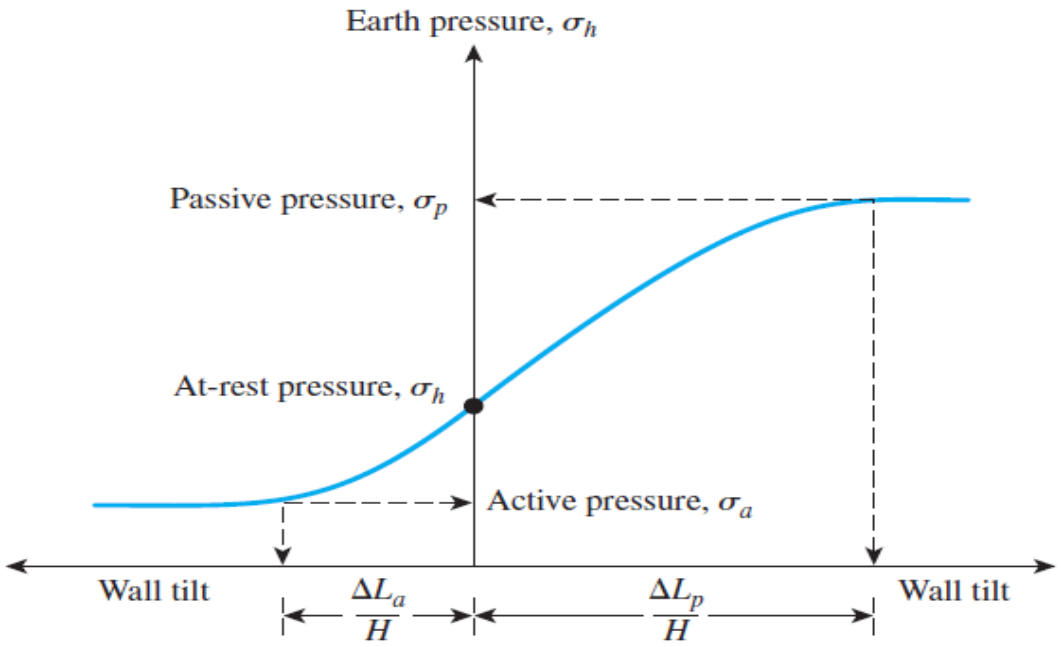

Fig. 2.10. Variation in lateral earth pressure with wall movement (Das, 2009)

Typical values of coefficient of active and passive earth pressures of loose and dense cohesionless soils (Barnes, 2010) are depicted in Figure 2.11

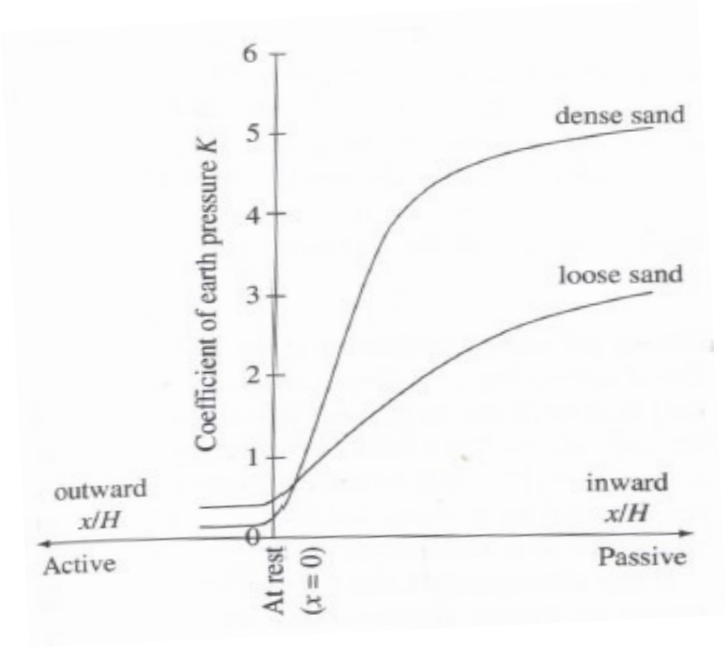

Fig. 2.11. Typical values of earth pressure coefficient (K) of cohesionless soils with wall movement (Barnes, 2010)

Mohr's circles for at-rest, active, and passive states are shown in Figure 2.12, in which: circle (I) presents for the at-rest state, circle (A) presents for the active state, and circle (B) presents for the passive state.

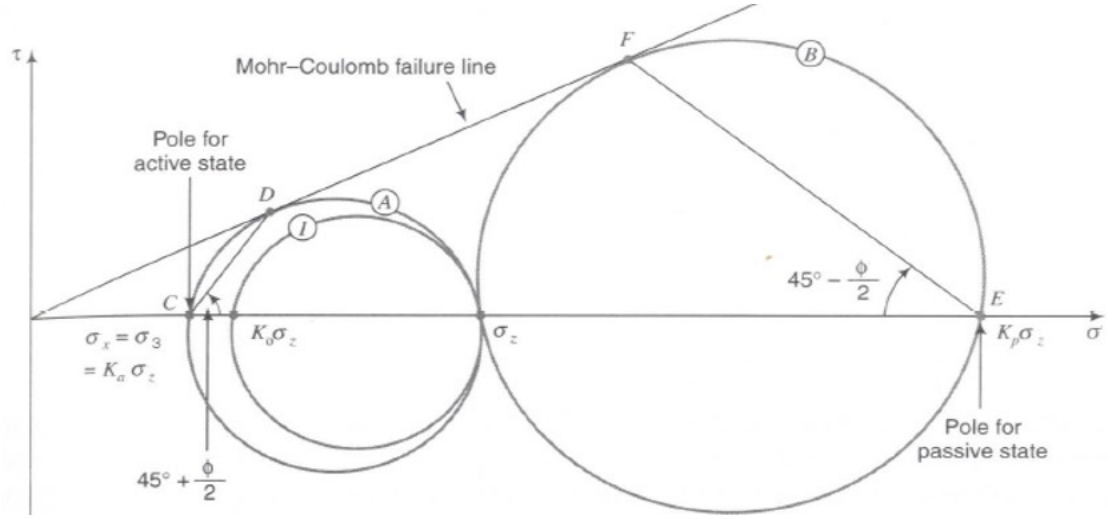

Fig. 2.12. Mohr's circles at-rest, active, and passive states (Budhu, 2008)

2.3.2. At-rest earth pressure

Generally, the at-rest earth pressure coefficient (K_0) depends on the angle of shearing resistance (ϕ'), plasticity index (PI), and stress history - overconsolidation ratio OCR (Liu and Evett, 2008).

Jaky (1944) proposed the empirical equation for estimation of at-rest earth pressure coefficient (K_0) for soils as follows:

$$K_0 = 1 - \sin\phi'_{cr} \qquad (2.8)$$

Where ϕ_{cr}' = critical state friction angle

However, the above Jaky's relationship just gives good results for backfill loose sand. The Jaky's relationship may grossly underestimate K_0 for backfill dense sand, resulting from the process of compaction backfill (Das, 2009).

Brooker and Ireland (1965) investigated experimentally the influence of stress history on the at-rest earth pressure coefficient (K_0) of remolded cohesive soils. Based on experimental results, the authors concluded that the at-rest earth pressure coefficient (K_0) depended on the angle of shearing resistance (ϕ'), the plasticity index (PI), and the soil's stress history as stated by the preconsolidation load or the overconsolidation ratio OCR. They confirmed that Jaky's equation was more accurate for the calculation of K_0 of cohesionless soils. For normally consolidated clay, a new empirical relationship was suggested as follows:

$$K_0 = 0.95 - \sin\phi'_{cr} \qquad (2.9)$$

Mackey and Kirk (1967) conducted the laboratory investigation into at-rest pressures acting on a rigid steel wall. In this investigation, three different sands which ranged from the loose to dense states were used. The authors indicated that the at-rest earth pressure in loose sand was in reasonable agreement with those of Jaky theory $K_0 = 1 - \sin \phi_{cr}'$; whereas, the at-rest earth pressure in dense sand was roughly equivalent to those of the simple Rankine passive pressure. It was confirmed again the Jaky's equation should not be used for backfill dense sand.

Alpan (1967) suggested a reasonably reliable procedure to roughly calculate the value of the at-rest earth pressure coefficient (K_0). He suggested that the following relationship should be used for clays: $K_0 = 0.19 + 0.233\log (PI)$ (PI – plasticity index – in %). (2.10)

Wroth (1973) proposed the empirical formula for estimation of at-rest earth pressure for overconsolidated sand.

$$K_{0(OC)} = K_{0(NC)} OCR - \left[\frac{\mu}{1-\mu}\right](OCR - 1) \qquad (2.11)$$

Where: $K_{0(NC)} = 1 - \sin \phi_{cr}'$; μ = Poisson's ratio (μ = 0.1 – 0.3 for loose sands; μ = 0.3 – 0.4 for dense sands)

Massarsch (1975) presented the new method for measuring in situ lateral earth pressure in soft clay. The method developed at the Royal Institute of Technology in Stockholm by using Glootzl measuring system. A spade-like, very thin (4mm) cell with large surface area (10x20cm) was installed at greater depths thanks to the protection of a steel casing. In this method, the at-rest earth pressure coefficient K_0 was estimated from the stress and pore pressure measurements.

They also reported that the at-rest earth pressure coefficient K_0 at 5 m depth was from 0.58 to 0.62.

Meyerhof (1976) proposed the following equation for estimating at-rest earth pressure coefficient (K_0): $K_{0(OC)} = (1 - \sin\phi')\sqrt{OCR}$ (2.12)

Massarsch (1979) introduced the empirical formula for predicting coefficient of at-rest earth pressure of normally consolidated clays as: $K_0 = 0.44 + 0.42\left[\frac{PI(\%)}{100}\right]$ (2.13)

For overconsolidated clays, the coefficient of at-rest earth pressure can be calculated by the following equation:

$$K_{0(OC)} = K_{0(NC)}\sqrt{OCR} \qquad (2.14)$$

Mayne and Kulhawy (1982) proposed the formula for estimation of at rest earth pressure coefficient of overconsolidated coarse-grained soils as follows:

$$K_{0(OC)} = (1 - \sin\phi')OCR^{\sin\phi'} \qquad (2.15)$$

Sherif et al. (1984) suggested for backfill dense sand, the following relationship should be employed:

$$K_0 = (1 - \sin\phi') + \left[\frac{\gamma_d}{\gamma_{d(\min)}} - 1\right]5.5 \qquad (2.16)$$

Where: γ_d= actual compacted dry unit weight of the backfill sand,

$\gamma_{d(min)}$ = dry unit weight of the sand in the loosest state

Duncan et al. (1991) stated that compaction of soil in layers adjacent to retaining walls induced lateral earth pressure above its pre-compaction values (normal at rest values). They developed charts for calculating K_0 by using a computer program, namely, EPCOMP2, based on the theory developed by Duncan and Seed called the hysteretic theory. These charts should be used for backfill cohesionless soil. They also expressed that for backfill clay soil, the high lateral pressures induced by compaction would be decreased gradually over time to normal at-rest values. Therefore, these charts should only be used to approximate the horizontal pressures in backfill clay soil immediately after compaction.

Mesri and Hayat (1993) performed laboratory investigation on undisturbed specimens of series of soft clay deposits. They introduced that an end-of-primary (EOP) coefficient of at-rest earth pressure, K_{op}, could be defined in terms of the constant-volume friction angle ϕ'_{cv}. The values of K_{op} for clay compositions and granular soils ranged from 0.31 to 0.67, corresponding to the value of ϕ'_{cv} from 19^0 to 44^0. They suggested the following equation for predicting K_{op} of sedimented, normally consolidated clays and granular soils: $K_{op} = 1 - \sin \phi'_{cv}$ (2.17)

In case of overconsolidated soil, they proposed the empirical formula as follows:

$$K_0 = (1 - \sin \phi_{cv}') \, OCR^{\sin \phi'cv} \quad (2.18)$$

Hamouche et al. (1995) reported the results of series of field tests (the self-boring pressuremeter, the Marchetti flat dilatometer, and the hydraulic fracturing) that were applied for three different clay deposits of eastern Canada. For an overconsolidated clay deposit, the values of K_0 from the experimental results were greater than that from using empirical relationship in theory: $K_{0(OC)} = K_{0(nc)} OCR^{\alpha}$ (2.19)

where: $\alpha = \sin \phi'$, $K_{0(nc)} = 1 - \sin \phi'$

They proposed that the equation (2.19) could be used to approximate the value of K_0 of overconsolidated clays, with a value of α between 0.75 and 1.15. It was necessary to determine K_0 directly by in situ tests for cases where accurate values of K_0 were required.

Landva et al. (2000) introduced a new apparatus, the split ring, to conduct one dimensional compression tests on municipal waste samples in order to measure at-rest earth pressure. They compared their measured values to typical values of granular materials and tire chips. They reported that the values of coefficient of earth pressure at-rest K_0 determined from the split ring test ranged from 0.23 to 0.40. The long term at-rest earth pressure coefficient of waste materials would be 0.47-0.49. They found that the at-rest earth pressure coefficient of waste materials decreased with an increasing amount of fibres (exposed belts). Therefore, the critical condition for coefficient of at-rest earth pressure of waste materials was the long term state when decomposable fibres was no longer available.

Michalowski (2005) revisited the Jaky's coefficient of at-rest earth pressure K_0, focusing on the problem of stress distribution in a wedge-shaped prism of sand. The author proposed the empirical relationship for the coefficient of at-rest earth pressure K_0 as follows:

$$K_0 = (1 - \sin \phi') \frac{1 + \frac{2}{3} \sin \phi'}{1 + \sin \phi'} \qquad (2.20)$$

The author also stated that the coefficient of at-rest earth pressure for overconsolidated soil $K_{0(OC)}$ was typically represented as a function of overconsolidation ratio OCR, but it was not dependent on the magnitude of the maximum consolidation stress. The $K_{0(OC)}$ not only was

affected by OCR but also was affected by some dependence on history including geologic features such as compaction bands.

Teerachaikkulpanich et al. (2007) introduced a method for estimation of at-rest earth pressure coefficient K_0 of kaolin clay by using the modified Oedometer covered with a pressurized chamber known as the COWK triaxial apparatus. Based on their study, the K_0 of normally consolidated clays was determined by using the equation below:

$$K_0 = \frac{CP - u_1}{\sigma'_{v0}} \qquad (2.21)$$

Where: CP = cell pressure, u_1 = pore water pressure measured by pressure transducers, σ'_{v0} = consolidation pressure during the preceding consolidation process.

They reported that the values of K_0 of normally consolidated kaolin used ranged from 0.68 to 0.75. Most of the values of K_0 of both normally and overconsolidated clays using empirical equations proposed by many researchers in the literature were lower than that from the experimental study.

Kalman (2008) attempted to determine K_0 of overconsolidated clay (Kiscelli clay) by two in situ measurements, namely, the Stresses Monitoring Station (borehole cells) and the flat jack. The results from these field tests supported their assumption which the values of K_0 of overconsolidated clay were more than 1. They demonstrated that the empirical relationship for estimation of K_0 proposed by Jaky always gave the result of K_0 less than 1. Jaky's formula should be only applied for geologically young and normally consolidated soils. Typically, for soft and plastic soils, the values of K_0 could be equal to 1. For overconsolidated soil/rock, the values of K_0 were greater than 1.

Hanna and Al-Romhein (2008) conducted an experimental investigation of the at-rest earth pressure of overconsolidated cohesionless soil acting on a vertical rough retaining wall with horizontal backfill. They proposed an empirical formula for determination of the at-rest earth pressure coefficient of overconsolidated cohesionless soil as follows:

$$K_{0\,(OC)} = (1 - \sin \phi') \, OCR^{(\sin \phi' - 0.18)} \qquad (2.22)$$

Where: OCR = the overconsolidation ratio, which is computed as $OCR = \frac{\sigma_v}{\gamma h}$ (σ_v = vertical pressure measured by the respective transducer at a given location, γh = theoretical overburden pressure calculated at that location).

They stated that the OCR was a function of the degree of the soil particles interlocking, stress history, and sand placing techniques employed in the laboratories. An increase of the OCR would result in significant increase of $K_{0(OC)}$. They also found that the friction angle between the wall and the sand (δ) had no effect on the measured coefficient of at-rest earth pressure.

Cai et al. (2011) attempted to assess the at-rest earth pressure coefficient K_0 based on the measurement of shear wave velocities from the seismic piezocone test (SCPTU). The empirical relationship in terms of K_0 was proposed as follows:

$$\frac{V_s(HV)}{V_s(HH)} = \frac{C_s(HV)}{C_s(HH)} \left(\frac{1 + K_0}{2K_0} \right)^{n_t} \qquad (2.23)$$

Where: V_s(HV) = the shear waves propagate in vertical direction, V_s(HH) = the shear wave propagate in horizontal direction; C_s(HV) and C_s(HH) = dimensional material constants, which could reflect the fabric anisotropy of the soil structure.

For granular soils, the ratio $\frac{V_s(HV)}{V_s(HH)} = 0.93$, and n_t = 0.25, while $\frac{C_s(HV)}{C_s(HH)} = 0.85$ for cohesive soils.

The author concluded that the shear wave velocity ratio $\frac{V_s(HV)}{V_s(HH)}$ was slightly influenced only by changes in the in-situ effective stress conditions.

El-Emam (2011) attempted to study at-rest lateral earth pressure of overconsolidated sand experimentally and numerically. The author reported that K_0 increased significantly by increasing overconsolidation ratio with repeated vibration compaction. Jaky's formula leaded to underestimate K_0 for overconsolidated sand. The author also found that the resultant of at-rest lateral earth pressure P_0 was located closer to 0.4H (H was the backfill height) from the wall base, which was above the 0.3H assumed by the classical earth pressure theory.

2.3.3. Passive earth pressure

Coulomb's theory

Coulomb theory (Das, 2009) for determination of lateral earth pressure based on limit equilibrium method, considering the wall soil friction angle δ. It is assumed that the soil is isotropic and homogeneous. The soil mass will slip along a plane inclined an angle α to the horizontal line. The slip plane can be determined by looking through the plane on which the maximum thrust acts.

Coulomb's passive earth pressure coefficient (K_p):

$$K_p = \frac{\cos^2(\phi'+\theta)}{\cos^2\theta\cos(\delta-\theta)\left[1-\sqrt{\frac{\sin(\phi'+\delta)\sin(\phi'+\beta)}{\cos(\delta-\theta)\cos(\beta-\theta)}}\right]^2} \qquad (2.24)$$

In which: ϕ' = the angle of shearing resistance of the backfill soil, θ = the angle of back side of wall and a horizontal line, β = the inclined backfill angle, and δ = the wall friction angle.

The passive thrust P_p is commonly assumed to act approximately a distance of (H/3) above the wall base. It is of interest to note that for a frictionless (δ=0) and vertical (θ=0) wall with a horizontal backfill (β=0), the above equation of K_p reduces to the Rankine's equation.

Rankine's theory

Rankine's theory (Liu and Evett, 2008; Das, 2009) for determination of lateral earth pressure is based on the stress state of soil and several assumptions. These assumptions are as follows:

- The wall is frictionless (no friction between wall and soil) and has to be vertical.
- The assumed failure plane is a function of the angle of shearing resistance (ϕ'), and the sliding wedge is along the assumed failure plane (Figure 2.13).
- The lateral earth pressure is various linearly with depth.
- The resultant force acts approximately a distance of (H/3) above the wall base, and it is parallel to the backfill surface.

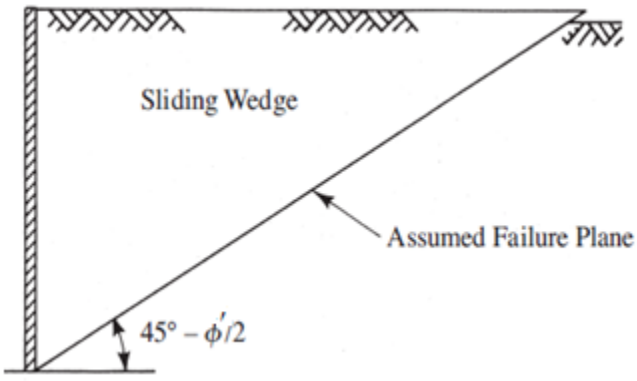

Fig. 2.13. Assumed failure plane for Rankine theory: Passive state (Liu and Evett, 2008)

Rankine's passive earth pressure coefficient: $K_P = \frac{1+\sin\phi'}{1-\sin\phi'} = \tan^2\left(45+\frac{\phi'}{2}\right)$ (2.25)

The total force per unit length of the wall: $P_p = \frac{1}{2}\gamma K_p H^2$ (2.26)

Figure 2.14 shows a frictionless wall retaining cohesive soils. The passive earth pressure acting on the wall at any depth below the ground surface can be expressed as follows:

$$\sigma_p = K_p\,\sigma_v + 2c'\sqrt{K_p} \quad (2.27)$$

The total passive force per unit length of the wall can be found from the area of the total pressure diagram as below:

$$P_p = \frac{1}{2}\gamma K_p H^2 + 2c' H\sqrt{K_p} \quad (2.28)$$

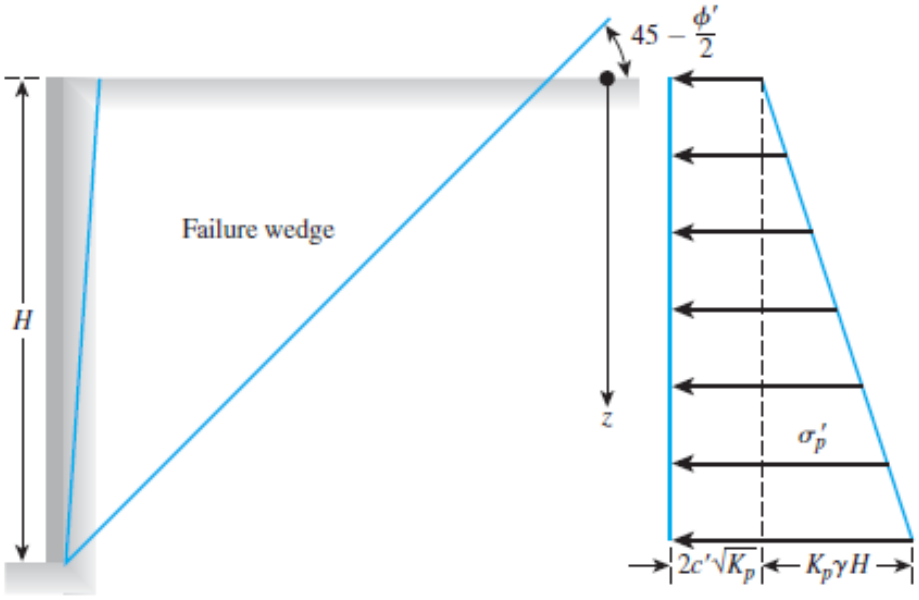

Fig. 2.14. Rankine's passive earth pressure distribution against a retaining wall with backfill cohesive soils (Das, 2009)

Narain et al. (1969) conducted series of laboratory tests with both the loose and dense sands to study passive earth pressure in sands. The test series involved translation of the wall, rotation of the wall about its bottom, and rotation of the wall about its top. The passive earth pressure coefficient K_p increased directly with the wall movements till a maximum value was reached. The magnitude of passive pressures and displacement required to cause maximum pressures were maximum in the case of rotation of the wall about its bottom and minimum in the case of rotation of the wall about its top. The distribution of passive pressures along the height of the wall was triangular only in the case of the wall that was translated; whereas the distribution of the passive pressures was parabolic in the case of the wall that was rotated. The location of the resultant force was above one third from bottom in the case of rotation of the wall about its bottom, while it was below one third from bottom in the case of rotation of the wall about its top.

Khoury (1994) investigated a laboratory experiment on the passive earth pressure of overconsolidated homogeneous and layered cohesionless soil acting on a retaining wall. The wall movement used in the tests was horizontal, no any rotation of the wall was allowed. The author proposed the following formula:

$$K_{pm} = b\sqrt{OCR}K_{pr} \qquad (2.29)$$

Where: K_{pm} = coefficient of passive earth pressure of overconsolidated sand; K_{pr} = coefficient of passive earth pressure by Rankine's method for normally consolidated sand; b = constant (b = 1 when OCR = 1.0; b = 2.5 when OCR>1.0).

Fang et al. (1994) performed laboratory experiments of passive earth pressure acting on vertical rigid wall with horizontal dry sand backfill. The entire retaining wall facility used in this

investigation comprised four components including model retaining wall, soil bin, driving system, and data acquisition system. The test series involved translational wall movement, rotation about a point above the top (RTT), and rotation about a point below the wall base (RBT) (Figure 2.15).

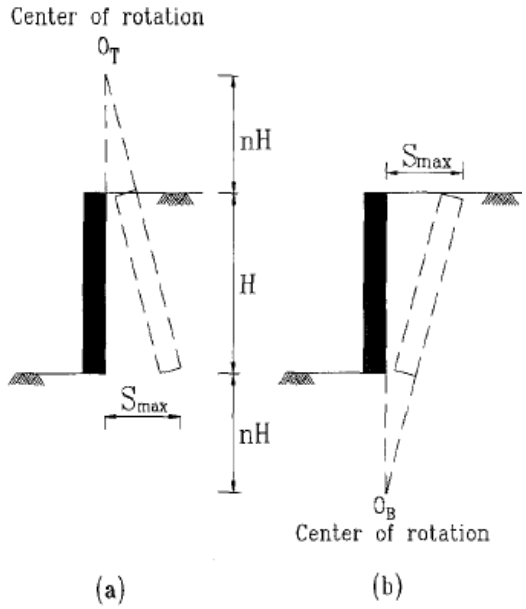

Fig. 2.15. Passive wall movement: (a) RTT mode; (b) RBT mode (Fang et al., 1994)

For the translational wall movement, the pressure distribution was fundamentally hydrostatic at every single stage of wall movement. At different depths of soil mass, the passive state was approximately simultaneously reached.

For the RTT wall movement (n = 0.00), the pressure distribution obtained was not close to linear. The resultant force P_p was evidently lower than that estimated using Coulomb and Rankine theories and its location was about 0.18H above the base of the wall.

For the RBT wall movement (n = 0.00), the pressure distribution obtained was nonlinear. The total force increased with an increase of wall movement continually, and the location of P_p was at about 0.55H above the base of the wall.

The authors also reported that the magnitude and location of the passive thrust P_p were importantly influenced by the wall movement mode when n value was small; whereas, the passive thrust P_p was slightly affected by the wall movement mode when n value was greater than about 2.0.

Fang et al. (1997) investigated experimentally passive earth pressures acting on a vertical rigid wall with inclined backfill dry sand. They reported that K_p increased with increasing backfill inclination. The experimental earth pressure distributions were approximately linear at every single stage of the wall motion up to failure. The experimental results presented a fairly good agreement with that determined by Coulomb's theory. However, Rankine's theory showed a tendency of underestimation of the passive thrust. They also found that K_p increased with wall motion before reaching the passive condition.

Kumar and Rao (1997) attempted to determine the coefficient of passive earth pressure of sand by method of slices. A design chart which showed the variation of K_p with δ/ϕ' was presented for determining the coefficient of passive earth pressure K_p for practical uses.

Mazindrani and Ganjali (1997) studied the earth pressure of inclined cohesive backfill. The empirical formula for estimating passive earth pressure coefficient K_p was proposed as follows:

$$K_p = \frac{1}{\cos^2 \phi'} \left\{ 2\cos^2 \beta + 2\left(\frac{c'}{\gamma z}\right)\cos\phi' \sin\phi' + \sqrt{\left[4\cos^2 \beta(\cos^2 \beta - \cos^2 \phi') + 4\left(\frac{c'}{\gamma z}\right)^2 \cos^2 \phi' + 8\left(\frac{c'}{\gamma z}\right)\cos^2 \beta \sin\phi' \cos\phi' \right]} \right\} - 1 \quad \text{(2-30)}$$

Where: ϕ' = angle of internal friction of soil, γ = unit weight of soil, z = depth to any point on the vertical back of the retaining wall from the level ground surface, c' = soil cohesion, β = inclined backfill angle.

They indicated that K_p increased with an increase of value of inclined backfill angle (β). K_p decreased with increasing value of soil cohesion (c').

Zhu and Qian (2000) proposed a new method for estimation of coefficient of passive earth pressure K_p using triangular slices based on the limit equilibrium method. The method was just applied for the case of cohesionless backfill without surcharge. They also provided tables and charts for determining K_p for practical application.

Duncan and Robert (2001) attempted to determine passive earth pressure using Log Spiral earth pressure theory along with special computer program corrected for 3D effects. They found that passive earth pressure for resisting structures movement was controlled by four main factors. These factors consisted of the amount and direction of the wall movement, strength and stiffness of the soil, friction and adhesion on the interface between the soil and structure, and the structure shape.

Fang et al. (2002) conducted experimentally investigation of passive earth pressure acting on a vertical rigid wall with horizontal backfill dry sand. The test series involved wall with backfill loose sand, wall with backfill medium dense sand, and wall with backfill dense sand. The research only focused on the translational wall movement to study the effect of soil density on the passive earth pressure.

For the wall with backfill loose sand, the passive earth pressure increased with increasing wall movement and lastly a limit passive pressure was reached. The passive earth pressure distributions was essentially linear at every single stage of wall movement. The passive thrust was slightly underestimated using Coulomb's theory.

For the wall with backfill dense sand, the passive earth pressure increased with increasing wall movement. After reaching a peak value, K_p decreased with increasing wall movement until reaching an ultimate value. In this case, the passive earth pressure would be overestimated using Coulomb's theory with the angle of shearing resistance at peak (ϕ'_{peak}). The authors recommended that the dilation and strength reduction of the backfill dense sand should be considered in estimation of the passive earth pressure.

Hanna and Khoury (2005) investigated a laboratory experiment on the passive earth pressure of overconsolidated cohesionless soil acting on a retaining wall. Tests were conducted on walls retaining homogeneous overconsolidated sand, strong overconsolidated cohesionless backfill overlying weak deposit, and weak overconsolidated cohesionless backfill overlying strong deposit.

For smooth walls (δ=0) retaining homogeneous overconsolidated sand:

$$K_{p(OC)} = b\sqrt{OCR}\,K_{p(NC)} \qquad (2.31)$$

Where: $OCR = \frac{\sigma_v}{\gamma h}$ (σ_v = vertical pressure measured by the respective transducer at a given location, γh = overburden pressure calculated at that location); $K_{p(NC)}$ = coefficient of passive earth pressure of normally consolidated sand (Rankine's value), and b = constant.

They found the constant b depended on the OCR: If the OCR was equal to 1, the constant b was equal to 1; whereas, if the OCR was greater than 1, the constant b was continuously

greater than 2. Generally, the constant b increased moderately with increasing the OCR.

For rough wall (1/2 $\phi' < \delta < 2/3\ \phi'$) retaining homogeneous overconsolidated sand:

$$K_{p(OC)} = K_{p(NC)}\left[1.5 - \left(\frac{\delta - 25}{100}\right)\right] OCR^{\sin\delta} \qquad (2.32)$$

The authors stated that compaction of cohesionless soil induced additional stresses in the soil mass. These stresses were locked in, causing the backfill soil becoming overconsolidated. Increasing the OCR leaded to the increase of passive earth pressure acting on the retaining wall. Moreover, they reported that for the case of a strong overconsolidated cohesionless backfill overlying a weak deposit, the passive earth pressures acting against the wall reduced significantly due to extending the failure mechanism to the weak deposit:

$$K_p\left(\frac{backfill}{deposit}\right) = \left[\frac{K_p(backfill) + K_p(deposit)}{2}\right] \qquad (2.33)$$

Where: K_p (backfill) = the coefficient of passive earth pressure of homogeneous backfill material, and K_p (deposit) = the coefficient of passive earth pressure of homogeneous lower deposits.

For the case of a weak overconsolidated cohesionless backfill overlying a strong deposit, the passive earth pressure acting against the wall could be estimated based on the condition of the backfill soil because the failure mechanism would remain confined in the backfill layer.

Vrecl – Kojc and Skrabl (2007) proposed a modified 3D failure mechanism for determination of the 3D passive earth pressure coefficient. The authors presented that the total passive earth force was defined by:

$$P = K_{p\gamma}\gamma\frac{h^2}{2}b + K_{pq}qhb + K_{pc}chb \qquad (2.34)$$

Where: $K_{p\gamma}$, K_{pq}, K_{pc} = earth pressure coefficient due to soil weight, vertical surcharge loading, and cohesion; q = surcharge loading; H = the height of the rigid retaining wall; c = cohesion; γ = unit weight

Hanna et al. (2011) developed numerical model using finite element method and the Mohr-Coulomb constitutive law to study the passive earth pressure on embedded vertical plate anchors in sand. They attempted to evaluate the stress and strain conditions during installation of anchor plates, and correspondingly evaluate the level of overconsolidation in the surrounding soils. They found that the passive earth pressure acting on anchor plates increased with increasing angle of shearing resistance ϕ' and the overconsolidation ratio of sand; whereas, it decreased with increasing the embedment depth of anchor. Eventually, design theories and design procedures were presented.

Poterasu (2013) attempted to study the influence of soil collapse on the passive earth pressure developed behind the retaining wall. The wall movement was translational. The author introduced that the passive earth pressure coefficient (K_p) decreased with increasing collapse potential C_p. When the backfill collapsible soil was saturated, K_p decreased with approximately 90% from the values estimated at initial condition.

Weng et al. (2014) studied the development of the passive earth pressure using PFC2D software based on the distinct element method (DEM). They presented that K_p increased with increasing the angle of shearing resistance (ϕ'). K_p also increased with increasing inter-particle stiffness. However, K_p would decreased with increasing the particle size.

Awn and Zakaria (2014) attempted to study the behavior of gravity retaining wall resting on collapsible soil by a small prototype model. The collapsible soil used in this study was gypsums soil with different gypsum percentages (5%, 20%, 30%, and 50%). The gypsums soil used to simulate the base soil was the fundamental factor controlling the behavior of the retaining wall. The gravity retaining wall model was backfilled with sandy soil. The authors then mixed 2.7% of cement with gypsums soil together as the soil improvement to reduce the vertical and tilting strain of the retaining wall. The authors reported that the collapsible soil layer (gypsums soil layer) experienced collapse when getting water percolation. They also revealed that with their test setup, the movement of the retaining wall was not uniform. The wall might fill toward or backward, settled in the toe faster than heel or the opposite when the collapsible becoming wet. However, after treating the embedded sypseous soil layer (the foundation of the retaining wall), the improvement in rotation settlement and collapse for the retaining wall model reached about 90% in compared to the values before the treatment.

Cai et al. (2016) proposed an analytical method to estimate the passive earth pressure acting on walls retaining cohesive soils subjected to the translation mode. The study was focused on the effects of several factors on passive earth pressure such as internal friction angle of backfill, wall – soil interface friction angle, surcharge pressure, cohesion, unit weight, and inclination angle of the slip surface on the passive earth pressure as well as on the slip-surface angle. The authors presented that the passive earth pressure increased when increasing the soil cohesion, the internal friction angle, and the uniformly distributed load on the surface of the cohesive backfill, respectively. The coefficient of passive earth pressure increased when

increasing the internal friction angle of the backfill. The authors proposed the following formula to estimate the passive earth pressure force on the rigid retaining wall:

$$P = K\left(qH + \frac{\gamma H^2}{2}\right) + (K-1)\frac{c'H}{\tan\phi'} \qquad (2.35)$$

where: K= coefficient of the passive earth pressure on the rigid wall

q = surcharge loading, H = the height of the rigid retaining wall, c' = cohesion of the backfill, ϕ' = angle of shearing resistance, γ = unit weight.

Hanna and Diab (2016) presented a numerical model for a wall retaining cohesionless backfill subjected to passive earth pressure under translation mode. The model applied the finite element technique, the constitutive law of the modified Cam-clay model, and the critical state soil mechanics (CSSM) concept. The model was also capable of incorporating the influence of the soil deformation and the stress history of the sand backfill on the values of passive earth pressure. Finally, the authors proposed the empirical formulae for estimation of the coefficients of passive earth pressure for normally consolidated sand and overconsolidated sand with the given values of the critical state parameters.

2.4. Discussion

Based on the literature review highlighted in this chapter, it can be drawn some main points as follows:

1. Collapsible soils have attracted a number of investigations from researchers/ scientists/engineers, but still need more research on them due to their complexity.
2. Numerous research works can be found dealing with at-rest and passive earth pressures theories for normally consolidated or over consolidated cohesionless soils. Few studies were made on cohesive soils. No investigations or attempts were made on the earth pressures of overconsolidated collapsible soils, accordingly no design theories for such type of soils were found in the literature.
3. The theories available in the literature are not applicable for prediction of the earth pressure acting the wall retaining collapsible soils subjected to inundation. The reason is that when inundated, the collapsible soils undergo sudden strength and volume reduction, which further influence the earth pressure of this soil on the wall.

CHAPTER 3
EXPERIMENTAL INVESTIGATION

3.1. General

The objective of the investigation was to establish the effect of soil collapse potential C_p and the overconcolidation ratio OCR on the at rest-earth and passive earth pressure of overconsolidated collapsible soil subjected to full inundation due to the rise of groundwater table. An experimental setup was designed and built in the laboratory to simulate the condition of retaining wall with backfill collapsible soil subjected to at-rest and passive earth pressures. Based on the wall movement, the pressure measured on the wall would be determined as at-rest or passive earth pressure. For the case of passive earth pressure, the wall was pushed toward the backfill soil horizontally without any rotation which generated compressive force on the soil mass. For the case of at-rest earth pressure, the wall was static, no horizontal force was applied to the wall.

3.2. Experimental setup

An experimental setup was developed in the laboratory to examine the earth pressure on the wall retaining dry or saturated collapsible soils. The model consists of testing tank, retaining wall, loading system, and water distribution system. Figure 3.1 presents the layout of the experimental setup used in this investigation. The testing tank was 1080 mm in length, 195 mm in width, and 405 mm in depth. A metal plate was positioned in the upper part of the testing tank to simulate the retaining wall.

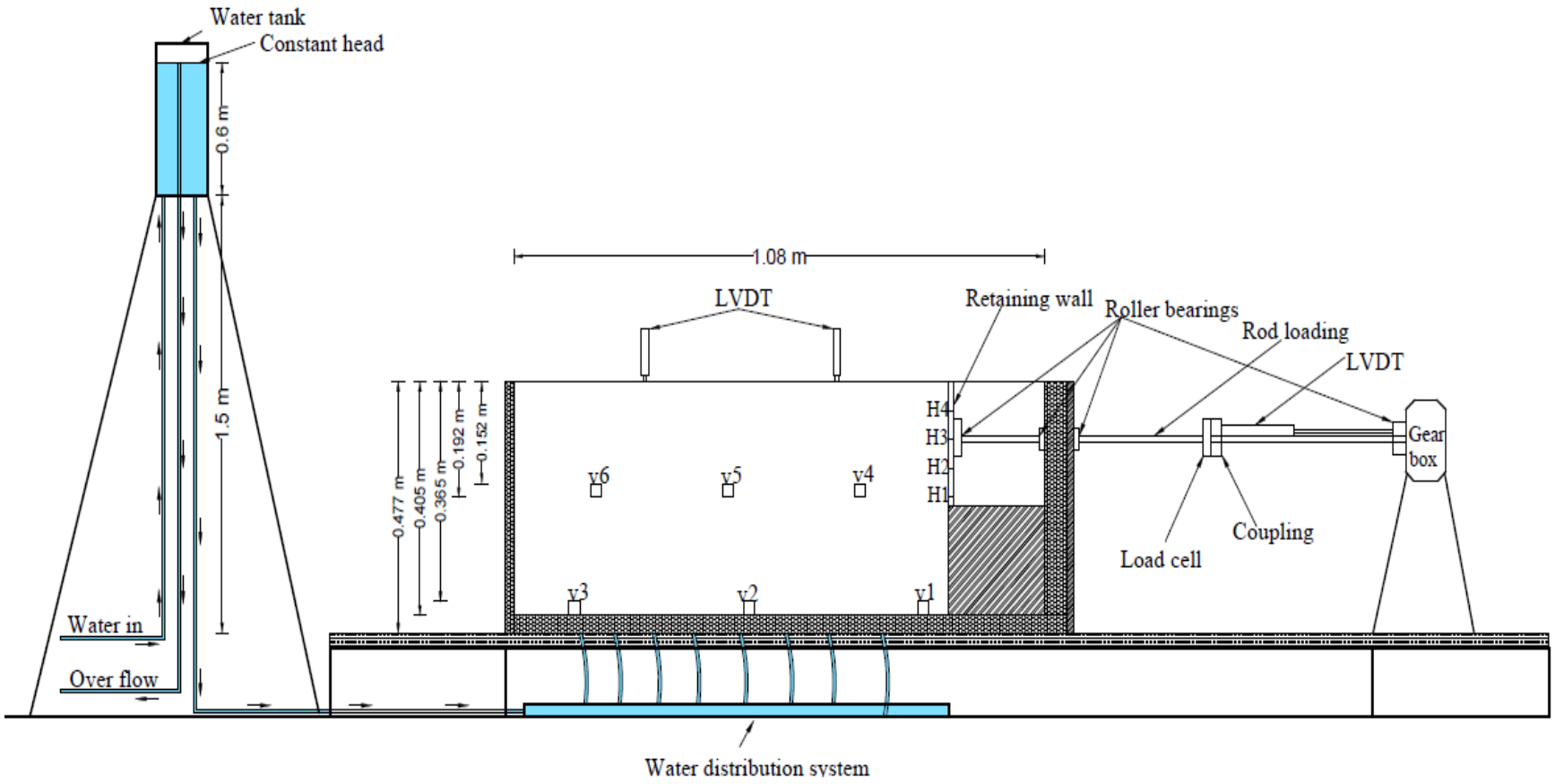

Fig. 3.1. Layout of the experimental setup

The model wall was 195 mm, 215 mm, and 19mm in width, height, and thickness, respectively. The wall was kept in the vertical position through a rod that was supported by two sets of roller. The rod was connected to a load cell to measure the total earth pressure acting on the retaining wall.

Four pressure transducers (H1, H2, H3, and H4) were installed at strategic points on the wall (Figure 3.2) to measure the earth pressure at these points and accordingly the earth pressure distribution acting on the wall. Six pressure transducers (v1 to v6) were placed in the soil mass at predetermined levels (these transducers were also placed in a staggered scheme in vertical direction to avoid boundary effects), to measure the vertical stresses in the soil mass (Figure 3.1). Three transducers were used for each selected level and they was situated at different location along the testing tank. Their readings could validate for the uniform soil mixture all over the testing tank. Each transducer was accommodated in a metal box (Figure 3.3), connected to the data acquisition system (DAS).

Furthermore, linear variable displacement transducers (LVDTs) were installed on the top of the testing tank to measure the collapse settlement of the soil behind the wall during the inundation. In order to develop the state of passive pressure in the retained collapsible soil mass, the wall was pushed horizontally toward the backfill without any rotation. A linear variable displacement transducer was installed to measure the displacement of the wall.

The pressure transducers used in this investigation were high stiffness, insensitive to temperature variation, simple to install, and water resistant. The transducers were individually calibrated in air and in sand prior to testing.

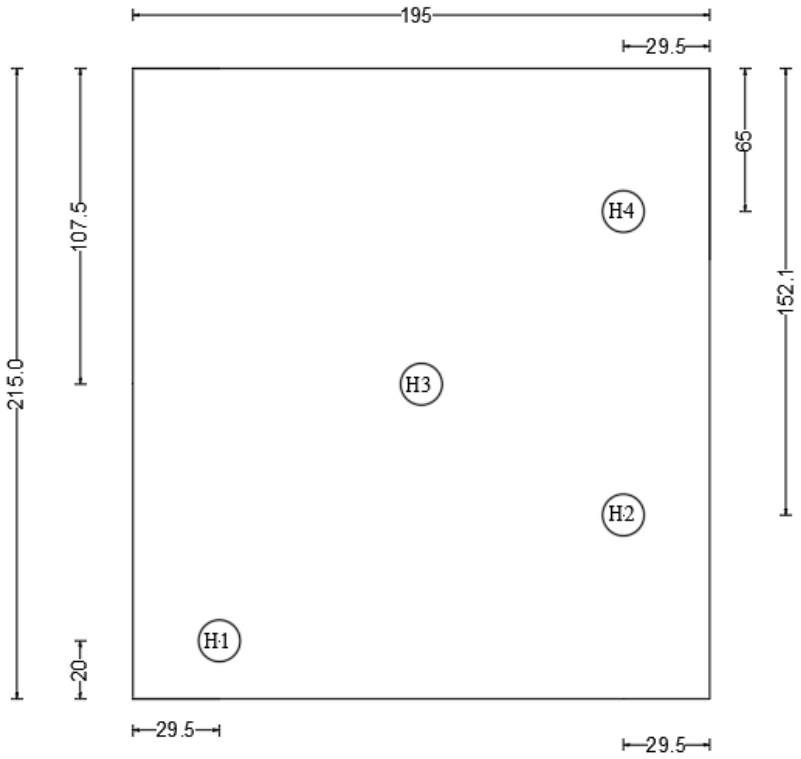

Fig. 3.2. Location of transducers on the model retaining wall

Fig. 3.3. Pressure transducers and its special box

An elevated water tank made of Plexiglas (Figure 3.4) , positioned on a stable wooden frame, connected to the testing tank through a plastic tube, through which the water was filled to the bottom of the testing tank, simulating the rise of groundwater. The water level in the water tank was remained unchanged during testing to assure laminar flow inside the soil in the testing tank. The water was filled in the water tank from the water source and one outflow pipe was fixed inside the water tank to keep the water at a constant level by draining the excess water. The second outflow pipe was connected to a water distributor (Figure 3.5) which introduced water to the soil tank through ten water inlets. To ensure even and uniform distribution of water throughout the collapsible soil during inundation, a thin layer of coarse silica sand was placed and slightly compacted at the bottom of the testing tank.

Fig. 3.4. Water tank

Fig. 3.5. Water distribution system

The loading system was composed of a gear box. The fixed gear box was used to generate horizontal forces which caused horizontal movement of the metal rod that was connected to the retaining wall. The horizontal forces generated by the gear box were measured by the load cell. One side of the load cell was connected to the horizontal retaining wall rod, another side of the load cell was connected to the horizontal rod of the gear box.

Figure 3.6 presents the photograph of main components of the experimental setup.

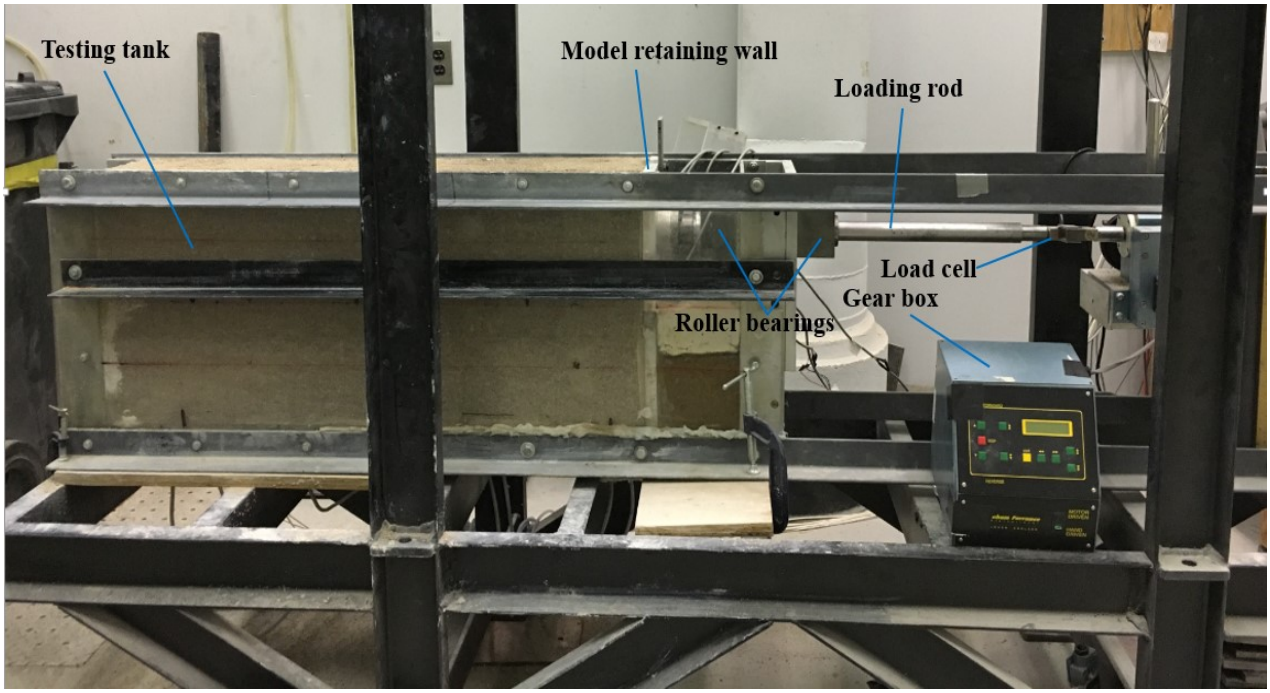

Fig. 3.6. Photograph of the experimental setup

In this experimental setup, an electric current of a constant voltage was used during the tests in order to supply the excitation voltages to the load cell, transducers, and LVDTs. Output readings from the load cell, transducers, and LVDTs were recorded on a computer in form of excel files through a Data Acquisition System (DAS) manufactured by Agilent Technologies by

using software. The software allowed data recording in the desired time intervals. The DAS allowed the measurement of millivolts from these device. The millivolt outputs from the load cell, transducers, and LVDTs were transformed to Newton (N), kilopascal (kPa), and millimeter (mm), respectively, based on the calibration of these device. Figure 3.7 illustrates schematically the connection between DAS and the other experimental instruments.

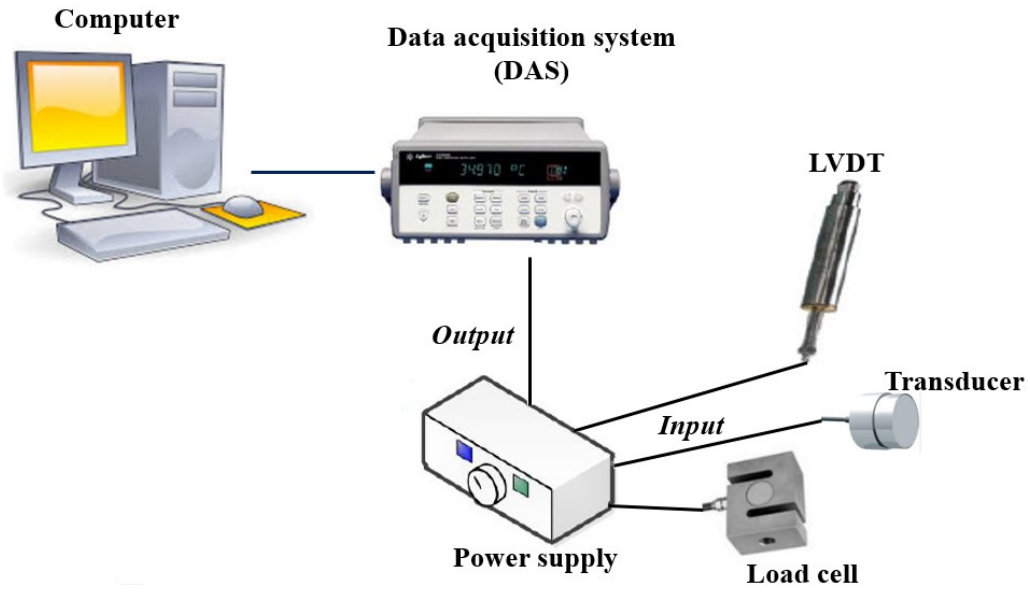

Fig. 3.7. Data acquisition system and measuring equipment

3.3. Collapsible soil preparation

The soil used in this investigation was a laboratory prepared collapsible soils formed by mixing Kaolin clay with fine sand. Generally, the higher the clay content the higher the collapse potential (C_p). Miller et al. (1998) reported that the maximum collapse occurs at around 18% of clay content. The clay played a role of cementing agent that bonds the sand particles at low water content. In this study, three different types of Kaolin clay, known commercially as Rogers,

Sapphire, and KT-Cast, were used to produce collapsible soil samples, to be tested under different water content, and the compaction energy to produce the desired collapse potential C_p, following ASTM D5333 (2003). Chemical analysis and physical properties of the three types of Kaolin clay provided by the manufacture are given in Tables 3.1 and 3.2. After a number of trials, it was concluded that the mixtures formed by Rogers clay produced the highest collapse potential C_p. Sand mixed with 6%, 8%, 10%, and 14% of Rogers clay at 5% water content will produce the soils having collapse potentials C_p of 4.2%, 9%, 12.5%, and 18%, respectively.

Collapse potential C_p is the key parameter used to define collapsible soil. Oedometer tests were conducted on these soil mixtures to determine the collapse potential of these mixtures, following ASTM D5333 (2003). Firstly, soil specimen (within the oedometer ring) is placed in the oedometer apparatus. Secondly, a predetermined vertical stress is gradually applied to the soil specimen until reaching a maximum load of 200 kPa. Thirdly, the soil specimen is inundated while the load is still maintained on the soil specimen. The collapse potential (C_p) is equal to the deformation of soil due to the addition of water, divided by the initial height of the specimen. In other words, the collapse potential (C_p) is the collapse strain due to inundation of the specimen under 200 kPa pressure in oedometer apparatus, as shown in equation (2.4): $C_p = \frac{\Delta h}{h_0} \cdot 100\%$

Table 3.3 presents summary of the response to wetting Oedometer tests on these mixtures used in this investigation. Table 3.4 presents a summary of the laboratory test results performed on these mixtures. The range of the collapse potential of 4.2% to 18% are defined as moderate to severe, which is widely encountered in the field, as in Table 3.5. Figure 3.8 presents the grain-size distribution for these mixtures.

Table 3.1. Chemical analysis of the Kaoline clay

Component elements properties	Rogers	Sapphire	KT-Cast
CaO (%)	0.28	0.2	0.09
MgO (%)	0.26	0.15	0.09
K_2O (%)	0.26	0.19	0.1
Na_2O (%)	0.12	0.1	0.09
TiO_2 (%)	1.3	1.4	1.64
Al_2O_3 (%)	37.5	38.15	38.8
SiO_2 (%)	46.5	46.25	45.1
Fe_2O_3 (%)	1.0	0.65	0.5

Table 3.2. Physical properties of the Kaoline clay

Physical properties	Rogers	Sapphire	KT-Cast
pH	4.8	4.8	5.5
Dry Modulus of rupture (psi)	400*	400*	225
Surface area (m^2/g)	16.5	16.5	12

Note: * Extruded 50% ball clay, 50%flint

Table 3.3. Summary of the response to wetting Oedometer tests on these mixtures used in this investigation

Mixtures	Rogers clay content (%)	Initial water content (%)	Compaction used for the soil mixtures placed the consolidation ring in Oedometer tests			C_p (%)
			Compaction weight (gm)	Number of drops	Height of drops (mm)	
A	6	5	100	8	150	4.2
B	8	5	100	8	150	9.0
C	10	5	100	8	150	12.5
D	14	5	100	6	150	18

Table 3.4. Physical properties of collapsible soil mixtures

Soil properties	**Soil – A** (C_p = 4.2%)	**Soil – B** (C_p = 9.0%)	**Soil – C** (C_p = 12.5%)	**Soil – D** (C_p = 18%)
Clay content in %	6	8	10	14
Water content in %	5	5	5	5
Unit weight (γ) in kN/m^3	16.28	16.25	16.2	15.3
Void ratio (e)	0.67	0.69	0.70	0.80
Specific gravity (Gs)	2.66	2.67	2.67	2.68
Cohesion (c') in kPa	9	12.5	15.5	18
Angle of shearing resistance (ϕ') in degree	40	38.5	35	31
Liquid limit (LL)	-	-	15.9	24.7
Plastic limit (PL)	-	-	13.35	17.3
Plasticity index (PI)	-	-	2.55	7.4
Coefficient of uniformity (C_u)	4	5.4	21.9	30
Coefficient of curvature (C_c)	1.27	1.65	6.47	8.53

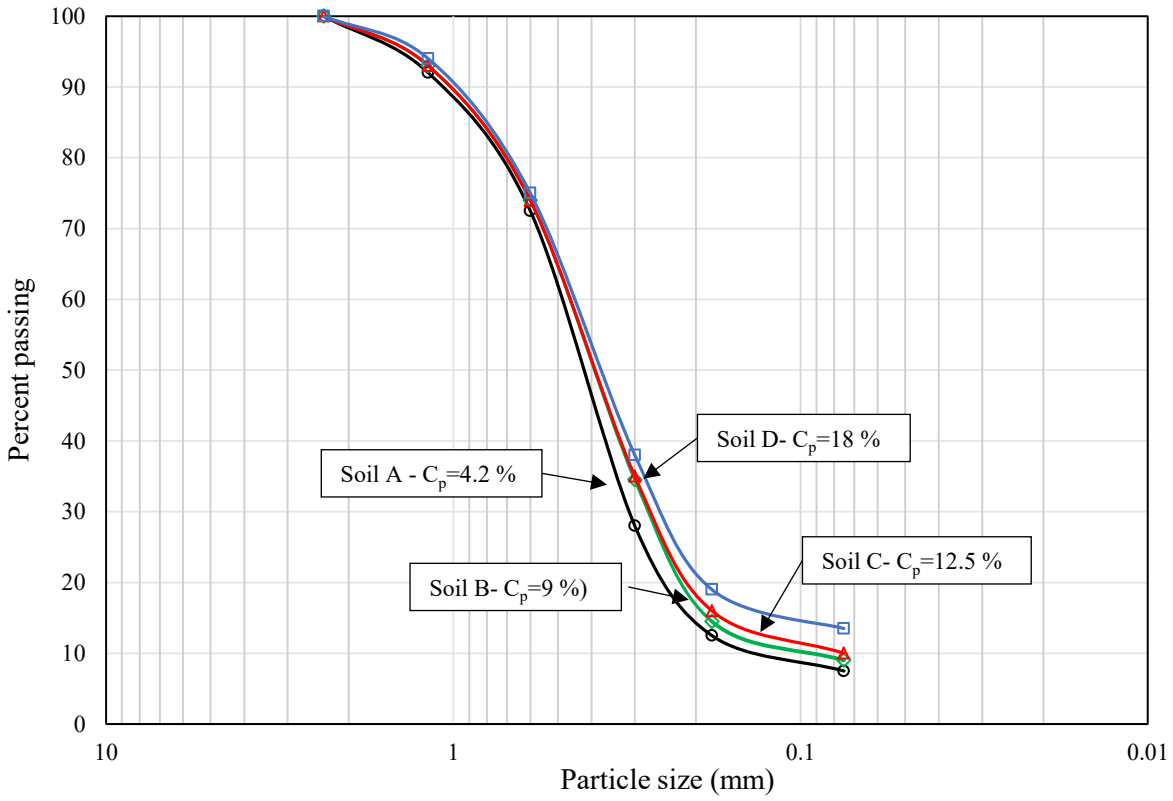

Fig. 3.8. Particle size distribution for the collapsible soil mixtures

Table 3.5. Mixtures classification based on collapse potential C_p

Classification	Collapsible soil mixtures			
	Soil – A (C_p = 4.2%)	Soil – B (C_p = 9.0%)	Soil – C (C_p = 12.5%)	Soil – D (C_p = 18%)
In terms of severity of foundation problem (Jennings and Knight, 1975)	Moderate trouble	Trouble	Severe trouble	Severe trouble
In terms of collapse potential (ASTM D5333, 2003)	Moderate	Moderately severe	Severe	Severe

3.4. Test procedure

a. Test was commenced by placing a thin layer of coarse silica sand at the bottom of the testing tank to ensure a uniform distribution of the water throughout the collapsible soil during inundation.

b. The prepared collapsible soil was then placed on the top of the coarse silica sand layer in four sublayers, and compacted by means of falling weight. The compaction was made of a 4.5 kg hammer that drops freely from a height of 45.7 cm on an aluminum plate placed on the top of the soil layer. The number of drops was predetermined for each layer to obtain uniform soil mixture in the testing tank.

c. When reaching the desired depth of the soil in the testing tank, tests, all measuring devices were connected and readings were recorded at regular interval by the DAS using a computer.

d. For the tests performed on the saturated soils, water was introduced to the soil from the bottom of the testing tank, at a slow rate, to simulate the rise of the groundwater table. This process continued until the full inundation of the soil in the testing tank was noted.

e. In order to produce overconsolidated soil in the testing tank, a rigid plate made of metal was placed on the top of the soil surface. A uniform static load – surcharge loading Ps (Figure 3.10) was subsequently applied on the plate, allowing loading and unloading.

   The process continued until no further increase in the vertical displacement, which was measured by the LVDTs mounted on the top of the plat.

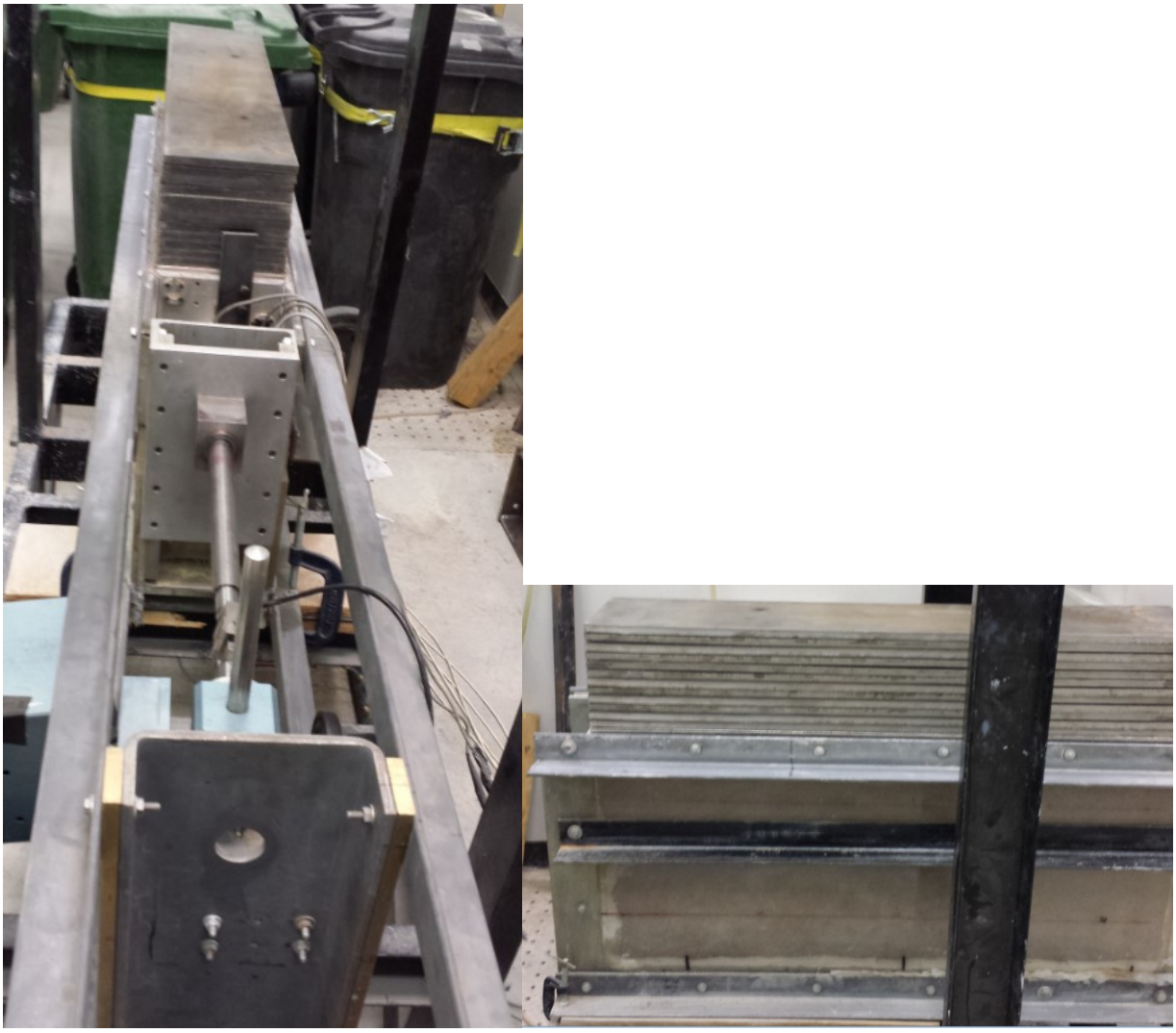

Fig. 3.9. Photograph of the application of the surcharge loading Ps

f. In order to generate the passive earth pressure condition, the wall was pushed toward the backfill soil horizontally without any rotation by the gear box according to the displacement steps of approximately 0.5mm/minute. Concurrently, all measuring devices were connected and readings were recorded at regular interval by the DAS.

3.5. Test program

The present investigation mainly focused on examining the role of the soil collapse potential C_p and stress history (overconsolidation ratio - OCR) as well as the effect of inundation on at-rest and passive earth pressures. In this investigation, tests were performed on both dry and saturated soils. Test program for at-rest case: the main test program is listed in Table 3.6, and a series of tests for the purpose of validation is shown in Table 3.7. Test program for passive case is presented in Table 3.8. Moreover, the list of the repeated tests to ensure the repeatability of the test results is presented in Table 3.9.

Table 3.6. Details of testing program for at-rest earth pressure (for the purpose of developing empirical formulae)

Test no.	Soil type	Surcharge Ps (kPa)	Testing condition
1	A (C_p = 4.2%)	0	Dry soil
2	C (C_p = 12.5%)	0	Dry soil
3	D (C_p = 18%)	0	Dry soil
4	A (C_p = 4.2%)	0	Saturated soil
5	C (C_p = 12.5%)	0	Saturated soil
6	D (C_p = 18%)	0	Saturated soil
7	A (C_p = 4.2%)	8	Dry soil
8	C (C_p = 12.5%)	8	Dry soil
9	D (C_p = 18%)	8	Dry soil
10	A (C_p = 4.2%)	8	Saturated soil
11	C (C_p = 12.5%)	8	Saturated soil
12	D (C_p = 18%)	8	Saturated soil

Table 3.7. Test program for at-rest earth pressure (for the purpose of validating the proposed empirical formulae)

Test no.	Soil type	Surcharge Ps (kPa)	Testing condition
13	A (C_p = 4.2%)	16	Dry soil
14	C (C_p = 12.5%)	16	Dry soil
15	D (C_p = 18%)	16	Dry soil
16	A (C_p = 4.2%)	16	Saturated soil
17	C (C_p = 12.5%)	16	Saturated soil
18	D (C_p = 18%)	16	Saturated soil
19	B (C_p = 9.0%)	0	Dry soil
20	B (C_p = 9.0%)	8	Dry soil
21	B (C_p = 9.0%)	16	Dry soil
22	B (C_p = 9.0%)	0	Saturated soil
23	B (C_p = 9.0%)	8	Saturated soil
24	B (C_p = 9.0%)	16	Saturated soil

Table 3.8. Details of testing program for passive earth pressure

Test No.	Soil type	Test series	Surcharge Ps (kPa)	Testing condition
1	A (C_p = 4.2%)	Se1	0	Dry soil
2	B (C_p = 9.0%)		0	Dry soil
3	C (C_p = 12.5%)		0	Dry soil
4	D (C_p = 18%)		0	Dry soil
5	A (C_p = 4.2%)	Se2	8	Dry soil
6	B (C_p = 9.0%)		8	Dry soil
7	C (C_p = 12.5%)		8	Dry soil
8	D (C_p = 18%)		8	Dry soil
9	A (C_p = 4.2%)	Se3	16	Dry soil
10	B (C_p = 9.0%)		16	Dry soil
11	C (C_p = 12.5%)		16	Dry soil
12	D (C_p = 18%)		16	Dry soil
13	A (C_p = 4.2%)	Se1’	0	Saturated soil
14	B (C_p = 9.0%)		0	Saturated soil
15	C (C_p = 12.5%)		0	Saturated soil
16	D (C_p = 18%)		0	Saturated soil
17	A (C_p = 4.2%)	Se2’	8	Saturated soil
18	B (C_p = 9.0%)		8	Saturated soil
19	C (C_p = 12.5%)		8	Saturated soil
20	D (C_p = 18%)		8	Saturated soil
21	A (C_p = 4.2%)	Se3’	16	Saturated soil
22	B (C_p = 9.0%)		16	Saturated soil
23	C (C_p = 12.5%)		16	Saturated soil
24	D (C_p = 18%)		16	Saturated soil

Table 3.9. Test program for studying the repeatability of the test results

Test no.	Test type	Surcharge Ps (kPa)	Soil type	Testing condition
3*	At-rest	0	D (C_p = 18%)	Dry soil
6*				Saturated soil
4*	Passive	0	D (C_p = 18%)	Dry soil
16*				Saturated soil

3.6. Validation of the experimental setup

Firstly, to consider the friction force in the bearings and the friction force between the wall and the testing tank during pushing the wall to simulate the passive earth pressure condition, Preliminary tests were conducted on the empty tank. After that, an average friction force was estimated and it was used to subtract the readings of all the passive tests.

Secondly, to ensure the suitability of the experimental setup, tests were conducted on homogenous loose sand and its coefficient of passive earth pressure (K_p) was calculated and validated by using Rankine's theory; while the coefficient of at-rest earth pressure (K_0) was computed and validated by using Jaky's equation.

*At-rest earth pressure test with homogenous loose sand: the wall was static, no horizontal force was applied to the wall. The horizontal earth pressure acting on the wall was measured by the transducers installed on the wall, and vertical pressure in the sand mass measured by the transducers placed in the sand mass. The test result is presented graphically in Figure 3.10.

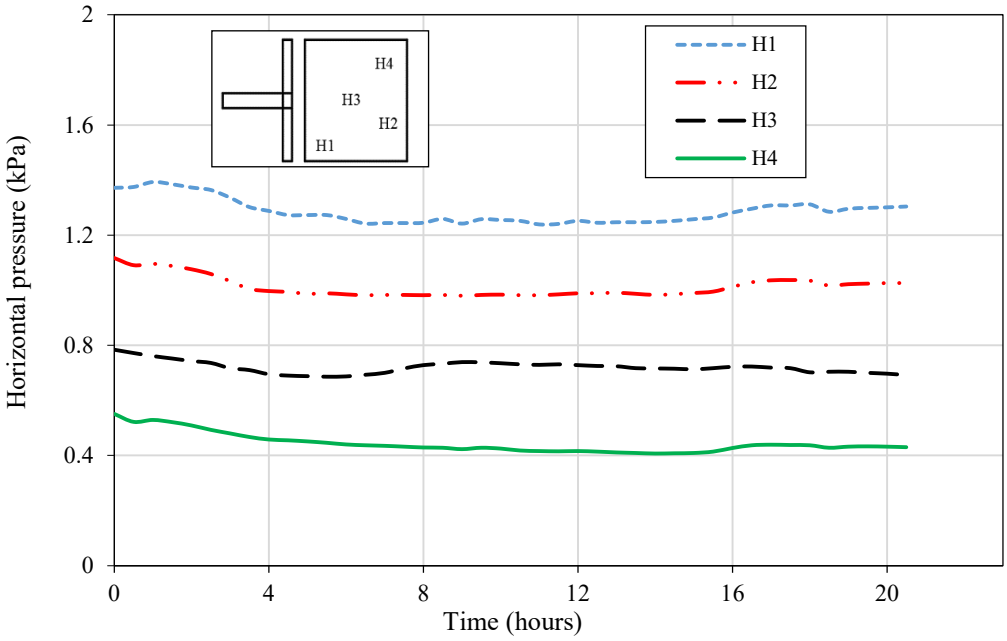

(a)

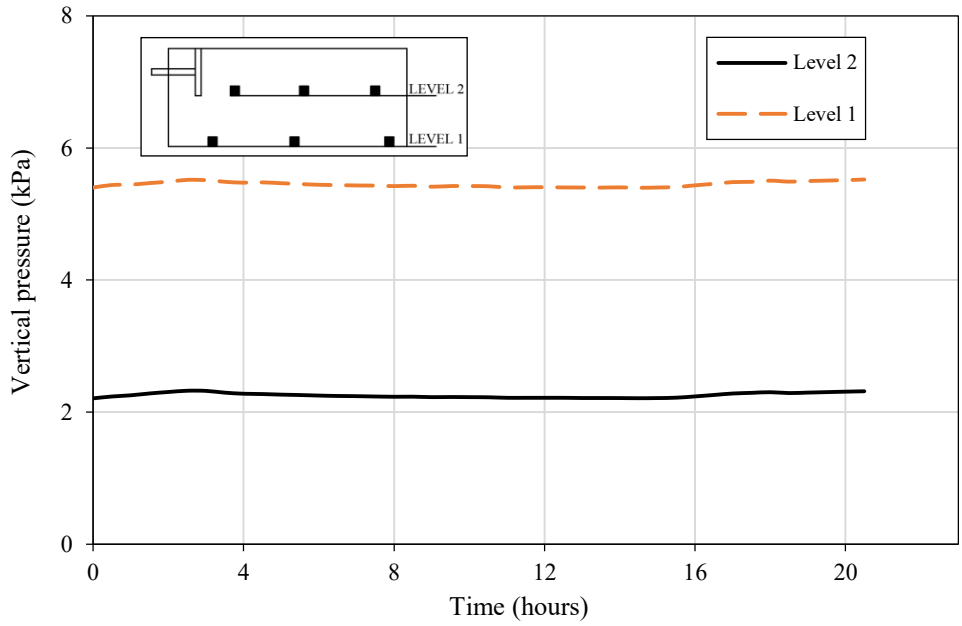

(b)

Fig. 3.10. Test results: (a) horizontal pressure measured by wall transducers versus time; (b) vertical pressure in the sand mass measured by transducers versus time

The experimental value of K_0 was estimated using the equation: $K_0 = \frac{\sigma'_h}{\sigma'_v}$; where σ'_h = at-rest earth pressure in kPa measured on the wall by the respective transducer; σ'_v = the corresponding vertical pressure at the same element. The experimental result of K_0 is 0.45.

In order to validate the result given by the experimental setup, K_0 was also calculated using Jaky's theory as the equation: $K_o = 1 - \sin\phi'$ = 1 - sin 33.26^0 = 0.452 (ϕ' =33.26^0 is angle of shearing resistance of the tested sand). It can be seen that the result given by the experimental setup agreed well with the result given by Jaky's theory.

* Passive earth pressure test with homogenous loose sand: the wall was pushed toward the retaining sand horizontally without any rotation by the gear box according to the displacement steps of approximately 0.5mm/minute in order to generate the passive earth pressure condition. The test result is presented diagrammatically in Figure 3.11.

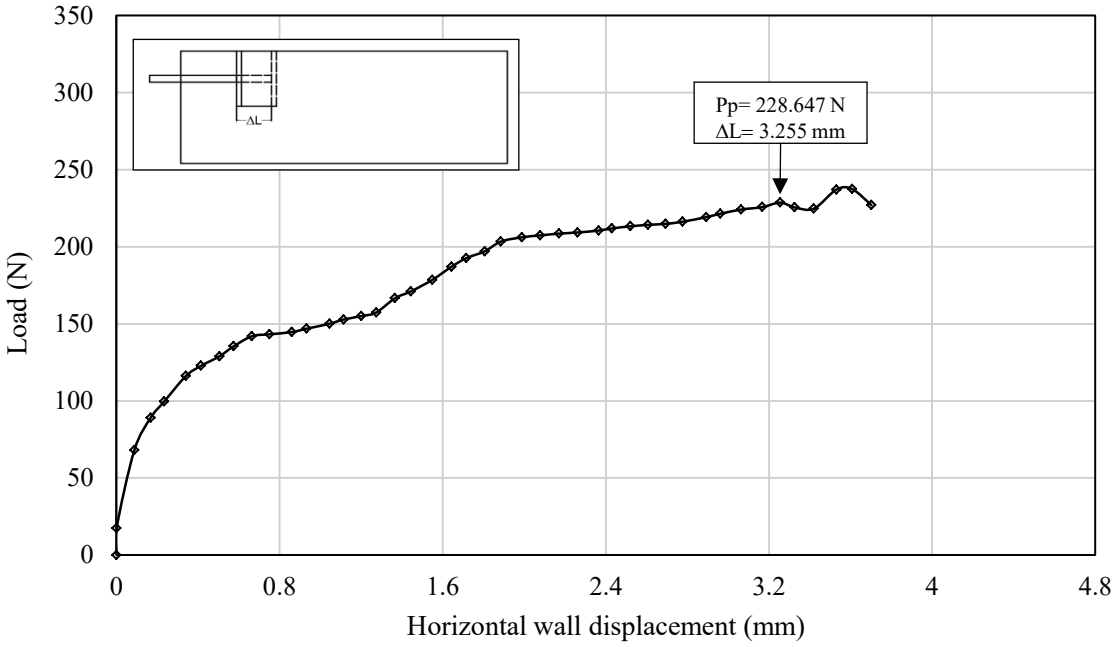

(a)

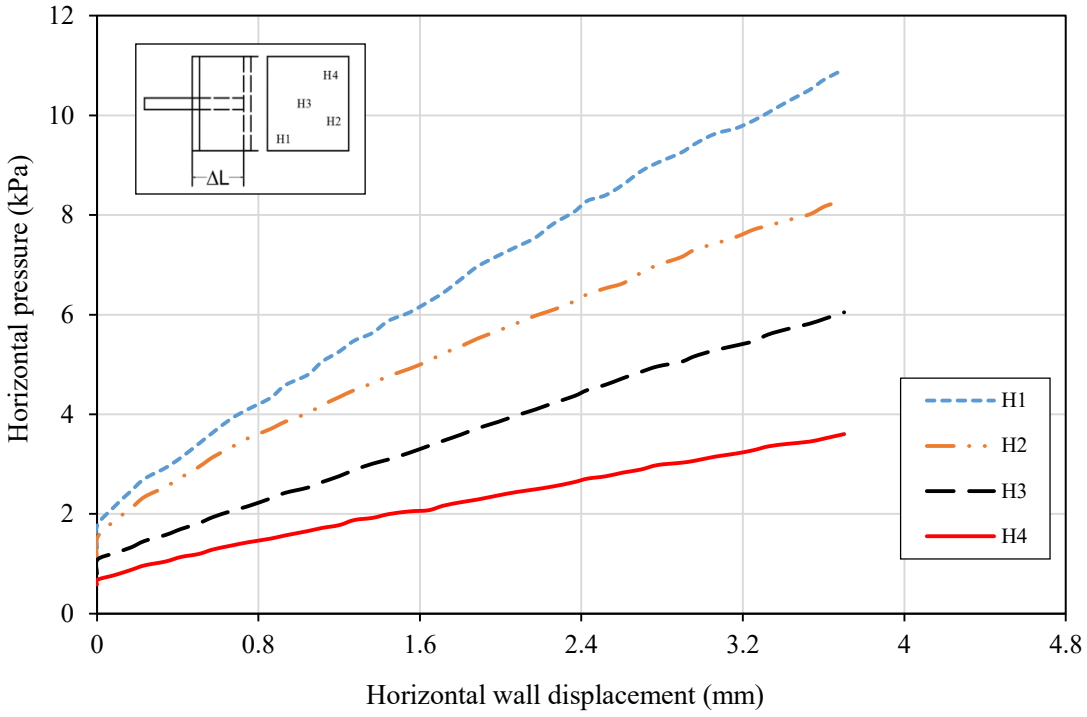

(b)

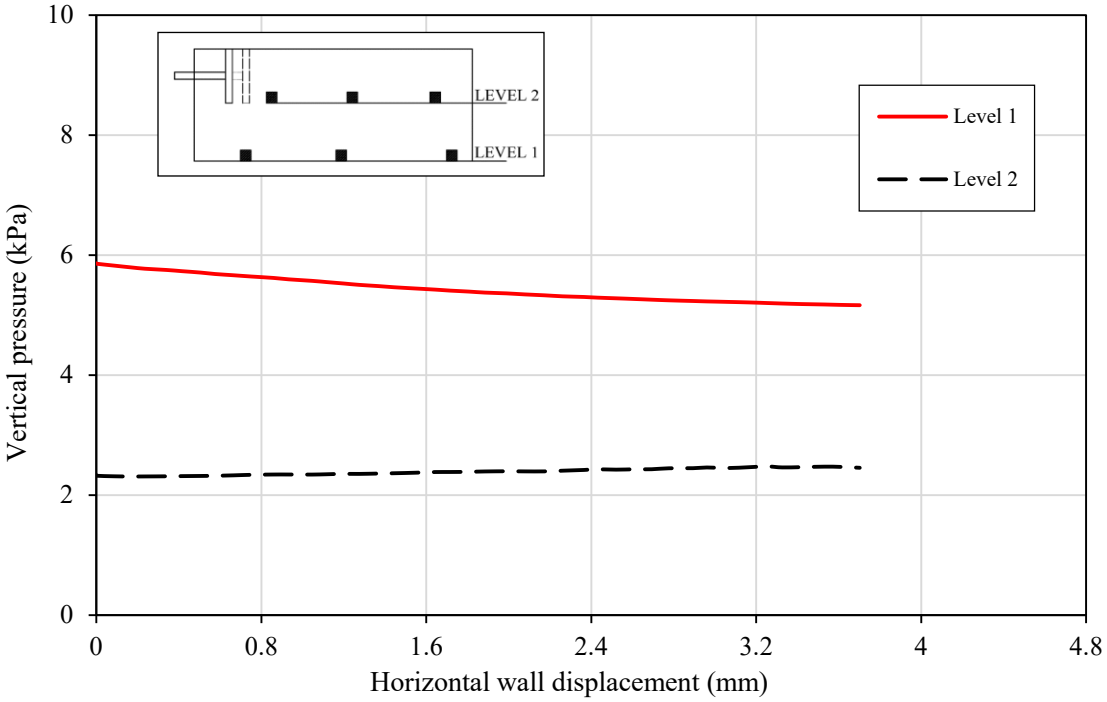

(c)

Fig. 3.11. Test results: (a) Load – displacement curve (load cell reading); (b) Load – displacement curves for each transducer; (c) Vertical pressure in the sand mass versus the wall displacement

The experimental value of K_p was estimated as followings: $K_p = \frac{P_p}{0.5\gamma H^2 b} = 3.42$

Where: P = passive earth force at failure (P = 228.647 N), measured by the load cell.

H = the height of the retaining wall (H= 215mm)

b = the width of the retaining wall (b=195mm)

γ = the unit weight of the sand (γ = 14.82 kN/m^3)

In order to validate the result given by the experimental setup, K_p was also calculated using Rankine's theory as followings: $K_p = \tan^2(45 + \frac{\phi'}{2}) = \tan^2\left(45 + \frac{33.26}{2}\right) = 3.43$

It can be seen that the result given by the experimental setup was in good agreement with the result given by the Rankine's theory.

CHAPTER 4
TEST RESULTS AND ANALYSIS FOR THE CASE OF AT-REST PRESSURE

4.1. General

In this chapter, the results obtained from the present experimental investigation are presented in form of figures, following by discussions about these results. A series of comparing figures have been developed to indicate the difference of soil behavior under the same or different conditions. Finally, empirical formulae and design charts are proposed based on the analysis of these results.

4.2. Results and analysis

Test no. 1 & 4 were performed on the dry and saturated soils, respectively, with 6% kaoline clay content, having collapse potential C_p of 4.2%. The test results are presented diagrammatically in Figure 4.1. From the Fig. 4.1a, it can be seen that at-rest earth pressure acting on the wall measured by transducers slightly changes with time for both dry and saturated soils. The decrease trend is more obvious in case of saturated soils. It can be seen from this figure that the at-rest earth pressure decreases slightly when the soil gets saturated. From the Fig. 4.1b, it can be seen that the vertical pressure in the soil mass slightly changes with time for both dry and saturated soils. The vertical pressure in the soil mass decreases when the soil is saturated.

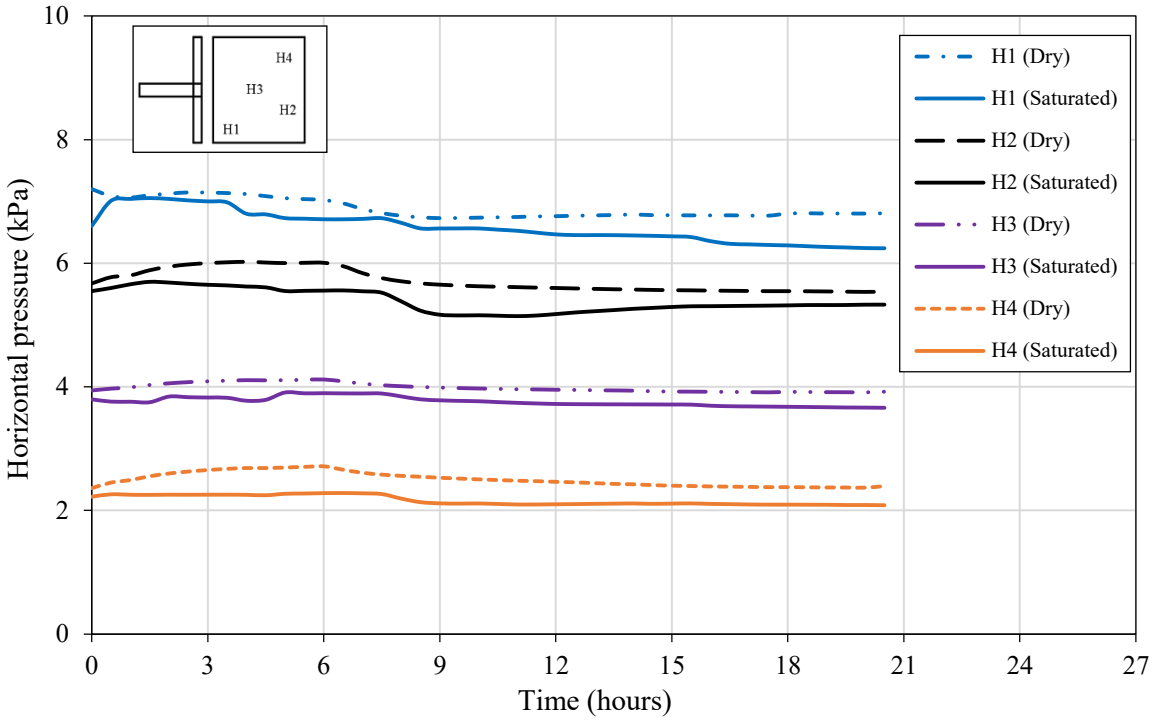

(a)

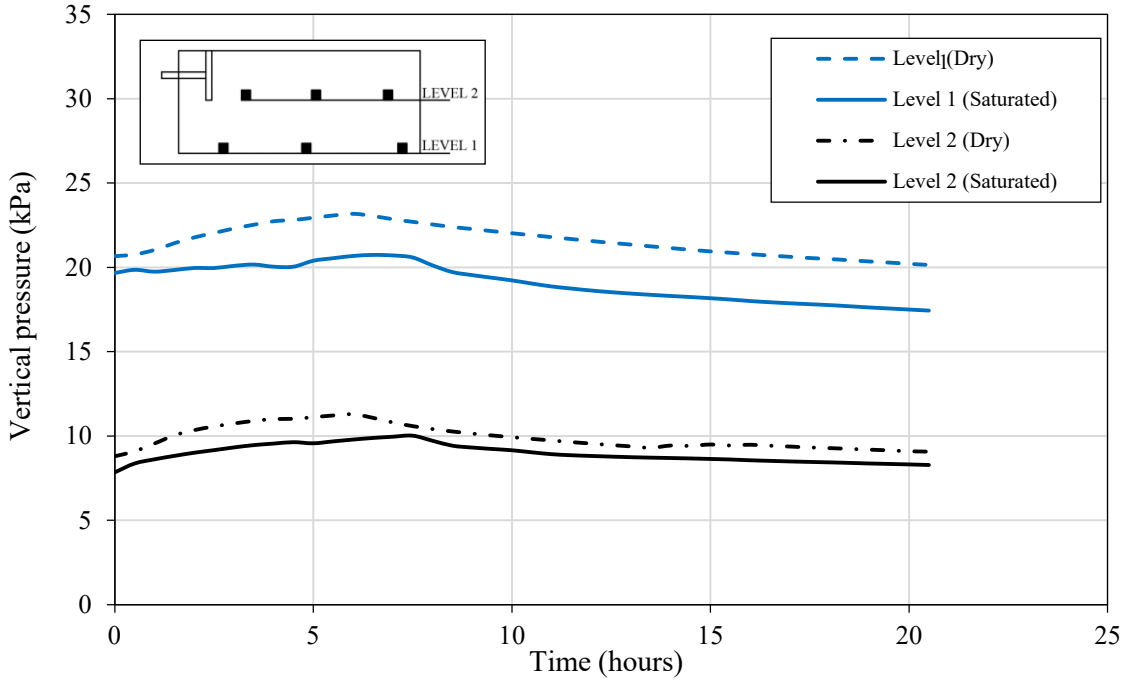

(b)

Fig. 4.1. Results from test no. 1 & 4 for soil – A (C_p=4.2%): (a) Horizontal pressure measured by wall transducers versus time; (b) Vertical pressure in the soil mass measured by transducers versus time

Test no. 2 & 5 were performed on the dry and saturated soils, respectively, with 10% kaoline clay content, having collapse potential C_p of 12.5%. The test results are presented diagrammatically in Figure 4.2. From the Fig. 4.2a, it can be seen that at-rest earth pressure measured on wall by transducers slightly changes with time for both dry and saturated soils. It can be seen from this figure that the at-rest earth pressure acting on the wall decreases considerably when the soil gets saturated. The at-rest earth pressure acting on the wall decreases with approximately 35% from dry soil to saturated soil. This decrease is strongly larger than that of the soil – C_p=4.2%. From the Fig. 4.2b, it can be seen that the vertical pressure in the soil mass slightly decreases with time for both dry and saturated soils. The vertical pressure in the soil mass undergoes a decrease when the soil is saturated.

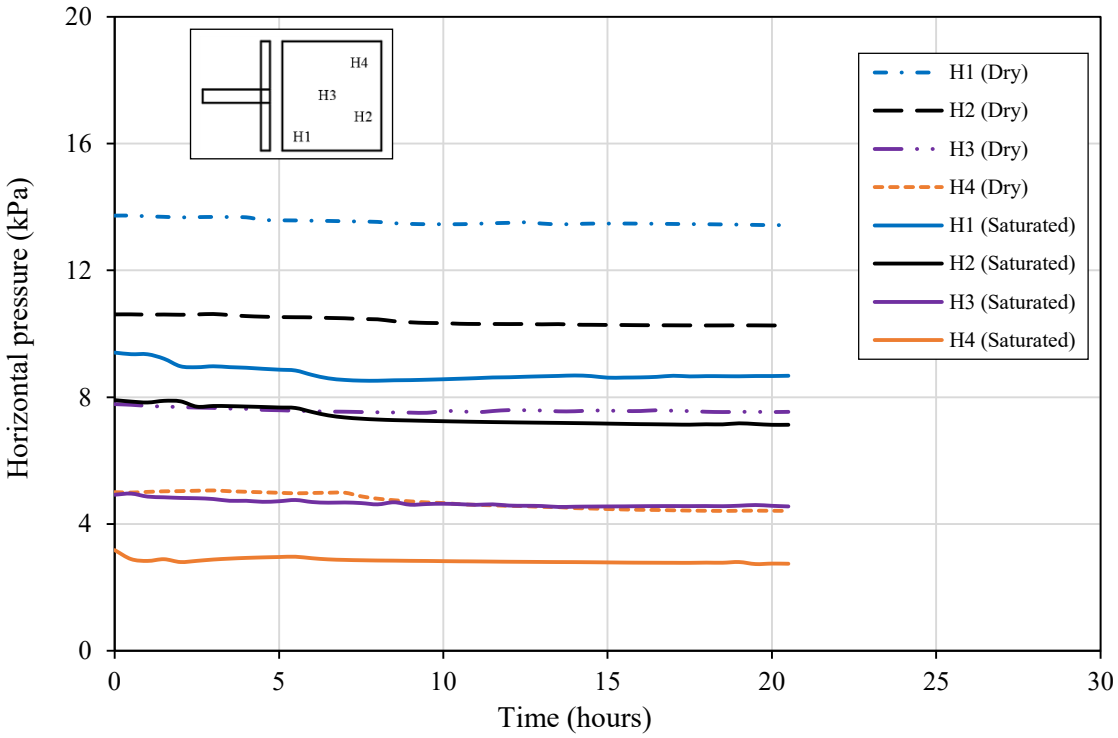

(a)

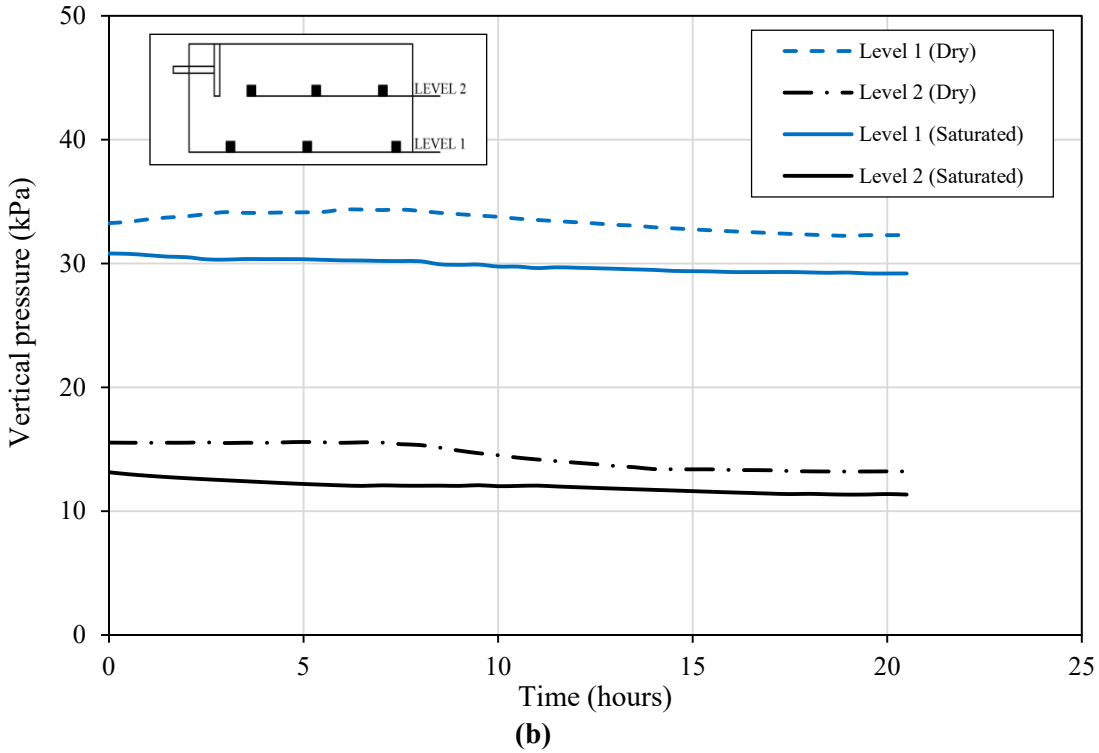

(b)

Fig. 4.2. Results from test no. 2 & 5 for soil – C (C_p=12.5%): (a) Horizontal pressure measured by wall transducers versus time; (b) Vertical pressure in the soil mass measured by transducers versus time

Test no. 3 & 6 were performed on the dry and saturated soils, respectively, with 14% kaoline clay content, having collapse potential of 18%. The test results are presented diagrammatically in Figure 4.3. From the Fig. 4.3a, it can be seen from this figure that the at-rest earth pressure acting on the wall decreases significantly when the soil behind the wall gets full inundated. The at-rest earth pressure acting on the wall decreases with roughly 80% from dry soil to saturated soil. From the Fig. 4.3b, it can be seen that the vertical pressure in the soil mass undergoes a significant decrease for the case of saturated soils. The vertical pressure in the soil mass decreases with about 80% from dry soil to saturated soil.

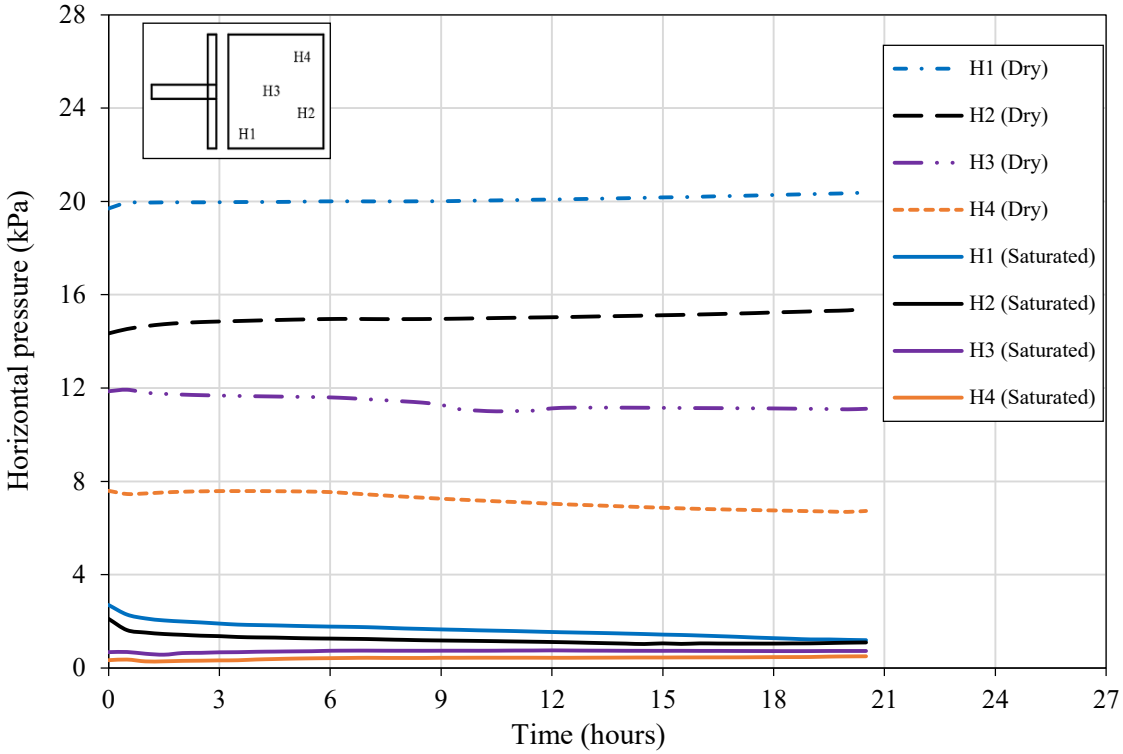

(a)

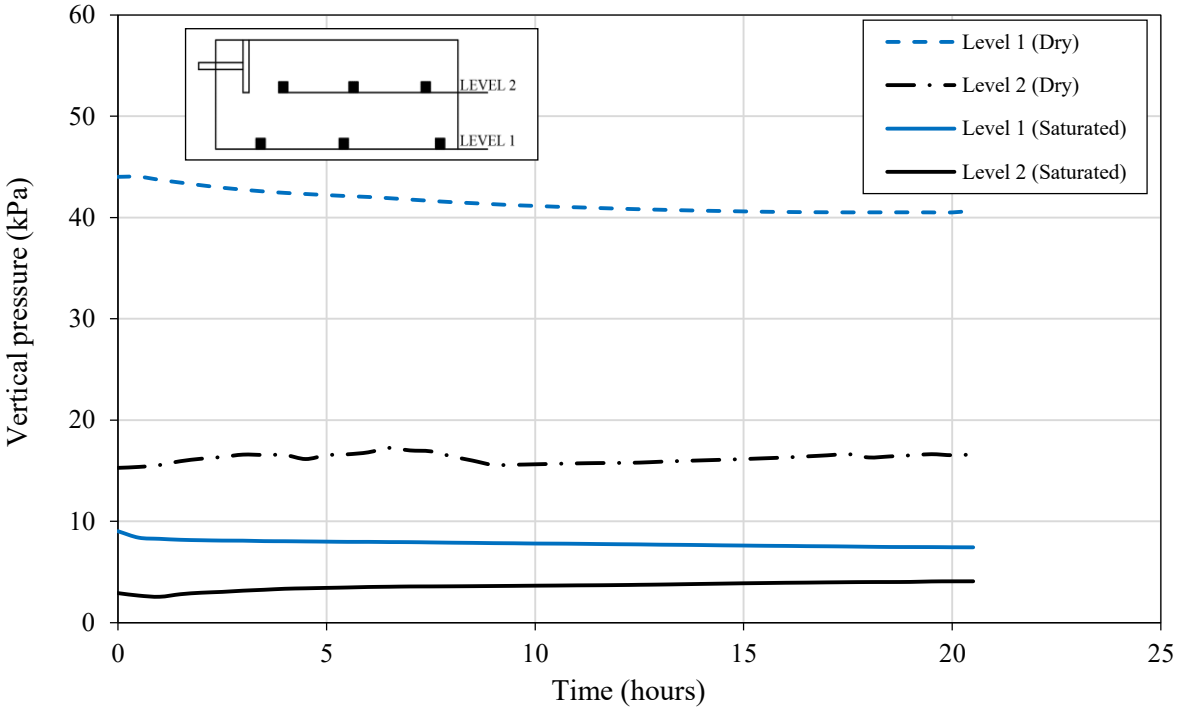

(b)

Fig. 4.3. Results from test no. 3 & 6 for soil – D (C_p=18%): (a) Horizontal pressure measured by wall transducers versus time; (b) Vertical pressure in the soil mass measured by transducers versus time

Test no. 7 & 10 were performed on the dry and saturated soils, respectively, with 6% kaoline clay content, having collapse potential C_p of 4.2%, applying surcharge Ps = 8 kPa. The test results are presented diagrammatically in Figure 4.4. It is obvious that the at-rest earth pressure increases considerably when increasing the stress level in the soil mass (OCR) by applying Ps. From the Fig. 4.4a, it can be seen that at-rest earth pressure acting on the wall varies from loading to unloading state. It should be noted that the at-rest earth pressure acting on the wall decreases slightly when the soil gets saturated. From the Fig. 4.4b, it can be seen that the vertical pressure in the soil mass slightly changes with time for both dry and saturated soils. The vertical pressure in the soil mass decreases when the soil is saturated.

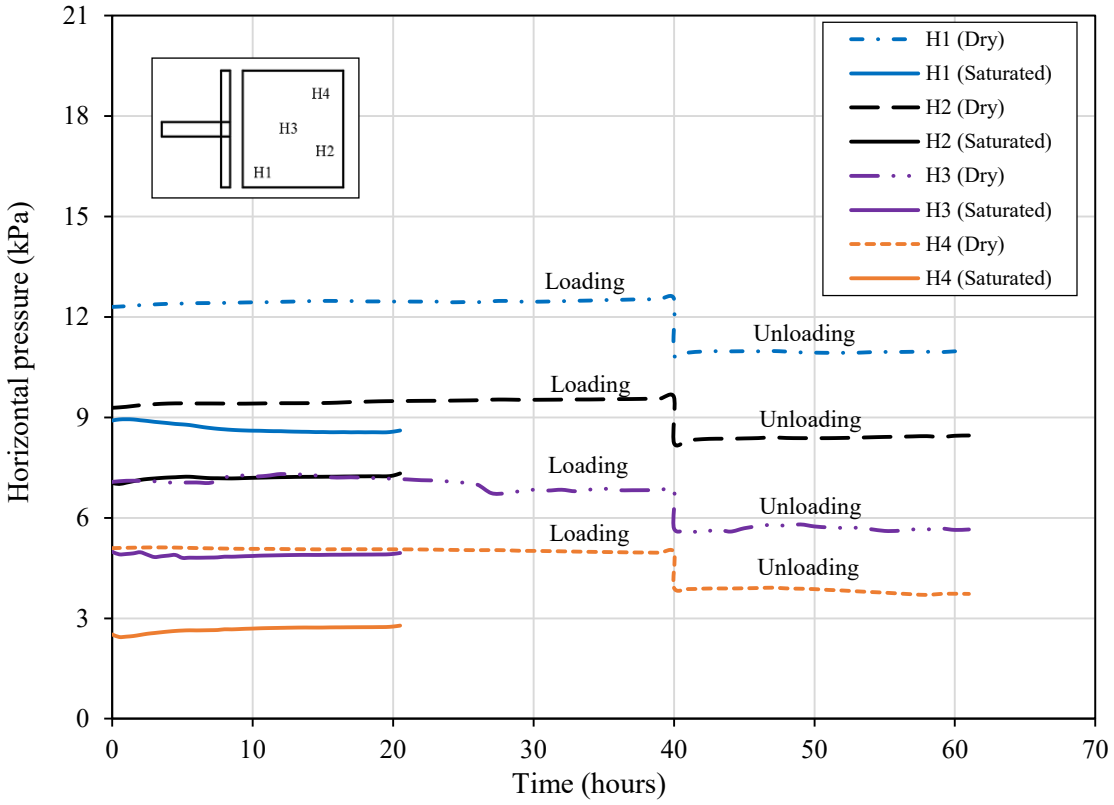

(a)

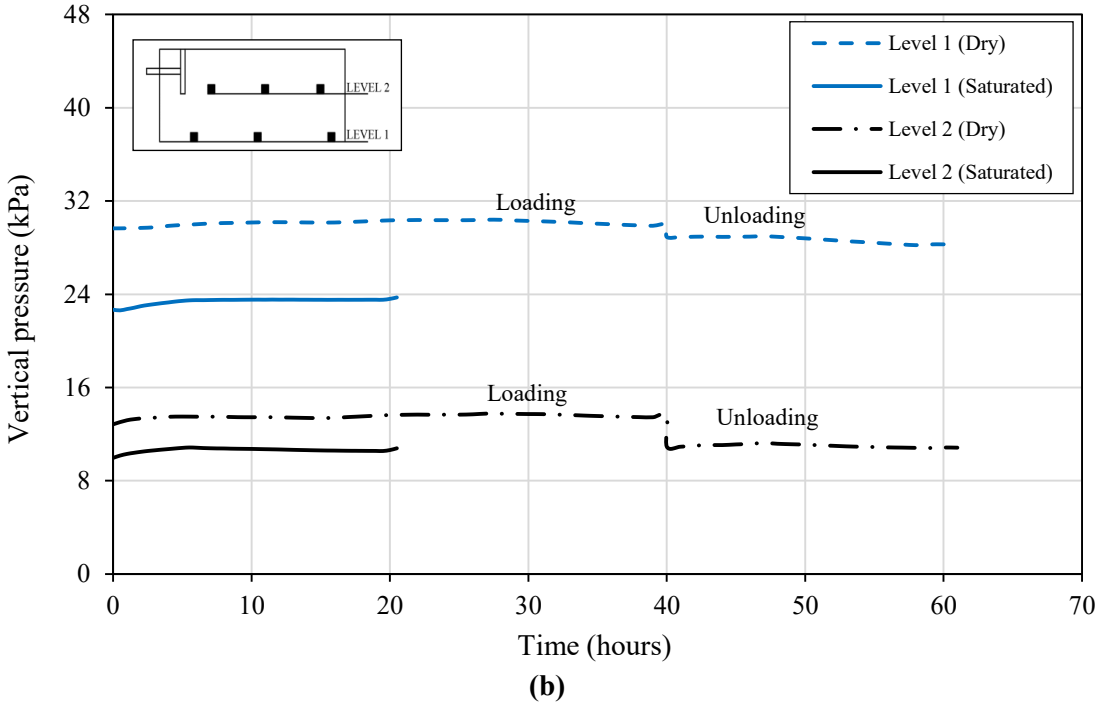

Fig. 4.4. Results from test no. 7 & 10 for soil – A (C_p=4.2%): (a) Horizontal pressure measured by wall transducers versus time; (b) Vertical pressure in the soil mass measured by transducers versus time

Test no. 8 & 11 were performed on the dry and saturated soils, respectively, with 10% kaoline clay content, having collapse potential C_p of 12.5%, applying surcharge Ps = 8 kPa. The test results are presented graphically in Figure 4.5. The at-rest earth pressure increases considerably when increasing the stress level in the soil mass (OCR) by applying Ps. From the Fig. 4.5a, it can be seen that at-rest earth pressure acting on the wall varies from loading to unloading condition. The difference of the values of at-rest earth pressure between loading and unloading also depends on the depth. It can be noted from this figure that the at-rest earth pressure acting on the wall decreases considerably when the soil behind the wall gets saturated. From the Fig. 4.5b, it can be seen that the vertical pressure in the soil mass slightly changes with time for both dry and saturated soils. The vertical pressure in the soil mass decreases slightly due to soil's saturation.

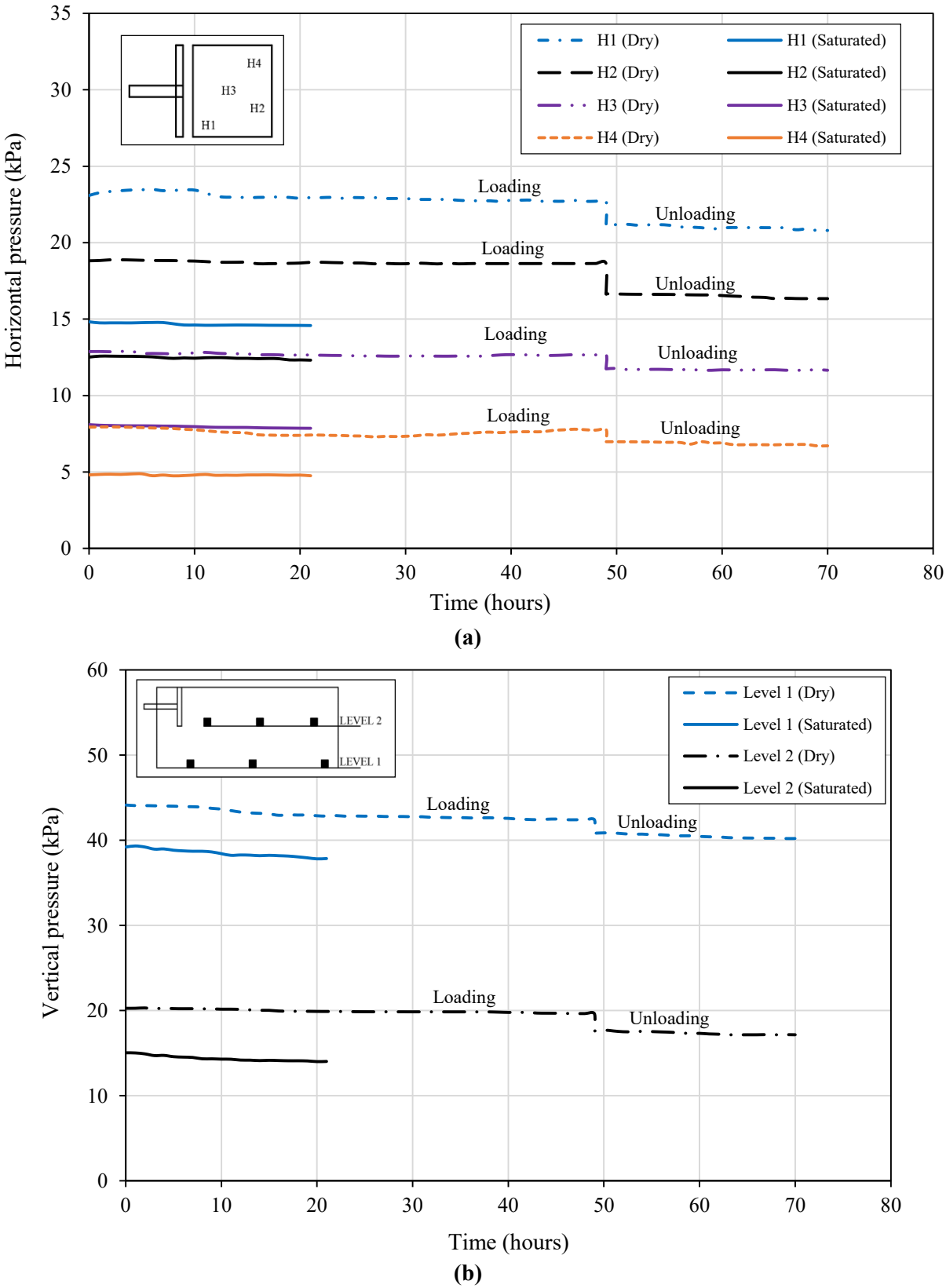

Fig. 4.5. Results from test no. 8 & 11 for soil – C (C_p=12.5%): (a) Horizontal pressure measured by wall transducers versus time; (b) Vertical pressure in the soil mass measured by transducers versus time

Test no. 9 & 12 were performed on the dry and saturated soils, respectively, with 14% kaoline clay content, having collapse potential C_p of 18%, applying surcharge Ps = 8 kPa. The test results is presented graphically in Figure 4.6. From the Fig. 4.6a, it can be seen that at-rest earth pressure acting on the wall varies from loading to unloading state. It is very clear from this figure that the at-rest earth pressure acting on the wall decreases significantly when the soil behind the wall gets full inundated. The at-rest earth pressure decreases approximately 90% due to the soil's saturation. From the Fig. 4.6b, it can be seen that the vertical pressure in the soil mass slightly changes with time for both dry and saturated soils. The vertical pressure in the soil mass decreases remarkably upon saturated.

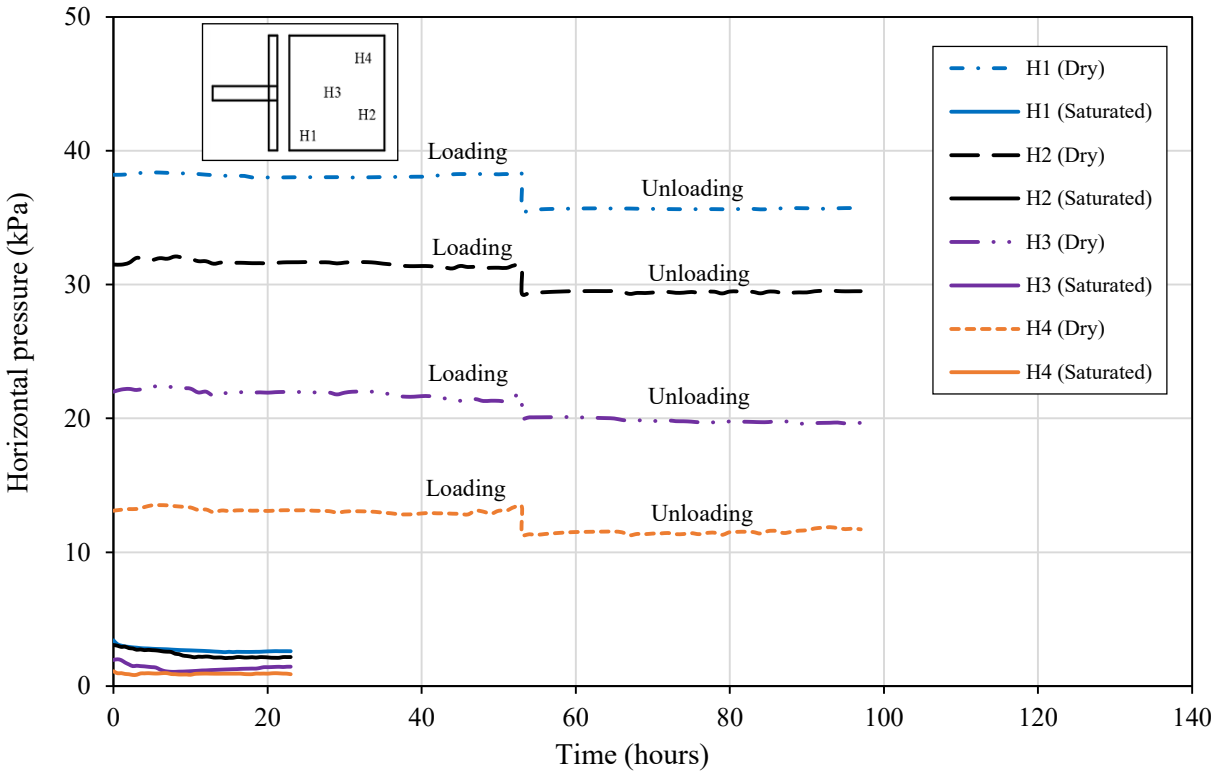

(a)

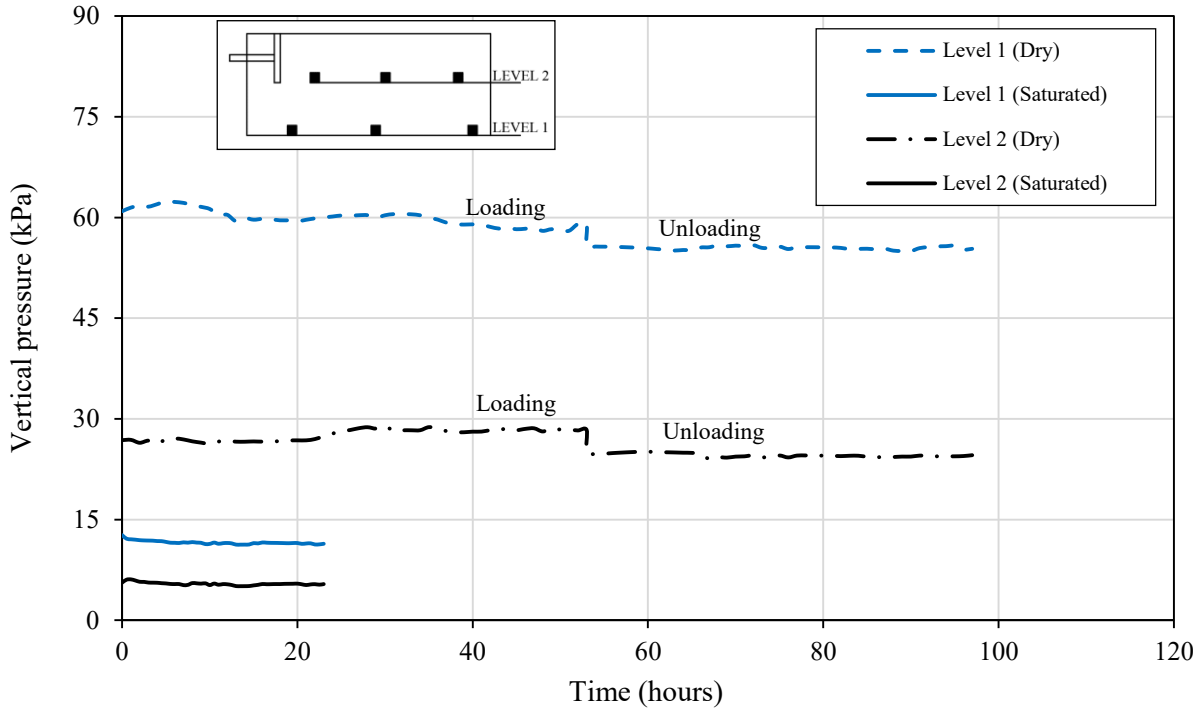

(b)

Fig. 4.6. Results from test no. 9 & 12 for soil – D (C_p=18%): (a) Horizontal pressure measured by wall transducers versus time; (b) Vertical pressure in the soil mass measured by transducers versus time

Test no. 13 & 16 were performed on the dry and saturated soils, respectively, with 6% kaoline clay content, having collapse potential C_p of 4.2%, applying surcharge Ps = 16 kPa. The test results are presented diagrammatically in Figure 4.7. It is obvious that the at-rest earth pressure increases considerably when increasing the stress level in the soil mass (OCR) by increasing value of Ps. From the Fig. 4.7a, it can be seen that at-rest earth pressure acting on the wall varies from loading to unloading state. It should be noted that the at-rest earth pressure acting on the wall decreases slightly when the soil is saturated. From the Fig. 4.7b, it can be seen that the vertical pressure in the soil mass slightly changes with time for both dry and saturated soils. The vertical pressure in the soil mass decreases when the soil gets saturated.

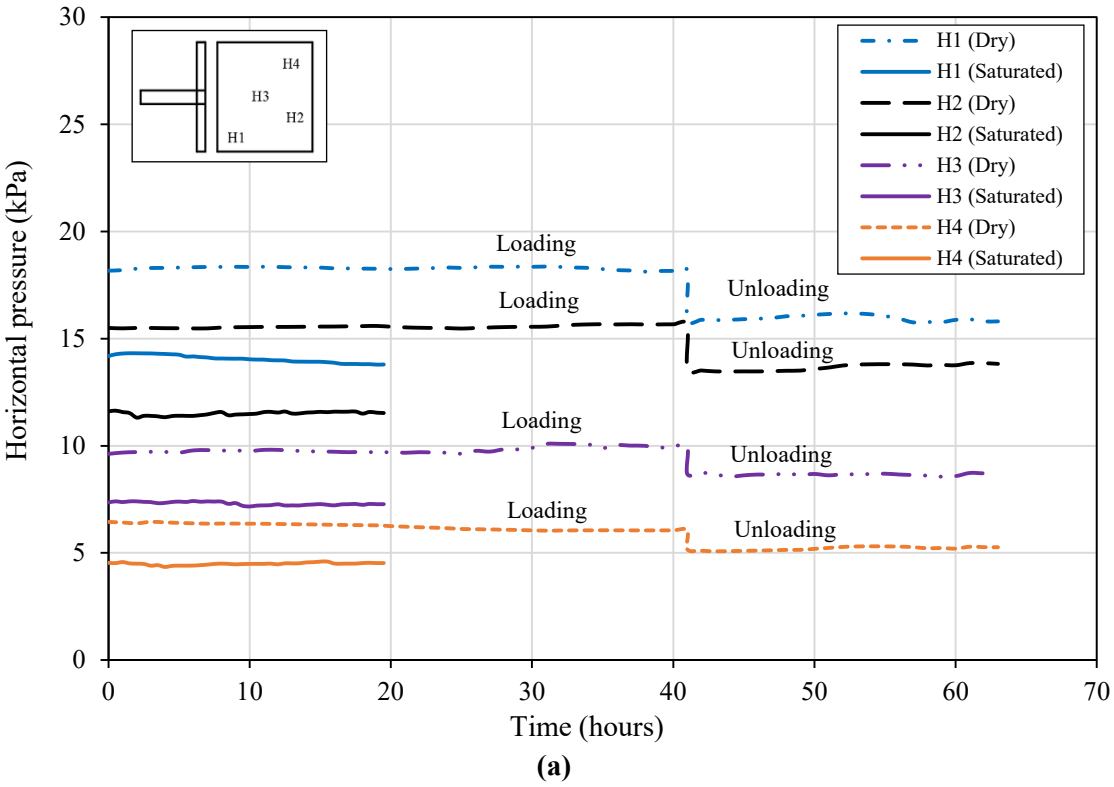

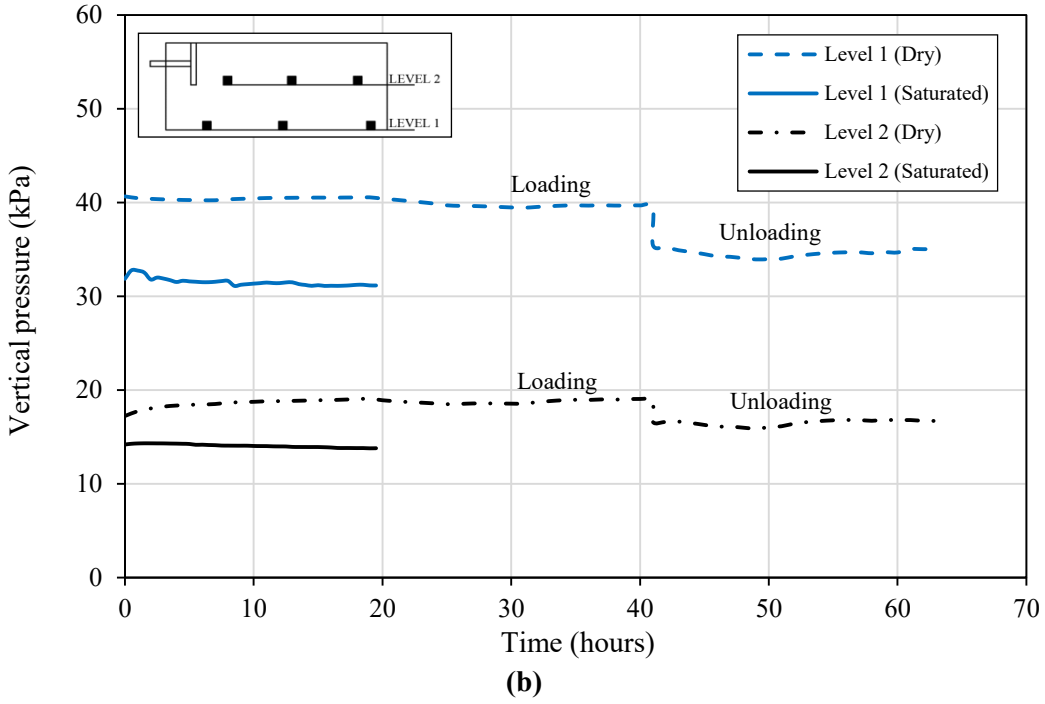

Fig. 4.7. Results from test no. 13 & 16 for soil – A (C_p=4.2%): (a) Horizontal pressure measured by wall transducers versus time; (b) Vertical pressure in the soil mass measured by transducers versus time

Test no. 14 & 17 were performed on the dry and saturated soils, respectively, with 10% kaoline clay content, having collapse potential C_p of 12.5%, applying Ps = 16 kPa. The test results are presented diagrammatically in Figure 4.8. It is obvious that the at-rest earth pressure increases considerably when increasing OCR by increasing Ps. From the Fig. 4.8a, it can be seen that at-rest earth pressure acting on the wall varies from loading to unloading state. It should be noted that the at-rest earth pressure acting on the wall decreases considerably due to the soil's saturation. It is of interest to note from the Fig.4.8a that the at-rest earth pressure decreases approximately 32% due to the soil's saturation. From the Fig. 4.8b, it can be seen that the vertical pressure on the soil mass slightly changes with time for both dry and saturated soils. The vertical pressure in the soil mass decreases due to the saturation of the soil.

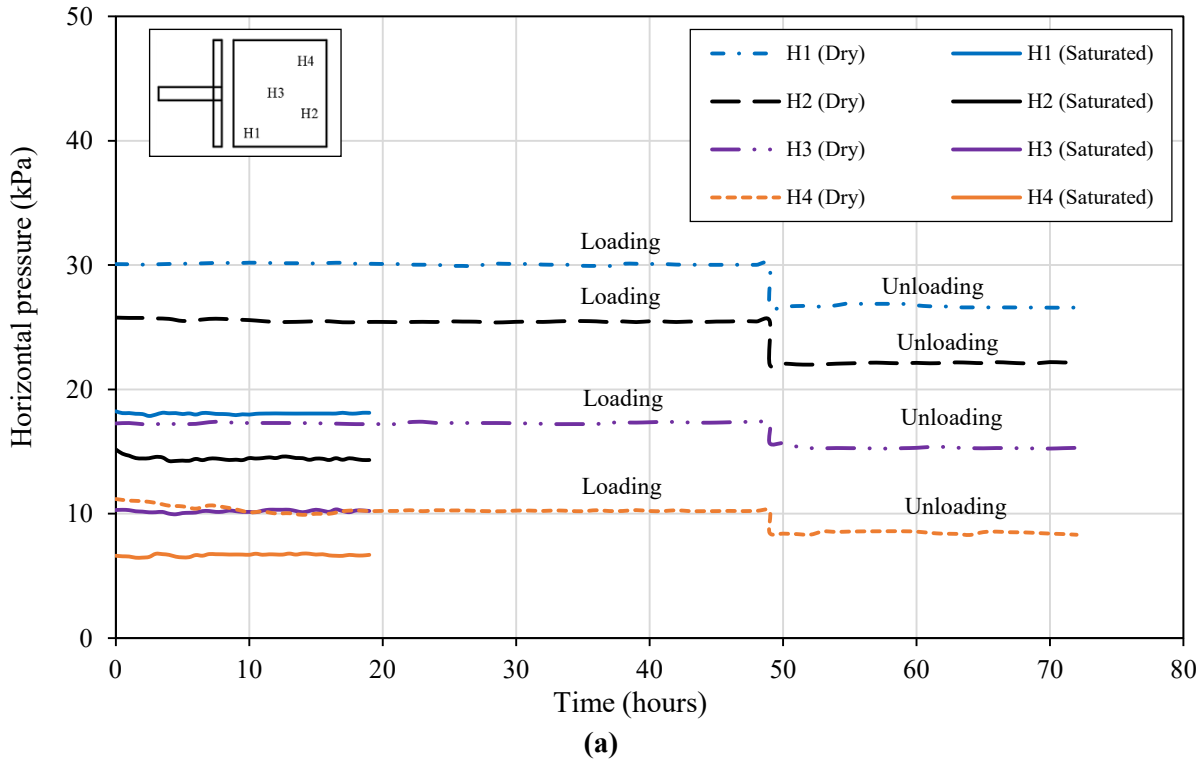

(a)

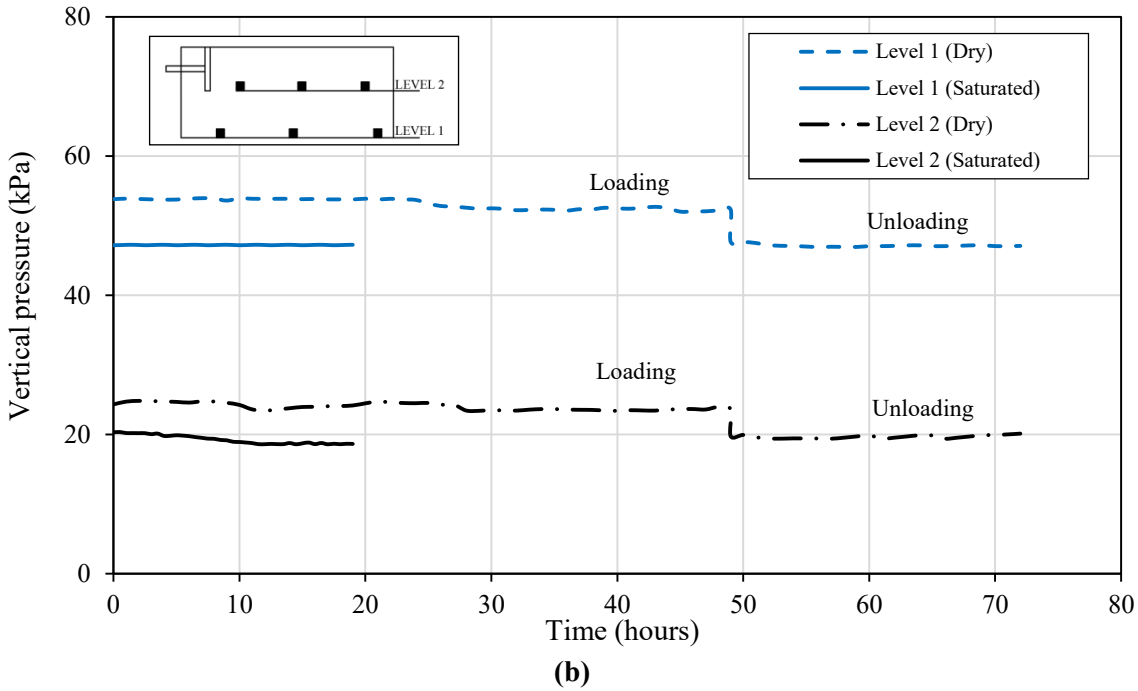

Fig. 4.8. Results from test no. 14 & 17 for soil – C (C_p=12.5%): (a) Horizontal pressure measured by wall transducers versus time; (b) Vertical pressure in the soil mass measured by transducers versus time

Test no. 15 & 18 were performed on the dry and saturated soils, respectively, with 14% kaoline clay content, having collapse potential C_p of 18%, applying Ps = 16 kPa. The test results are presented diagrammatically in Figure 4.9. Firstly, it is noted that the at-rest earth pressure increases considerably when increasing OCR by increasing Ps. From the Fig. 4.9a, it can be seen that at-rest earth pressure acting on the wall changes from loading to unloading conditions. It should be noted that the at-rest earth pressure acting on the wall decreases significantly due to the soil's full inundation. The at-rest earth pressure decreases approximately 90% from dry condition to saturated condition. From the Fig. 4.9b, it can be seen that the vertical pressure in the soil mass decreases outstandingly due to the saturation of the soil. The vertical pressure in the soil mass decreases around 75% due to the soil's saturation.

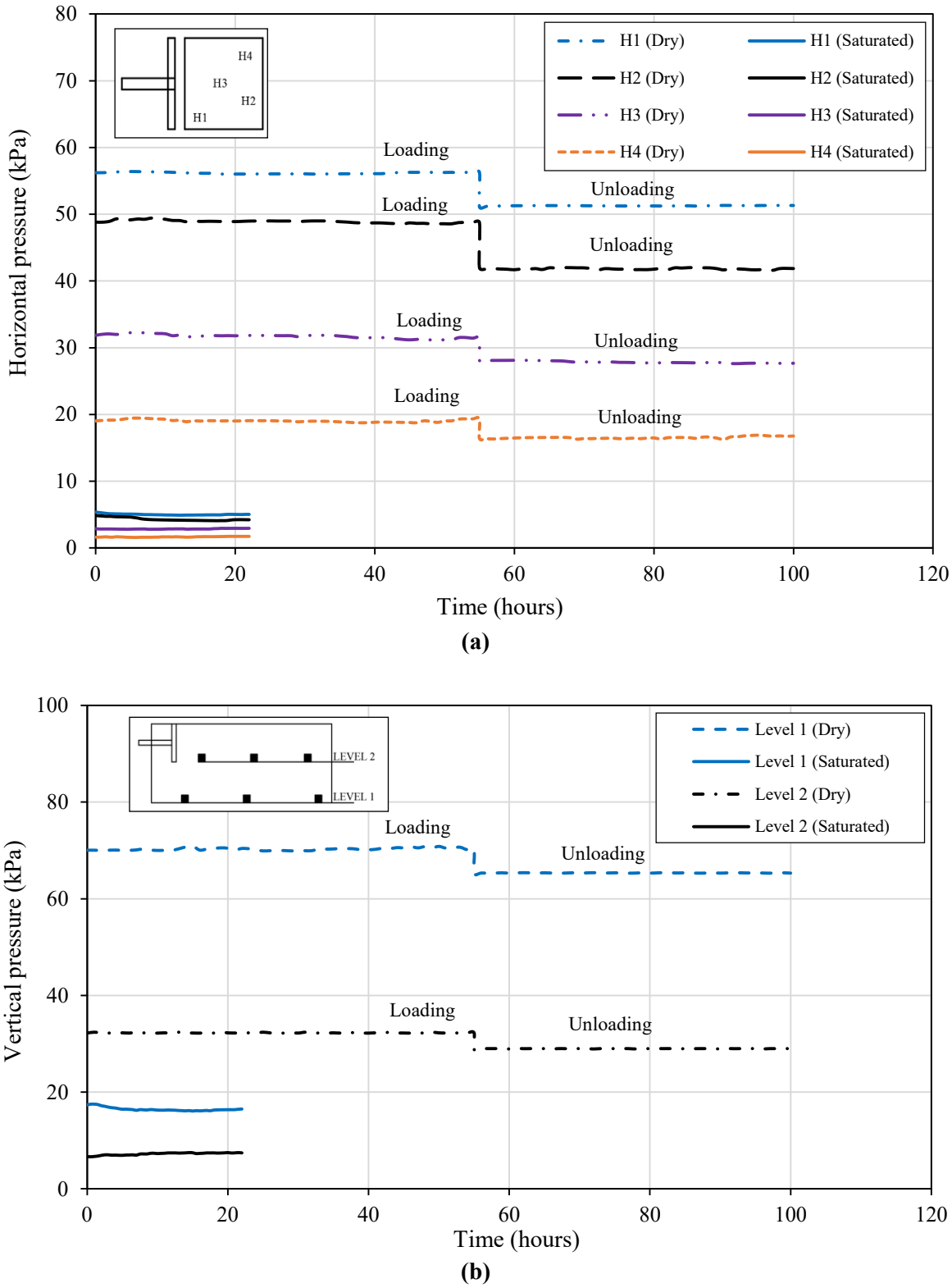

Fig. 4.9. Results from test no. 15 & 18 for soil – D (C_p=18%): (a) Horizontal pressure measured by wall transducers versus time; (b) Vertical pressure in the soil mass measured by transducers versus time

Test no. 19 & 22 were performed on the dry and saturated soils, respectively, with 8% kaoline clay content, having collapse potential C_p of 9.0%. The test results are presented diagrammatically in Figure 4.10. From the Fig. 4.10a, it can be seen that at-rest earth pressure measured on wall by transducers slightly changes with time for both dry and saturated soils. It can be seen from this figure that the at-rest earth pressure on the wall decreases moderately when the soil gets saturated. From the Fig. 4.10b, it can be seen that the vertical pressure in the soil mass slightly decreases with time for both dry and saturated soils. The vertical pressure in the soil mass experiences a decrease when the soil gets saturated.

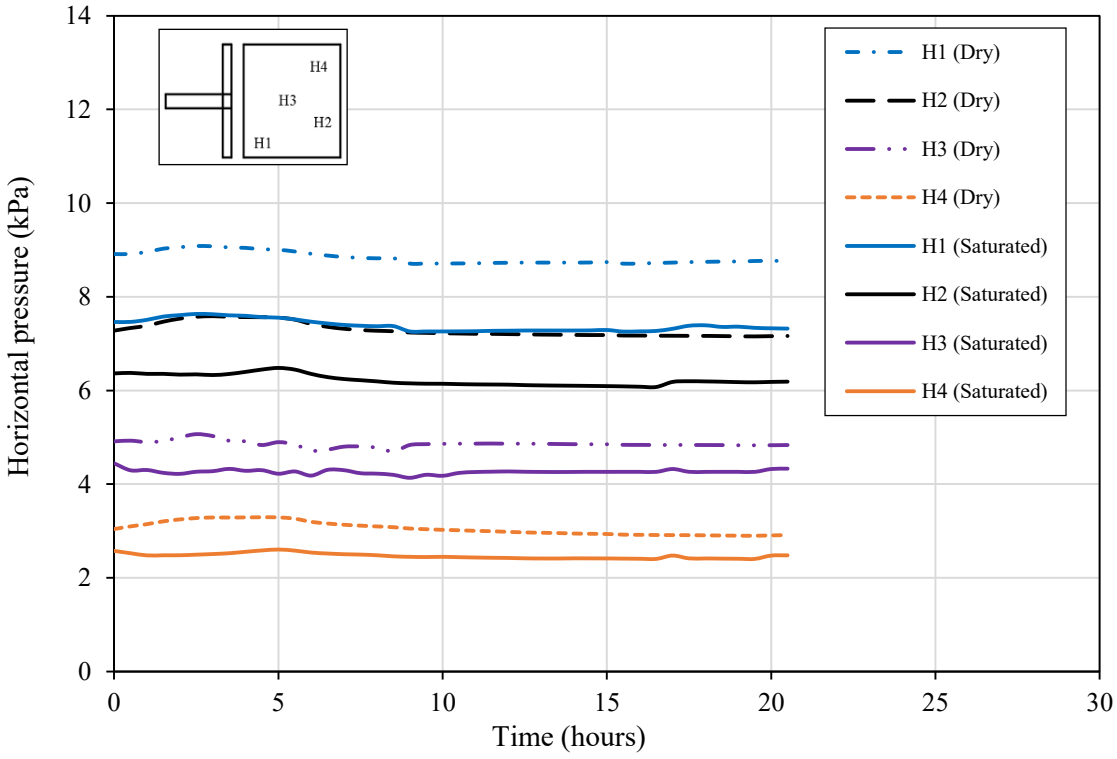

(a)

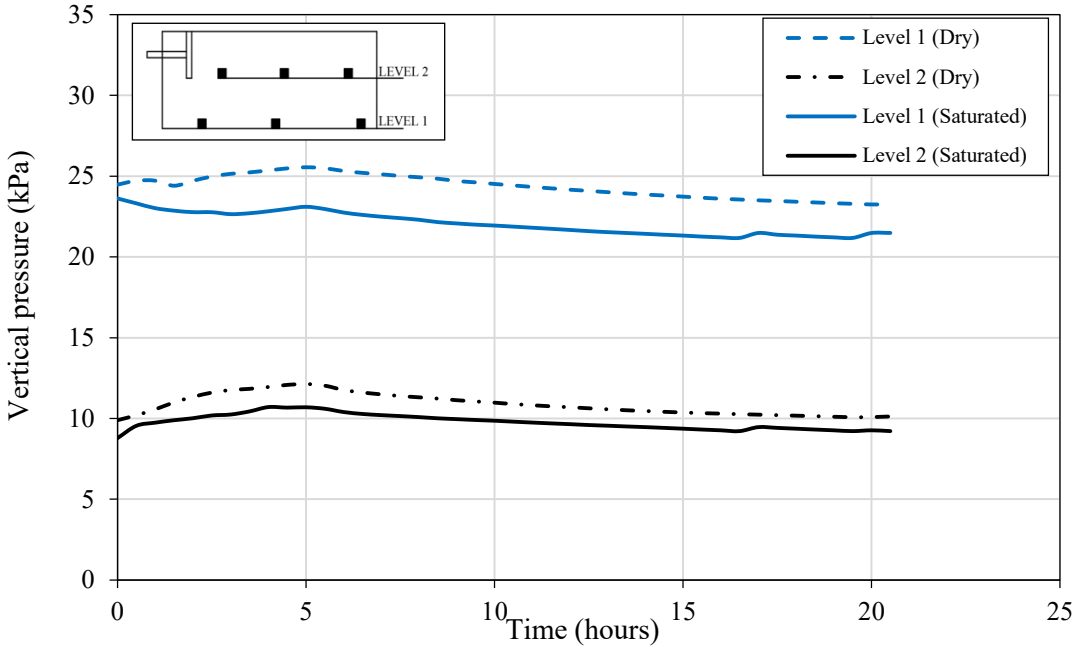

(b)

Fig. 4.10. Results from test no. 19 & 22 for soil – B (C_p=9.0%): (a) Horizontal pressure measured by wall transducers versus time; (b) Vertical pressure in the soil mass measured by transducers versus time

Test no. 20 &23 were performed on the dry and saturated soils, respectively, with 8% kaoline clay content, having collapse potential of 9.0%, applying Ps = 8 kPa. The test results are presented graphically in Figure 4.11. It is clear that the at-rest earth pressure increases considerably when increasing the stress level in the soil mass (OCR) by applying Ps. From the Fig. 4.11a, it can be seen that at-rest earth pressure acting on the wall varies from loading to unloading state. It can be noted from this figure that the at-rest earth pressure acting on the wall decreases moderately due to saturation of the soils. From the Fig. 4.11b, it can be seen that the vertical pressure in the soil mass slightly changes with time for both dry and saturated soils. The vertical pressure in the soil mass decreases due to soil's saturation.

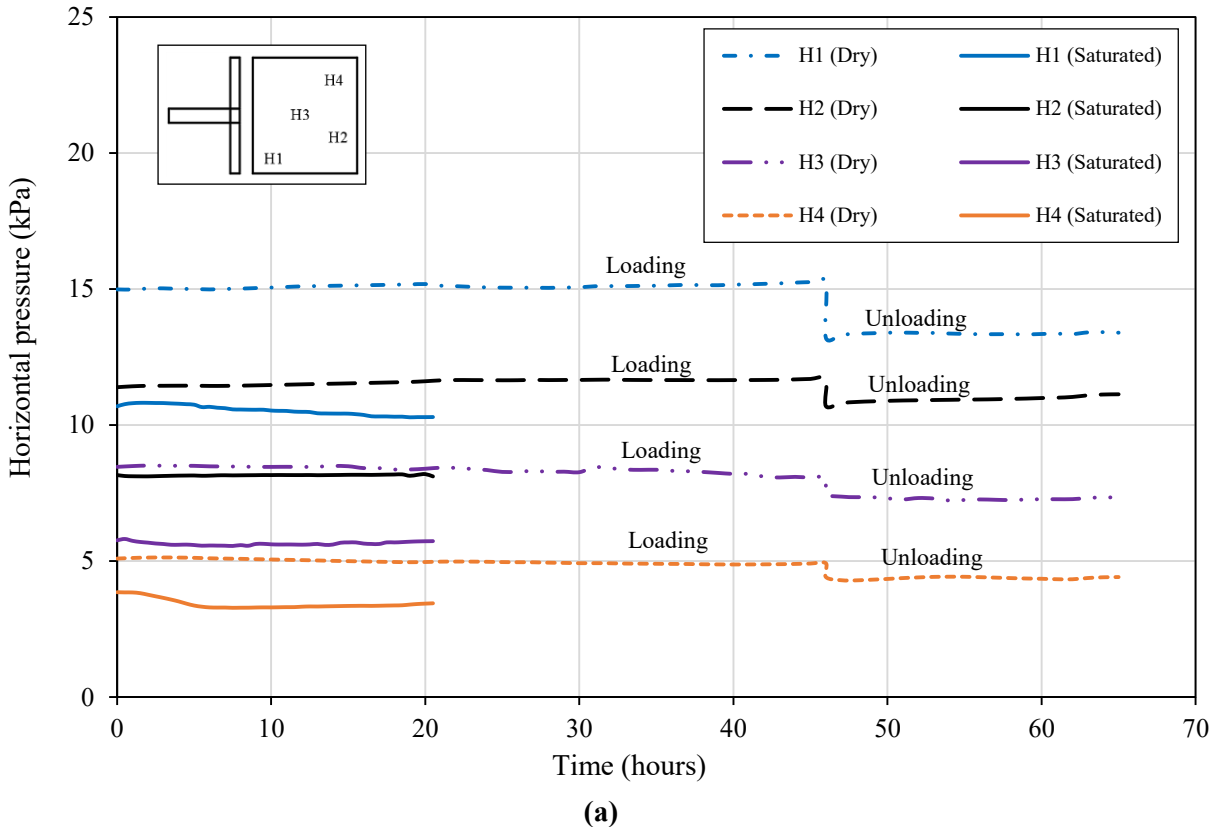

(a)

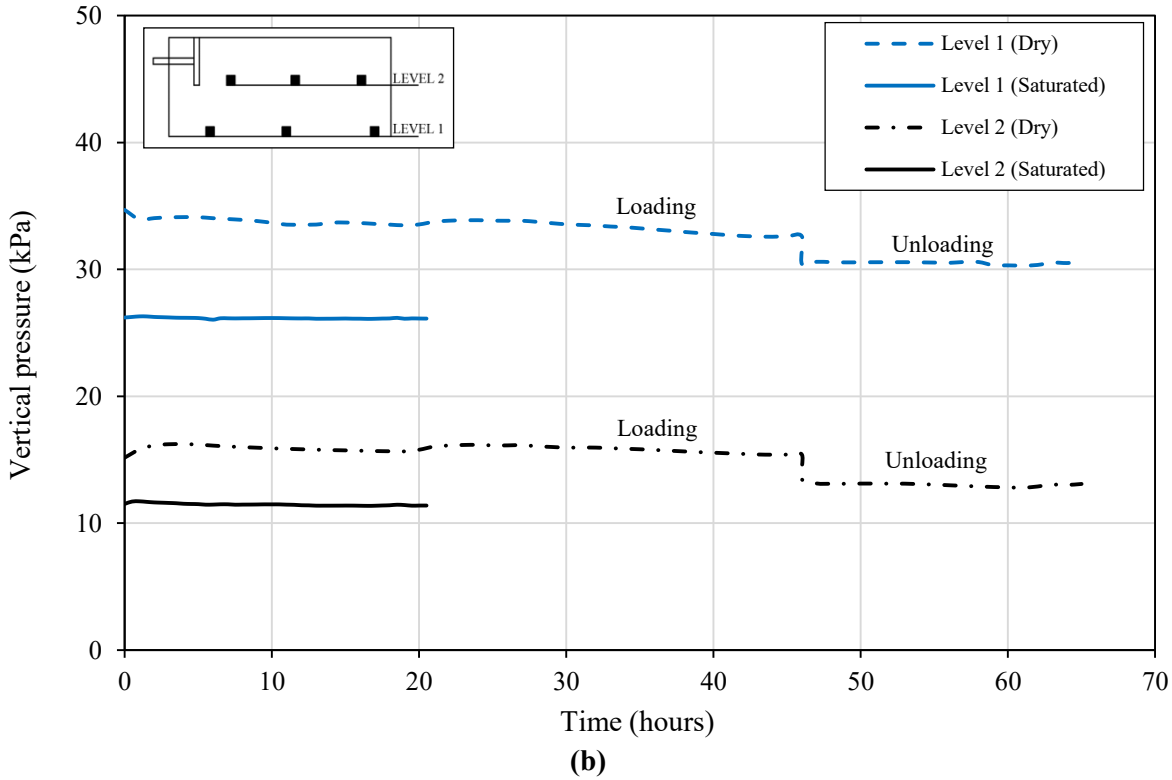

(b)

Fig. 4.11. Results from test no. 20 & 23 for soil – B (C_p=9.0%): (a) Horizontal pressure measured by wall transducers versus time; (b) Vertical pressure in the soil mass measured by transducers versus time

Test no. 21 & 24 were performed on the dry and saturated soils, respectively, with 8% kaoline clay content, having collapse potential C_p of 9.0%, applying Ps = 16 kPa. The test results are presented diagrammatically in Figure 4.12. It is obvious that the at-rest earth pressure increases considerably when increasing OCR by increasing Ps. From the Fig. 4.12a, it can be seen that at-rest earth pressure acting on the wall varies from loading to unloading state. It should be noted from this figure that the at-rest earth pressure acting on the wall decreases moderately due to the soil's full inundation. From the Fig. 4.12b, it can be seen that the vertical pressure on the soil mass slightly varies with time for both dry and saturated soils. The vertical pressure in the soil mass decreases upon saturated.

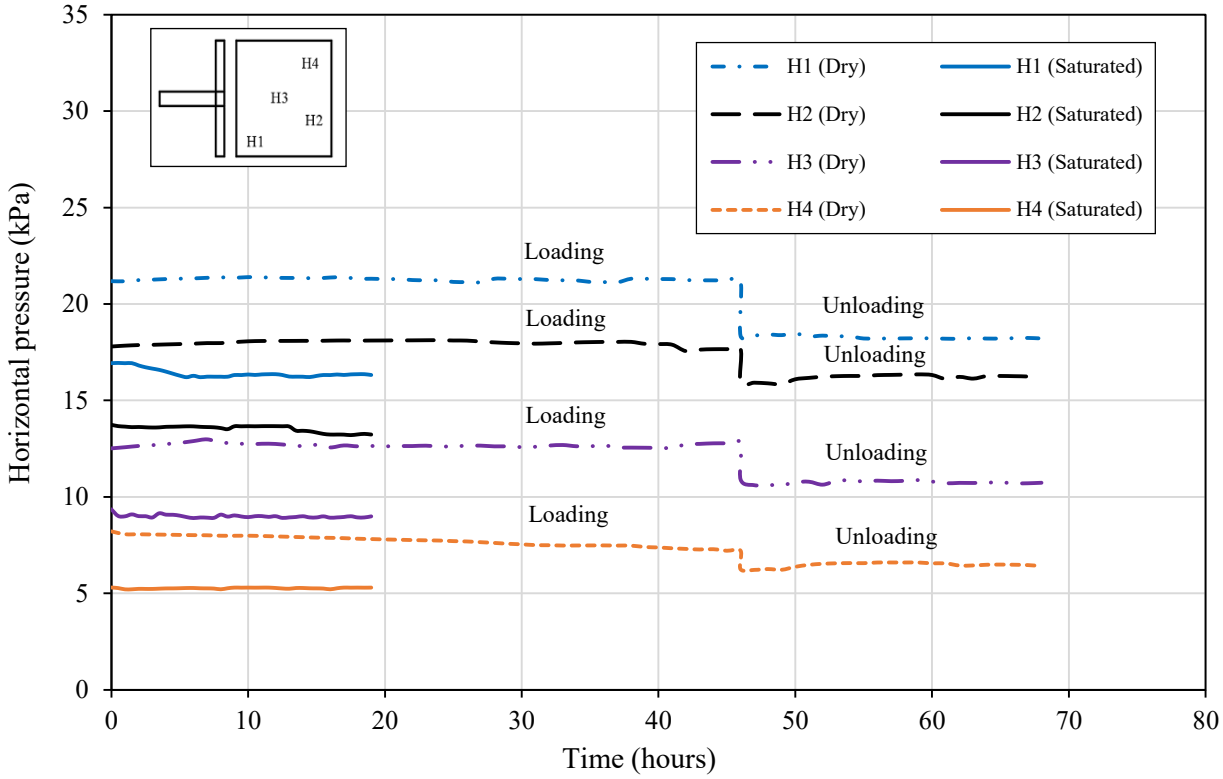

(a)

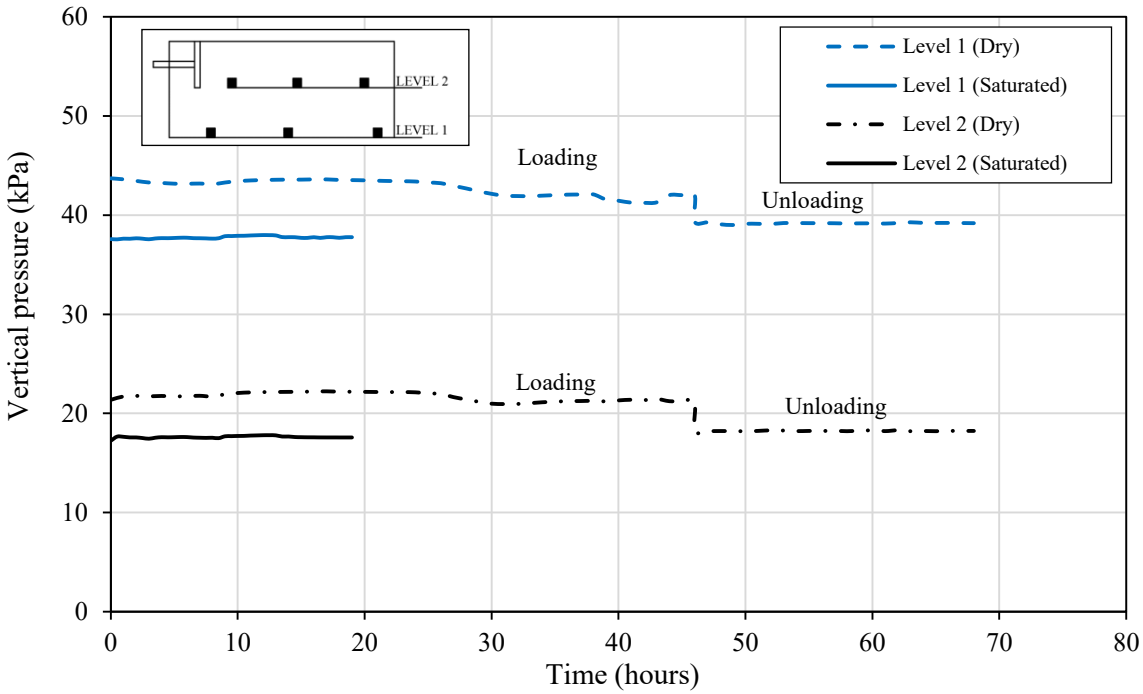

(b)

Fig. 4.12. Results from test no. 21 & 24 for soil – B (C_p=9.0%): (a) Horizontal pressure measured by wall transducers versus time; (b) Vertical pressure in the soil mass measured by transducers versus time

Results from repeatability tests (for studying the repeatability test results): These results are presented graphically in Figures 4.13 to 4.14.

It is essential to check the repeatability of the test results by conducting some tests under the same conditions to check the variation in the results between these tests.

The first set of repeated tests were performed on the dry soil. The second set of the repeated tests were conducted on the saturated soil. The results of two tests (original and repeated) performed under the same conditions with the same soil were compared together. Figure 4.13 and 4.14 presents the original and repeated at-rest earth pressure test results for the dry and saturated soil D (C_p=18%), respectively. It can be generally seen from these figures that the results obtained from two tests performed on the same soil under the same conditions are almost identical.

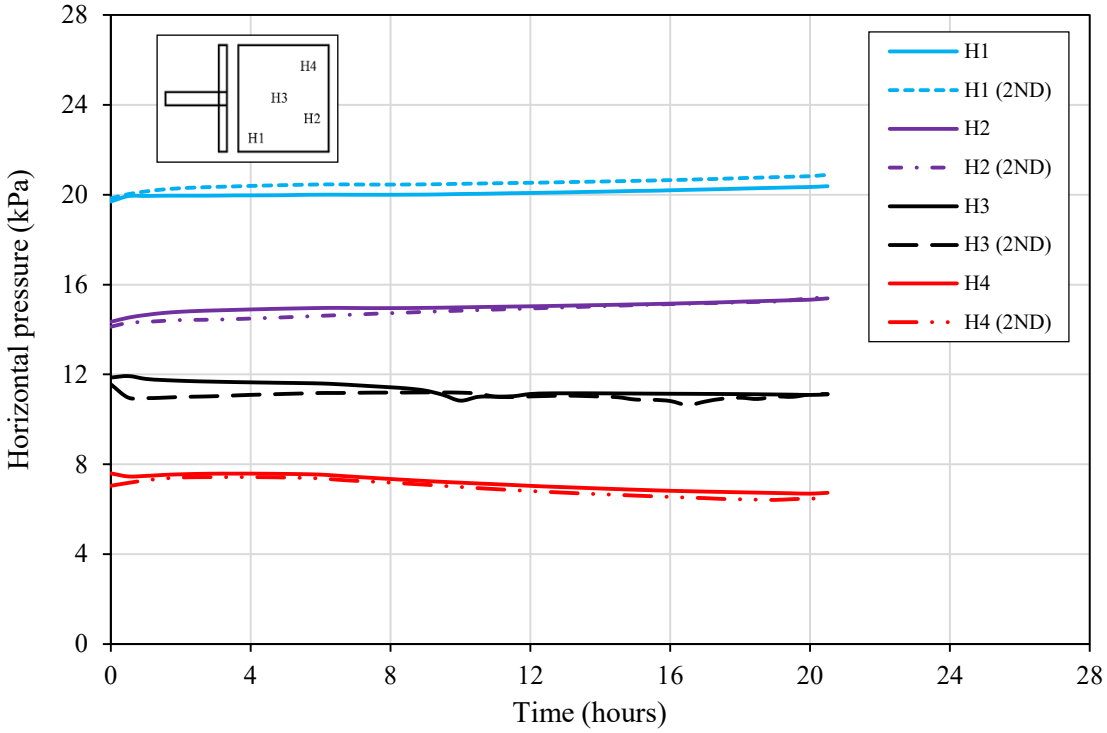

(a)

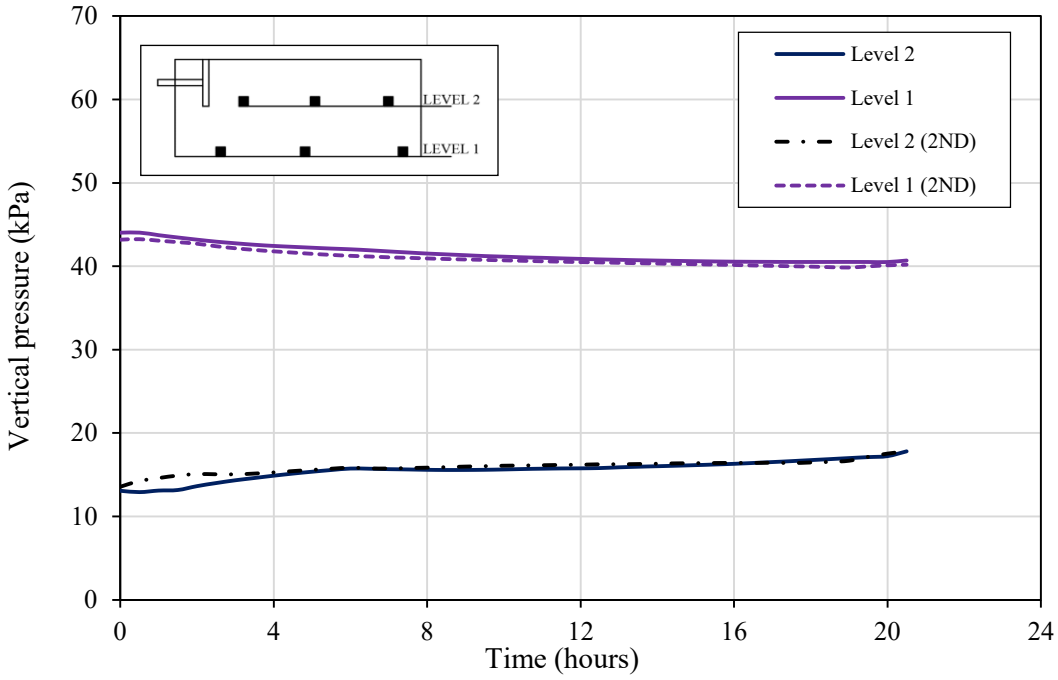

(b)

Fig. 4.13. Results from test no. 3 and test no. 3* (2^{ND}) performed on dry soil - D (C_p =18%: (a) Horizontal pressure measured by wall transducers versus time; (b) Vertical pressure in the soil mass measured by transducers versus time

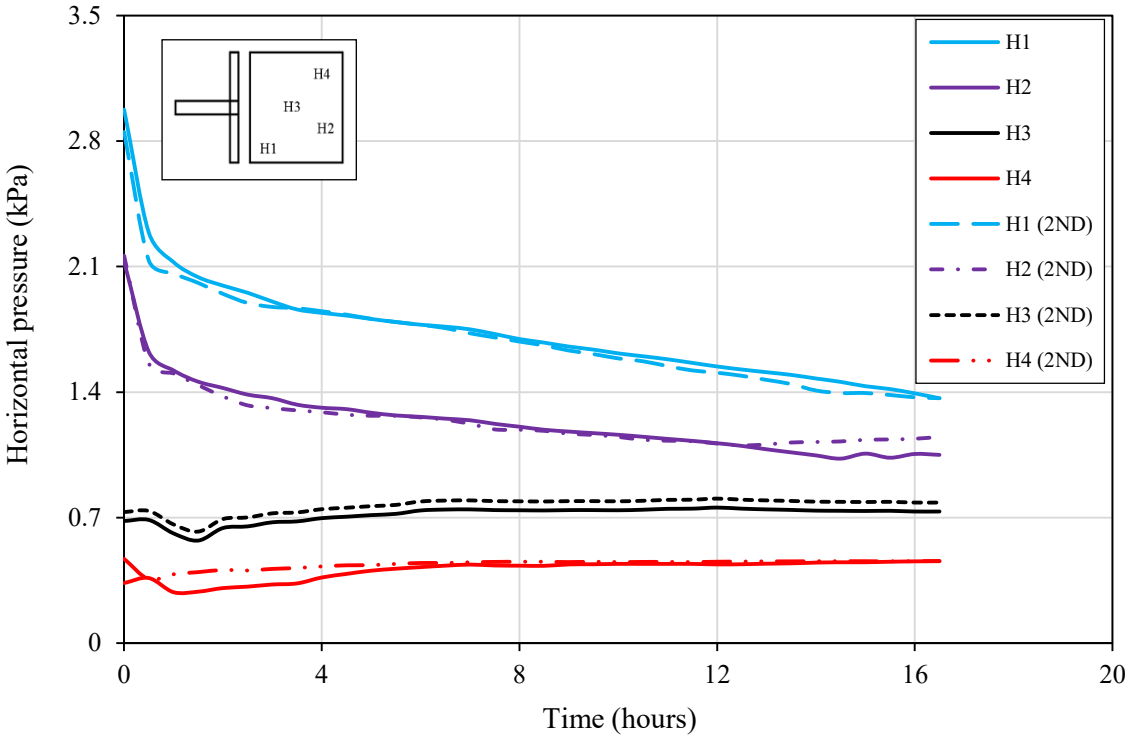

(a)

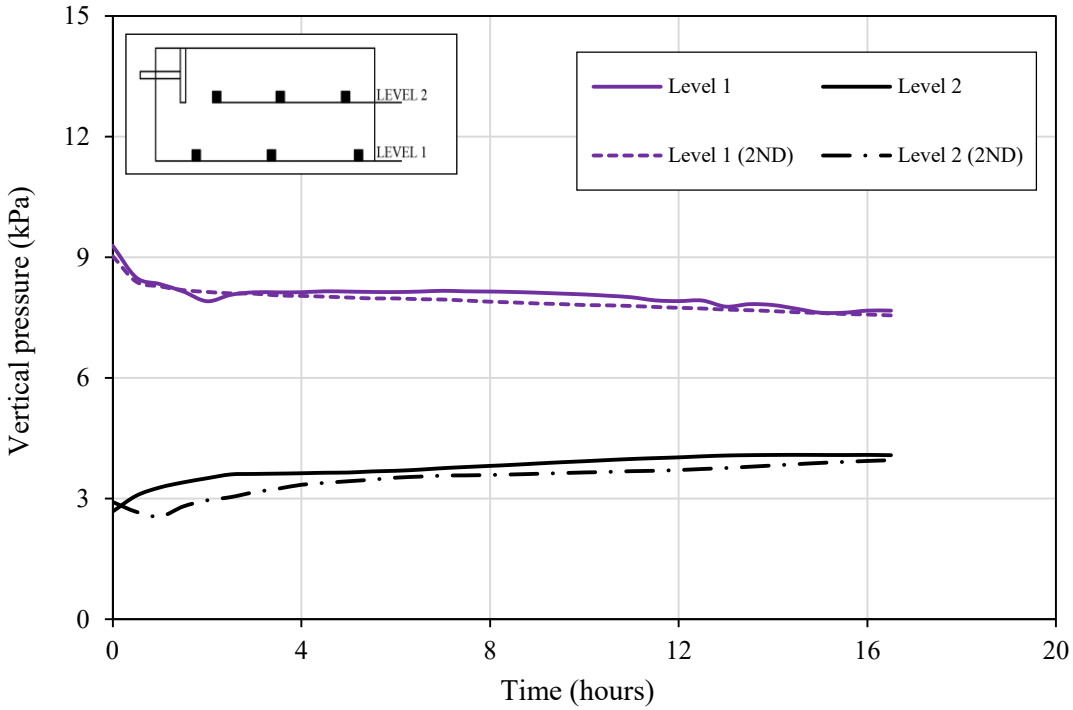

(b)

Fig. 4.14. Results from test no.6 and test no. 6* (2^{ND}) performed on the saturated soil - D (C_p=18%): (a) Horizontal pressure measured by wall transducers versus time; (b) Vertical pressure in the soil mass measured by transducers versus time

Collapse settlement due to inundation

In this experimental investigation, the correlation of the collapse settlement due to inundation and time during inundation process is examined and presented graphically in Figure 4.15. It can be noted that the collapse settlement increases during the inundation process and reaches maximum when reaching 100% saturation.

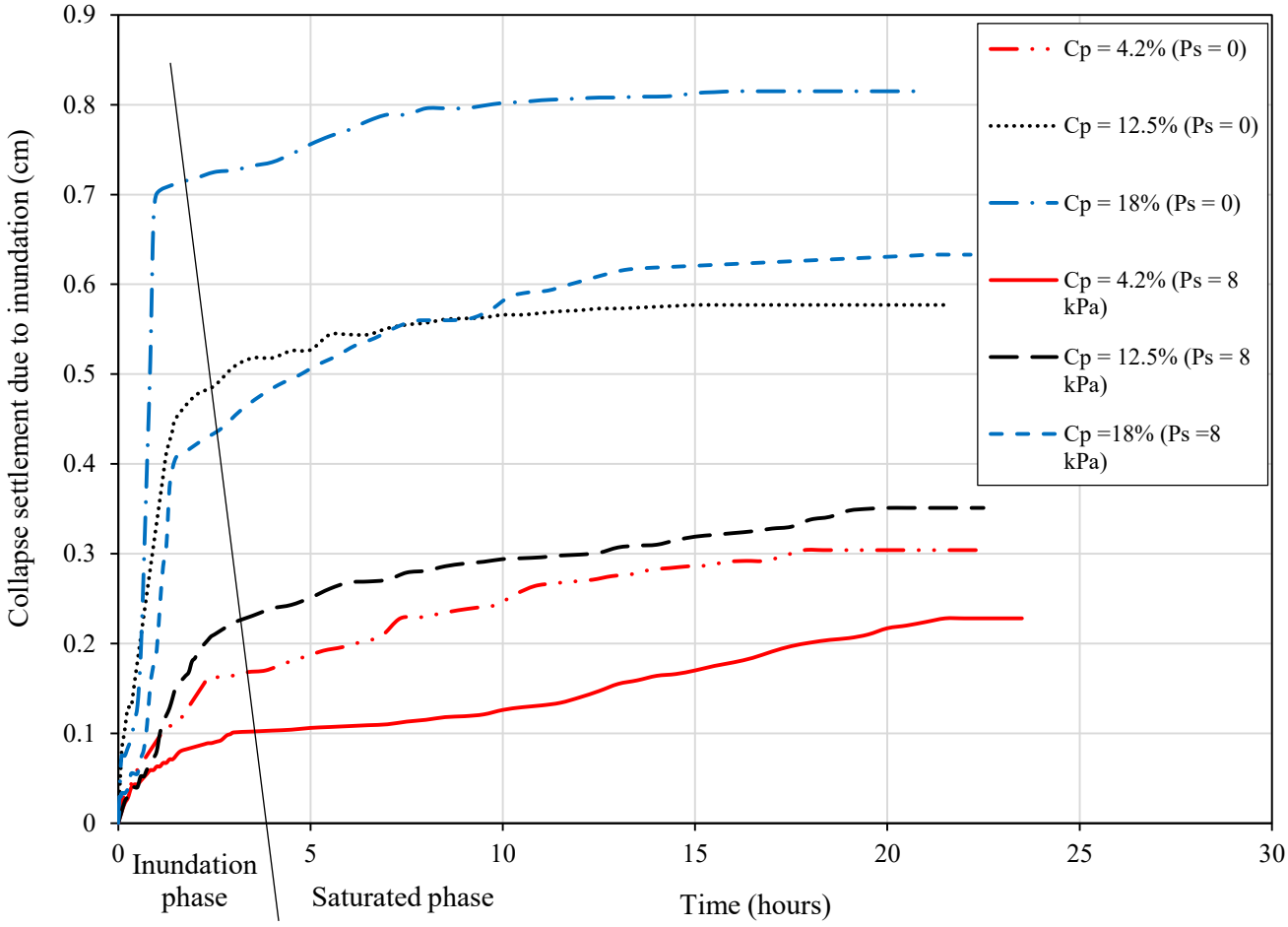

Fig. 4.15. Test result: collapse settlement due to inundation versus time

Furthermore, the collapse settlement increases rapidly up to a degree of saturation of about 80% then increases gradually until it reaches 100% saturation. It should be reported herein that for a given value of the OCR, the collapse settlement increases with the increase of the collapse potential C_p. It is of interest to note that collapse settlement takes place in relatively short period

for higher values of the C_p, while it takes longer period for higher OCR. It is of interest to report herein that the collapse settlement does not end at 100% satuartion but rather continues at a lower rate after, up to 20-40% of the collapse settlement at 100% saturation.

4.3. Developing empirical formulae

In this investigation, the overconsolidation ratio OCR values for the case of dry and saturated collapsible soils were determined from Equations (4.1) and (4.2), respectively:

$$OCR_{(dry)} = \frac{\sigma'_v}{\gamma' h} \tag{4.1}$$

$$OCR_{(saturated)} = \frac{\sigma_v - u_w}{\gamma' h} \tag{4.2}$$

The coefficients of at-rest earth pressure K_0 for the dry and saturated soil conditions were determined as follows:

$$K_{0(dry)} = \frac{\sigma'_h}{\sigma'_v} \tag{4.3}$$

$$K_{0(saturated)} = \frac{\sigma'_h}{\sigma'_v} = \frac{\sigma_h - u_w}{\sigma_v - u_w} \tag{4.4}$$

Where

σ_v= total vertical pressure at a given level measured by the transducer;

σ_h= total horizontal pressure measured on the wall by the respective transducer;

$\sigma'_v = \sigma_v - u_w$= effective vertical pressure at a given level;

$\sigma'_h = \sigma_h - u_w$ = effective horizontal pressure at a given level;

$u_w = \gamma_w h$ = pore water pressure;

$\gamma' h$ = theoretical effective overburden pressure at that level.

It should be reported herein that for dry soils, the OCR increases gradually due to the increase of the clay content (C_p) in the soil. The OCR also increases when increasing the surcharge loading on the soil mass. It can be also seen from Table 4.1 that the OCR decreases considerably due to the saturation of the soil. Upon saturated, the soil with greater C_p experiences larger decrease in the OCR.

Table 4.1. Summary of all test results for at-rest earth pressure

Test No.	Soil type	C_p (%)	Surcharge Ps (kPa)	Condition	OCR	K_0
1	A	4.2	0	Dry	3.3	0.613
2	C	12.5	0	Dry	5.5	0.864
3	D	18	0	Dry	7.2	1.049
4	A	4.2	0	Saturated	2.8	0.602
5	C	12.5	0	Saturated	4.7	0.615
6	D	18	0	Saturated	1.1	0.215
7	A	4.2	8	Dry	4.5	0.709
8	C	12.5	8	Dry	6.9	0.979
9	D	18	8	Dry	9.9	1.275
10	A	4.2	8	Saturated	3.7	0.689
11	C	12.5	8	Saturated	5.9	0.732
12	D	18	8	Saturated	1.8	0.275
13	A	4.2	16	Dry	6.0	0.831
14	C	12.5	16	Dry	8.2	1.082
15	D	18	16	Dry	11.7	1.449
16	A	4.2	16	Saturated	4.9	0.802
17	C	12.5	16	Saturated	7.0	0.812
18	D	18	16	Saturated	2.7	0.340
19	B	9	0	Dry	3.9	0.722
20	B	9	8	Dry	5.1	0.821
21	B	9	16	Dry	6.6	0.923
22	B	9	0	Saturated	3.3	0.605
23	B	9	8	Saturated	4.1	0.696
24	B	9	16	Saturated	5.7	0.811

Furthermore, it can be noted from this table that the coefficient of at-rest earth pressure of dry soils increases moderately by increasing the C_p, which can be modelled in a linear relation, while it also increases due to the increase of stress level (OCR) in the soil. It can be noted that the coefficient of at-rest earth pressure dropped considerably when the soil was fully inundated.

This can be explained that collapsible soil due to its unstable soil fabric, the bond strength between particles is easy to be weakened and/or broken due to the presence of water, causing collapse, which is associated with loss of strength and significant settlement. It is of interest to note that the at-rest earth pressure for saturated soil decreases with the increase of the collapse potential C_p of the soil and increases with the increase of the "OCR".

4.3.1. Proposed formula for estimating coefficient of at-rest earth pressure K_0 for collapsible soils at dry state

Test results of the present experimental investigation were used to develop the following empirical formula, which predict the coefficient of earth pressure at-rest for given OCR and C_p values for collapsible soils in the dry state:

$$K_0 = (0.007\,C_p + 0.4)(0.18\,OCR + 0.8) \qquad (4.5)$$

Table 4.2 presents the values of the coefficient of at-rest earth pressure K_0 estimated by Eq. (4.5) for dry soils for given OCR and C_p values, together with the theoretical values of Meyerhof (1976), Massarsch (1979), Mayne & Kulhawy (1982), and Hanna and Al-Romhein (2008), where good agreement can be noted.

Furthermore, the values predicted by Eq. (4.5) for normally consolidated soils were also compared with the values given by Jaky (1944). These values are given in Table 4.3, and reasonable agreement can be seen.

For convenience, the theoretical values evaluated using Eq. (4.5) were presented in graphical form in Figure 4.16.

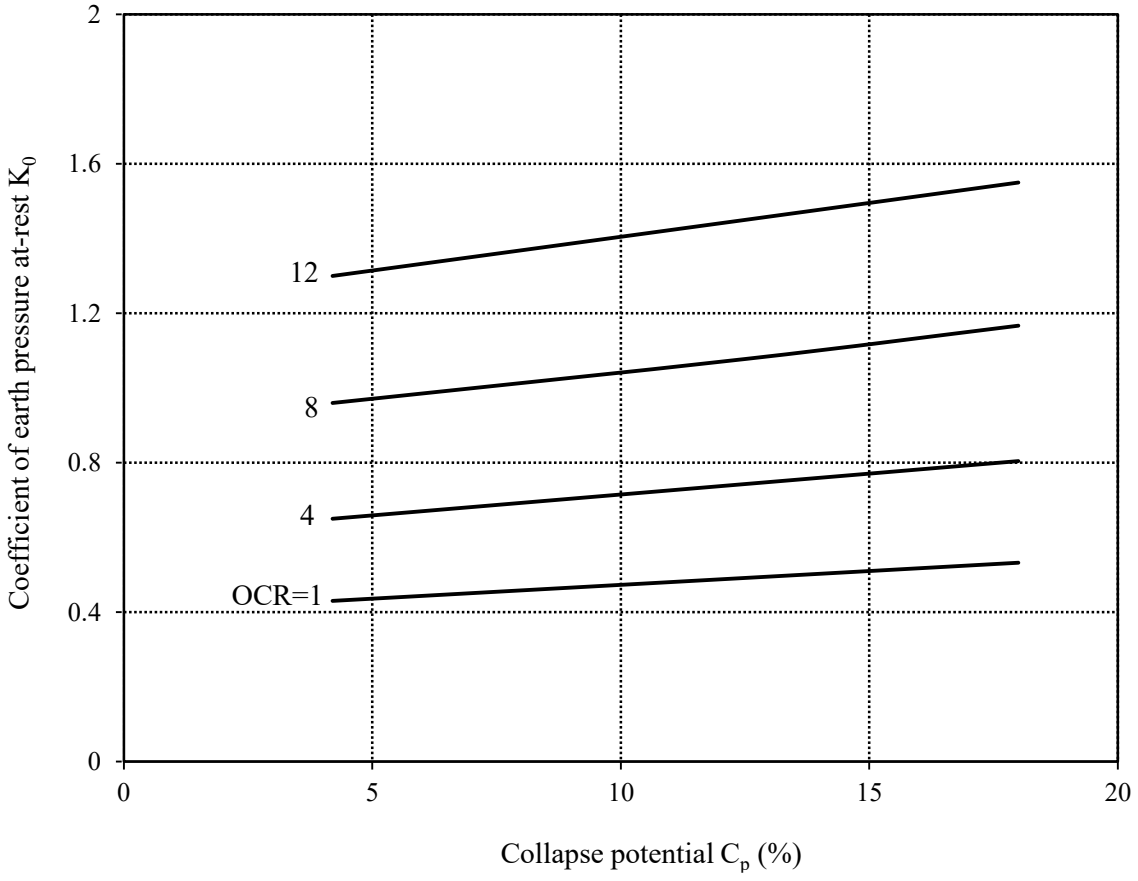

Fig. 4.16. The theoretical values of K_0 obtained from the proposed formula [Eq. (4.5)] for the dry state

Table 4.2. Comparison between Experimental and Theoretical values of K_0 for overconsolidated collapsible soil at dry state

Experimental data							Theoretical results K_0				
Test no.	Soil properties				OCR	K_0	Meyerhof 1976	Massarch 1979	Mayne & Kulhawy 1982	Hanna & Al-Romhein 2008	Proposed formula [Eq.(4.5)]
	Soil type	C_p (%)	ϕ' (degree)	PI (%)							
1	A	4.2	40	-	3.3	0.613	0.649	-	0.768	0.621	0.600
2	C	12.5	35	2.55	5.5	0.864	0.999	1.057	1.134	0.834	0.878
3	D	18	31	7.4	7.2	1.049	1.301	1.264	1.340	0.940	1.112
7	A	4.2	40	-	4.5	0.709	0.757	-	0.939	0.717	0.700
8	C	12.5	35	2.55	6.9	0.979	1.119	1.184	1.291	0.912	1.001
9	D	18	31	7.4	9.9	1.275	1.526	1.482	1.579	1.045	1.368
13	A	4.2	40	-	6.0	0.831	0.875	-	1.130	0.819	0.810
14	C	12.5	35	2.55	8.2	1.082	1.221	1.291	1.426	0.976	1.114
15	D	18	31	7.4	11.7	1.449	1.659	1.611	1.721	1.206	1.538
19	B	9	38.5	-	3.9	0.722	0.745	-	0.881	0.689	0.700
20	B	9	38.5	-	5.1	0.821	0.852	-	1.041	0.776	0.800
21	B	9	38.5	-	6.6	0.923	0.970	-	1.222	0.870	0.923

Table 4.3. Comparison between the predicted values of K_0 obtained from Eq. (4.5) and the values given by Jaky (1944) for the case of normally consolidated soils at dry state

Soil properties			Coefficient of at-rest earth pressure, K_0	
C_p (%)	ϕ' (degree)	OCR	Jaky (1944)	Proposed formula [Eq. (4.5)]
4.2	40	1	0.357	0.430
9.0	38.5	1	0.377	0.460
12.5	35	1	0.426	0.492
18	31	1	0.485	0.530

4.3.2. Proposed formula for estimating coefficient of at-rest earth pressure K_0 for collapsible soils for the case after full inundation

Test results of the present experimental investigation after full inundation were used to develop the following empirical formula, which predict the coefficient of earth pressure at-rest for given OCR and C_p values for collapsible soils in the saturated state:

$$K_0 = (0.41 - 0.014C_p)\,(0.39OCR + 0.64) \qquad (4.6)$$

For practical use, the theoretical values evaluated using Eq. (4.6) were plotted in Figure 4.17. Considering that no experimental results available in the literature to validate the results predicted by the proposed Eq. (4.6) for the case of saturated collapsible soil, additional tests were conducted only for the purpose to validate the proposed empirical formula. The results of these comparisons are presented in Tables 4.4 and 4.5, where good agreement can be noted.

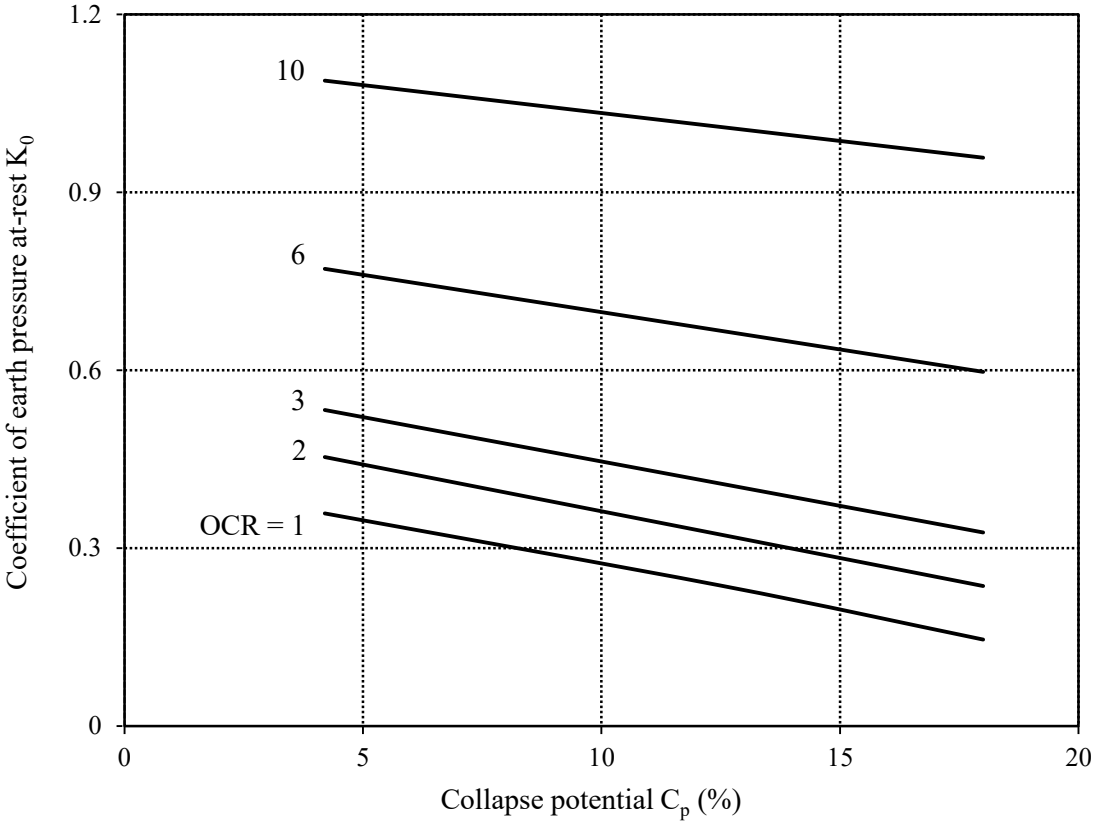

Fig. 4.17. The theoretical values of K_0 obtained from the proposed formula [Eq. (4.6)] for the case after full inundation

Table 4.4. Comparison between Experimental and Theoretical values of K_0 for the overconsolidated collapsible soil after full inundation

Test No.	Experimental results				Theoretical results of K_0
	Soil type	C_p (%)	OCR	K_0	Proposed formula [Eq.(4.6)]
4	A	4.2	2.8	0.602	0.608
5	C	12.5	4.7	0.615	0.581
6	D	18	1.1	0.215	0.170
10	A	4.2	3.7	0.689	0.730
11	C	12.5	5.9	0.732	0.693
12	D	18	1.8	0.275	0.212

Table 4.5. Comparison between Theoretical and Experimental results from the additional Tests of K_0 for the overconsolidated collapsible soil after full inundation.

Test No.	Experimental results				Theoretical results of K_0
	Soil type	C_p (%)	OCR	K_0	Proposed formula [Eq. (4.6)]
16	A	4.2	4.9	0.802	0.890
17	C	12.5	7.0	0.812	0.792
18	D	18	2.7	0.340	0.277
22	B	9	3.3	0.605	0.560
23	B	9	4.1	0.696	0.660
24	B	9	5.7	0.811	0.813

4.3.3. Proposed design charts for predicting coefficient of at-rest earth pressure K_0 for unsaturated collapsible soils at different degree of saturation

After validating the proposed empirical formulae given in Eqs. (4.5) and (4.6) for the dry and saturated states, respectively, these formulae were used to develop design charts given in Figure 4.18 to predict the values of coefficient of at-rest earth pressure of overconsolidated collapsible soil K_0 as the function of the collapse potential (C_p), the overconsolidation ratio (OCR) and the degree of saturation (S) of the soil. In these charts, it was assumed that the coefficient of at-rest earth pressure K_0 decreases linearly with the increase of the degree of saturation (S).

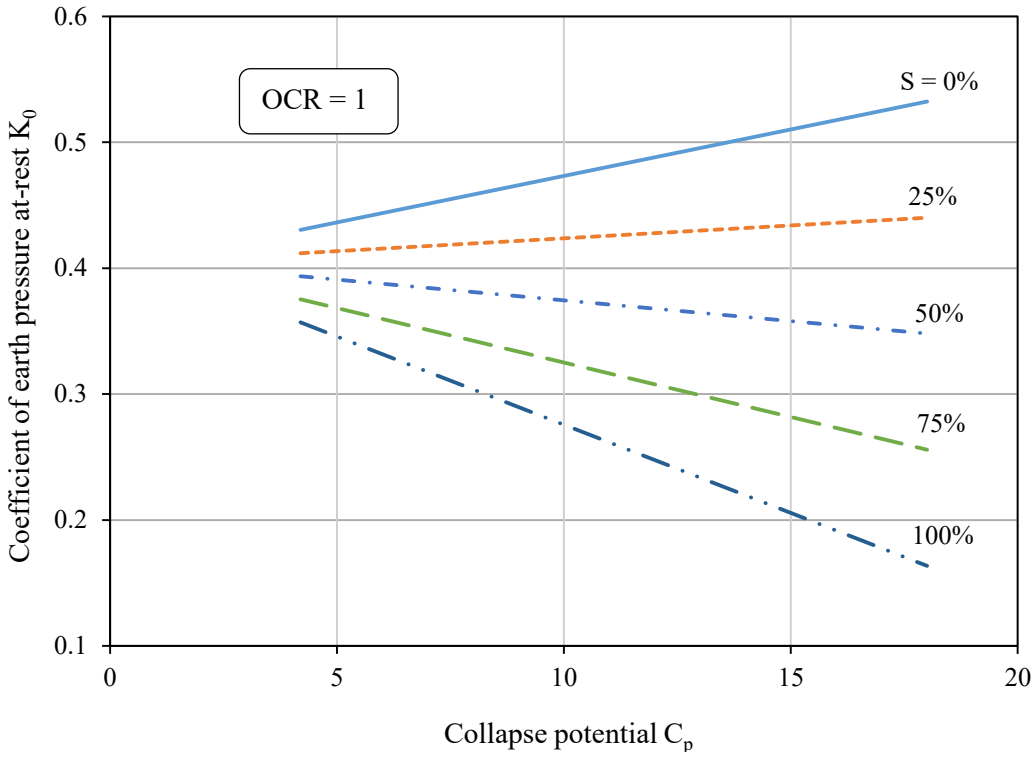

(a)

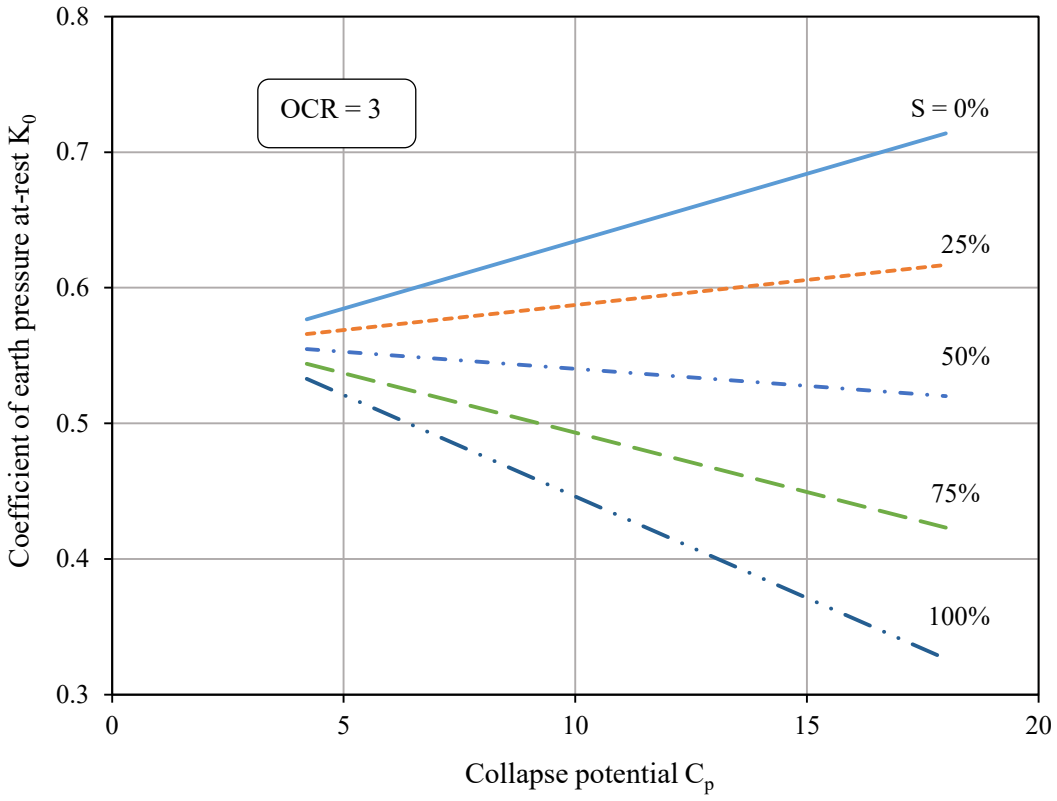
OCR = 3
S = 0%
25%
50%
75%
100%
Coefficient of earth pressure at-rest K_0
Collapse potential C_p
0.8
0.7
0.6
0.5
0.4
0.3
0
5
10
15
20

(b)

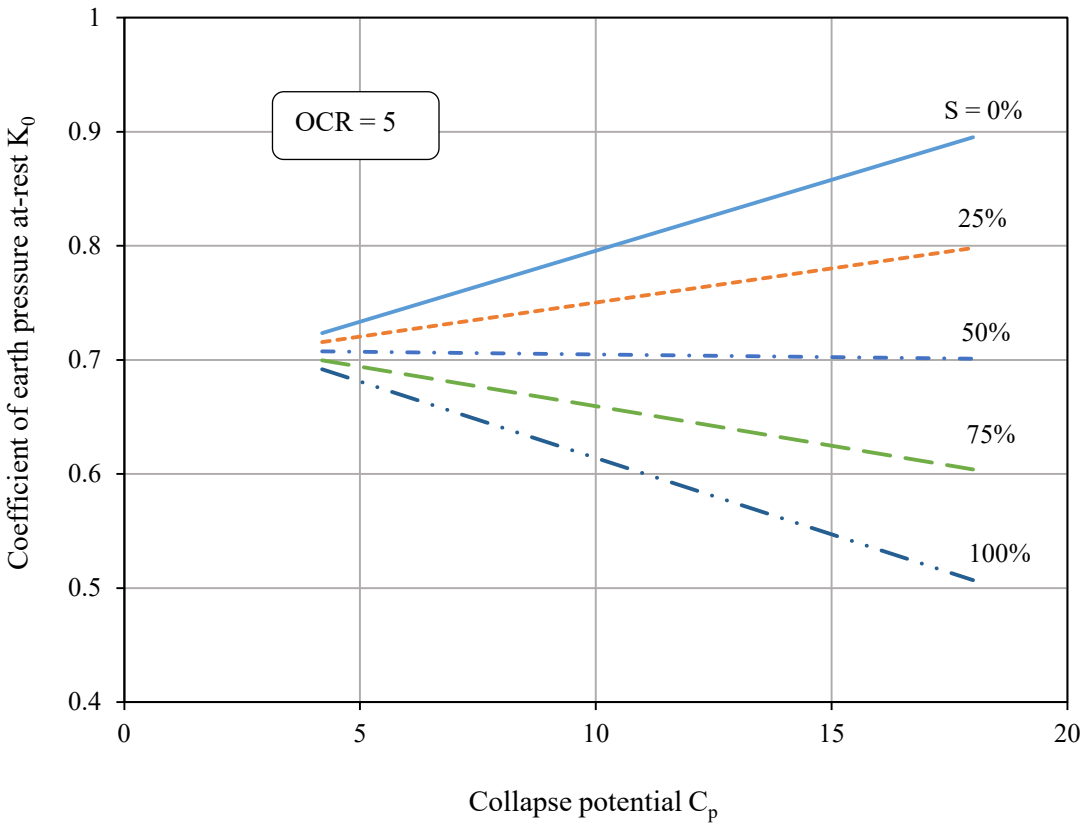
OCR = 5
S = 0%
25%
50%
75%
100%
Coefficient of earth pressure at-rest K_0
Collapse potential C_p
1
0.9
0.8
0.7
0.6
0.5
0.4
0
5
10
15
20

(c)

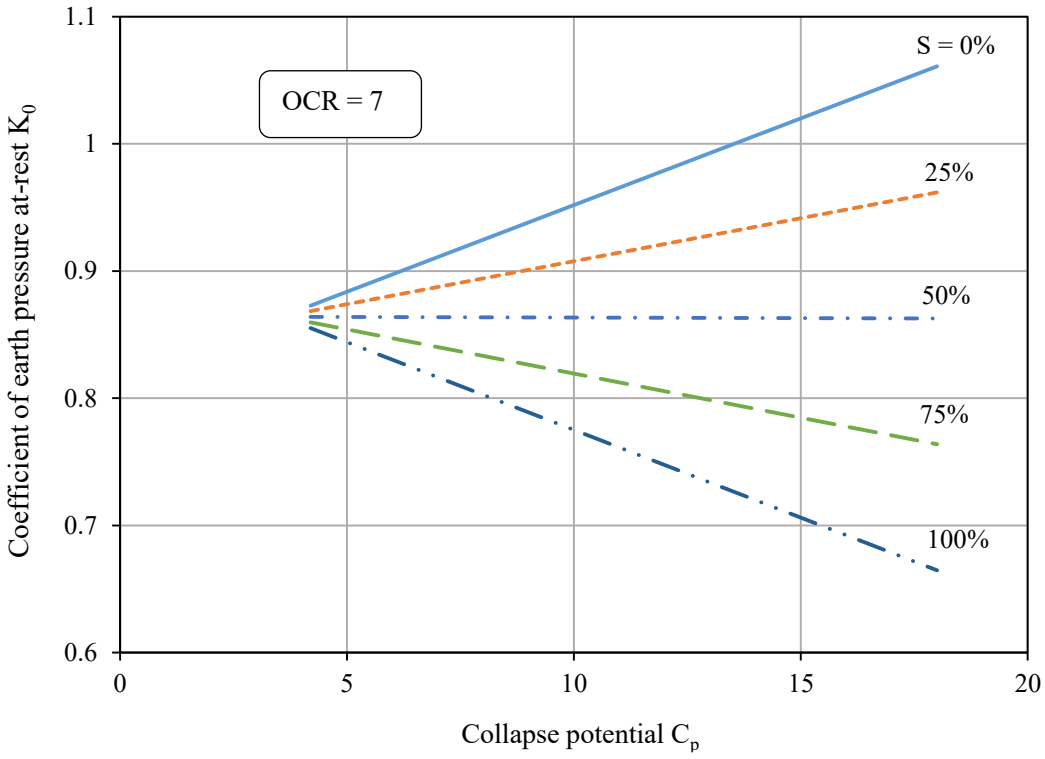

(d)

Fig. 4.18. Design charts: The theoretical values of K_0 for unsaturated collapsible soils: (a) OCR = 1; (b) OCR = 3; (c) OCR = 5; (d) OCR = 7.

CHAPTER 5
TEST RESULTS AND ANALYSIS FOR THE CASE OF PASSIVE PRESSURE

5.1. General

In this chapter, the results obtained from the present experimental investigation are presented in form of figures. A series of comparing figures have been developed to indicate the difference of soil behavior under the same or different conditions. An analytical model was developed to predict the passive earth force P_p and the coefficient of passive earth pressure K_p of collapsible soils. The analytical model developed in this investigation was used to develop results for a wide range of parameters. These results are presented as design chart, which will assist designers to estimate the coefficient of passive earth pressure K_p for given OCR and C_p values for dry collapsible soils. Moreover, the reduction factor was introduced to take into account the effect of the soil collapse on the coefficient of passive earth pressure K_p for the case of inundated collapsible soils.

5.2. Results and analysis

The experimental results are presented in graphical form in Figures 5.1 to 5.24. It can be noted that the passive earth force (P_p) and the horizontal wall displacement (ΔL) recorded at the failure point of the soil are also highlighted and indicated.

Results for test no. 1

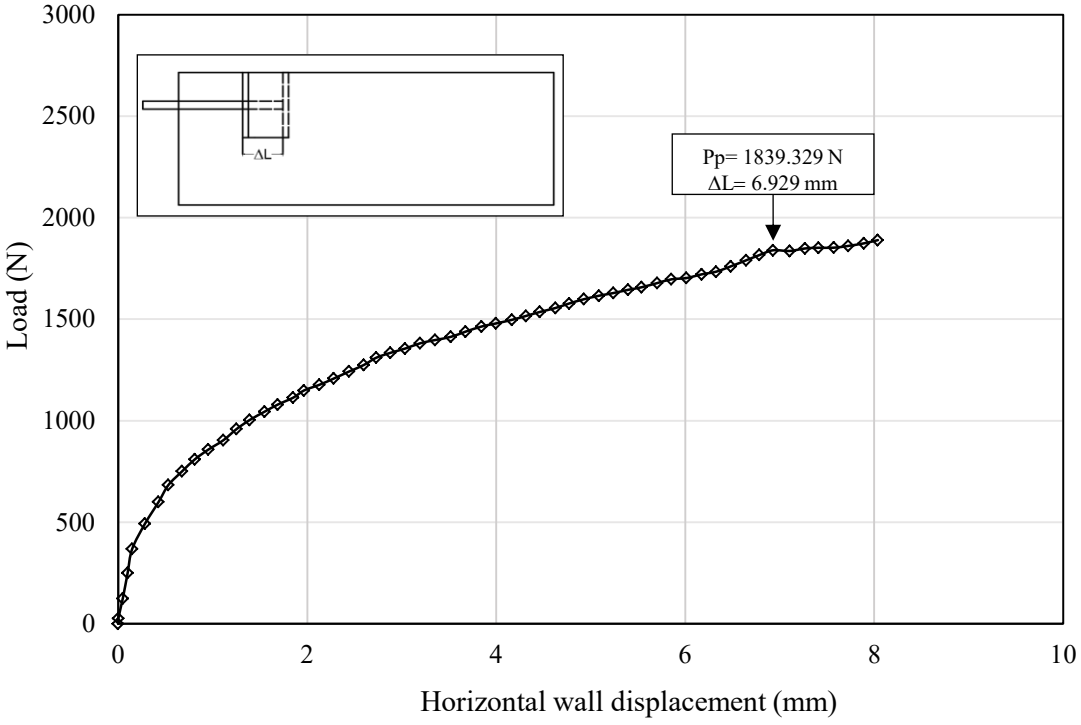

(a)

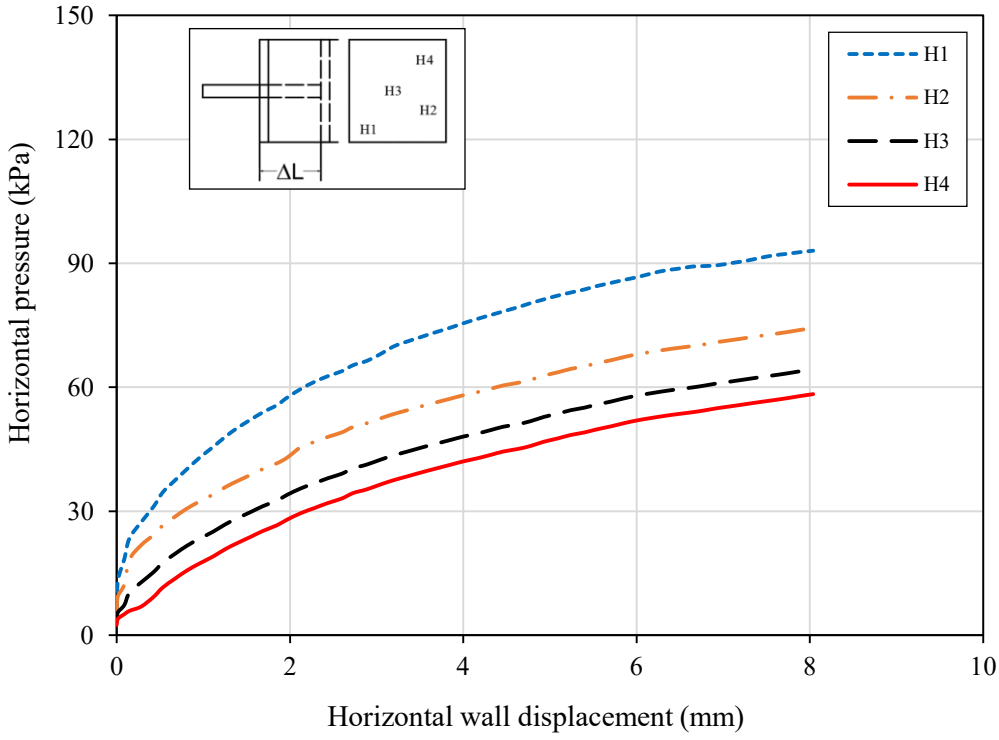

(b)

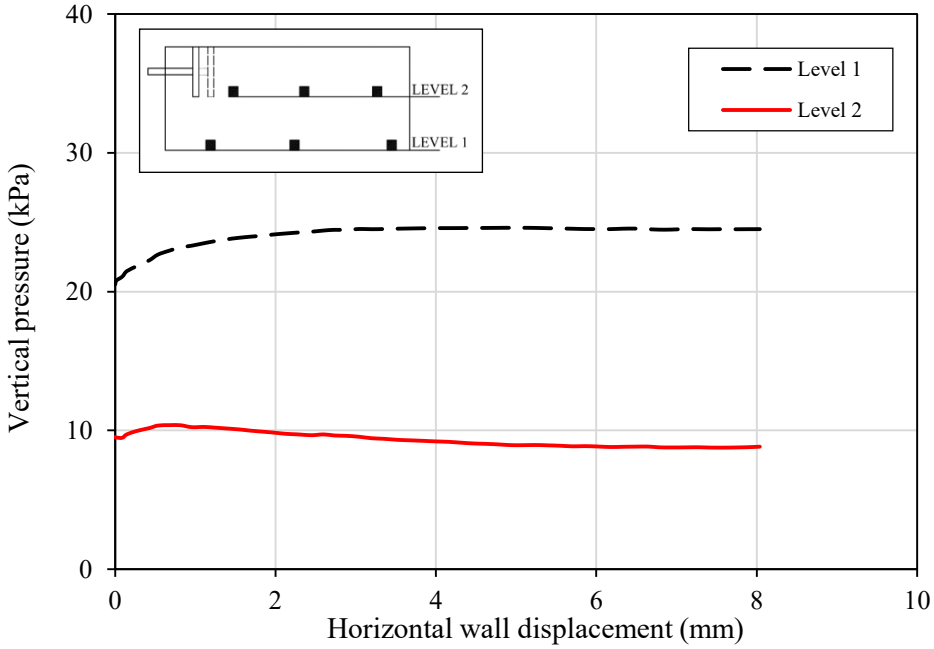

(c)

Fig. 5.1. Results for test no.1 (Se1) for soil A – C_p =4.2%: (a) Load – displacement curve (load cell reading); (b) Load – displacement curves for each transducer; (c) Vertical pressure in the soil mass versus the wall displacement

Results for test no. 2

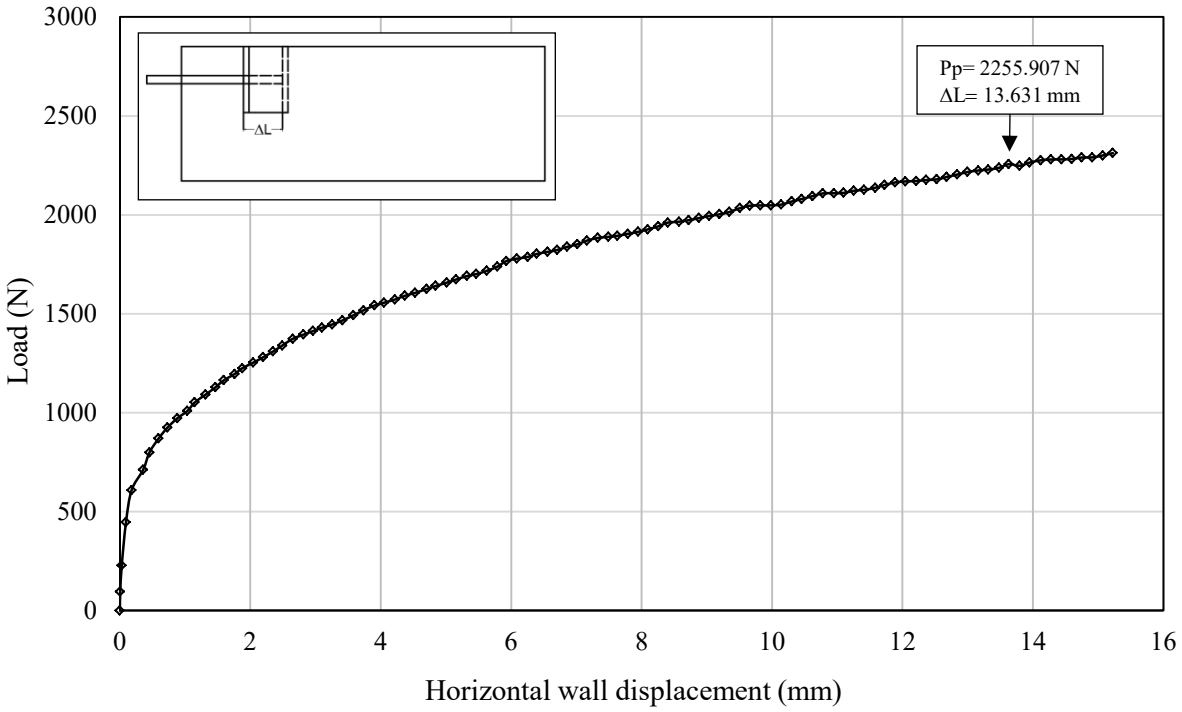

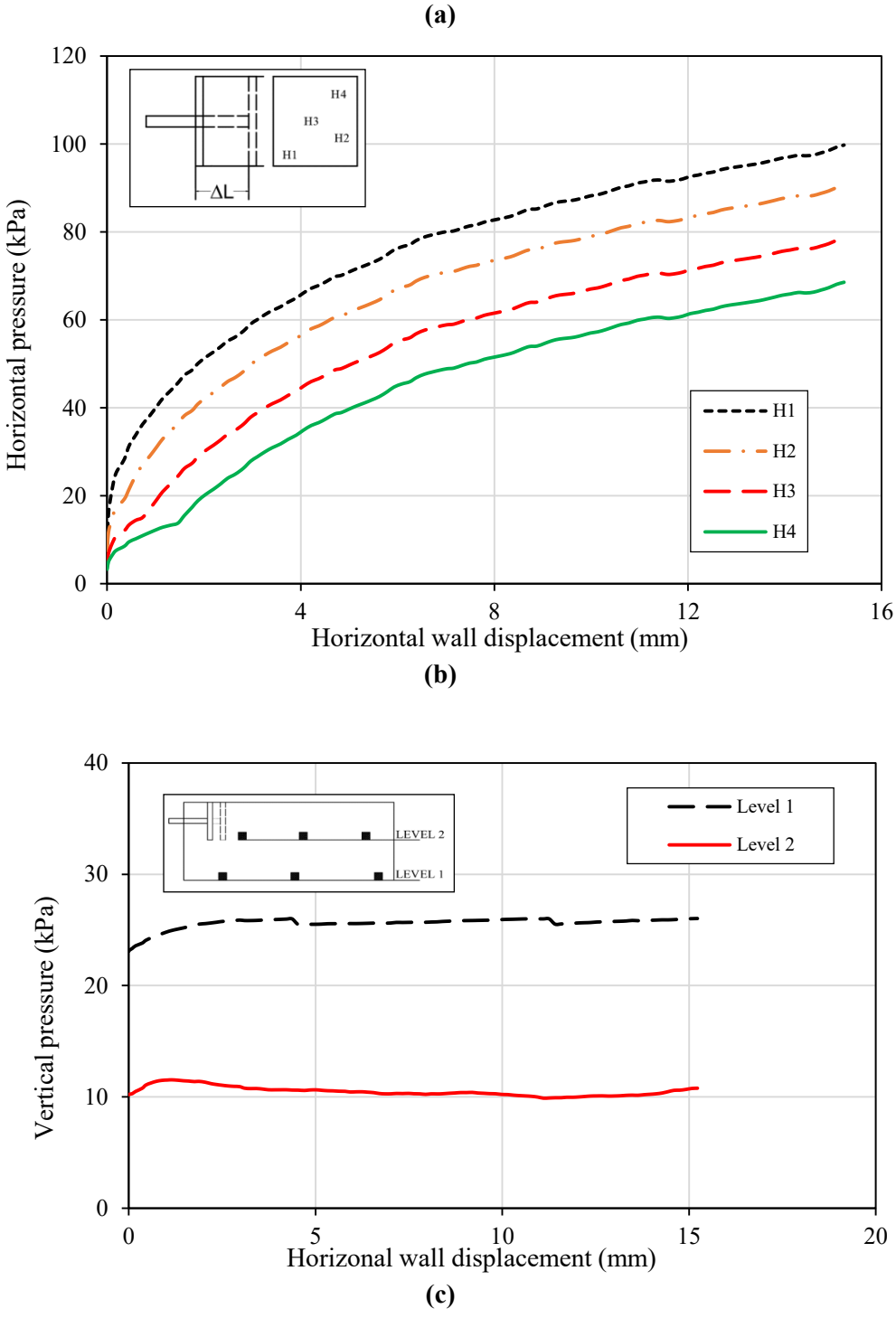

Fig. 5.2. Results for test no.2 (Se1) for soil B – C_p =9.0%: (a) Load – displacement curve (load cell reading); (b) Load – displacement curves for each transducer; (c) Vertical pressure in the soil mass versus the wall displacement

Results for test no. 3

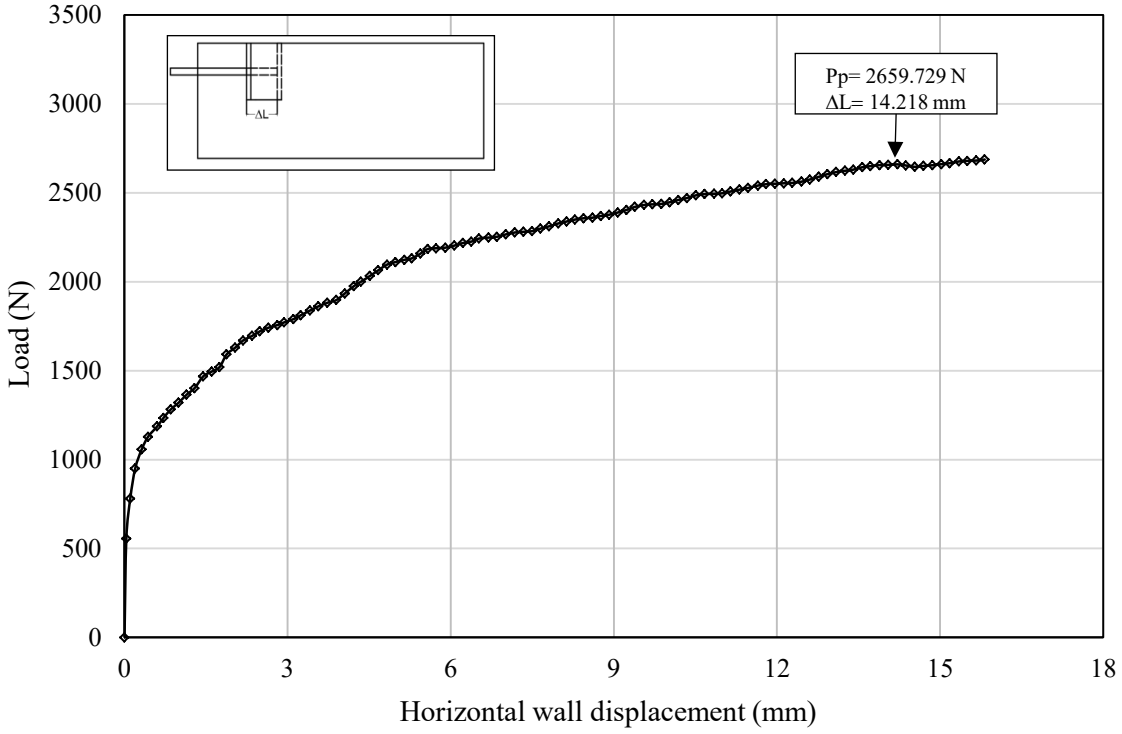

(a)

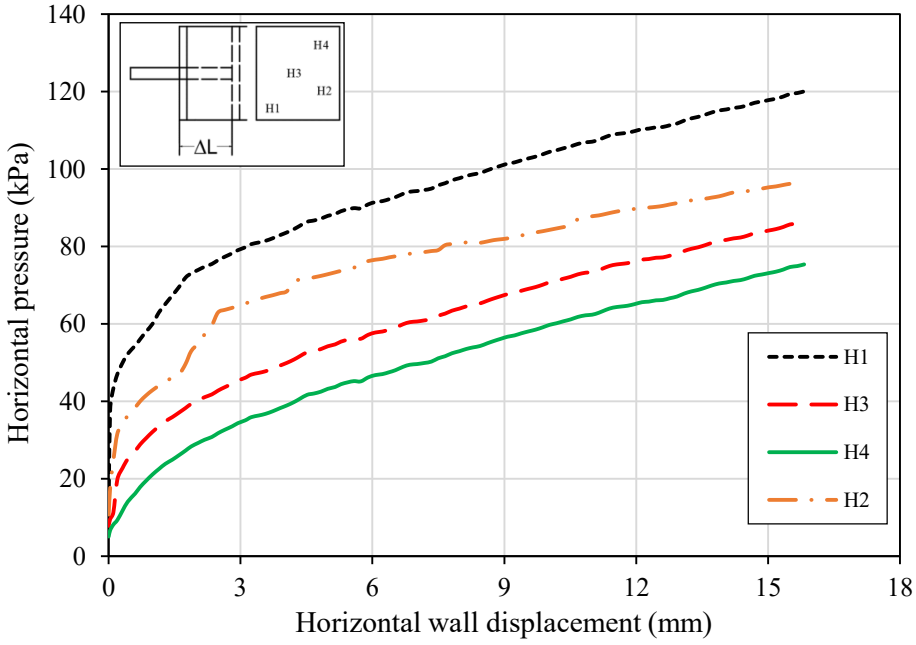

(b)

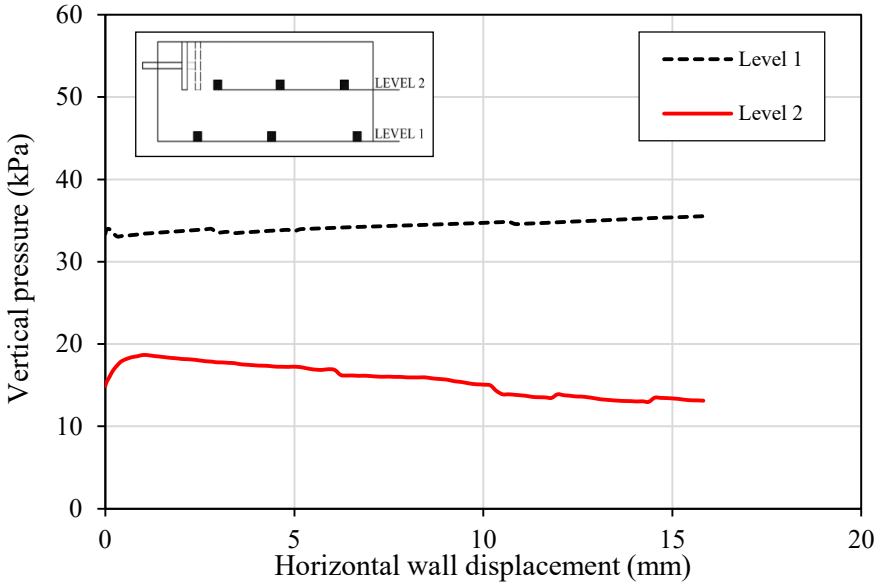

(c)

Fig. 5.3. Results for test no. 3 (Se1) for soil C – C_p =12.5%: (a) Load – displacement curve (load cell reading); (b) Load – displacement curves for each transducer; (c) Vertical pressure in the soil mass versus the wall displacement

Results for test no. 4

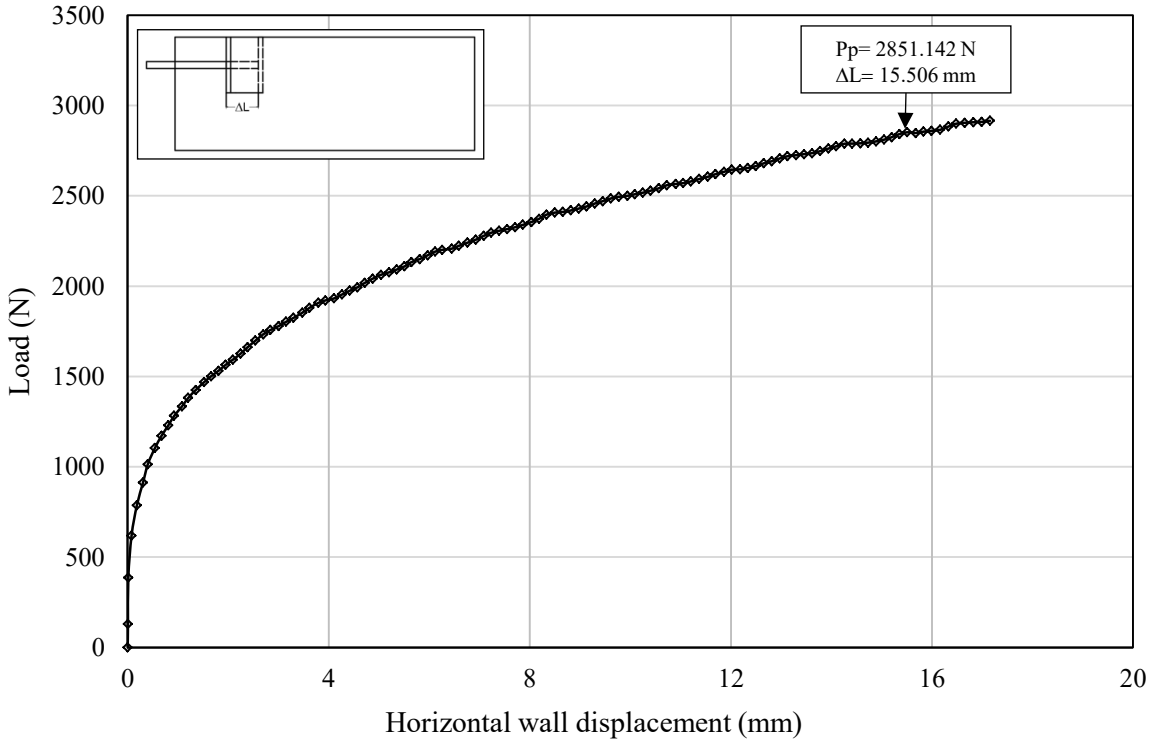

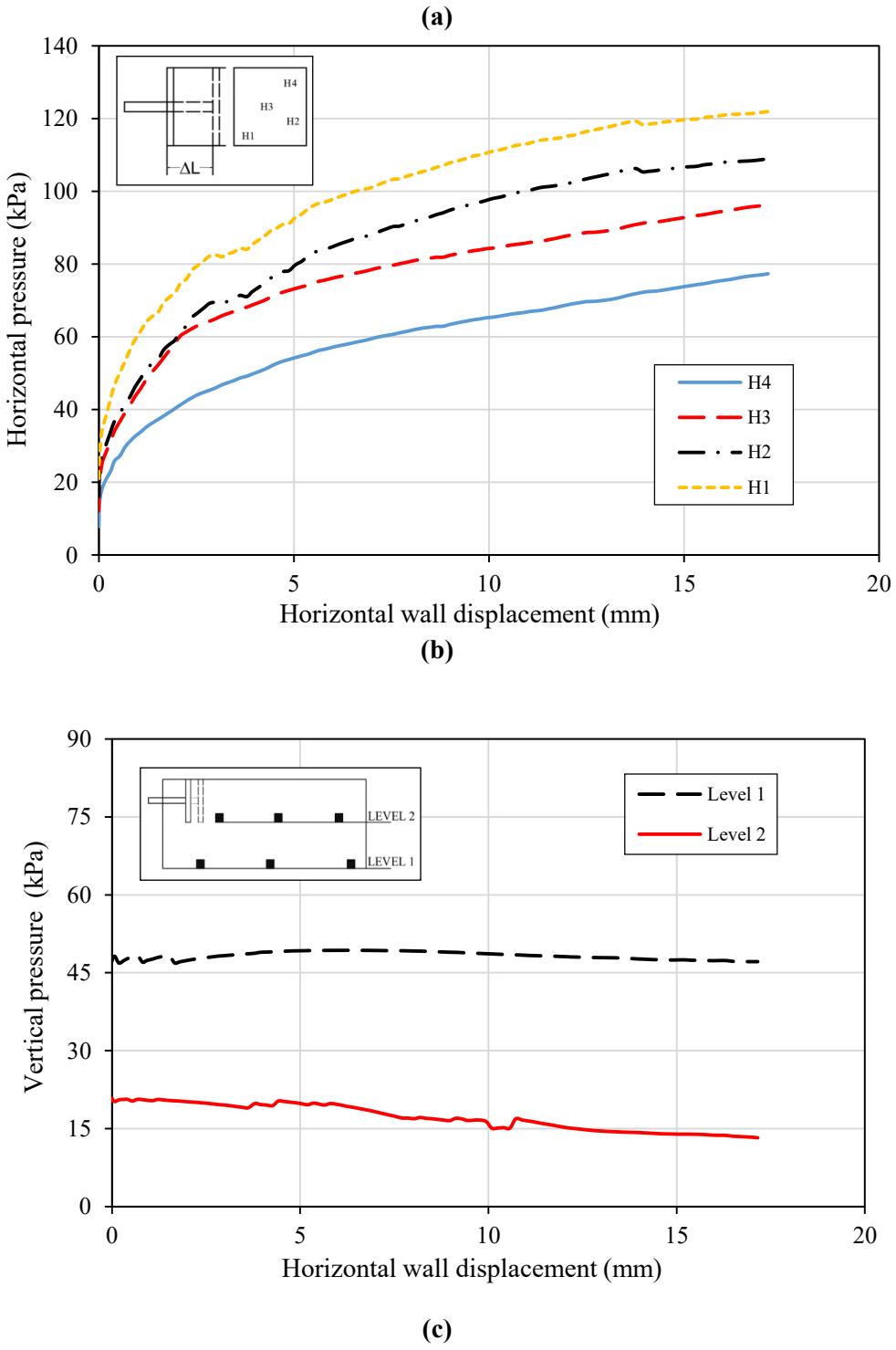

Fig. 5.4. Results for test no. 4 (Se1) for soil D – C_p =18%: (a) Load – displacement curve (load cell reading); (b) Load – displacement curves for each transducer; (c) Vertical pressure in the soil mass versus the wall displacement

Results for test no. 5

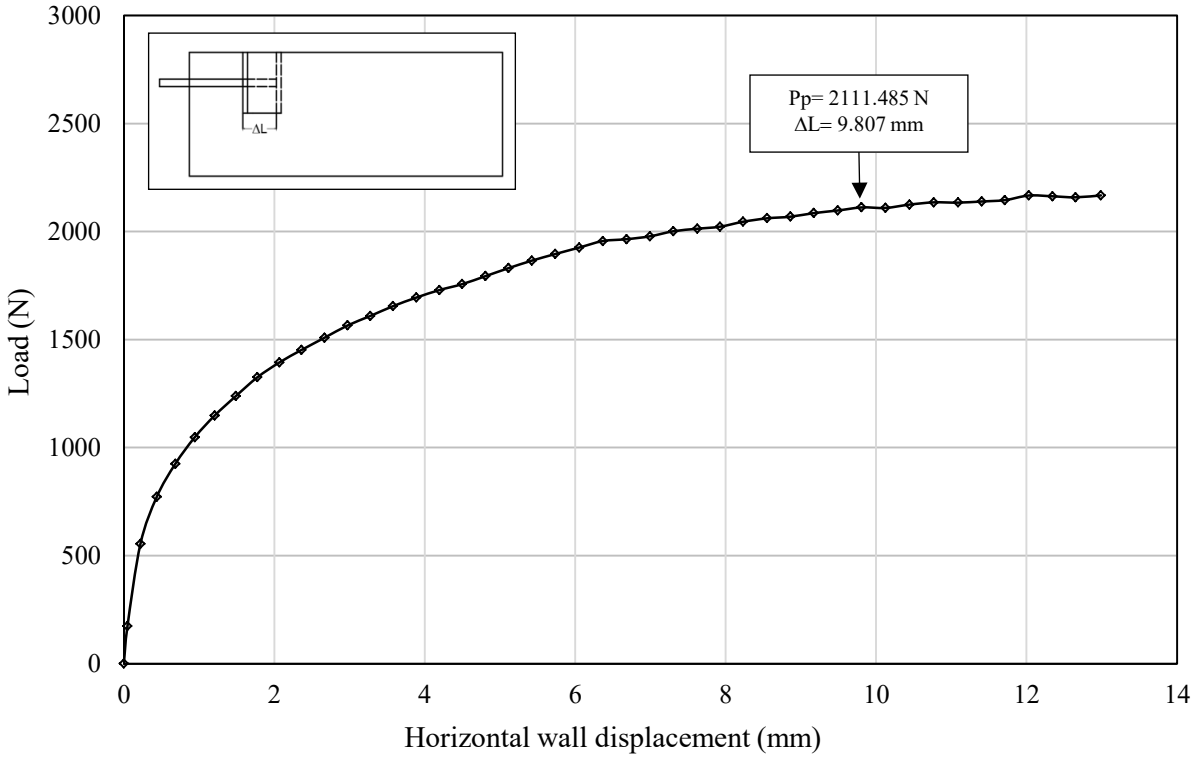

(a)

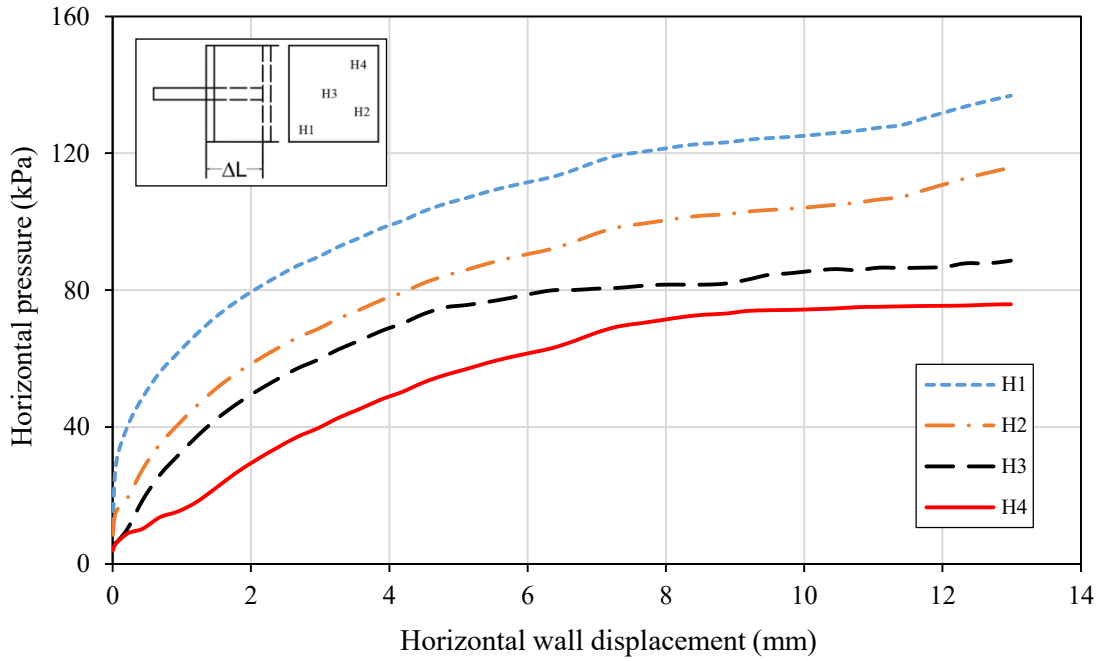

(b)

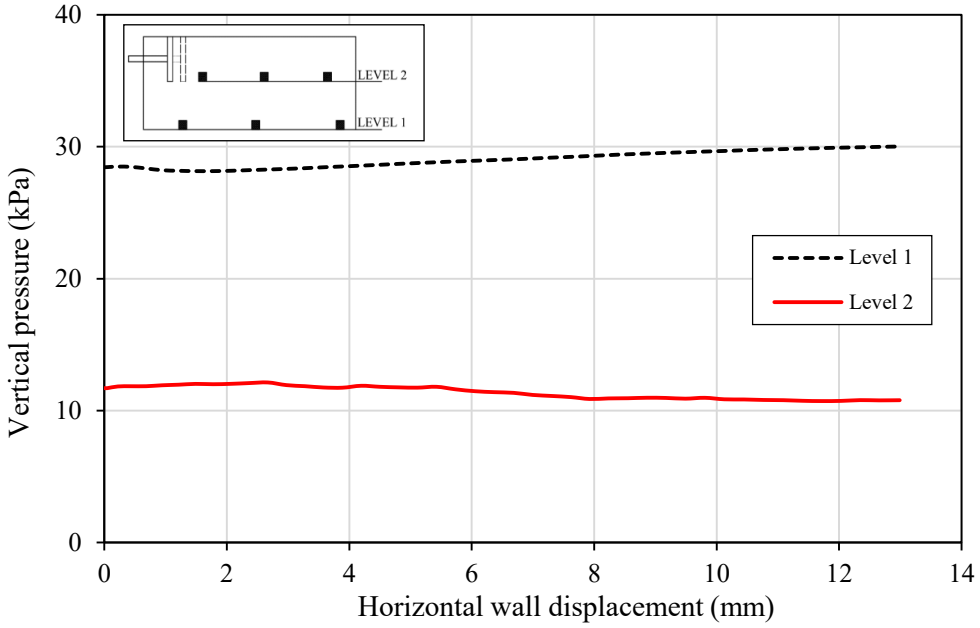

(c)

Fig. 5.5. Results for test no. 5 (Se2) for soil A – C_p =4.2%: (a) Load – displacement curve (load cell reading); (b) Load – displacement curves for each transducer; (c) Vertical pressure in the soil mass versus the wall displacement

Results for test no. 6

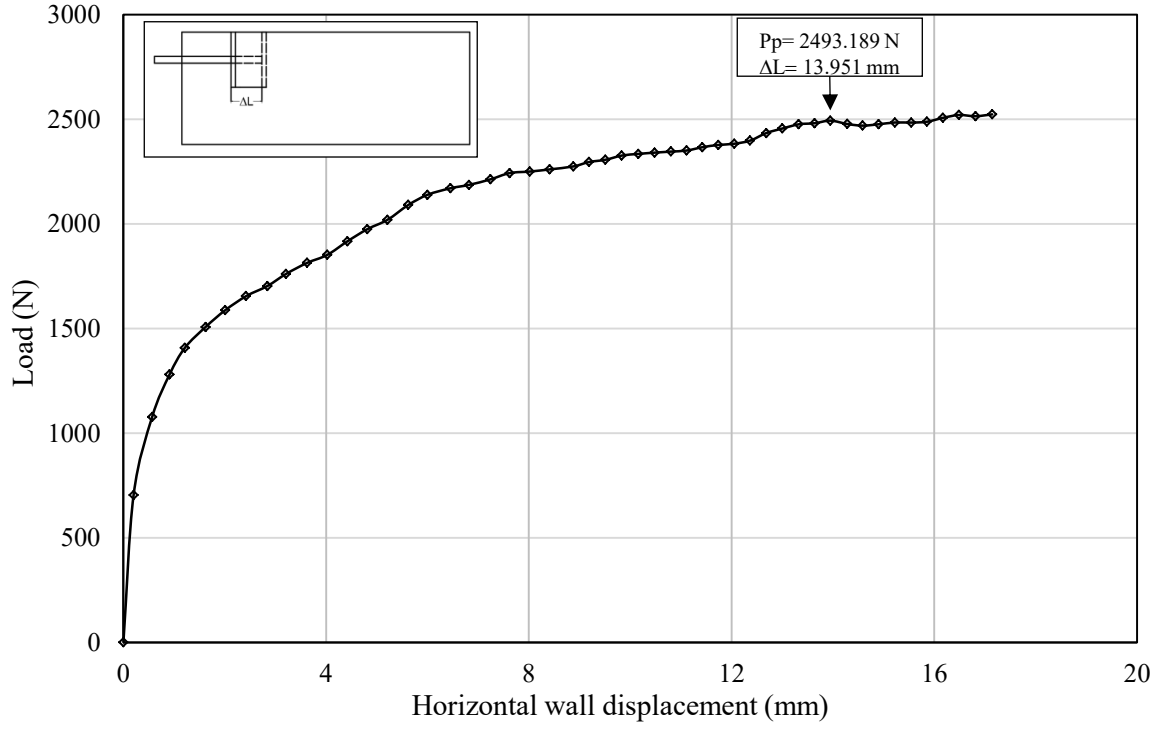

(a)

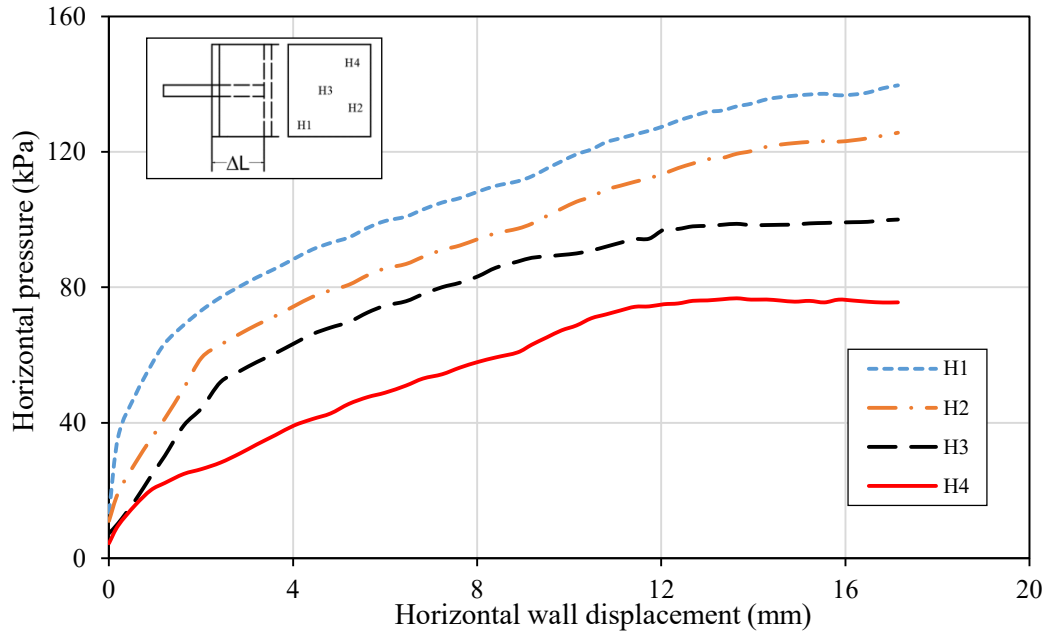

(b)

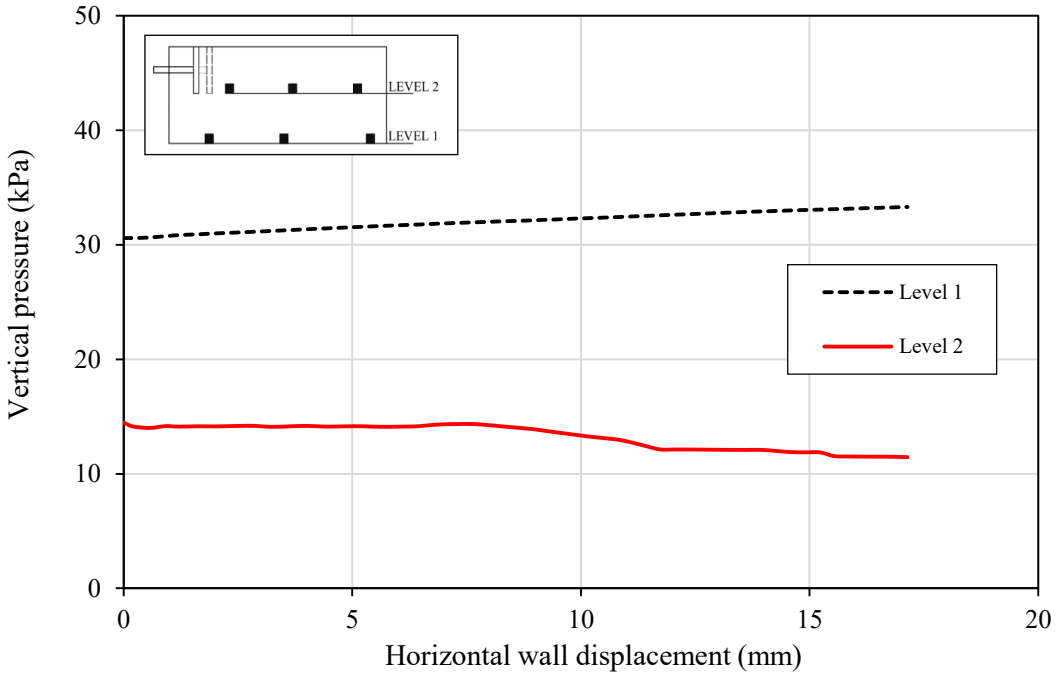

(c)

Fig. 5.6. Results for test no. 6 (Se2) for soil B – C_p =9.0%: (a) Load – displacement curve (load cell reading); (b) Load – displacement curves for each transducer; (c) Vertical pressure in the soil mass versus the wall displacement

Results for test no. 7

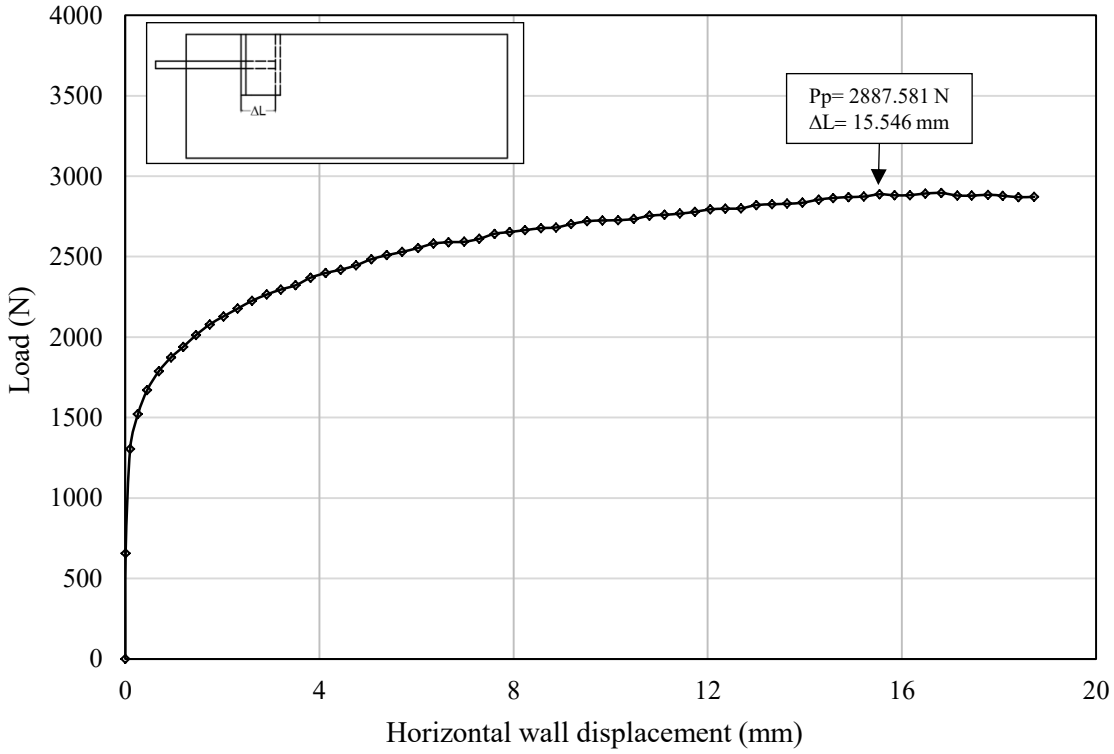

(a)

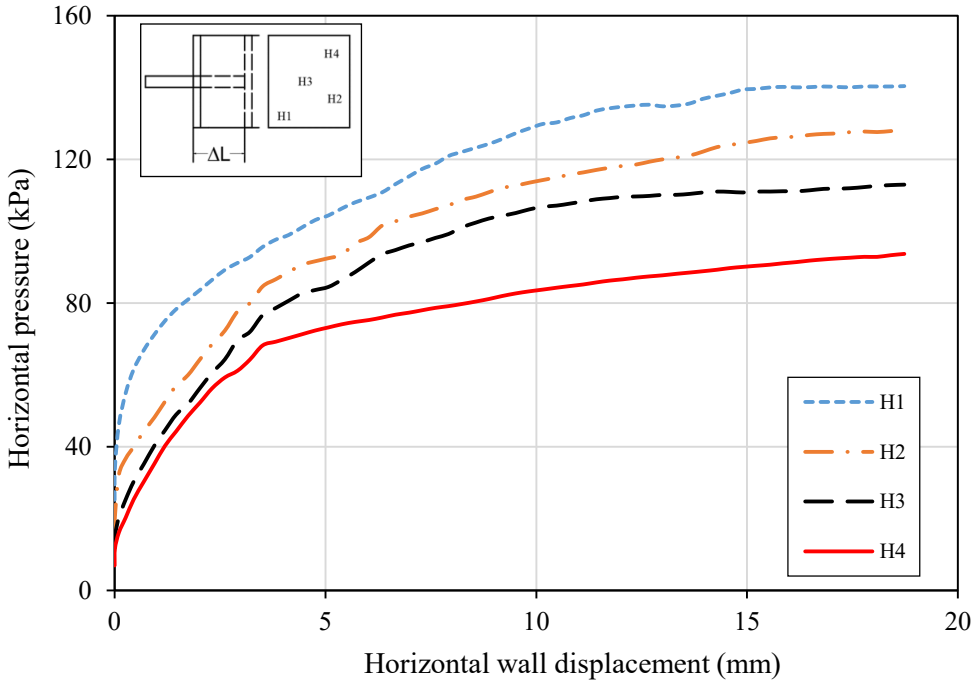

(b)

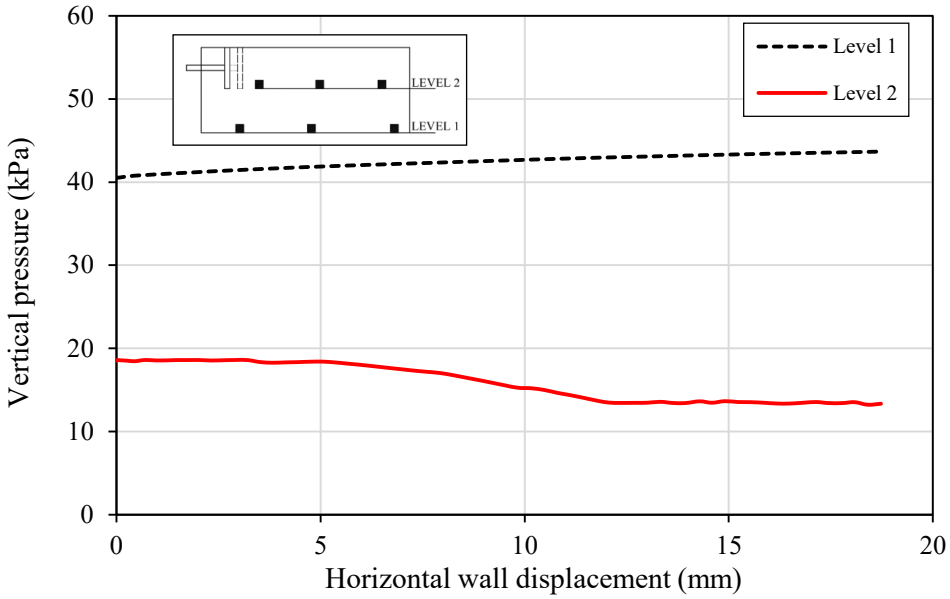

(c)

Fig. 5.7. Results for test no. 7 (Se2) for soil C – C_p =12.5%: (a) Load – displacement curve (load cell reading); (b) Load – displacement curves for each transducer; (c) Vertical pressure in the soil mass versus the wall displacement

Results for test no. 8

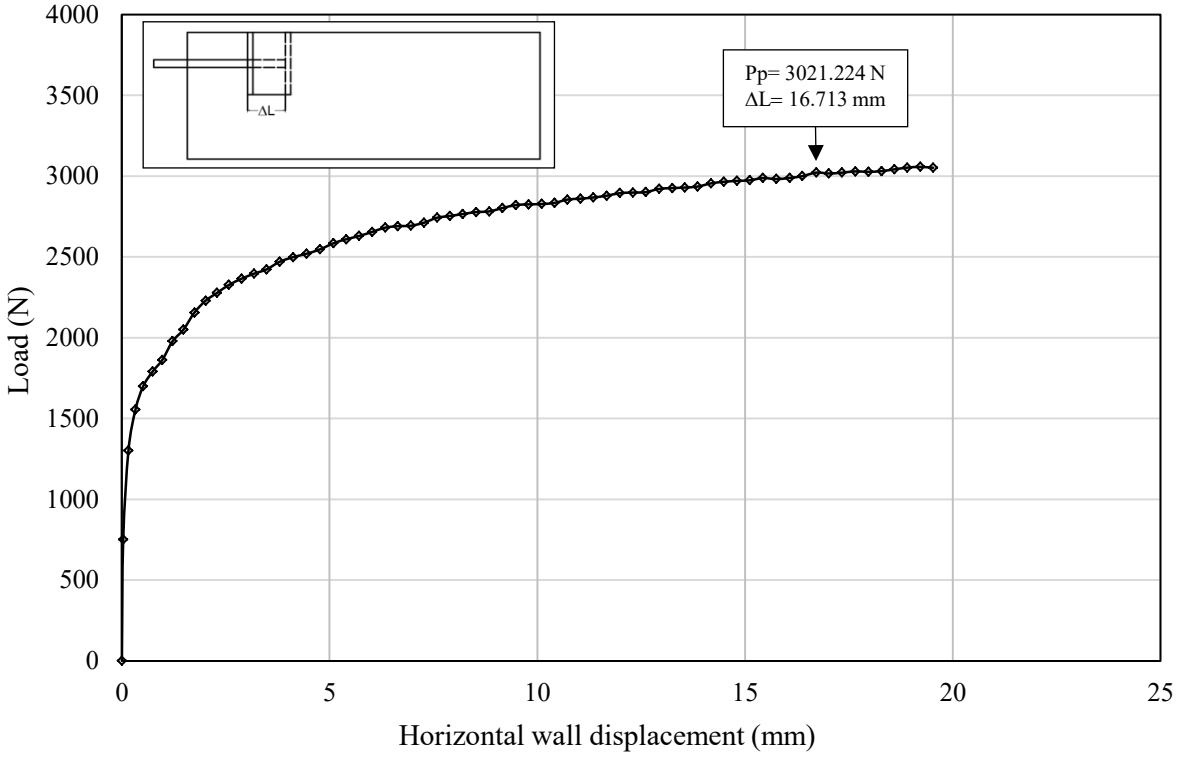

(a)

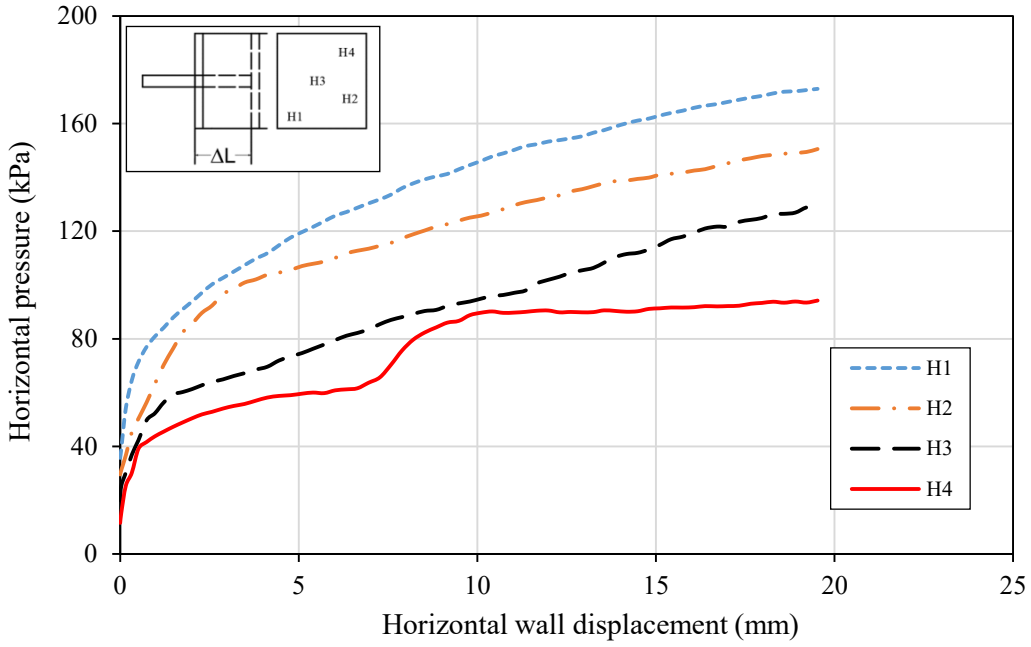

(b)

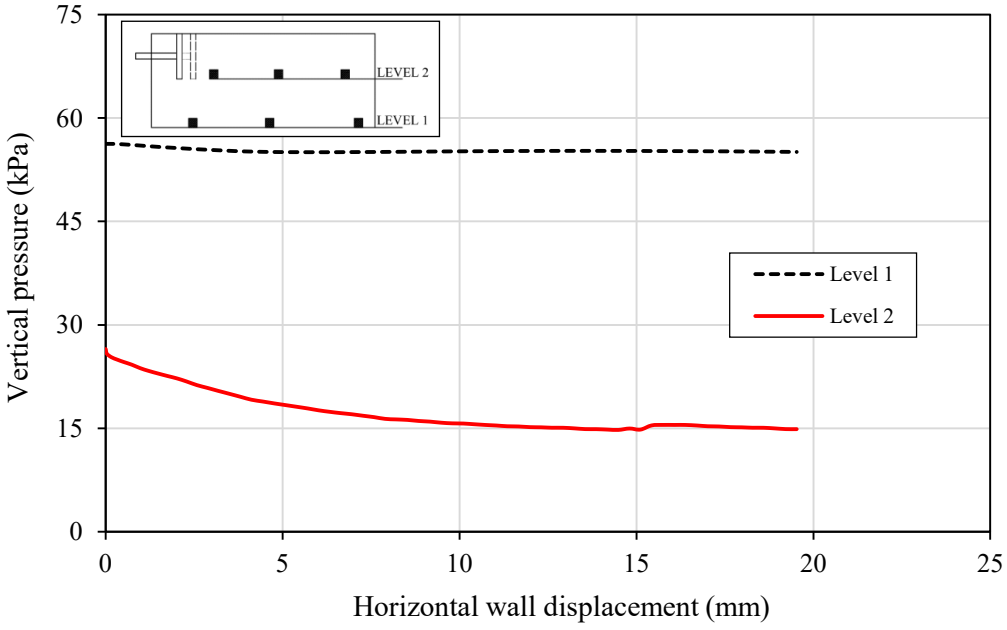

(c)

Fig. 5.8. Results for test no. 8 (Se2) for soil D – C_p =18%: (a) Load – displacement curve (load cell reading); (b) Load – displacement curves for each transducer; (c) Vertical pressure in the soil mass versus the wall displacement

Results for test no. 9

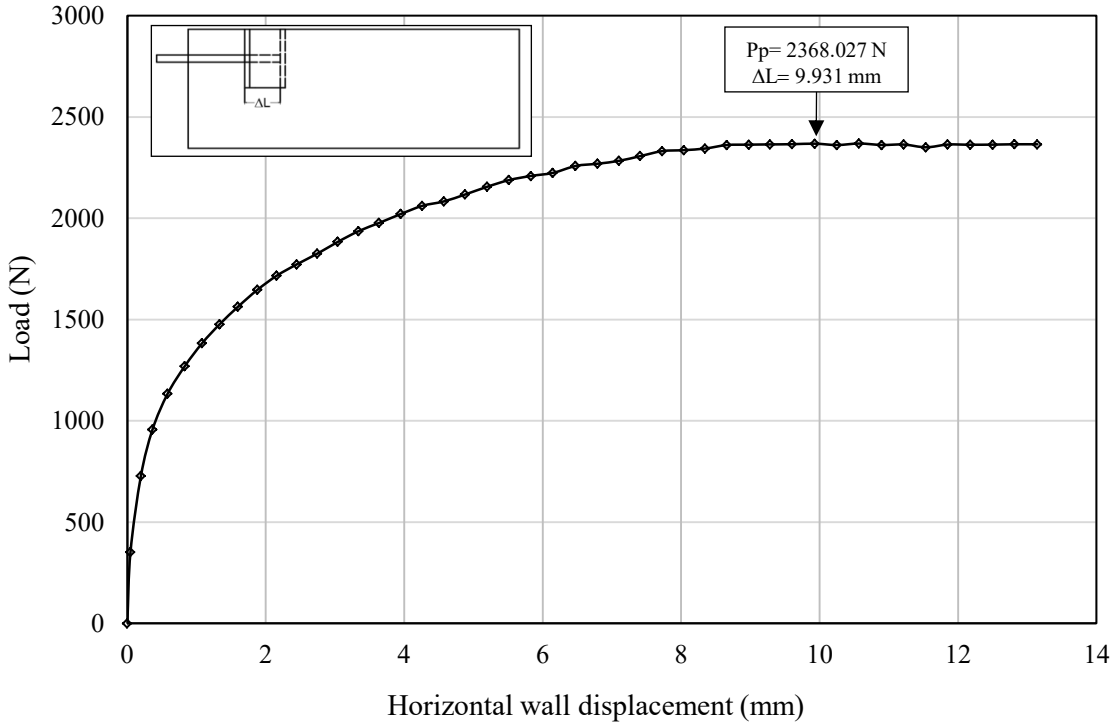

(a)

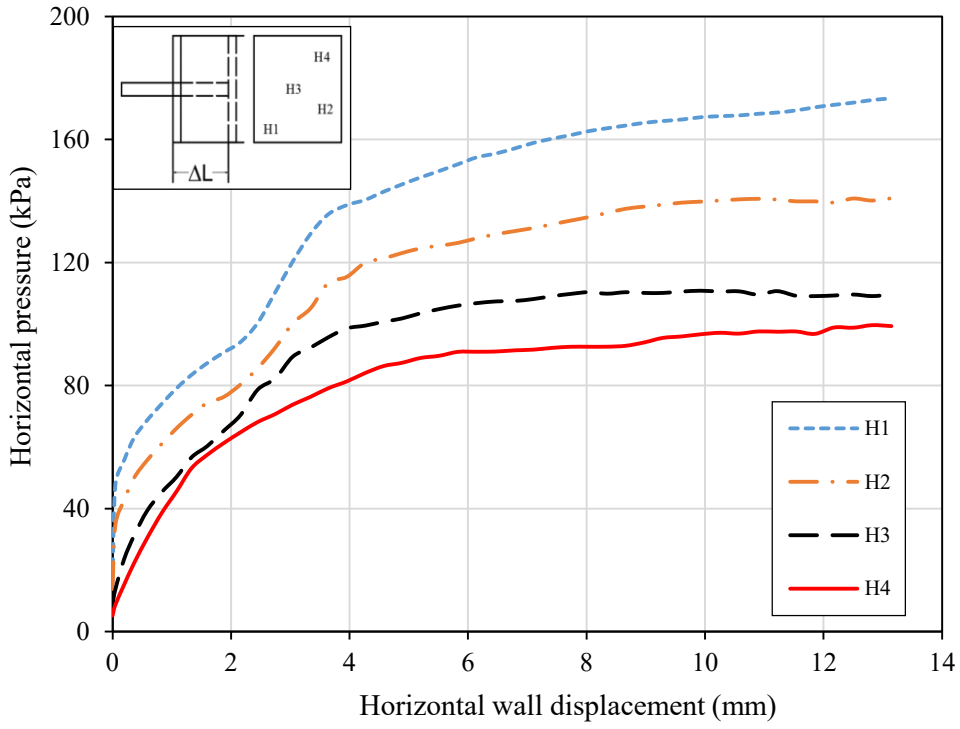

(b)

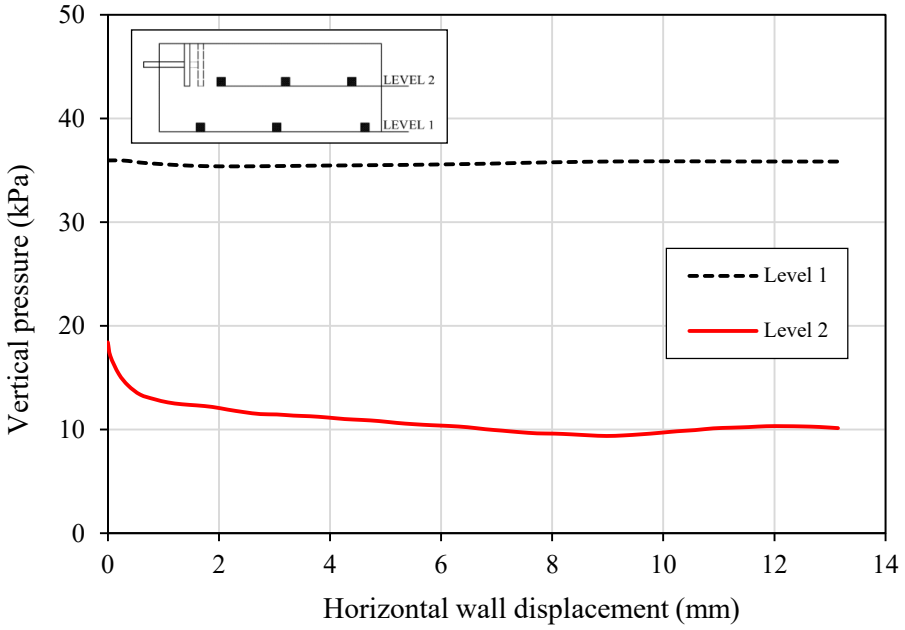

(c)

Fig. 5.9. Results for test no. 9 (Se3) for soil A – C_p =4.2%: (a) Load – displacement curve (load cell reading); (b) Load – displacement curves for each transducer; (c) Vertical pressure in the soil mass versus the wall displacement

Results for test no. 10

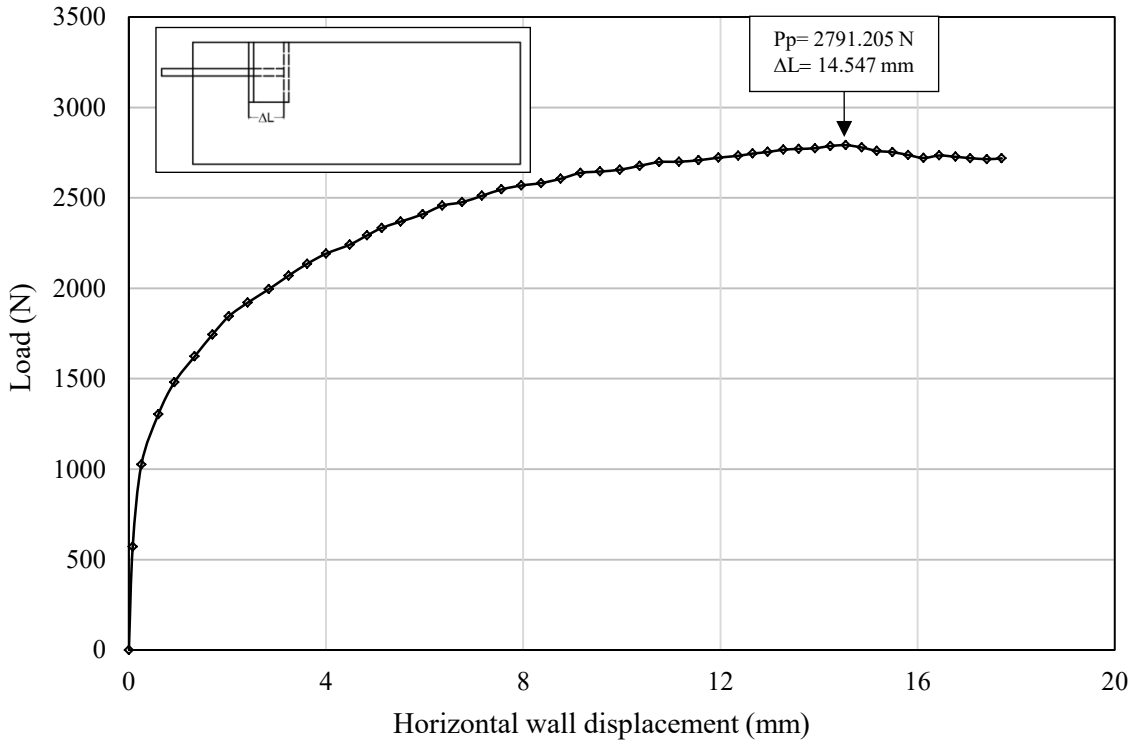

(a)

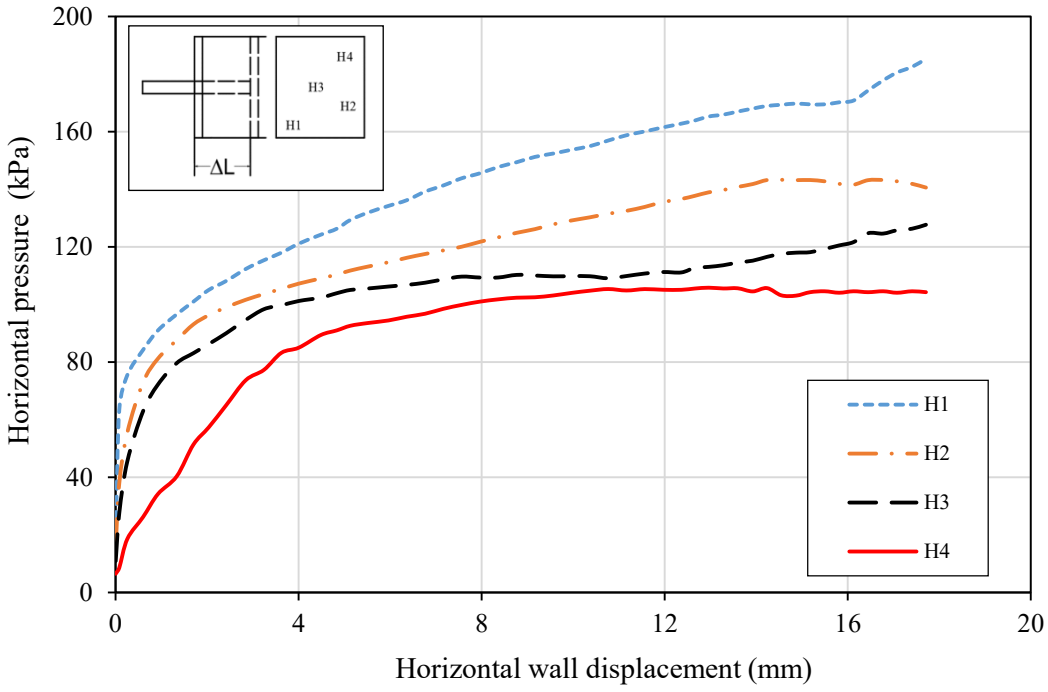

(b)

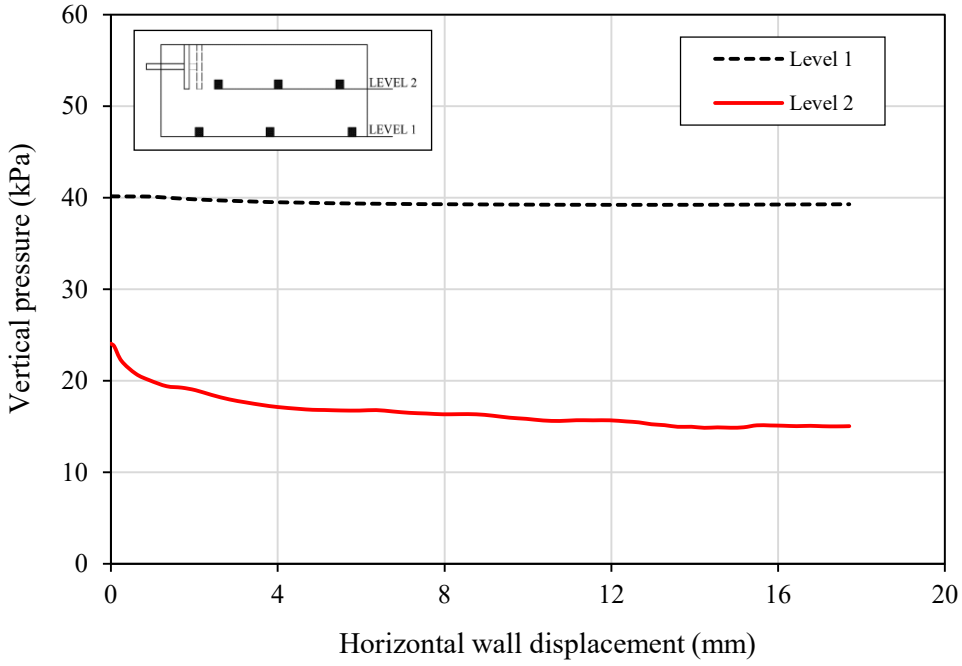

(c)

Fig. 5.10. Results for test no.10 (Se3) for soil B – C_p =9.0%: (a) Load – displacement curve (load cell reading); (b) Load – displacement curves for each transducer; (c) Vertical pressure in the soil mass versus the wall displacement

Results for test no. 11

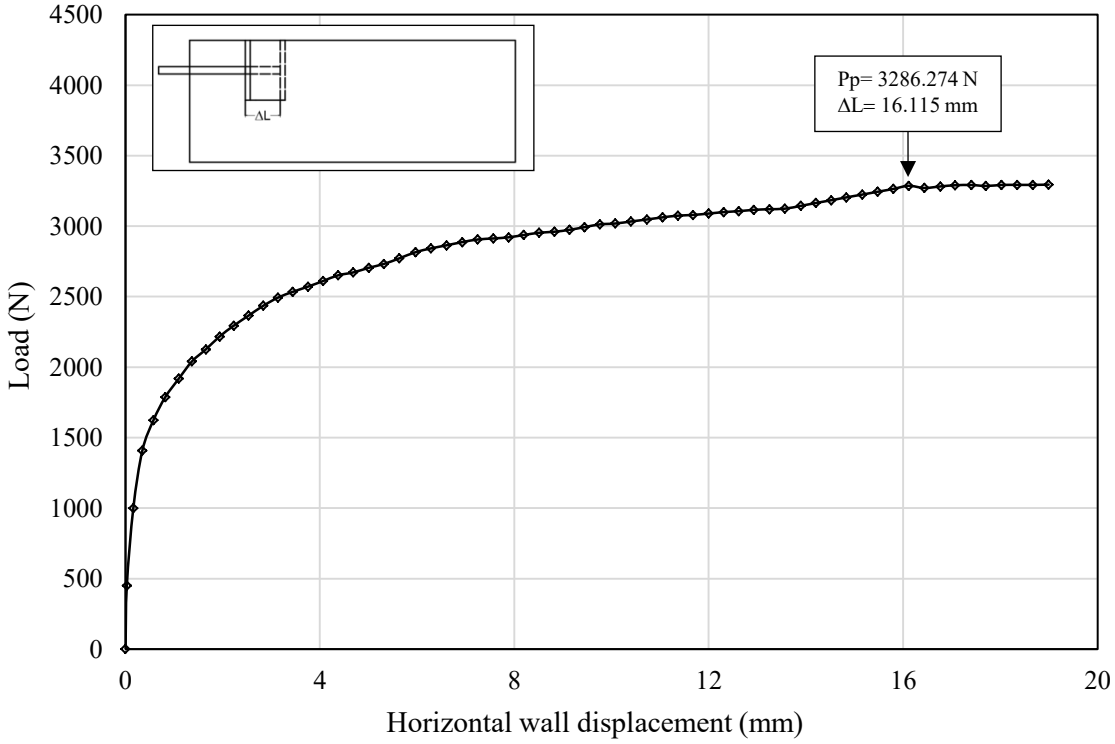

(a)

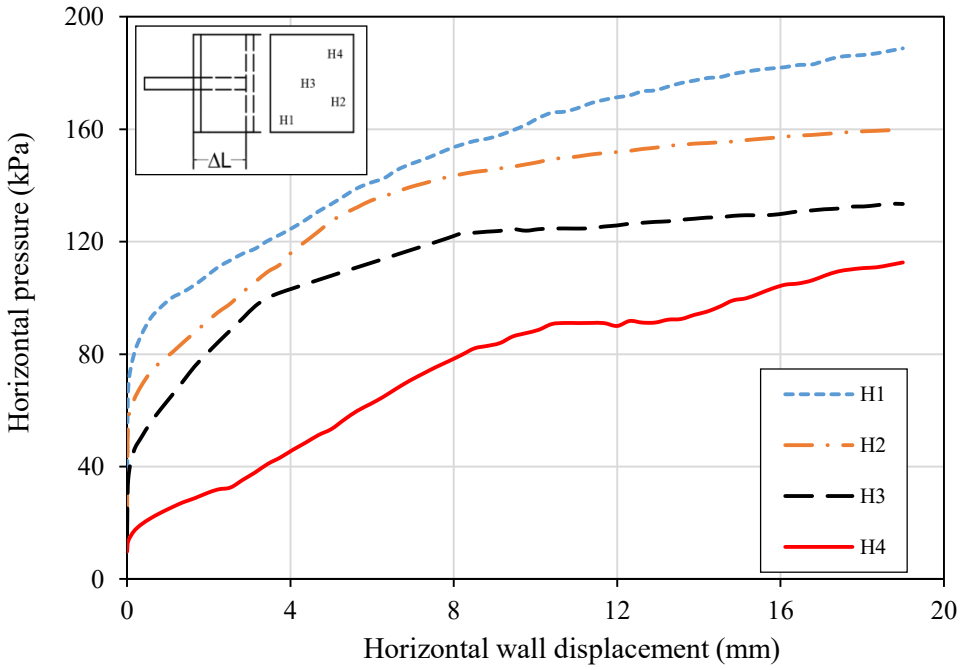

(b)

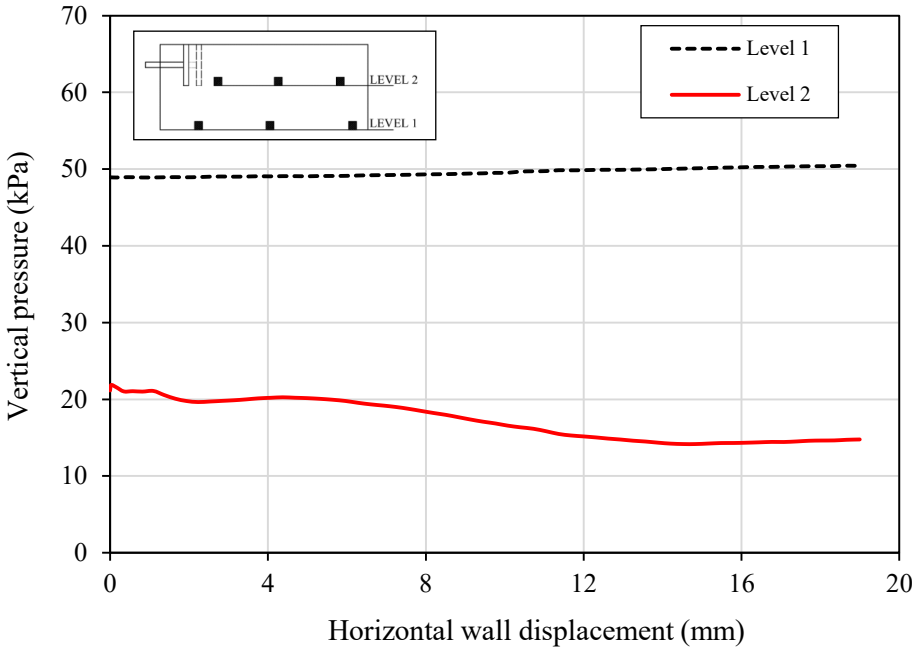

(c)

Fig. 5.11. Results for test no. 11 (Se3) for soil C – C_p =12.5%: (a) Load – displacement curve (load cell reading); (b) Load – displacement curves for each transducer; (c) Vertical pressure in the soil mass versus the wall displacement

Results for test no. 12

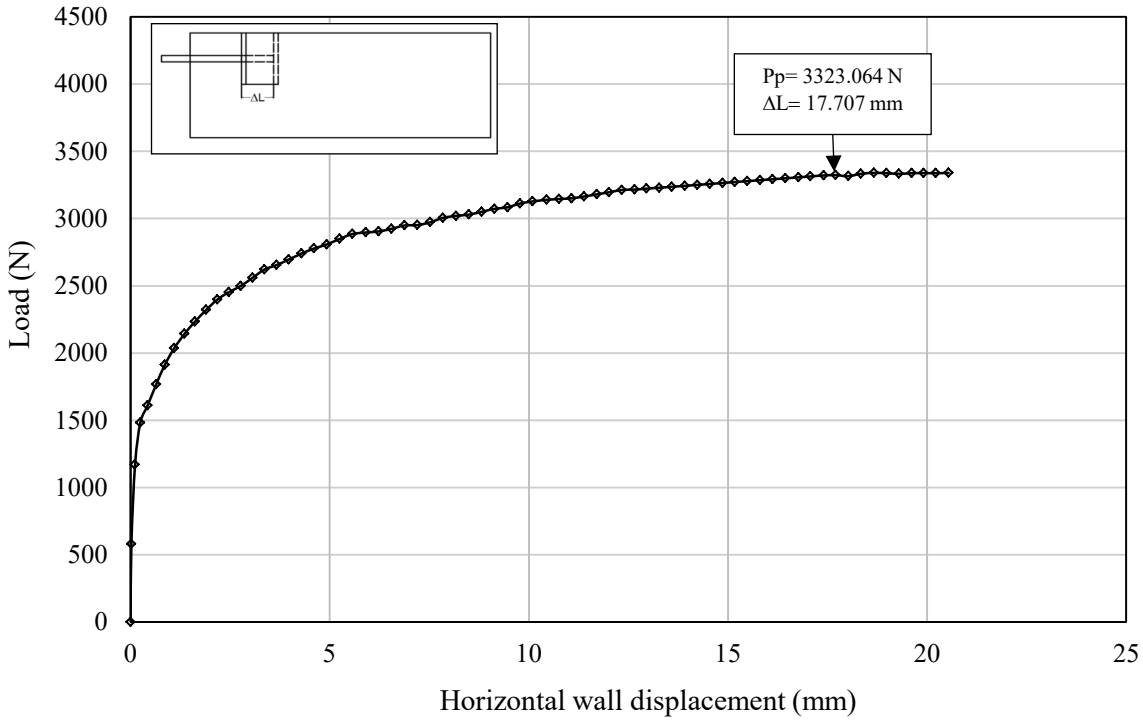

(a)

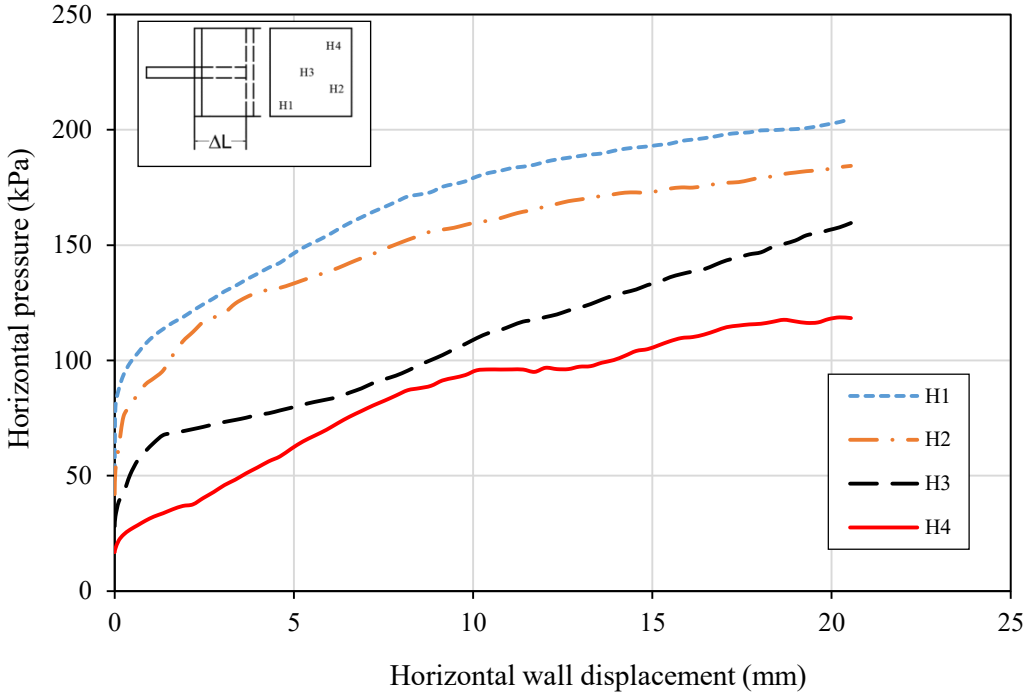

(b)

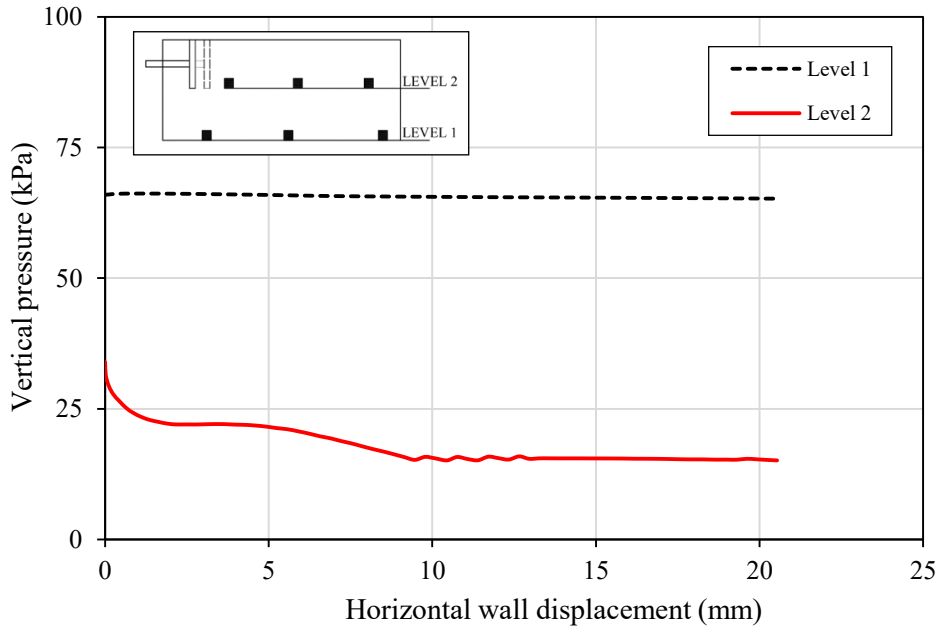

(c)

Fig. 5.12. Results for test no. 12 (Se3) for soil D – C_p =18%: (a) Load – displacement curve (load cell reading); (b) Load – displacement curves for each transducer; (c) Vertical pressure in the soil mass versus the wall displacement

Results for test no. 13

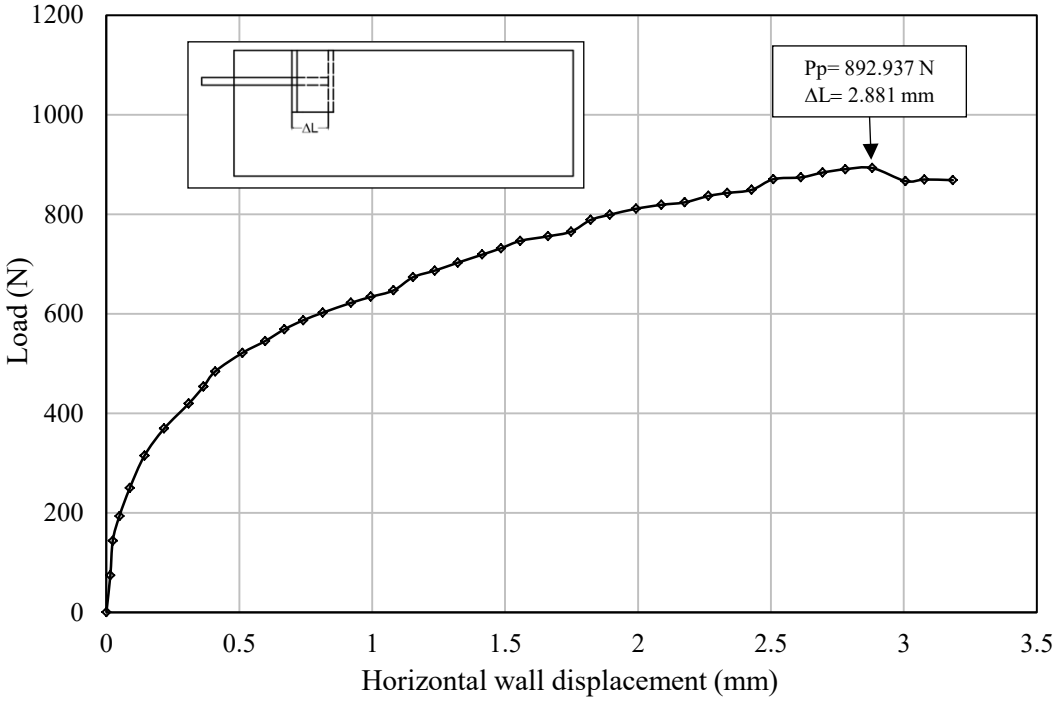

(a)

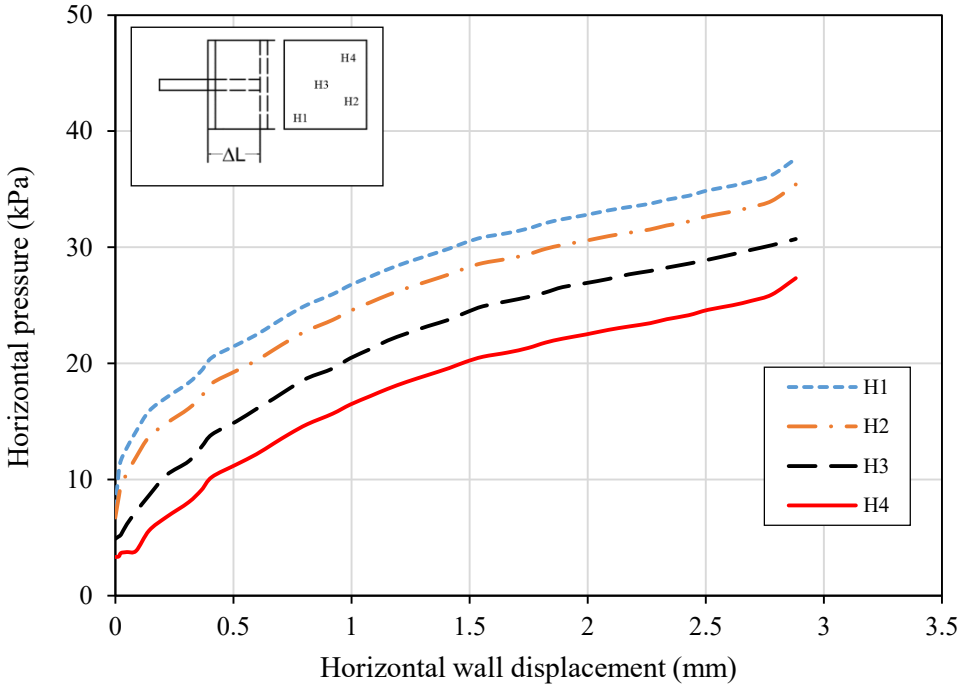

(b)

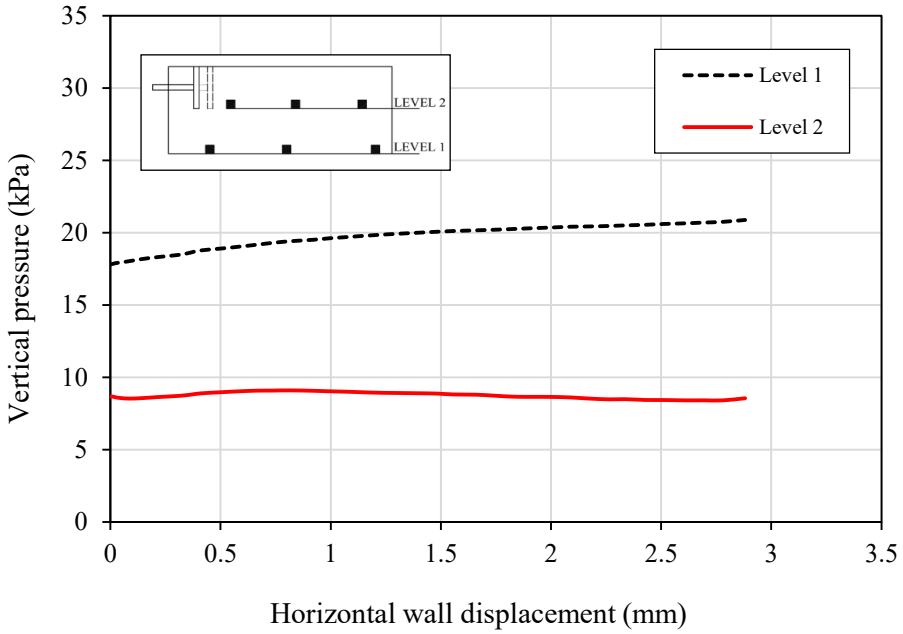

(c)

Fig. 5.13. Results for test no.13 (Se1') for soil A – C_p =4.2%: (a) Load – displacement curve (load cell reading); (b) Load – displacement curves for each transducer; (c) Vertical pressure in the soil mass versus the wall displacement

Results for test no. 14

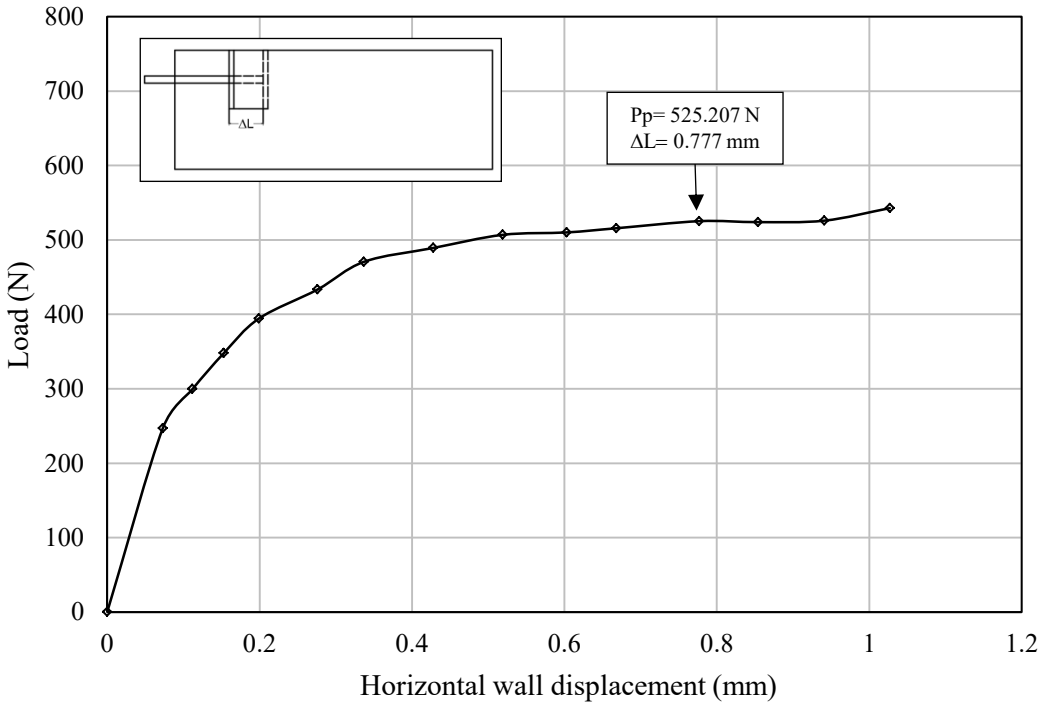

(a)

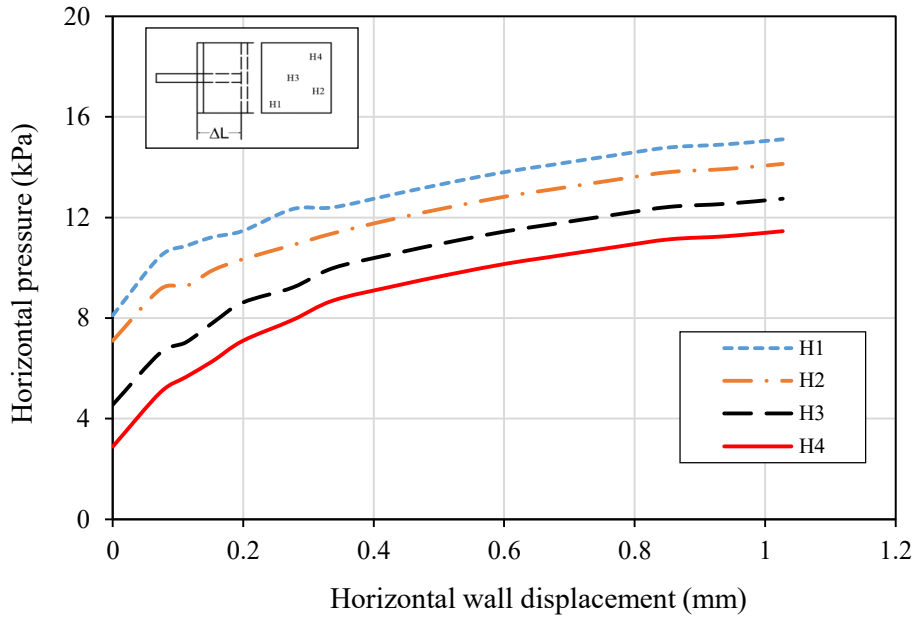

(b)

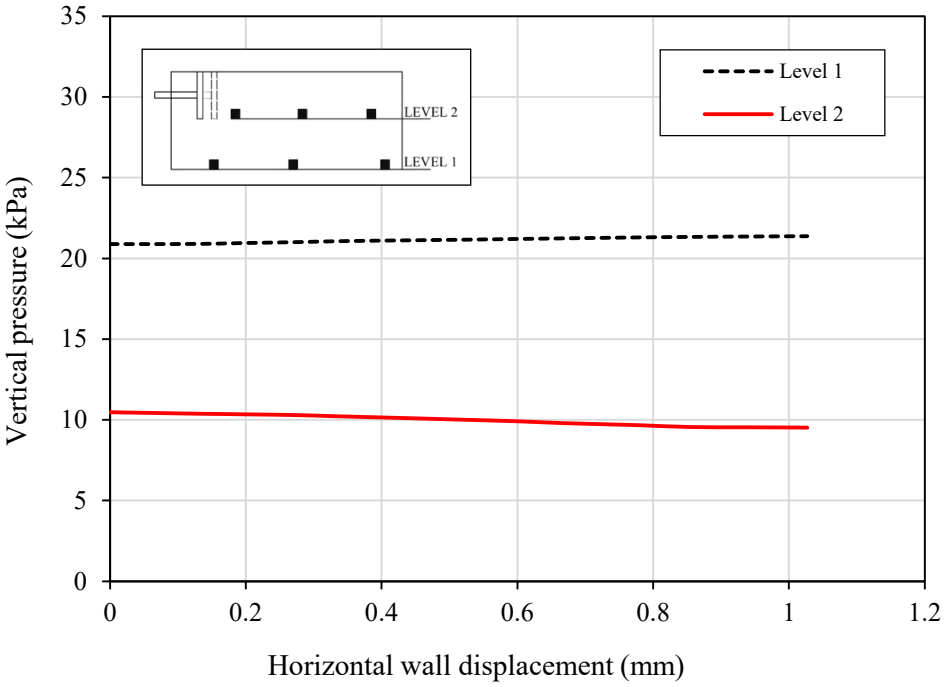

(c)

Fig. 5.14. Results for test no.14 (Se1') for soil B – C_p =9.0%: (a) Load – displacement curve (load cell reading); (b) Load – displacement curves for each transducer; (c) Vertical pressure in the soil mass versus the wall displacement

Results for test no. 15

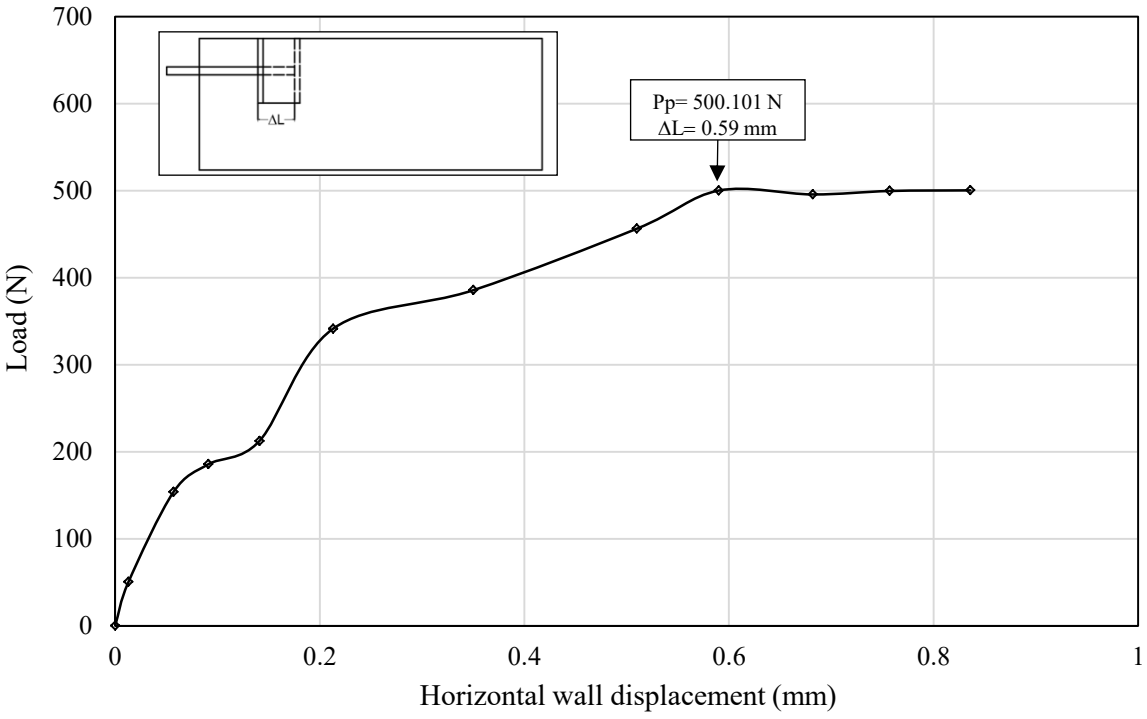

(a)

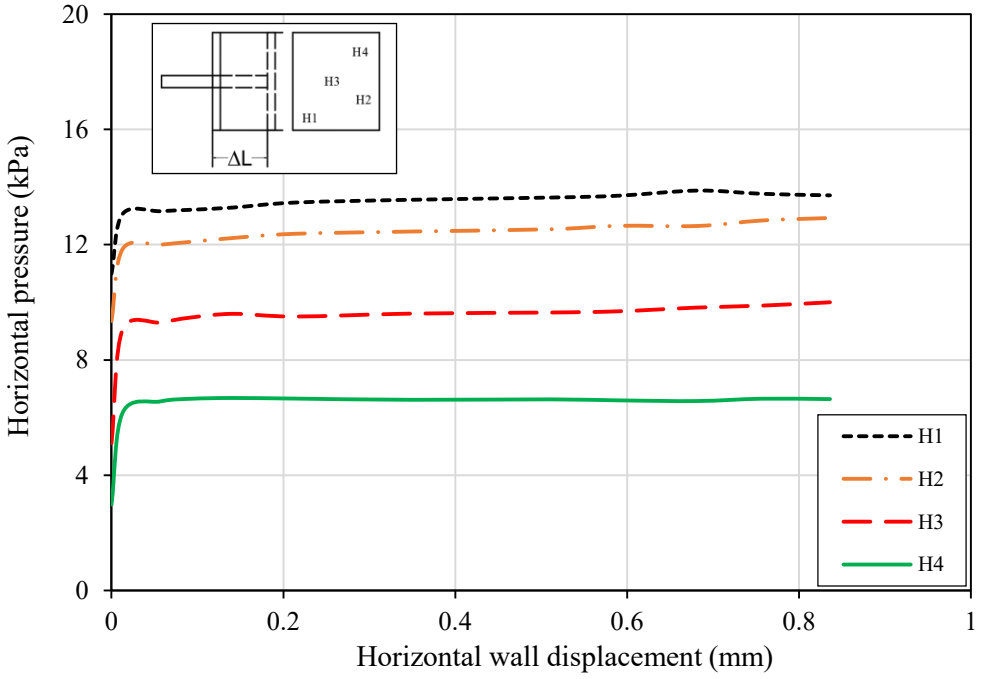

(b)

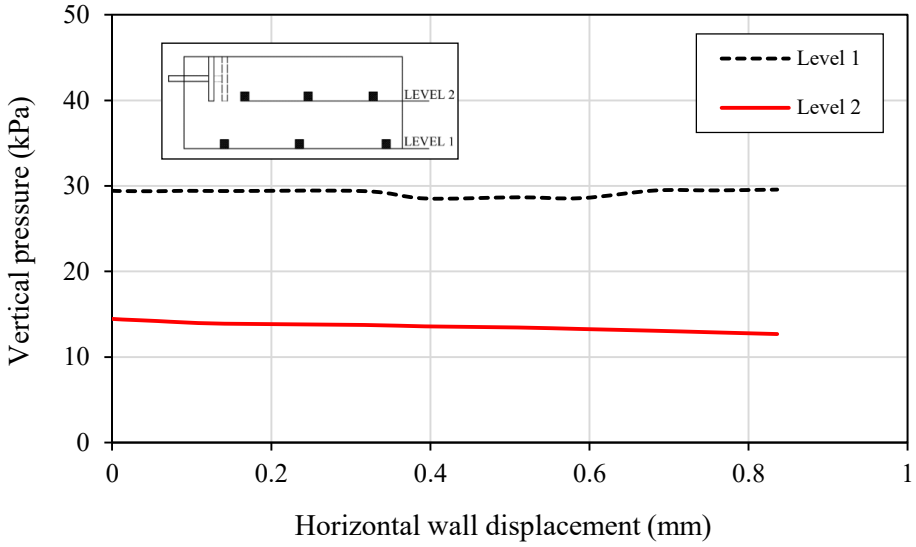

(c)

Fig. 5.15. Results for test no. 15 (Se1') for soil C – C_p =12.5%: (a) Load – displacement curve (load cell reading); (b) Load – displacement curves for each transducer; (c) Vertical pressure in the soil mass versus the wall displacement

Results for test no. 16

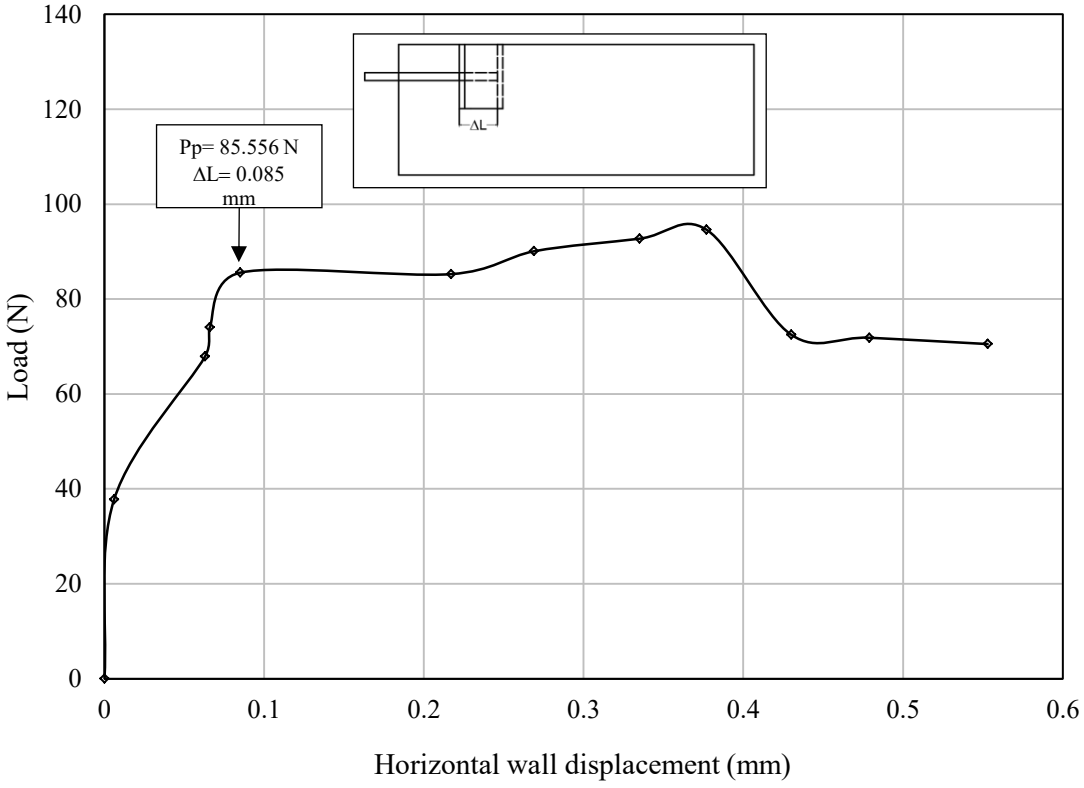

(a)

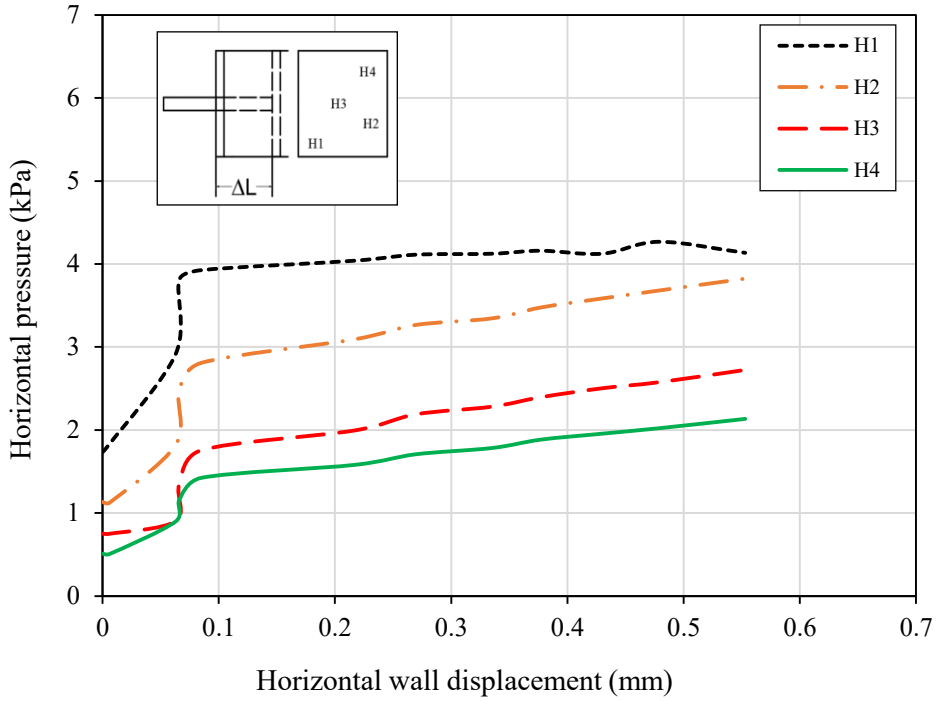

(b)

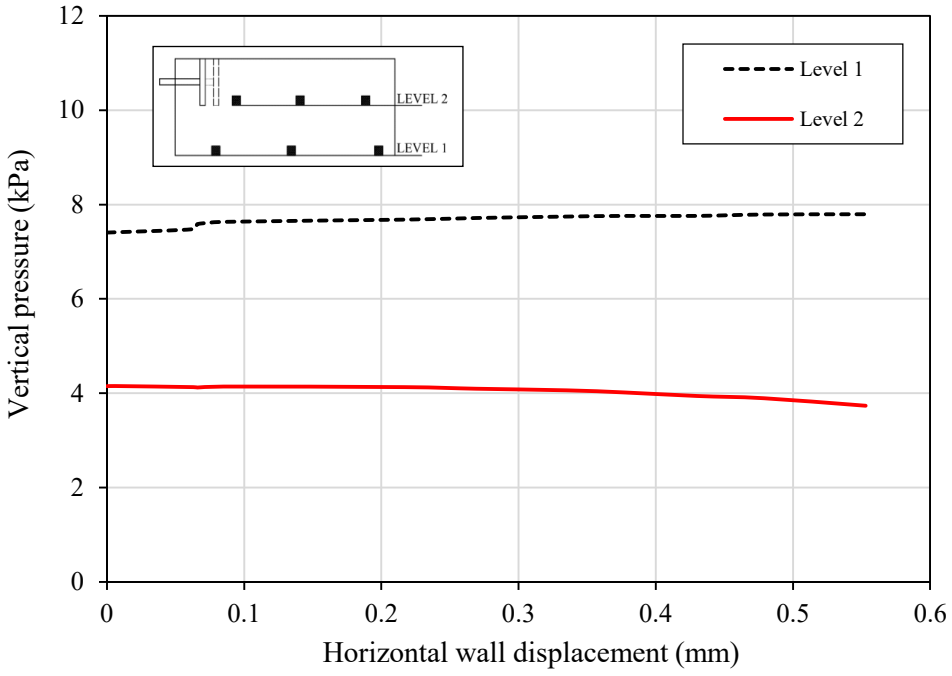

(c)

Fig. 5.16. Results for test no.16 (Se1') for soil D – C_p =18%: (a) Load – displacement curve (load cell reading); (b) Load – displacement curves for each transducer; (c) Vertical pressure in the soil mass versus the wall displacement

Results for test no. 17

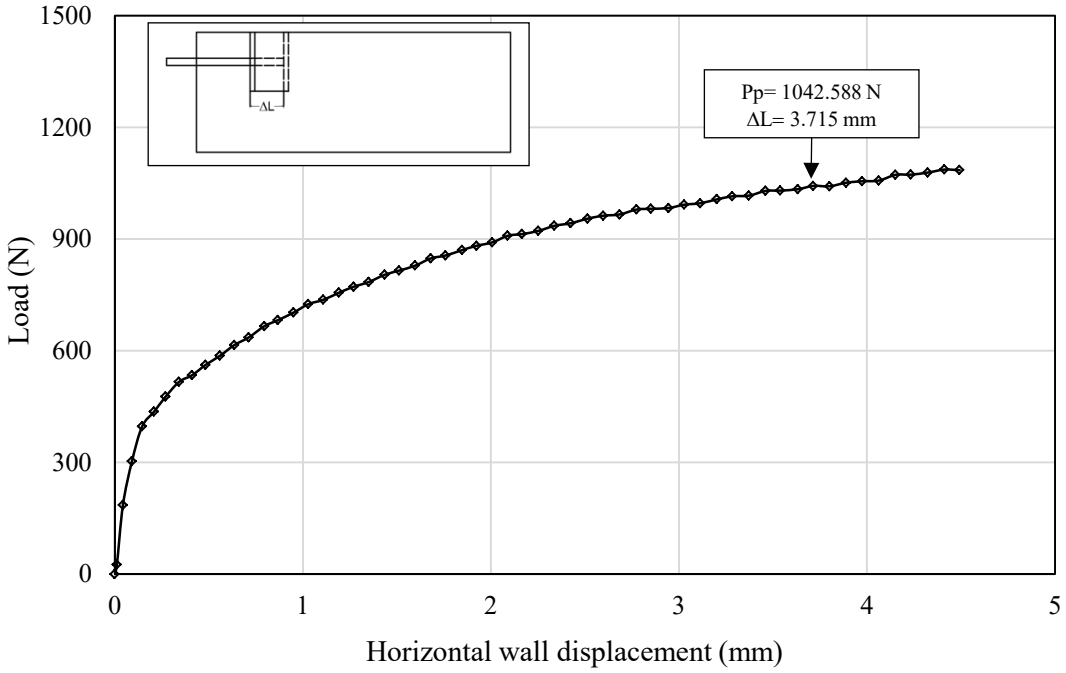

(a)

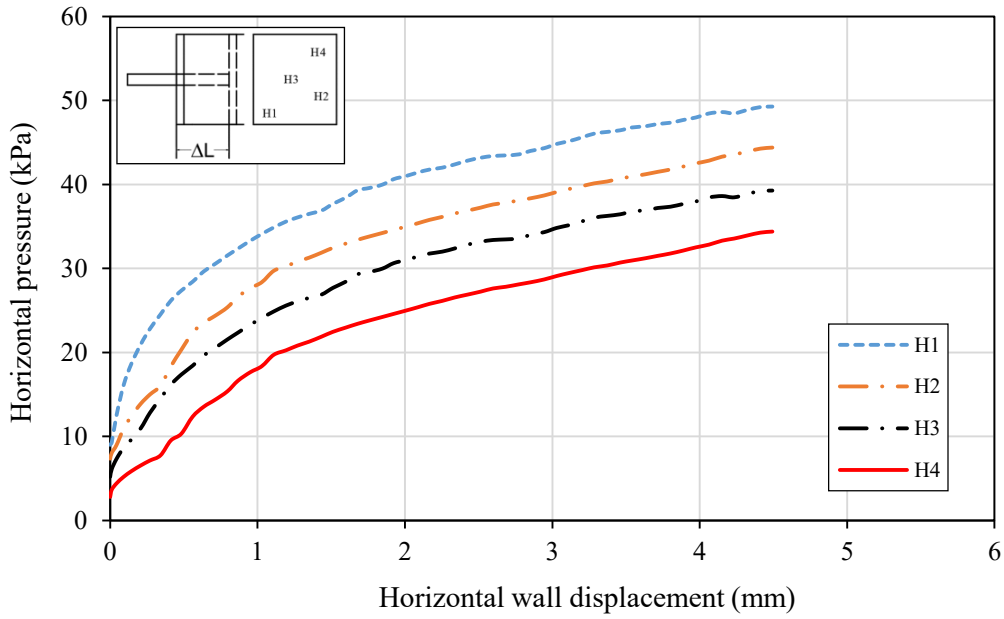

(b)

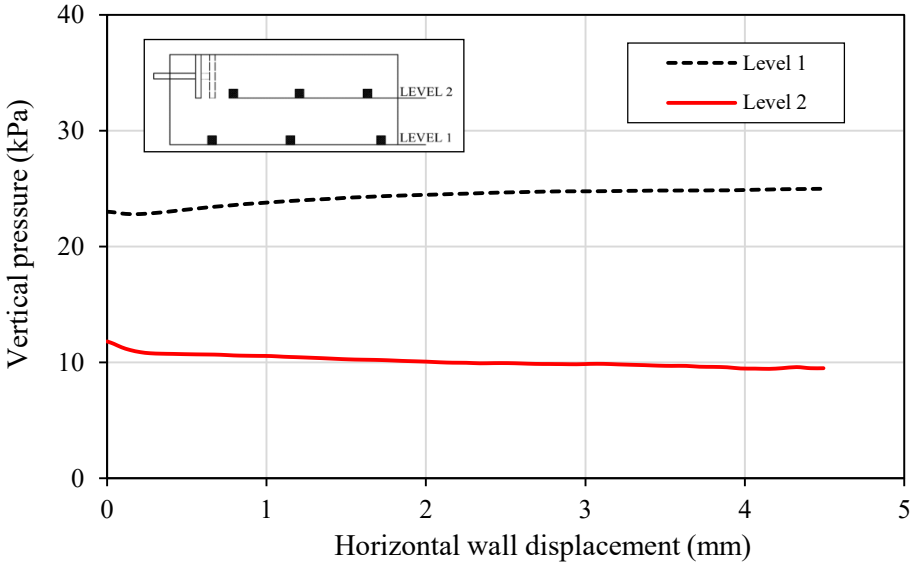

(c)

Fig. 5.17. Results for test no. 17 (Se2') for soil A – C_p =4.2%: (a) Load – displacement curve (load cell reading); (b) Load – displacement curves for each transducer; (c) Vertical pressure in the soil mass versus the wall displacement

Results for test no. 18

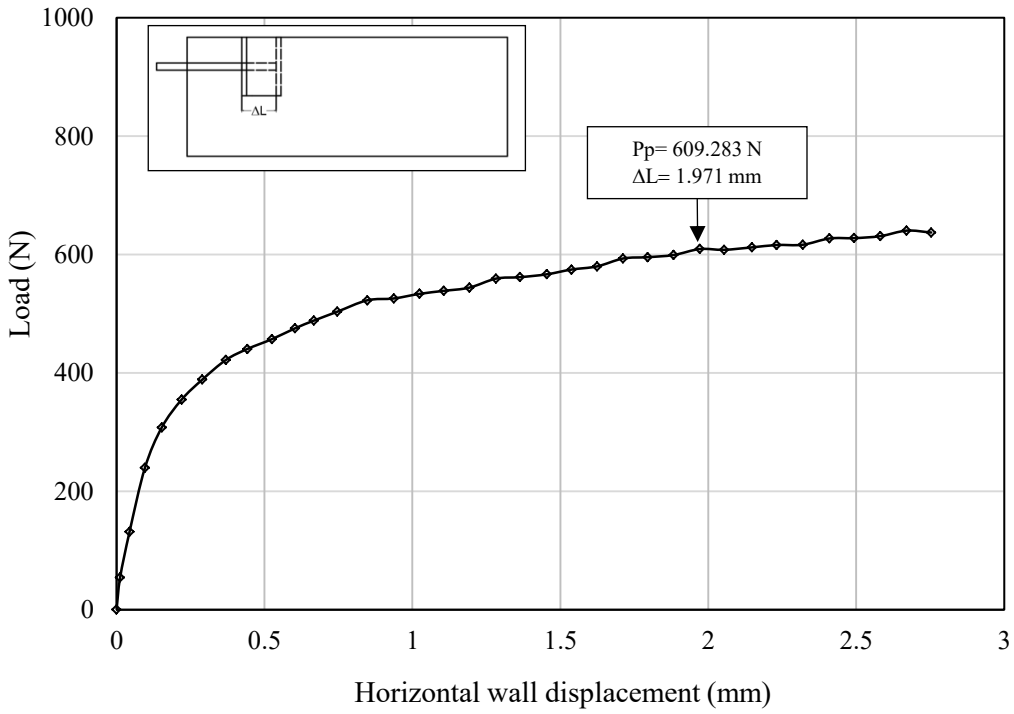

(a)

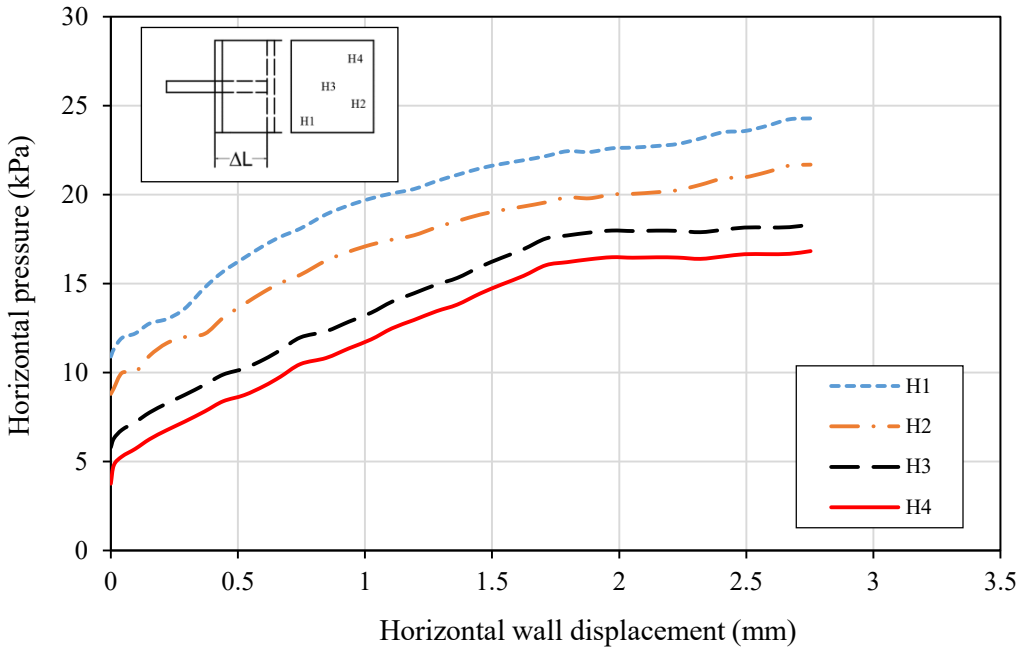

(b)

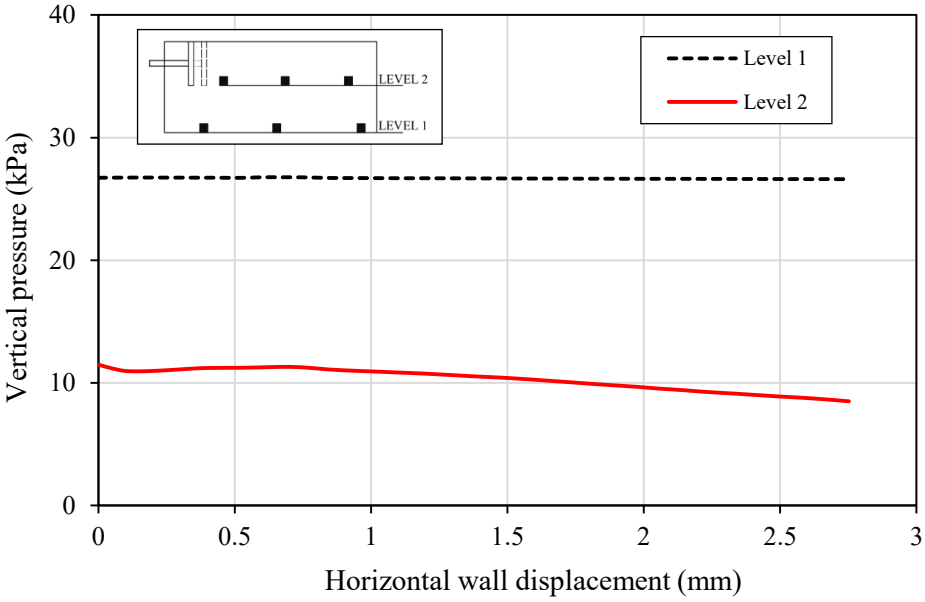

(c)

Fig. 5.18. Results for test no.18 (Se2') for soil B – C_p =9.0%): (a) Load – displacement curve (load cell reading); (b) Load – displacement curves for each transducer; (c) Vertical pressure in the soil mass versus the wall displacement

Results for test no. 19

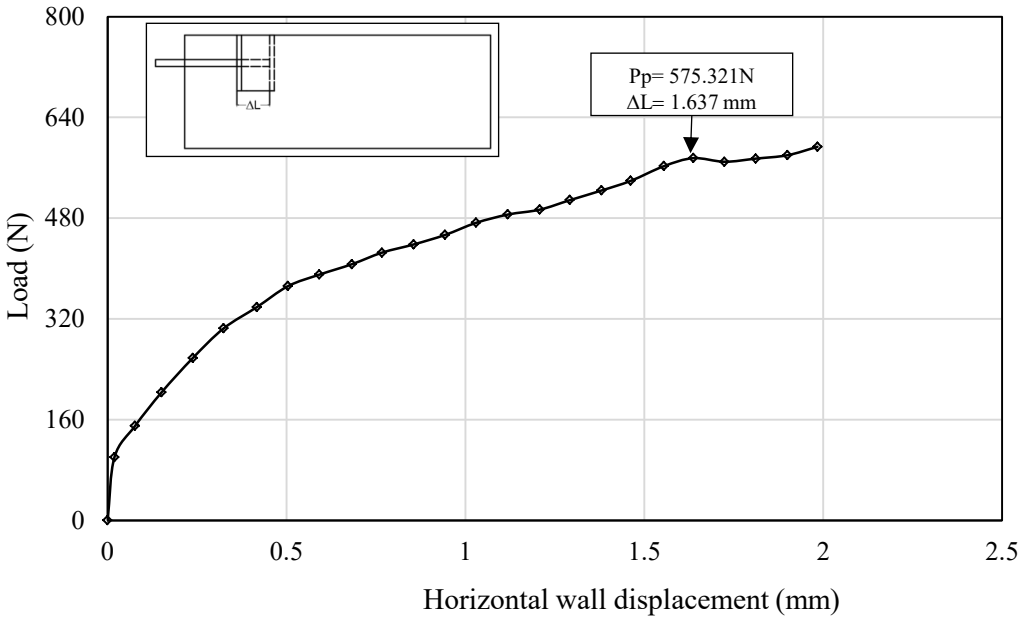

(a)

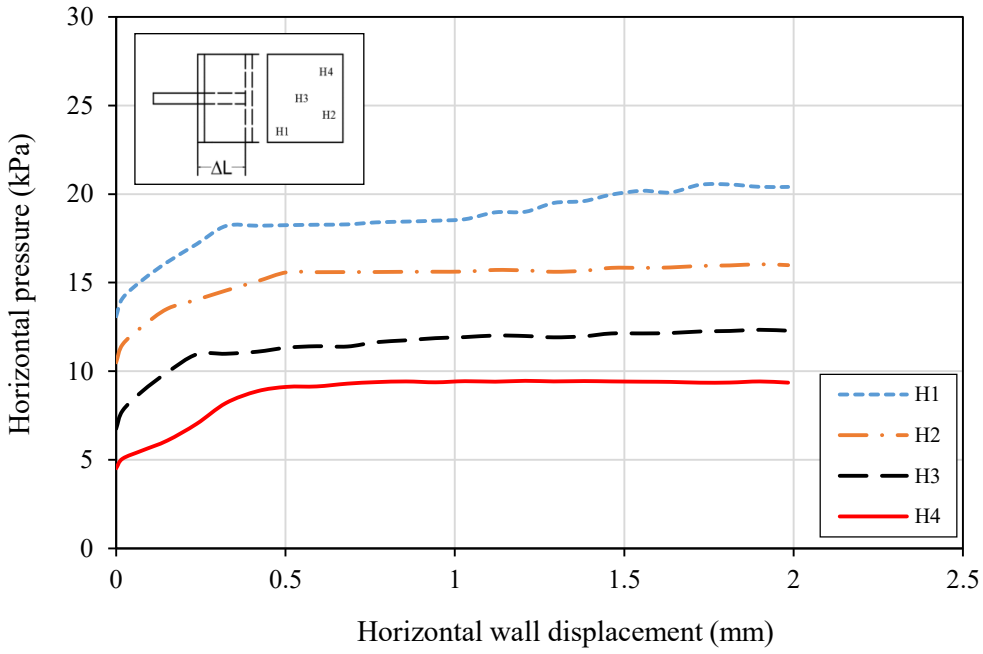

(b)

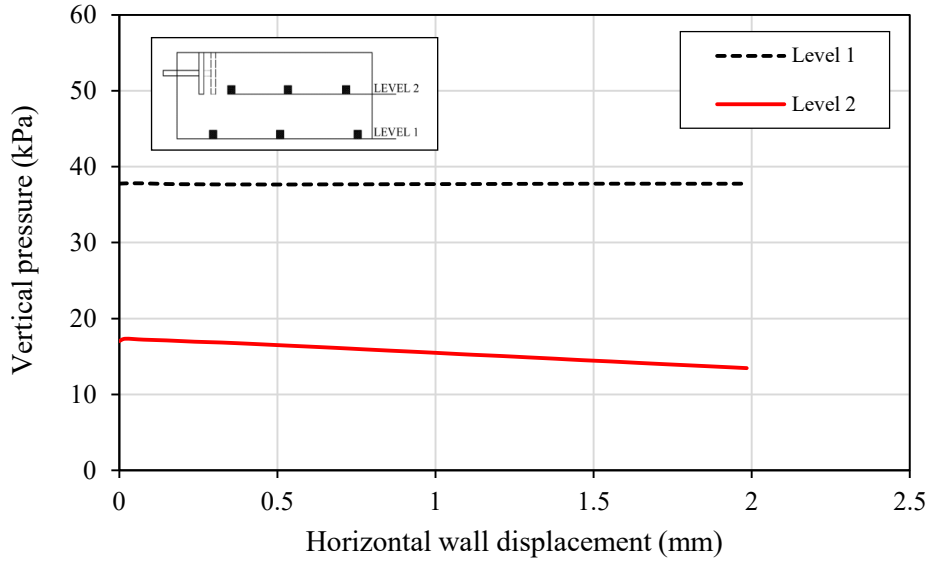

(c)

Fig. 5.19. Results for test no.19 (Se2') for soil C – C_p =12.5%): (a) Load – displacement curve (load cell reading); (b) Load – displacement curves for each transducer; (c) Vertical pressure in the soil mass versus the wall displacement

Results for test no. 20

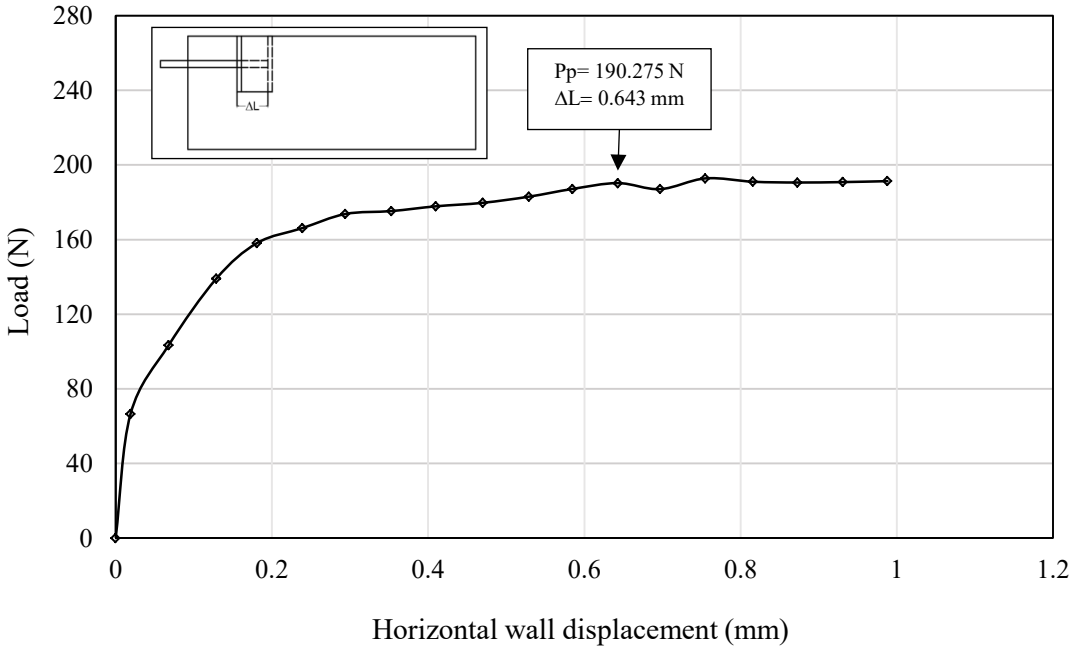

(a)

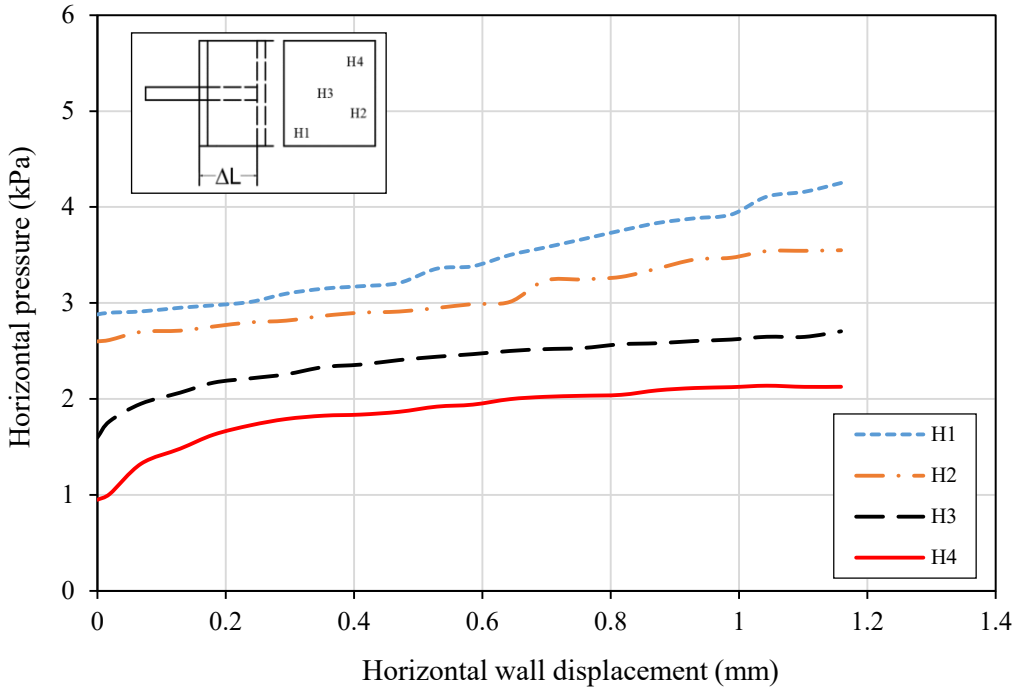

(b)

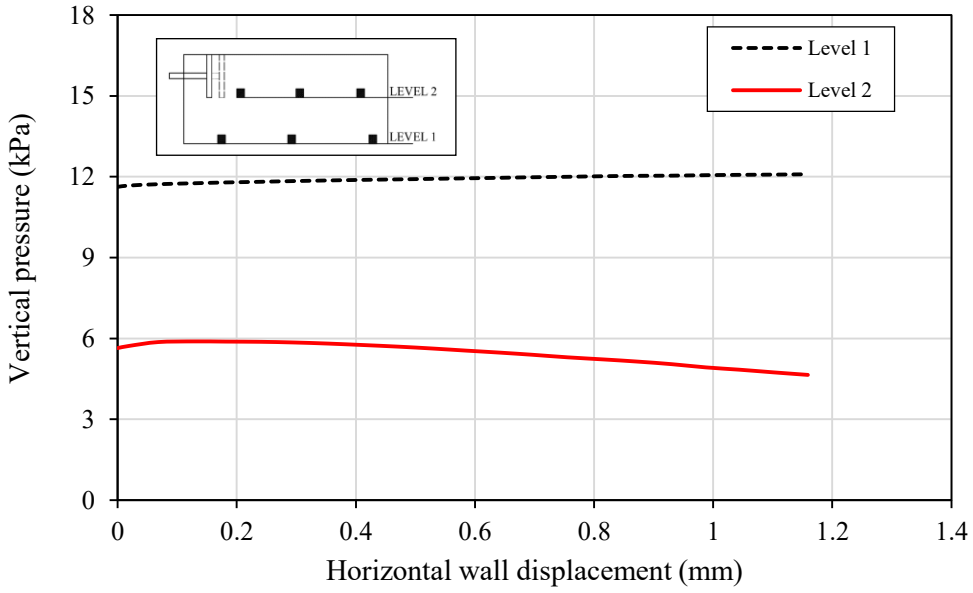

(c)

Fig. 5.20. Results for test no. 20 (Se2') for soil D – C_p =18%: (a) Load – displacement curve (load cell reading); (b) Load – displacement curves for each transducer; (c) Vertical pressure in the soil mass versus the wall displacement

Results for test no. 21

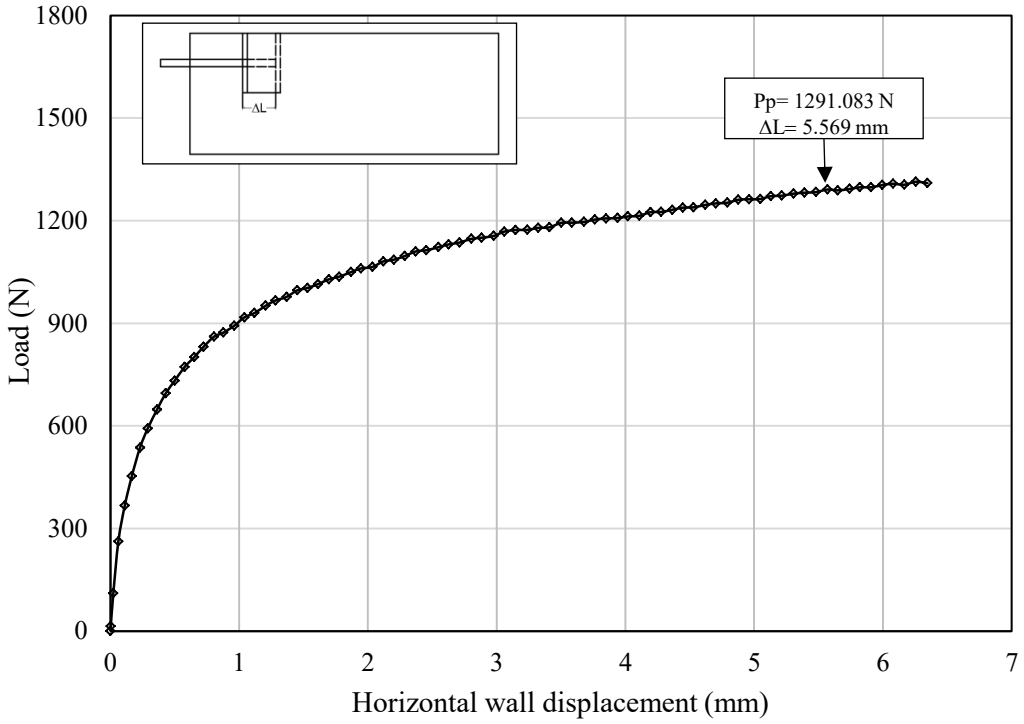

(a)

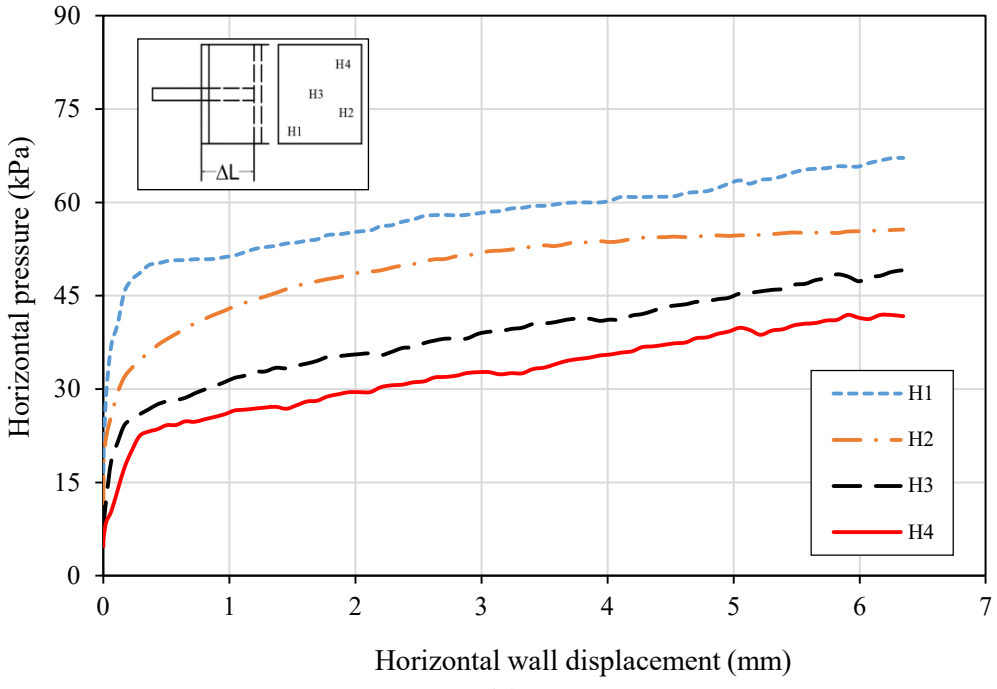

(b)

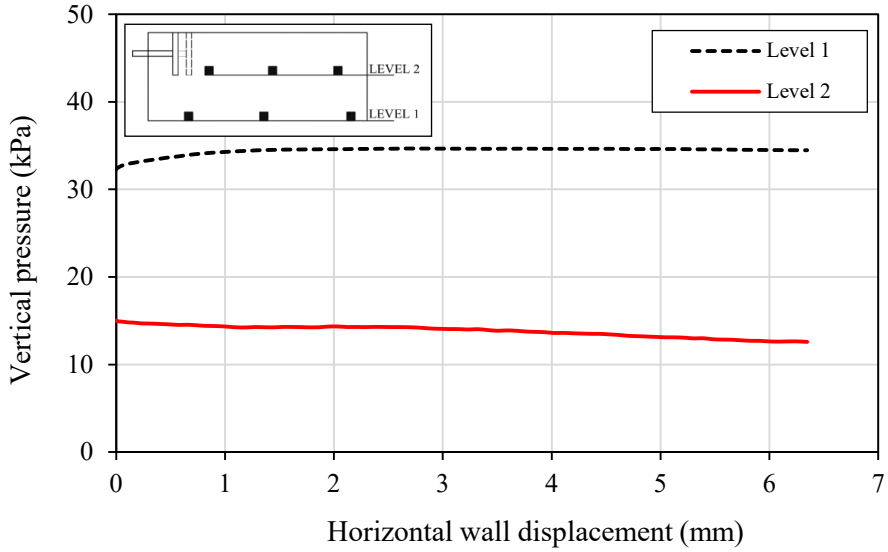

(c)

Fig. 5.21. Results for test no.21 (Se3') for soil A – C_p =4.2%: (a) Load – displacement curve (load cell reading); (b) Load – displacement curves for each transducer; (c) Vertical pressure in the soil mass versus the wall displacement

Results for test no. 22

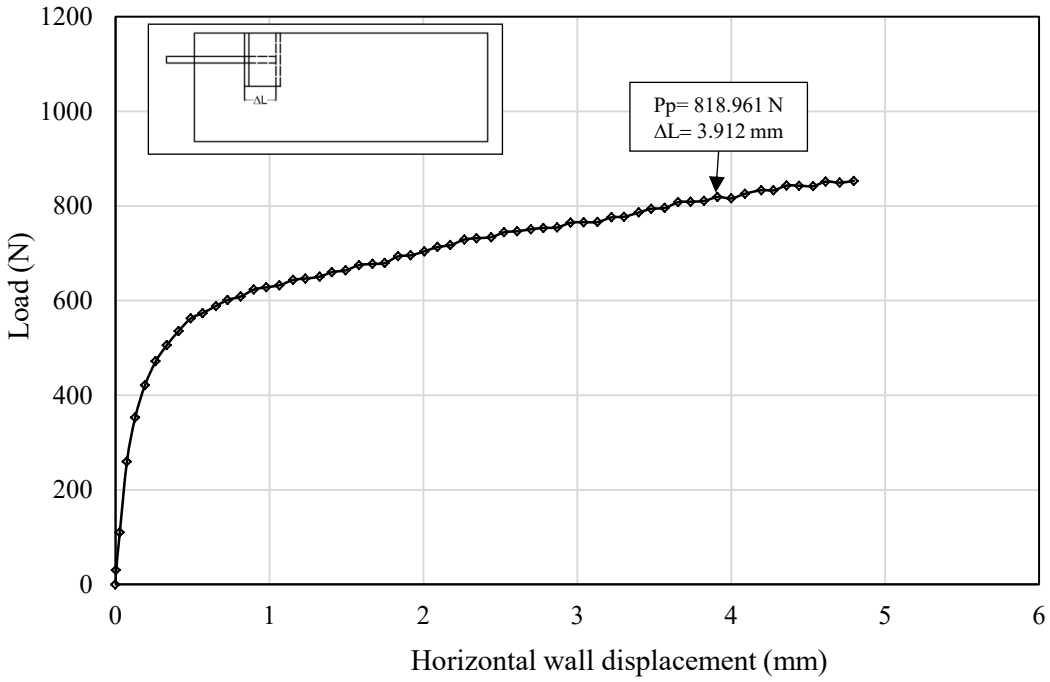

(a)

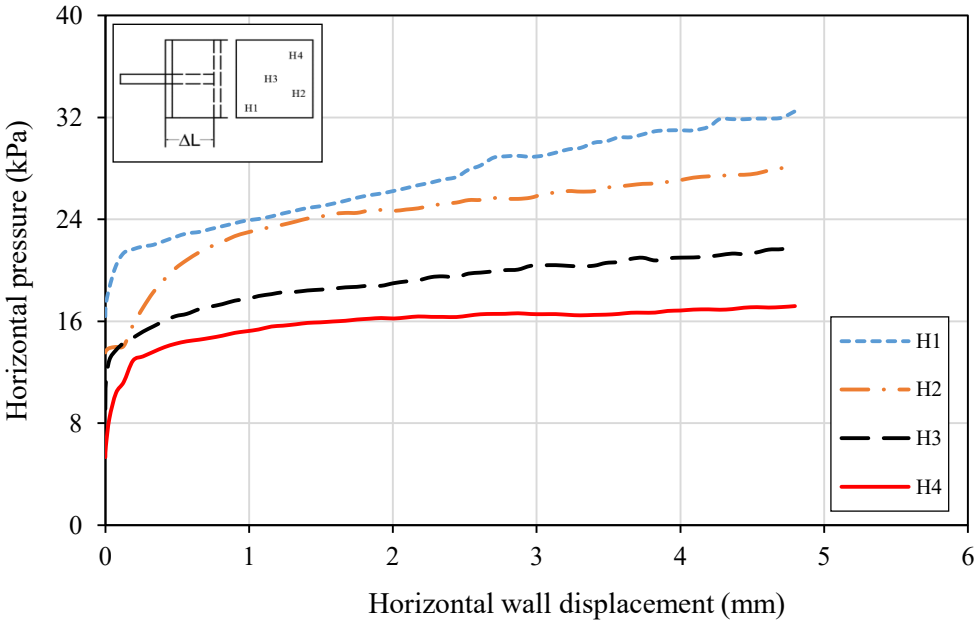

(b)

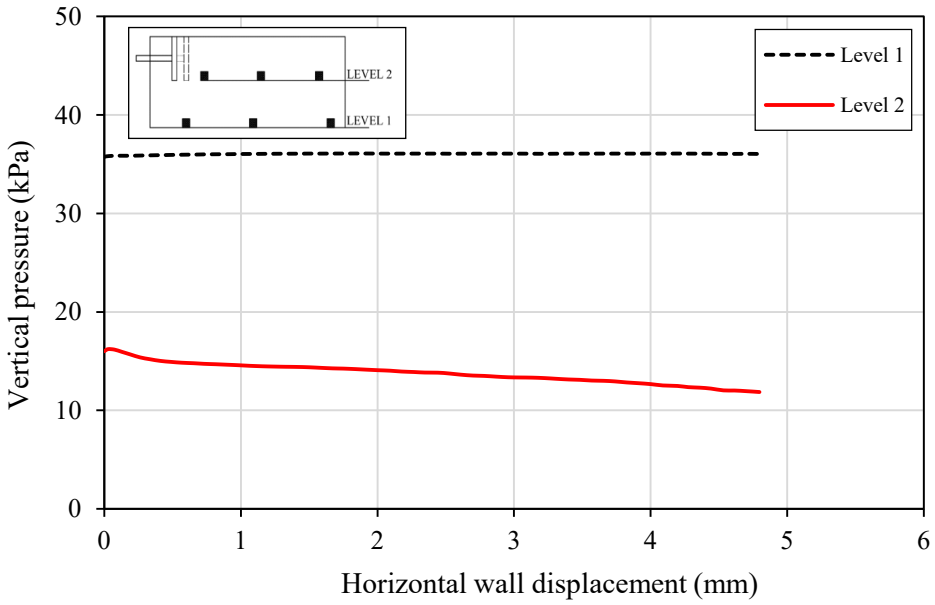

(c)

Fig. 5.22. Results for test no. 22 (Se3') for soil B – C_p =9.0%: (a) Load – displacement curve (load cell reading); (b) Load – displacement curves for each transducer; (c) Vertical pressure in the soil mass versus the wall displacement

Results for test no. 23

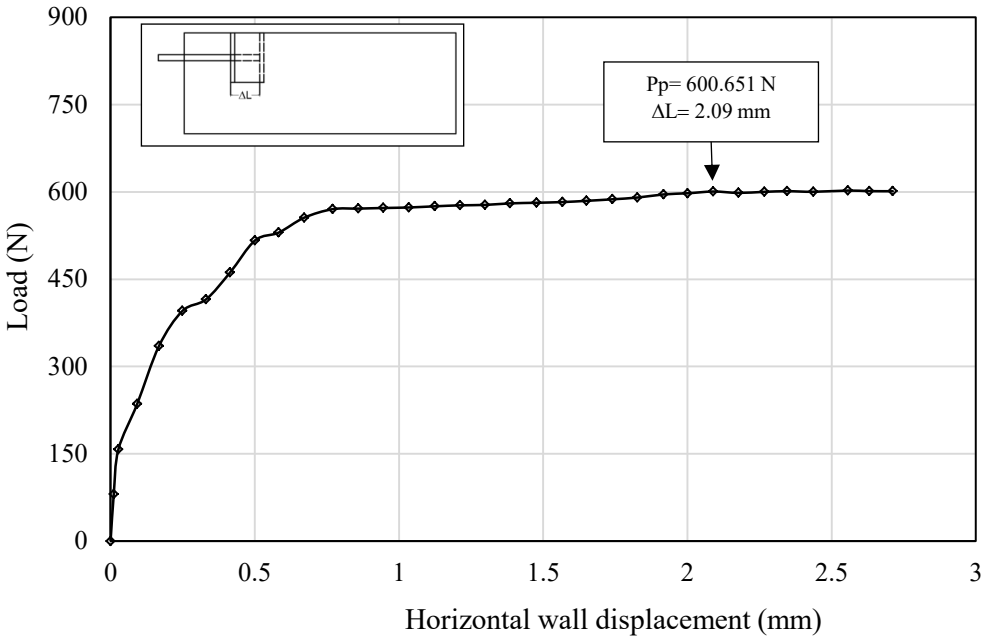

(a)

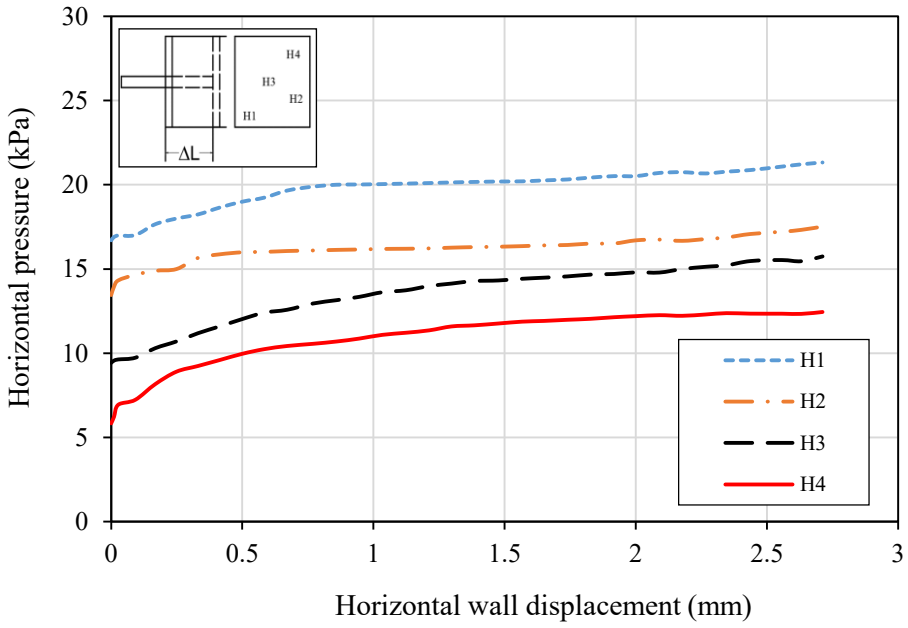

(b)

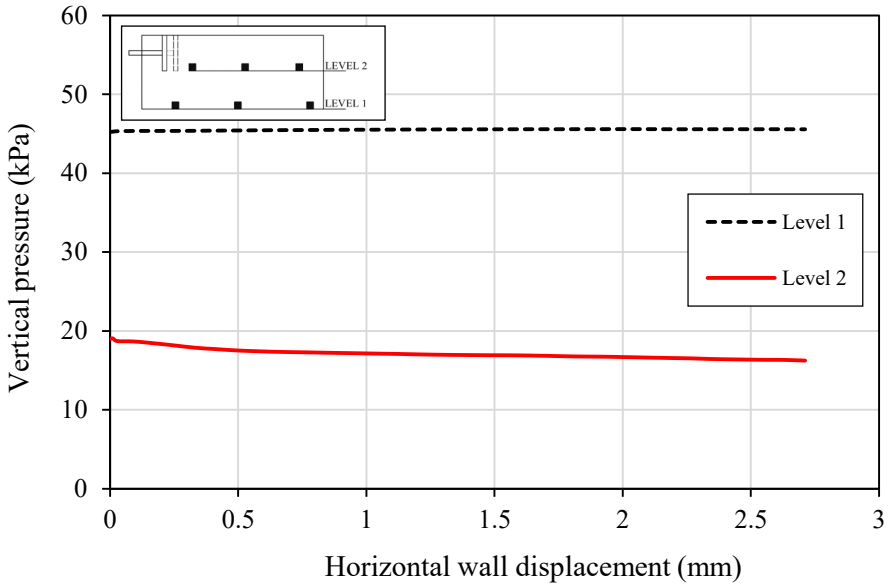

(c)

Fig. 5.23. Results for test no. 23 (Se3') for soil C – C_p =12.5%: (a) Load – displacement curve (load cell reading); (b) Load – displacement curves for each transducer; (c) Vertical pressure in the soil mass versus the wall displacement

Results for test no. 24

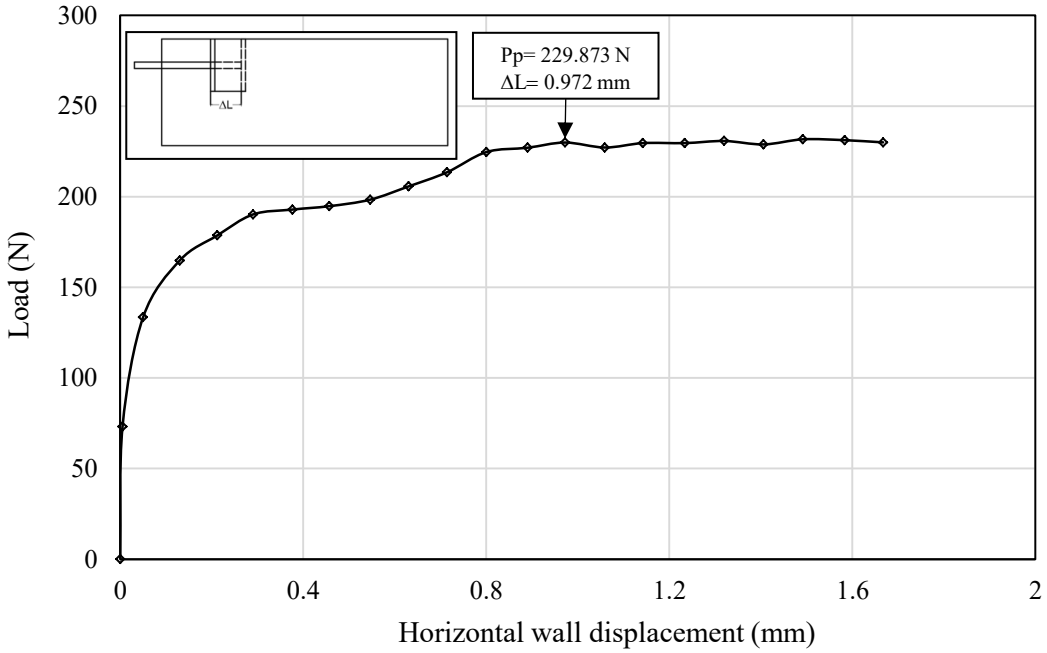

(a)

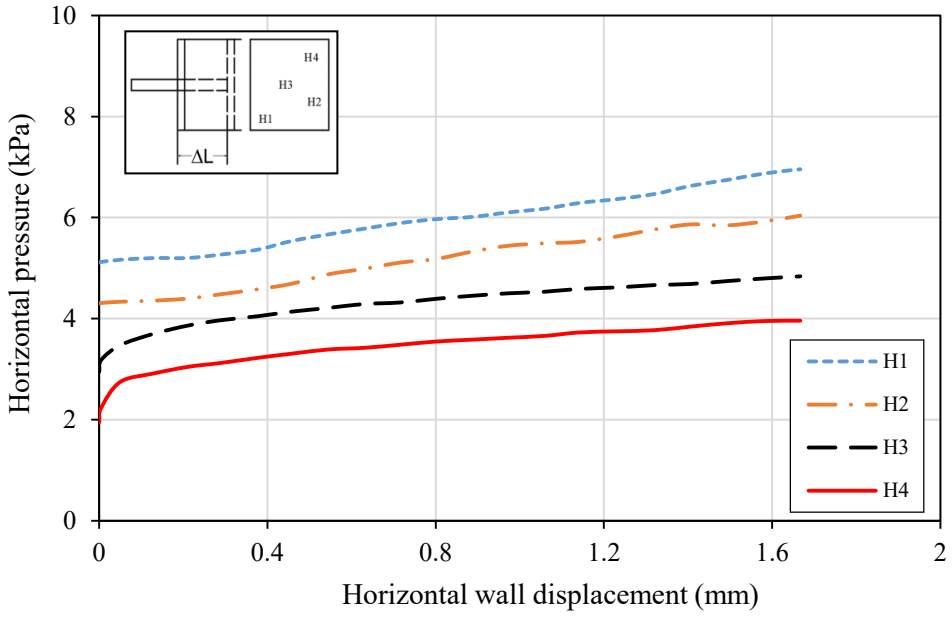

(b)

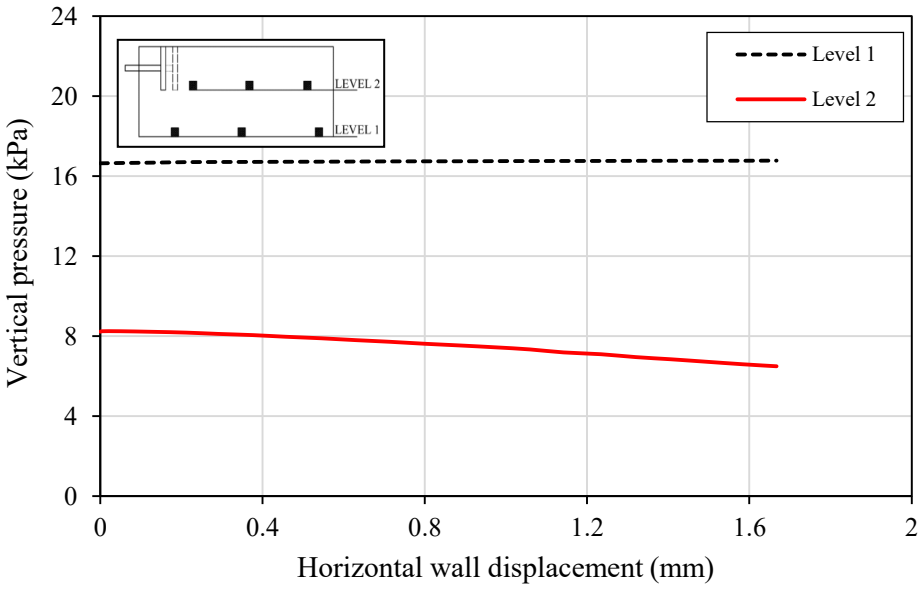

(c)

Fig. 5.24. Results for test no. 24 (Se3') for soil D – C_p =18%: (a) Load – displacement curve (load cell reading); (b) Load – displacement curves for each transducer; (c) Vertical pressure in the soil mass versus the wall displacement

Results from repeatability tests (for studying the repeatability test results): These results are presented graphically in Figures 5.25 to 5.26.

The first set of repeated tests were performed on the dry soil. The second set of the repeated tests were conducted on saturated soil. The results of two tests (original and repeated) performed under the same conditions with the same soil were compared together. Figures 5.25 and 5.26 present the original and repeated passive earth pressure test results for the dry and saturated soil D $-C_p$=18%, respectively. It can be generally seen from these figures that the results obtained from two tests performed on the same soil under the same conditions are almost identical. Thus, the comparison shows acceptable consistency in the test results.

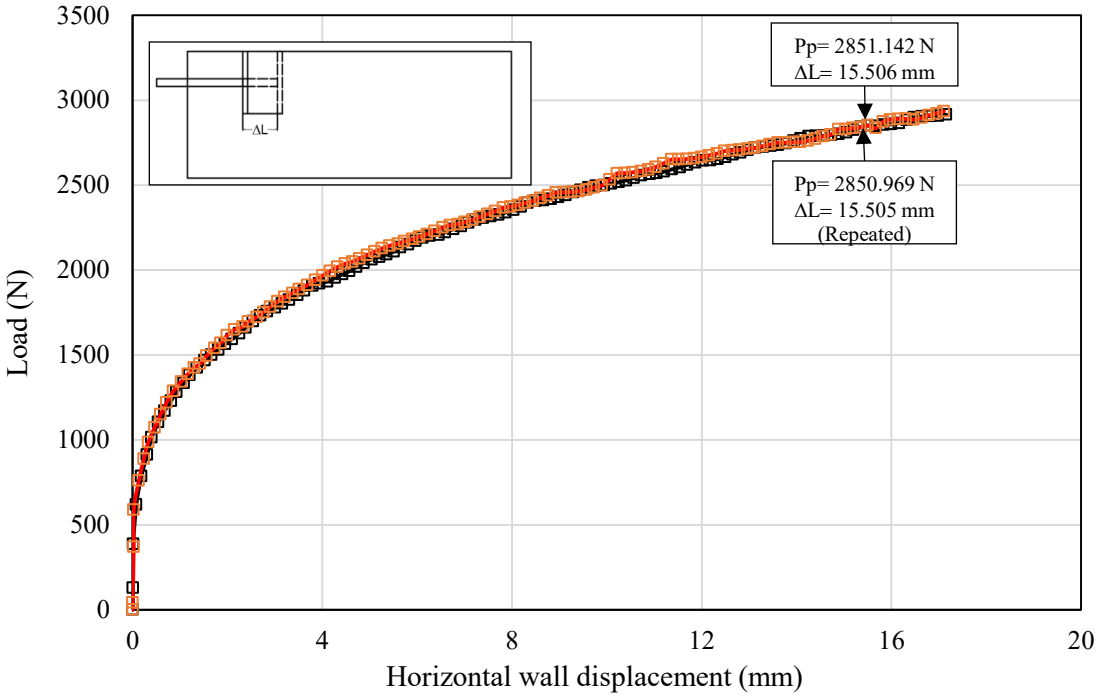

(a)

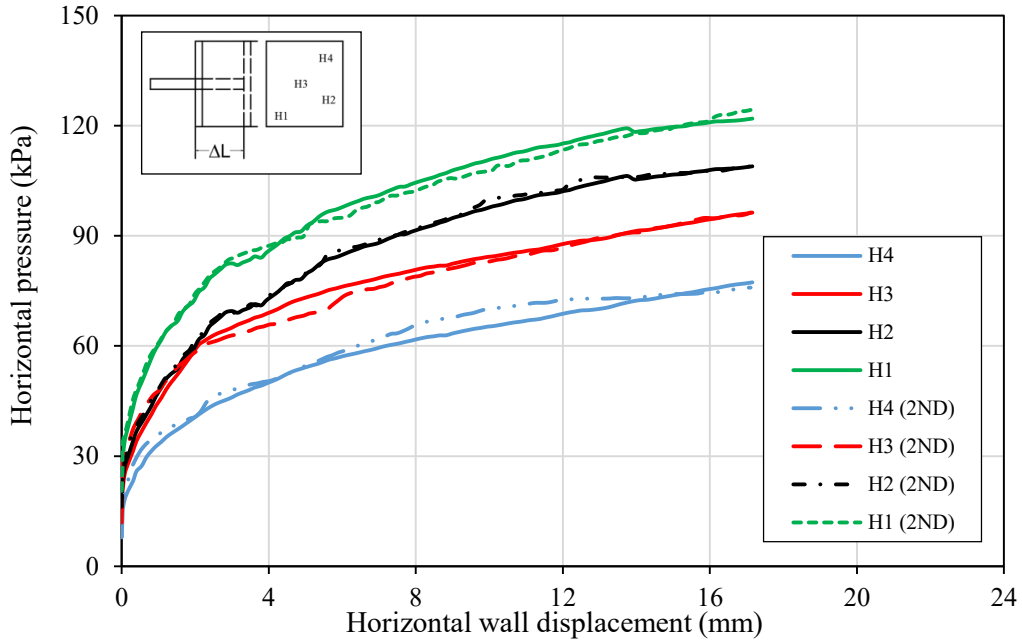

(b)

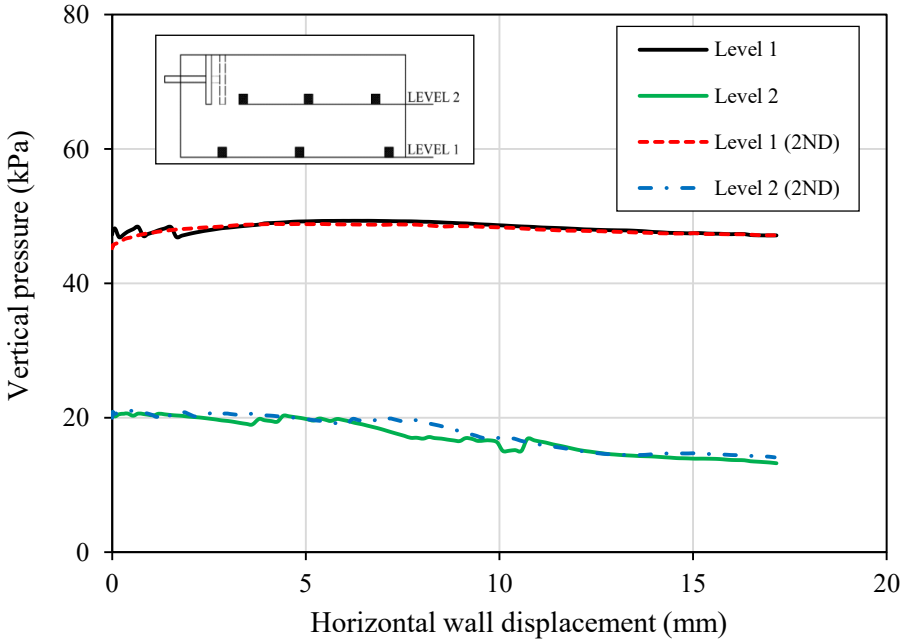

(c)

Fig. 5.25. Results from test no. 4 and test no. 4* (2^{ND}) performed on the dry soil D – C_p=18%: (a) Load – displacement curve (load cell reading); (b) Load-displacement curve (transducers readings); (c) Vertical pressure in the soil mass versus horizontal wall displacement

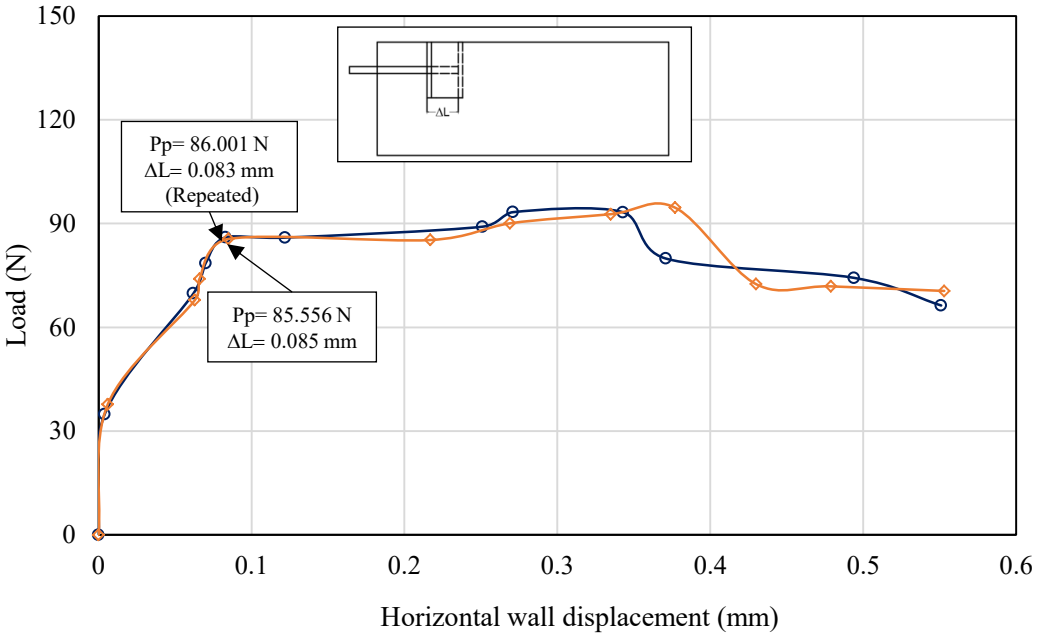
Pp= 86.001 N
ΔL= 0.083 mm
(Repeated)
Pp= 85.556 N
ΔL= 0.085 mm
ΔL
Load (N)
Horizontal wall displacement (mm)
0
30
60
90
120
150
0
0.1
0.2
0.3
0.4
0.5
0.6

(a)

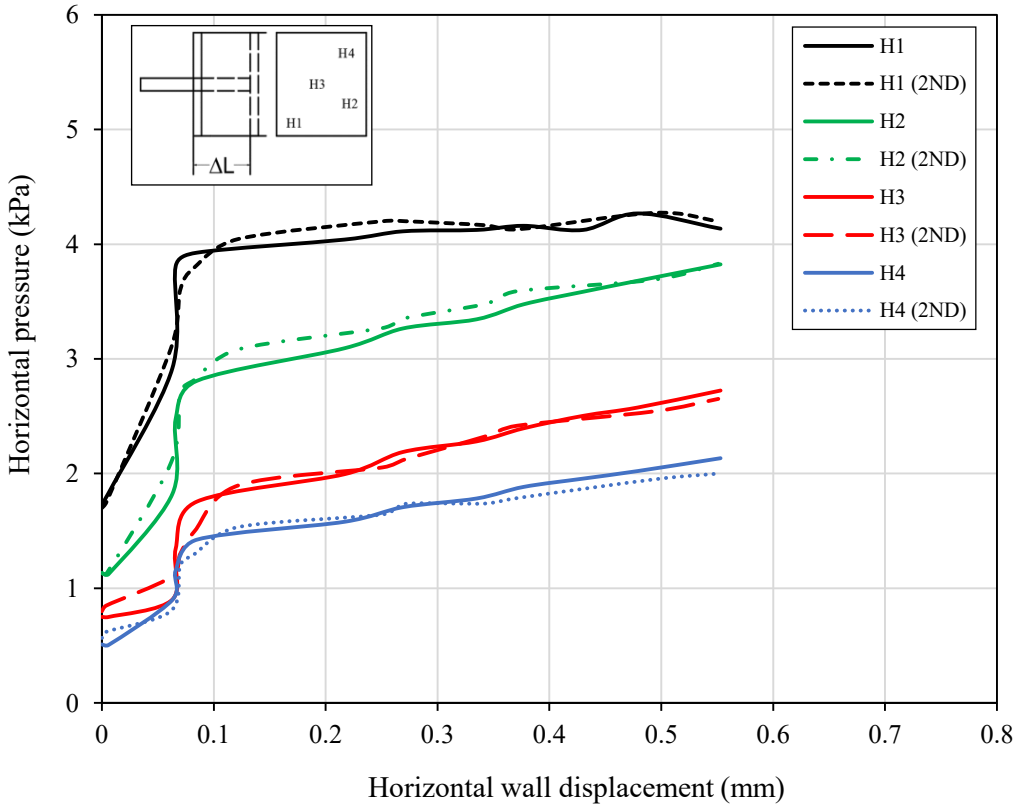
H1
H1 (2ND)
H2
H2 (2ND)
H3
H3 (2ND)
H4
H4 (2ND)
H4
H3
H2
H1
ΔL
Horizontal pressure (kPa)
Horizontal wall displacement (mm)
0
1
2
3
4
5
6
0
0.1
0.2
0.3
0.4
0.5
0.6
0.7
0.8

(b)

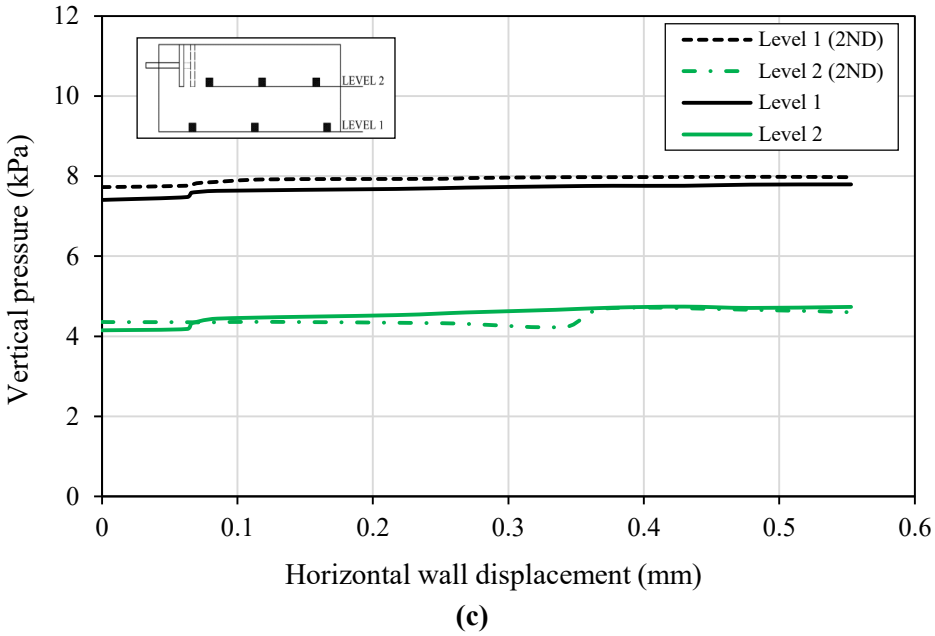

(c)

Fig. 5.26. Results from test no.16 and test no.16* (2^{ND}) performed on the saturated soil D – C_p=18%: (a) Load – displacement curve (load cell reading); (b) Load-displacement curve (transducers readings); (c) Vertical pressure in the soil mass versus horizontal wall displacement

5.3. Parametric study

Effect of clay content (collapse potential) on the passive earth pressure for dry collapsible soil

Figure 5.27 shows the variation in the passive earth force with respect to the horizontal wall displacement for different soil mixtures with different clay content, accordingly different collapse potential. It can be seen that the passive earth force and the wall displacement at failure increase with the increase of the collapse potential C_p of the soil. Accordingly, increasing the clay content in the mixture will increase the passive resistance of the soil. This can be explained by the fact that the clay is acting as a bonding agent, which increases the strength for the retained soil. It is of interest to note from this figure that by increasing the clay content from 6% to 8%, the passive earth force increases about 18%. The increase of the passive earth force is approximately 43% when increasing clay content from 6% to 14%.

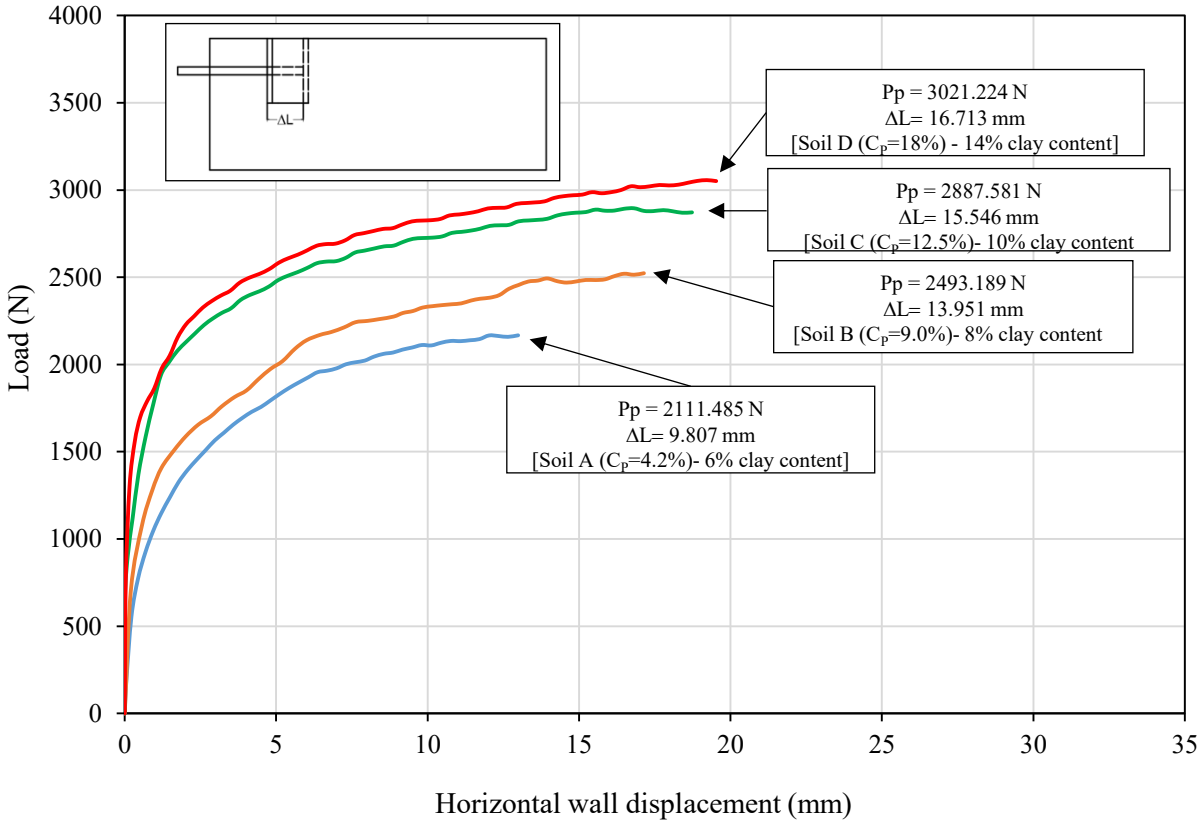

Fig. 5.27. Load – displacement curves (Se2) for dry collapsible soils with different clay content (different collapse potential)

Effect of collapse potential on the passive earth pressure for saturated collapsible soil

Figure 5.28 shows the variation in the passive earth force with respect to the horizontal wall displacement for different soil mixtures having different collapse potential C_p for the case of after full inundation. It can be observed that the passive earth force and horizontal wall displacement at failure decrease considerably with the increase of the collapse potential C_p of the soil in saturated condition. Increasing the collapse potential C_p of the soil results in the decrease of the passive resistance of the soil. It can be seen from this figure that by increasing the collapse potential C_p from 4.2% to 9.0%, the passive earth force decreases about 42%. The decrease of the passive earth force is around 82% when increasing the collapse potential C_p from 4.2% to

18%. Generally, for the case of after full inundation, the higher the collapse potential of the soil, the larger the decrease in the passive earth force and the wall displacement at failure.

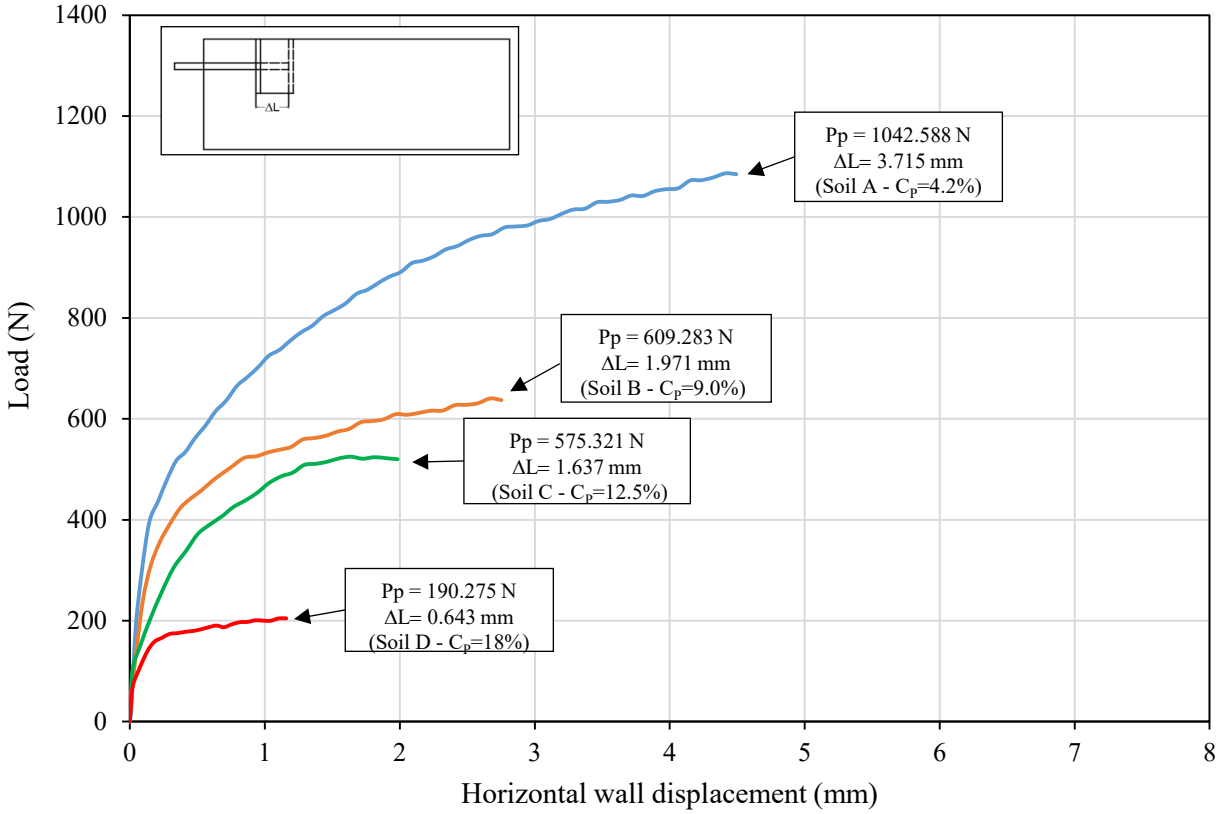

Fig. 5.28. Load – displacement curves (Se2') for saturated collapsible soils having different collapse potential

Effect of inundation of collapsible soil on passive earth pressure

In order to examine the effect of inundation on passive earth pressure of collapsible soils, load – displacement curves for the tests conducted on the same soil mixture under dry and saturated conditions are plotted in the same figure. Figure 5.29 presents the load-displacement curves for the tests performed on dry and saturated soil A - C_p = 4.2% (tests no. 5 and 17). It can be observed from this figure that the passive earth force of the dry soil is reduced by 51% after

inundation. Similarly, the wall displacement at failure is decreased about 62% for the case of after full inundation.

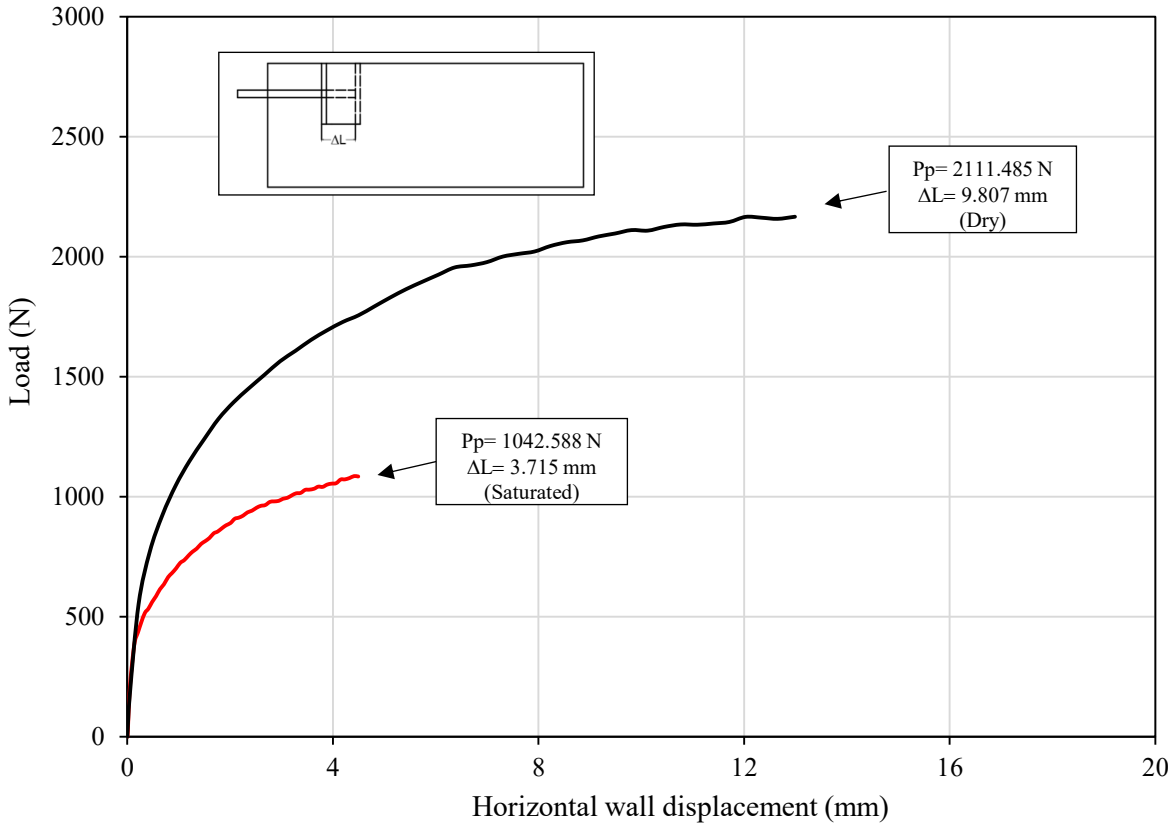

Fig. 5.29. Load – displacement curves for dry and saturated collapsible soil A - C_p = 4.2% (tests no. 5 and 17)

Figure 5.30 illustrates the load-displacement curves for the tests performed on dry and saturated soil D - C_p = 18% (tests no. 8 and 20). It can be noted that the passive earth force of the dry soil is dropped by 94% after inundation. Similar observation is noted for the wall displacement. This can be explained by the fact that at full saturation, the soil loses most of its strength, which leads to premature failure at low value of wall displacement.

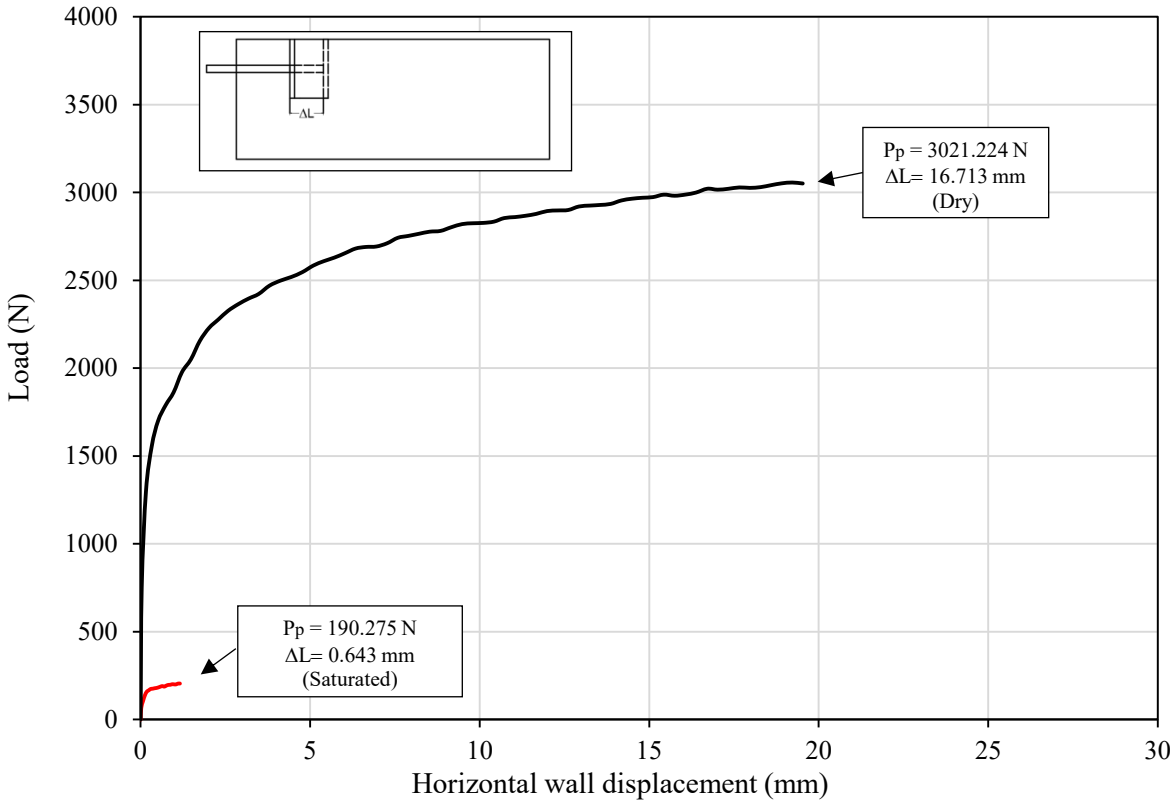

Fig. 5.30. Load – displacement curves for dry and saturated collapsible soil D - C_p = 18% (tests no. 8 and 20)

It can be noted from Figures 5.29 and 5.30 that the passive earth pressure of collapsible soils are significantly affected by the inundation. Upon full inundated, the decrease of passive earth pressure of the soil A (C_p = 4.2%) is moderate. However, the decrease of passive earth pressure of the soil D (C_p = 18%) is very remarkable. It can be firstly concluded that the higher the collapse potential, the larger the decrease in passive earth pressure of collapsible soils under inundation condition.

In this investigation, the experimental values of the earth force P_p acting on the wall were used to determine the coefficient of passive earth pressure K_p for the dry and saturated collapsible soils, as follows:

$$P_{p(dry)} = \frac{1}{2} K_p \gamma' b H^2 + 2c' b H \sqrt{K_p} \qquad (5.1)$$

$$P_{p(saturated)} = \frac{1}{2} K_p \gamma' b H^2 + 2c' b H \sqrt{K_p} + \frac{1}{2} \gamma_w b H^2 \qquad (5.2)$$

Where

P_p = passive earth force at the failure point measured by the load cell;

γ' = effective unit weight of the soil;

γ_w = unit weight of water;

c' = effective cohesion of the soil;

H = the height of the wall;

b = the width of the wall.

Table 5.1 presents a summary of the test results of the present experimental investigation for passive case.

It can be seen from this table that the coefficient of passive earth pressure K_p of dry collapsible soils decreases gradually by increasing the collapse potential C_p, and increases considerabky with the increase of the OCR; while at full saturation, it decreases with the increase of the collapse potential C_p of the soil and increases with the increase of the OCR.

In general, at full saturation, the higher the collapse potential C_p the larger the decrease in coefficient of passive earth pressure K_p.

Table 5.1. Summary of the test results of passive earth pressure

Test No.	Soil type	Surcharge Ps (kPa)	Testing condition	OCR	P_p (N)	H1 (kPa)	H2 (kPa)	H3 (kPa)	H4 (kPa)	ΔL (mm)	K_p
1	A (C_p = 4.2%)	0	Dry soil	3.3	1839	89.52	70.93	60.91	54.96	6.93	4.15
2	B (C_p = 9.0%)	0	Dry soil	3.9	2256	95.96	86.77	74.78	64.80	13.63	3.61
3	C (C_p = 12.5%)	0	Dry soil	5.5	2660	115.78	93.96	82.09	71.10	14.22	3.45
4	D (C_p = 18%)	0	Dry soil	7.2	2851	120.31	107.40	93.61	74.72	15.51	3.10
5	A (C_p = 4.2%)	8	Dry soil	4.5	2111	124.79	103.80	84.96	74.23	9.81	5.14
6	B (C_p = 9.0%)	8	Dry soil	5.1	2493	134.20	120.21	98.36	76.40	13.95	4.31
7	C (C_p = 12.5%)	8	Dry soil	6.9	2888	140.05	125.88	111.07	90.71	15.55	4.00
8	D (C_p = 18%)	8	Dry soil	9.9	3021	167.23	144.25	121.69	92.04	16.71	3.40
9	A (C_p = 4.2%)	16	Dry soil	6.0	2368	167.20	139.79	110.82	96.67	9.93	6.25
10	B (C_p = 9.0%)	16	Dry soil	6.6	2791	169.31	143.28	117.53	103.17	14.55	5.20
11	C (C_p = 12.5%)	16	Dry soil	8.2	3286	182.11	157.38	130.09	104.71	16.12	4.80
12	D (C_p = 18%)	16	Dry soil	11.7	3323	198.91	178.23	146.01	115.62	17.71	4.06
13	A (C_p = 4.2%)	0	Saturated soil	2.8	893	37.63	35.41	30.71	27.34	2.88	1.05
14	B (C_p = 9.0%)	0	Saturated soil	3.3	525	14.50	13.52	12.14	10.85	0.78	0.20
15	C (C_p = 12.5%)	0	Saturated soil	4.7	500	13.39	12.65	9.70	6.60	0.59	0.149
16	D (C_p = 18%)	0	Saturated soil	1.1	86	3.50	2.81	1.76	1.42	0.09	0.001
17	A (C_p = 4.2%)	8	Saturated soil	3.7	1043	47.2	41.5	37.2	31.5	3.72	1.41
18	B (C_p = 9.0%)	8	Saturated soil	4.1	609	22.61	20.01	17.99	16.49	1.97	0.27
19	C (C_p = 12.5%)	8	Saturated soil	5.9	575	20.09	15.86	12.15	9.40	1.64	0.20
20	D (C_p = 18%)	8	Saturated soil	1.8	190	4.98	3.01	2.50	2.00	0.64	0.01
21	A (C_p = 4.2%)	16	Saturated soil	4.9	1291	65.27	55.08	46.92	40.51	5.57	1.91
22	B (C_p = 9.0%)	16	Saturated soil	5.7	819	31.00	26.95	20.95	17.81	3.91	0.37
23	C (C_p = 12.5%)	16	Saturated soil	7.0	601	25.70	19.74	14.79	12.26	2.09	0.29
24	D (C_p = 18%)	16	Saturated soil	2.7	230	6.10	5.44	4.50	3.62	0.97	0.015

5.4. Analytical model

Analytical model using limit equilibrium method was developed to simulate the case of a vertical wall retaining overconsolidated collapsible soil, as shown in Figure 5.31.

The model uses the constitutive law of Mohr-Coulomb criterion and Spencer method of analysis. The Spencer method considers both shear and normal inter-slice forces, and assumes a constant inter-slice force function. The Spencer factor of safety satisfies all conditions of equilibrium, including moment and force equilibrium. The Spencer method works well for any shape of slip surface.

The model operates with the angle of shearing resistance (ϕ_{cr}'), cohesion (c'), and the unit weight (γ'). The material properties of the collapsible soil used in the experimental investigation (Table 3.4) was used as an input data set for this model.

In this analysis, a line load representing the passive earth force was applied at 1/3 of the wall.

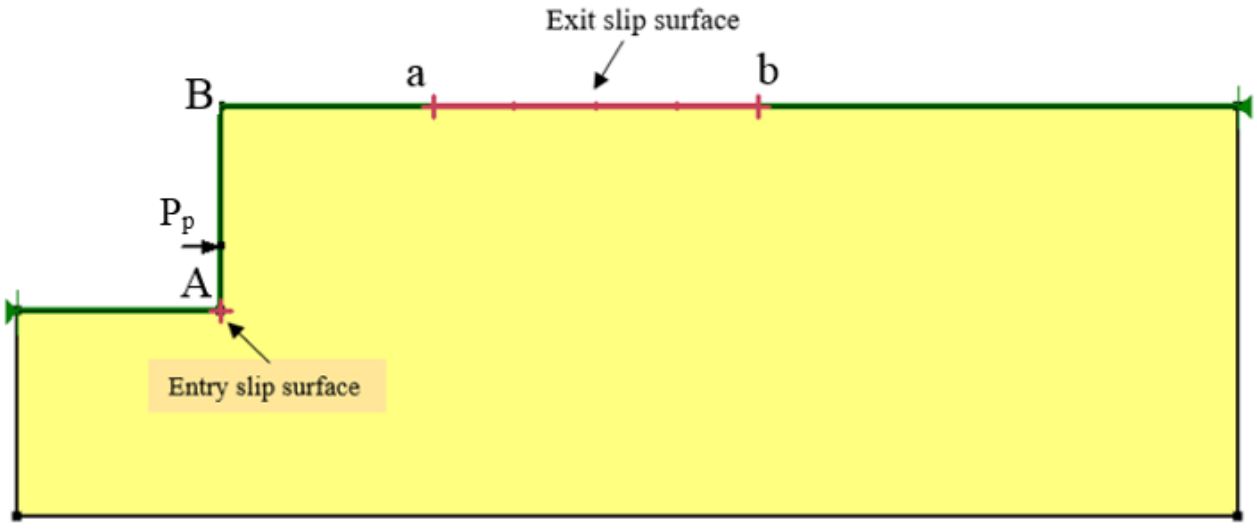

Fig. 5.31. Geometry of the model used

After obtaining the load on the wall at failure, the analysis proceeded by trial and error to find the critical slip surface, which could produce the experimental value of the passive earth force, and accordingly the factor of safety being about one.

It should be reported herein that based on the limit equilibrium method of analysis, the factor of safety is the ratio between the forces/moments resisting (R) movement and the forces/moments motivating (M) movement.

$$FS = \frac{\sum R}{\sum M} \qquad (5.3)$$

In performing these trials, the entry point of the slip surface was assigned at the toe of the wall (A), while the exit points were taken within the range of points (a) to (b) as shown in Figure 5.31. Point (a) was taken at a distance from the wall equal to the wall height, while point (b) was taken at a distance from the wall equal four times of the wall height.

This range was wisely chosen to cover all possible critical slip surface. About 20 trials were performed for each soil type to search for the critical slip surface. The program “GeoStudio” was used to perform the analysis using planar and curved surfaces in order to determine the critical slip surface.

Figures 5.32 to 5.35 present results of all the trial slip surfaces, including the critical slip surface (accordingly the factor of safety of about one), for soils A, B, C and D, respectively.

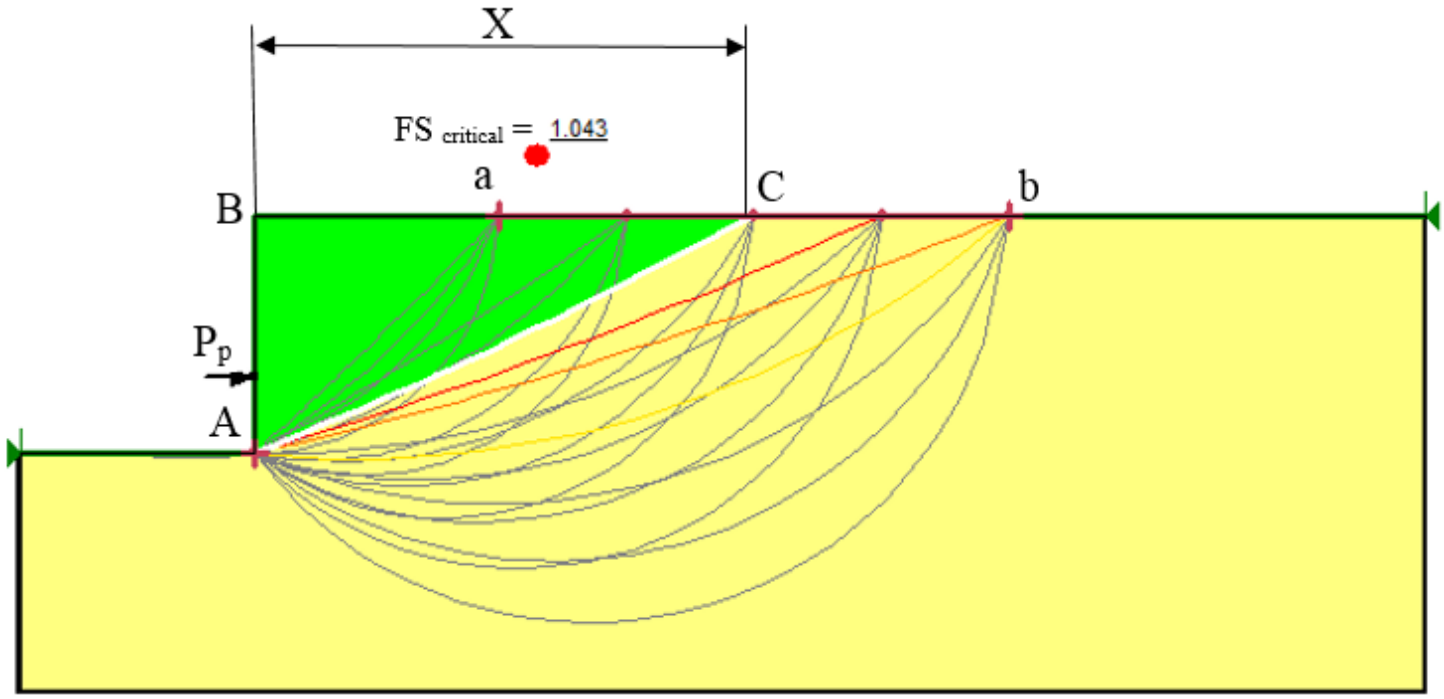

Fig. 5.32. Trial slip surfaces for soil A

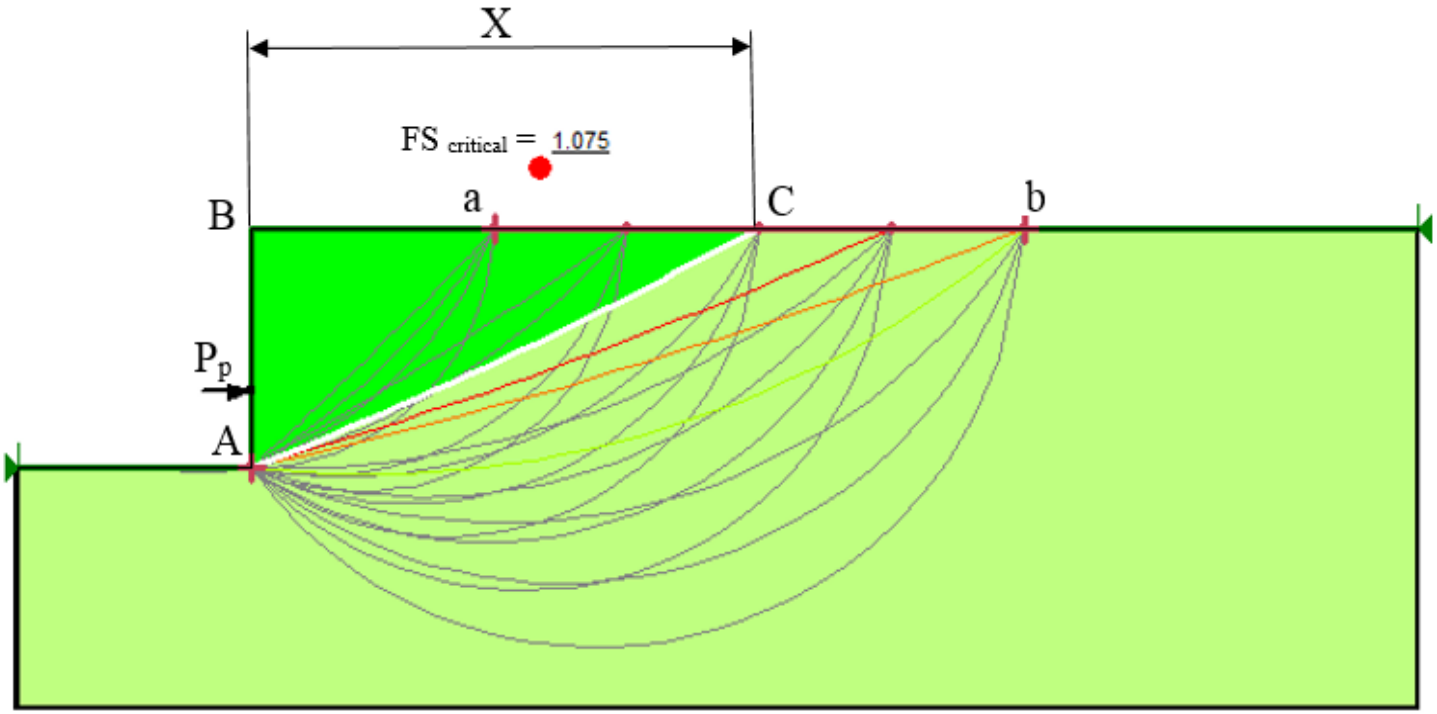

Fig. 5.33. Trial slip surfaces for soil B

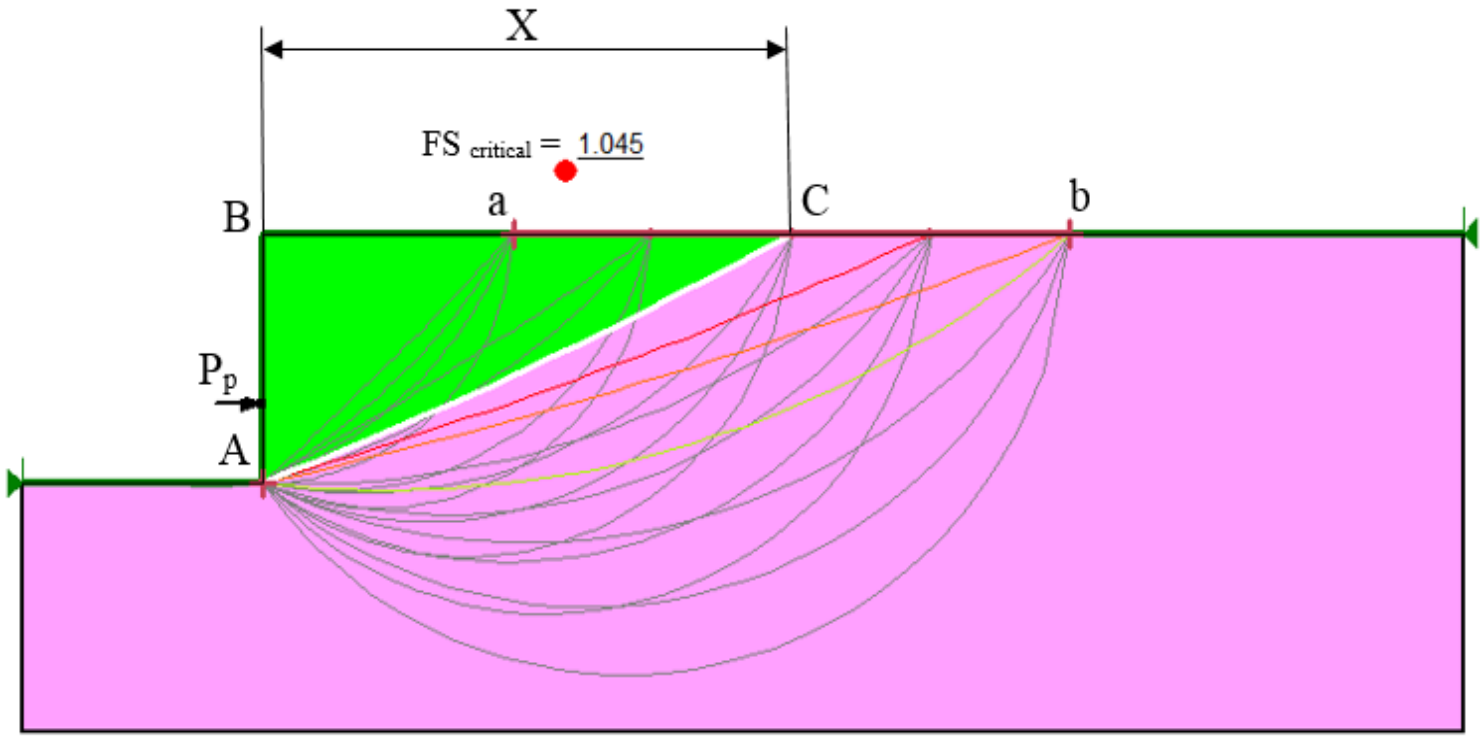

Fig. 5.34. Trial slip surfaces for soil C

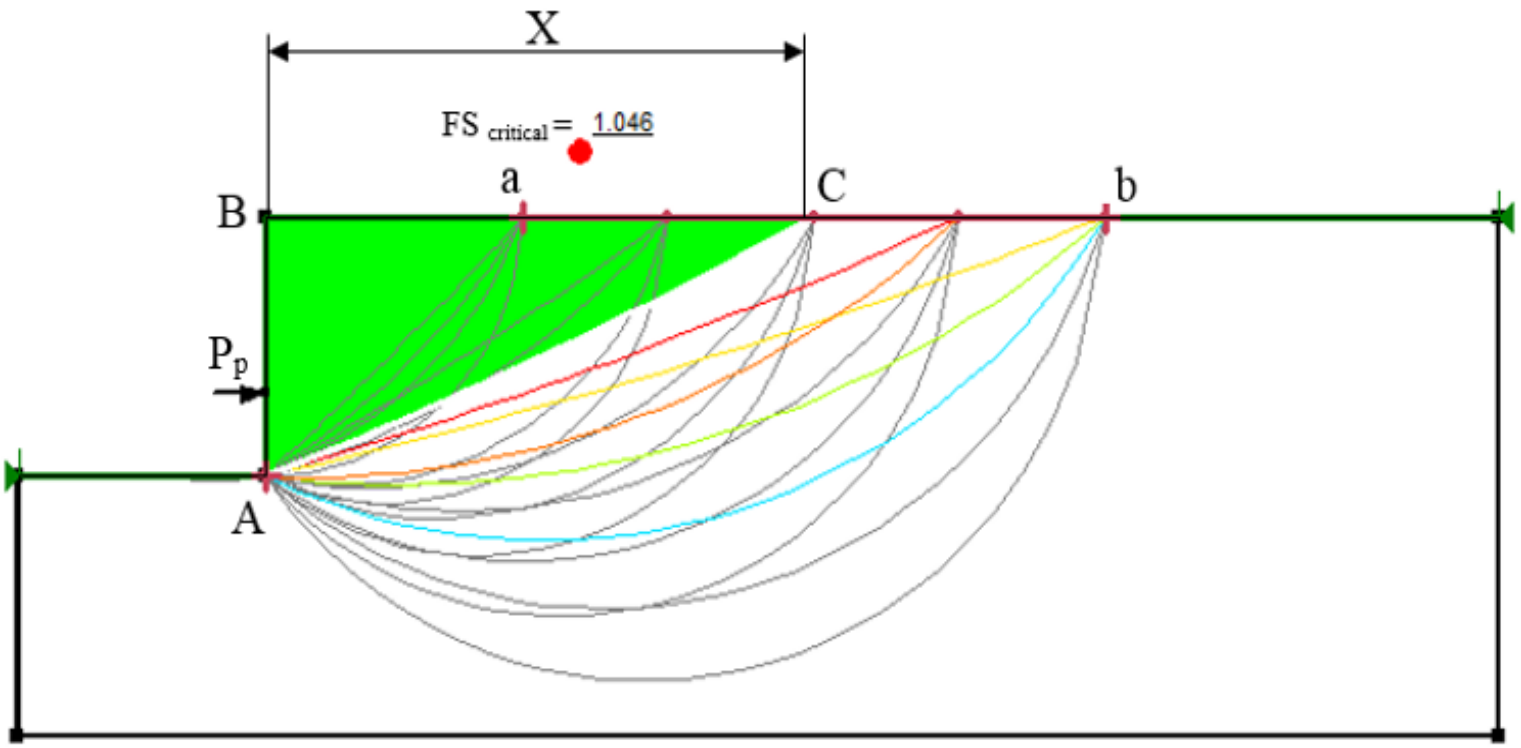

Fig. 5.35. Trial slip surfaces for soil D

Tables 5.2 to 5.5 present the results of this analysis performed on samples A, B, C and D respectively, and accordingly, the critical slip surfaces of each sample were identified.

It can be noted that the factor of safety of about one for all samples tested in this investigation was determined by planar slip surface. Therefore, the planar slip surface is the critical slip surface. Furthermore, the factor of safety increases with increasing the distance "X", which reflect on the angle (α), defined as the slope of the slip surface with the horizontal. It is of interest to note that with the same value of "X", the curved slip surfaces give higher factor of safety than that of planar slip surfaces.

Table 5.2. Summary of the trials considered for soil A (C_p = 4.2%)

Trial slip #	Shape of trial slip	X (m) Distance from the wall to the exit point of the slip surface	α (^{0}) angle of inclination of the slip surface	FS Factor of safety
1	Planar	0.69	17.574	1.163
2		0.57	21.045	1.108
3		**0.45**	**26.000**	**1.043**
4		0.35	32.152	0.559
5		0.22	45.258	0.497
6	Curved	0.57	-0.512	1.726
7		0.45	-4.967	1.321
8		0.45	-9.1879	1.545
9		0.35	-10.376	1.185
10		0.57	-16.686	2.138
11		0.35	-21.808	1.336
12		0.69	-21.967	2.824
13		0.45	-22.999	1.811
14		0.57	-31.311	2.573
15		0.45	-35.324	2.093
16		0.69	-37.118	3.475
17		0.57	-44.082	3.038
18		0.69	-50.109	4.176

Table 5.3. Summary of the trials considered for soil B (C_p = 9.0%)

Trial slip #	Shape of trial slip	X (m) Distance from the wall to the exit point of the slip surface	α (^{0}) angle of inclination of the slip surface	FS Factor of safety
1	Planar	0.71	17.055	1.229
2		0.60	20.002	1.137
3		**0.47**	**25.012**	**1.075**
4		0.36	31.429	0.564
5		0.22	44.889	0.501
6	Curved	0.60	-1.155	1.798
7		0.47	-5.606	1.384
8		0.47	-9.928	1.603
9		0.36	-11.026	1.218
10		0.60	-17.445	2.236
11		0.36	-22.509	1.374
12		0.71	-22.697	2.971
13		0.47	-23.823	1.884
14		0.60	-32.149	2.699
15		0.47	-36.198	2.182
16		0.71	-37.917	3.668
17		0.60	-44.957	3.195
18		0.71	-50.931	4.419

Table 5.4. Summary of the trials considered for soil C (C_p = 12.5%)

Trial slip #	Shape of trial slip	X (m) Distance from the wall to the exit point of the slip surface	α (^{0}) angle of inclination of the slip surface	FS Factor of safety
1	Planar	0.73	16.625	1.225
2		0.61	19.830	1.119
3		**0.49**	**24.100**	**1.045**
4		0.37	30.735	0.759
5		0.23	44.131	0.540
6	Curved	0.61	-1.466	1.758
7		0.49	-5.904	1.367
8		0.49	-10.29	1.564
9		0.37	-11.346	1.183
10		0.61	-17.813	2.189
11		0.37	-22.991	1.325
12		0.73	-23.049	2.917
13		0.49	-24.225	1.840
14		0.61	-32.554	2.647
15		0.49	-36.623	2.133
16		0.73	-38.301	3.608
17		0.61	-45.379	3.136
18		0.73	-51.325	4.352

Table 5.5. Summary of the trials considered for soil D (C_p = 18%)

Trial slip #	Shape of trial slip	X (m) Distance from the wall to the exit point of the slip surface	α (^{0}) angle of inclination of the slip surface	FS Factor of safety
1	Planar	0.75	16.350	1.262
2		0.64	18.924	1.139
3		**0.52**	**23.00**	**1.046**
4		0.39	29.695	0.757
5		0.24	42.851	0.477
6	Curved	0.64	-1.771	1.234
7		0.75	-6.195	1.396
8		0.52	-10.645	1.645
9		0.39	-11.663	1.811
10		0.64	-18.173	2.208
11		0.39	-23.195	1.336
12		0.75	-23.392	1.801
13		0.52	-24.62	1.851
14		0.64	-32.951	2.673
15		0.75	-38.676	3.653
16		0.64	-45.792	3.171
17		0.75	-51.71	4.413

Furthermore, the deduced angle of inclination (α) of the failure plane to the horizontal versus the collapse potentials C_p of the soil samples is presented in Figure 5.36.

It can be noted from this figure that the angle (α) decreases due to the increase of the collapse potential C_p.

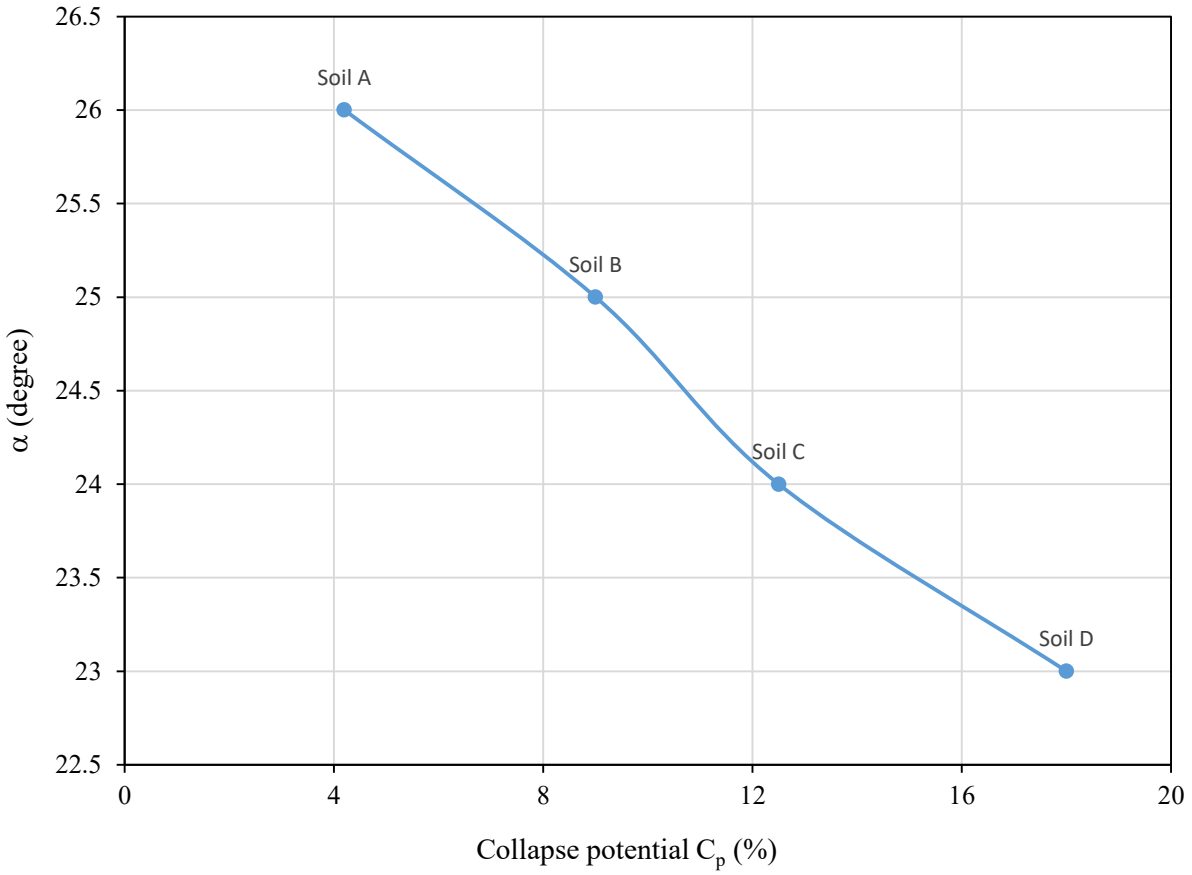

Fig. 5.36. Analytical results: the angle (α) versus the collapse potential C_p (Ps = 0)

Figure 5.37 presents the deduced angle (α) with the corresponding overconsolidation ratio OCR values, where the angle (α) decreases due to the increase of the overconsolidation ratio OCR.

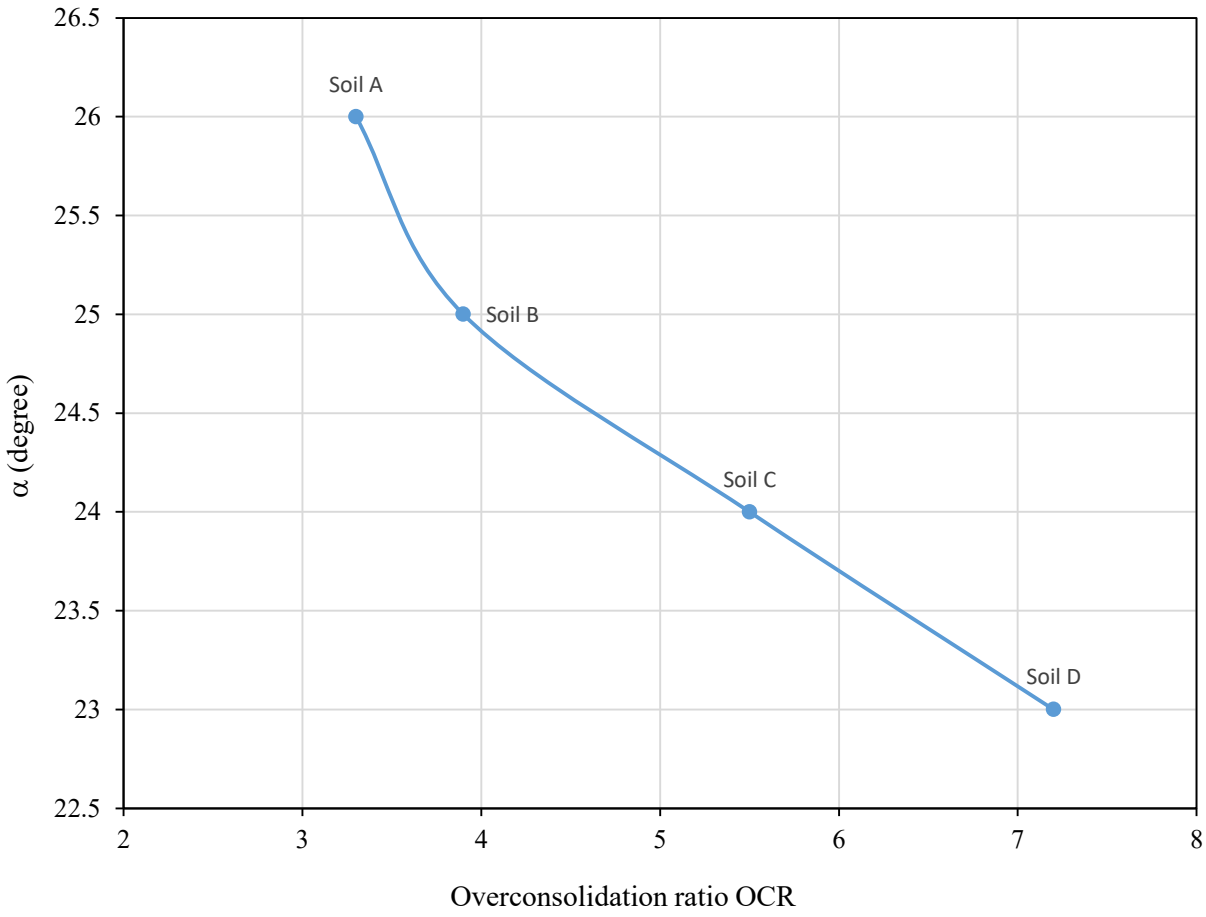

Fig. 5.37. Analytical results: the angle (α) versus OCR (Ps = 0)

Figure 5.38 presents the deduced slip surface at failure from the analytical model. The failing wedge was analyzed using limit equilibrium method of analysis to determine the passive earth pressure for all samples tested, as shown in Figure 5.39. Thus

$$\sum F_X = 0$$

$$E + dE - E - R\sin(\alpha + \phi_{cr}^{'}) + c'L\cos\alpha = 0 \qquad (5.4)$$

Or

$$dE = R\sin(\alpha + \phi_{cr}^{'}) + c'L\cos\alpha \qquad (5.5)$$

Where:

α= Angle of inclination of the failure plane with the horizontal

ϕ_{cr}' = Critical state friction angle of the backfill soil;

c' = Cohesion of the backfill soil;

R = Resultant of the tangential and normal forces on the failure plane;

E and E + dE = horizontal forces on the element;

L = element length;

W = element weight.

Furthermore,

$$\sum F_Y = 0$$

$$W + X + dX - X - R\cos(\alpha + \phi_{cr}^{'}) + c'L\sin\alpha = 0 \qquad (5.6)$$

Where: X and X + dX = shear forces acting on the sides of the element

Therefore

$$W + dX + c'L\sin\alpha = R\cos(\alpha + \phi_{cr}^{'}) \qquad (5.7)$$

Or

$$R = \frac{W + dX + c'L\sin\alpha}{\cos(\alpha + \phi_{cr}^{'})} \qquad (5.8)$$

Substituting R from Eq. (5.8) into Eq. (5.5):

$$dE = W\tan(\alpha + \phi_{cr}^{'}) + dX\tan(\alpha + \phi_{cr}^{'}) + c'L\sin\alpha\tan(\alpha + \phi_{cr}^{'}) + c'L\cos\alpha$$

(5.9)

The change of the vertical shear force across an element, dX, was equated to zero (Bishop, 1955).

Therefore, the passive earth force of this element:

$$dE = W\tan(\alpha + \phi_{cr}^{'}) + c'L\left[\sin\alpha\tan(\alpha + \phi_{cr}^{'}) + \cos\alpha\right] \qquad (5.10)$$

Accordingly,

The passive earth force P_p of the failure wedge can be estimated as:

$$P_p = W_{wedge}\tan(\alpha + \phi_{cr}^{'}) + c'L_{wedge}\left[\sin\alpha\tan(\alpha + \phi_{cr}^{'}) + \cos\alpha\right] \qquad (5.11)$$

In which: W_{wedge} = weight of the failure wedge, L_{wedge} = the length of the failure surface of the wedge.

And

$$P_P = 0.5\gamma H^2 K_P + (K_P - 1)\frac{c' H}{\tan\phi'} \qquad \text{(Cai et al., 2016)} \qquad (5.12)$$

Therefore, the coefficient of passive earth pressure K_p:

$$K_P = \frac{P_p \tan\phi_{cr}^{'} + c' H}{0.5\gamma' H^2 \tan\phi_{cr}^{'} + c' H} \qquad (5.13)$$

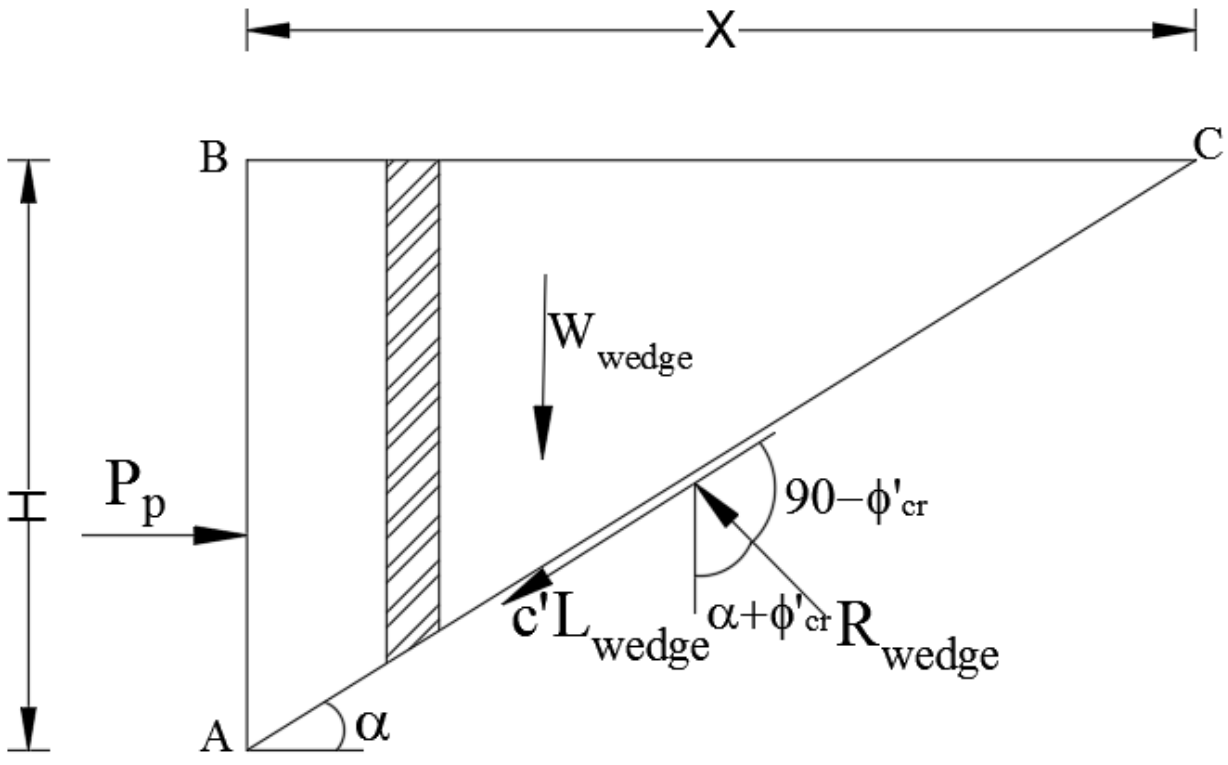

Fig. 5.38. Failure wedge with planar surface

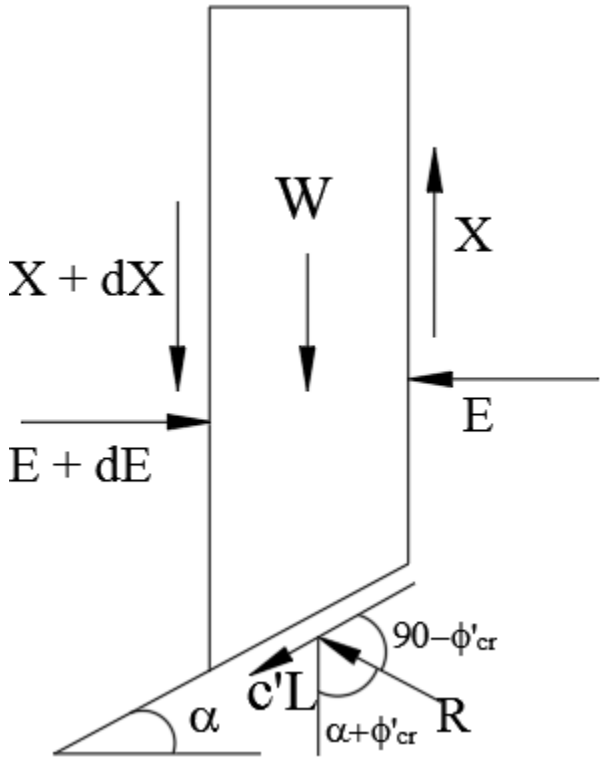

Fig.5.39. Forces acting on typical element of failure wedge

The proposed analytical model [Eq. (5.11) and Eq. (5.13)] was validated using the experimental results for dry collapsible soils. Table 5.6 presents the results of this analysis together with the experimental values of the passive earth force P_p and the coefficient of passive earth pressure K_p, where good agreement can be noted.

Table 5.6. Comparison between the predicted and the experimental values of the passive earth force P_p and the coefficient of passive earth pressure K_p

Test no.	Soil type	OCR	Theoretical values			Experimental values	
			α (^{0})	P_p (kN) [Eq. (5.11)]	K_p [Eq. (5.13)]	P_p (kN)	K_p
1	A (C_p = 4.2%)	3.3	26	1.95	4.41	1.84	4.15
2	B (C_p = 9.0%)	3.9	25	2.48	4.01	2.26	3.61
3	C (C_p = 12.5%)	5.5	24	2.81	3.73	2.66	3.45
4	D (C_p = 18%)	7.2	23	3.04	3.24	2.85	3.10
5	A (C_p = 4.2%)	4.5	22	1.99	4.77	2.11	5.14
6	B (C_p = 9.0%)	5.1	21	2.57	4.42	2.49	4.31
7	C (C_p = 12.5%)	6.9	20	2.99	4.10	2.89	4.00
8	D (C_p = 18%)	9.9	19	3.32	3.56	3.02	3.40
9	A (C_p = 4.2%)	6.0	19	2.10	5.81	2.37	6.25
10	B (C_p = 9.0%)	6.6	18.5	2.71	4.95	2.79	5.20
11	C (C_p = 12.5%)	8.2	18	3.16	4.52	3.29	4.80
12	D (C_p = 18%)	11.7	17	3.55	4.10	3.32	4.06

In this investigation, the analytical model developed in this investigation was used to develop results for a wide range of parameters. These results are presented herein as design charts in Figure 5.40, which will assist designer to predict the coefficient of passive earth pressure K_p for given OCR and C_p values for dry collapsible soils.

Figure 5.41 presents comparison between the theoretical and experimental values of K_p of the present investigation, where good agreement can be observed.

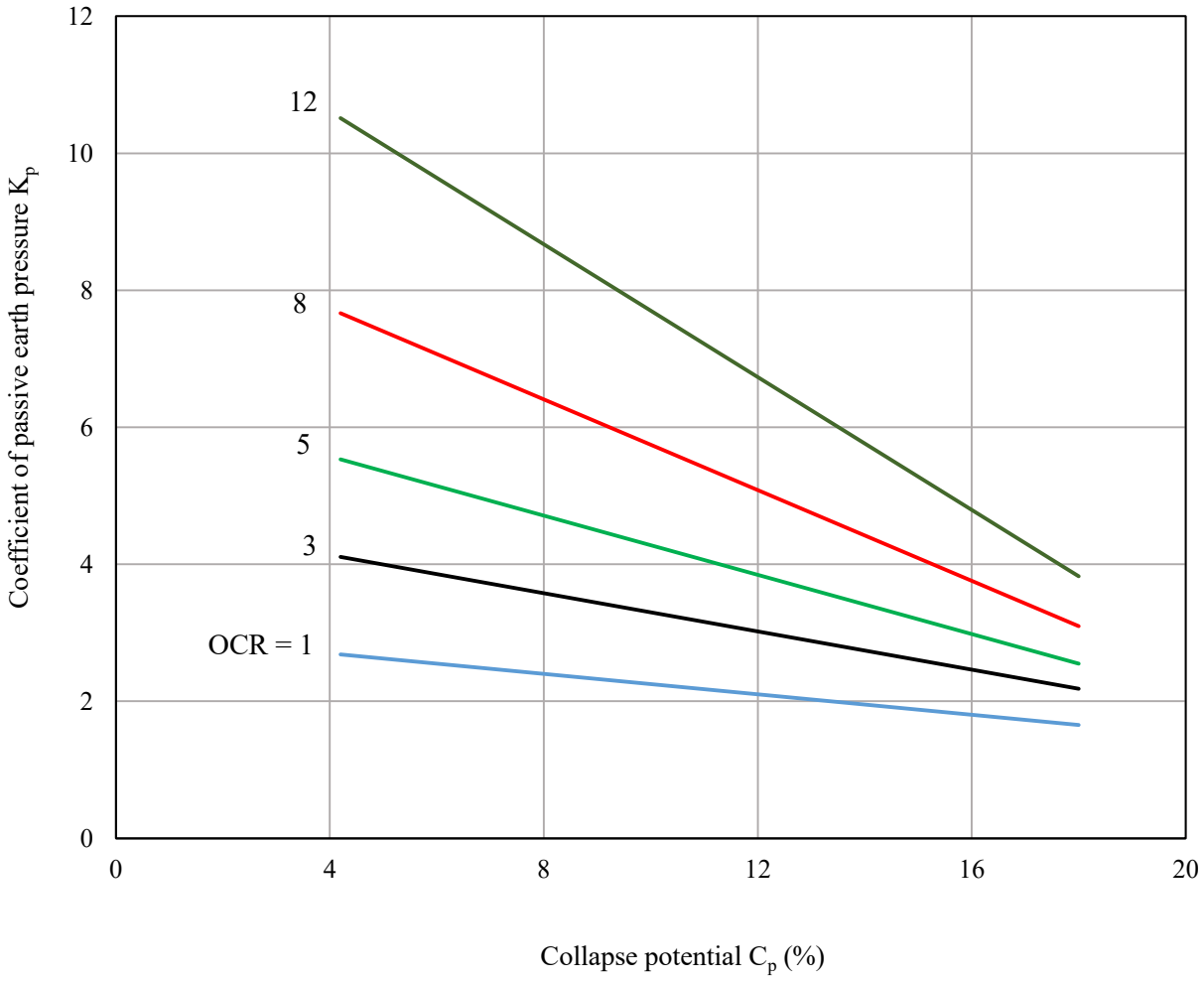

Fig. 5.40. Design chart: coefficient of passive earth pressure K_p of collapsible soil at dry state

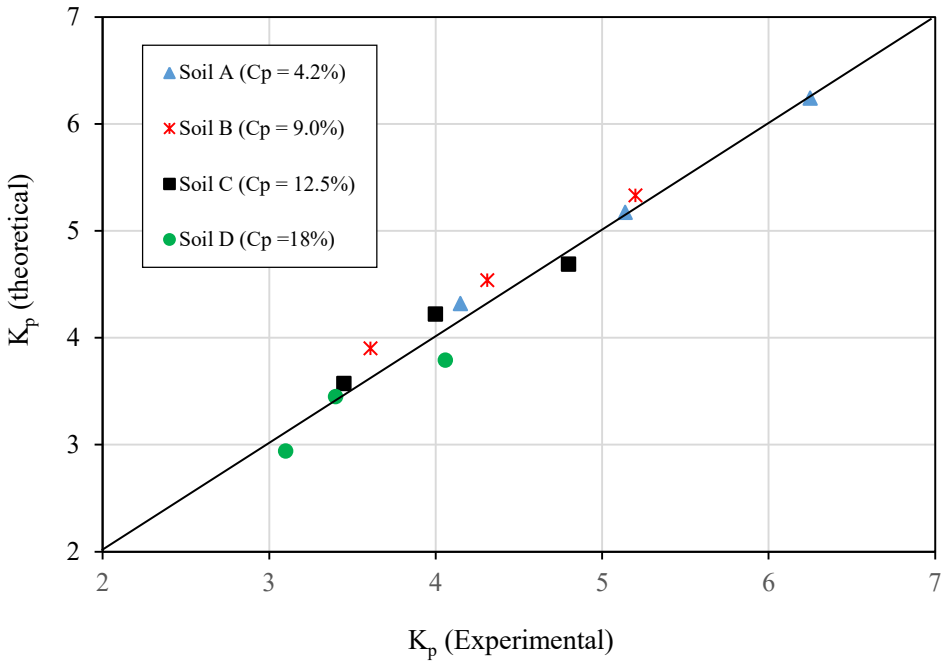

Fig. 5.41. Comparison between the results obtained from the present theory and the experimental results of the present investigation for the dry state.

For the case of inundated collapsible soil, a reduction factor R_F was introduced to take into account the effect of the soil collapse on the coefficient of passive earth pressure K_p. Thus, the coefficient of passive earth pressure of saturated collapsible soils can be determined as follows:

$$K_{P(sat)} = R_F K_{P(dry)} \qquad (5.14)$$

It should be reported herein that the results of saturated collapsible soils in the present investigation were divided into two groups: the first group of the data were used to determine the reduction factor R_F (Figure 5.42), and the second group (the remaining data) were used to validate the results.

Figure 5.43 presents the theoretical values of K_p determined from Eq. (14) and the remaining experimental values of the present investigation, where a good agreement can be found.

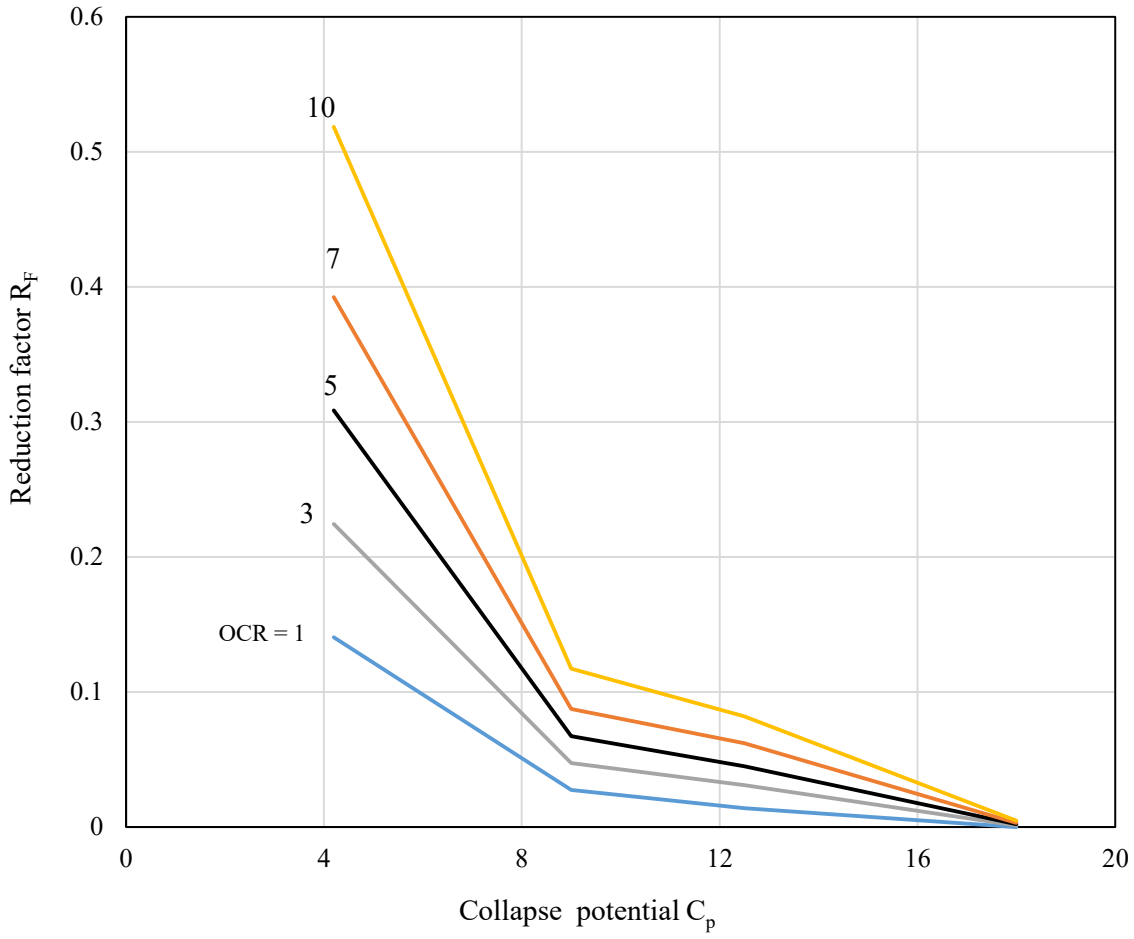

Fig. 5.42. Reduction factor R_F

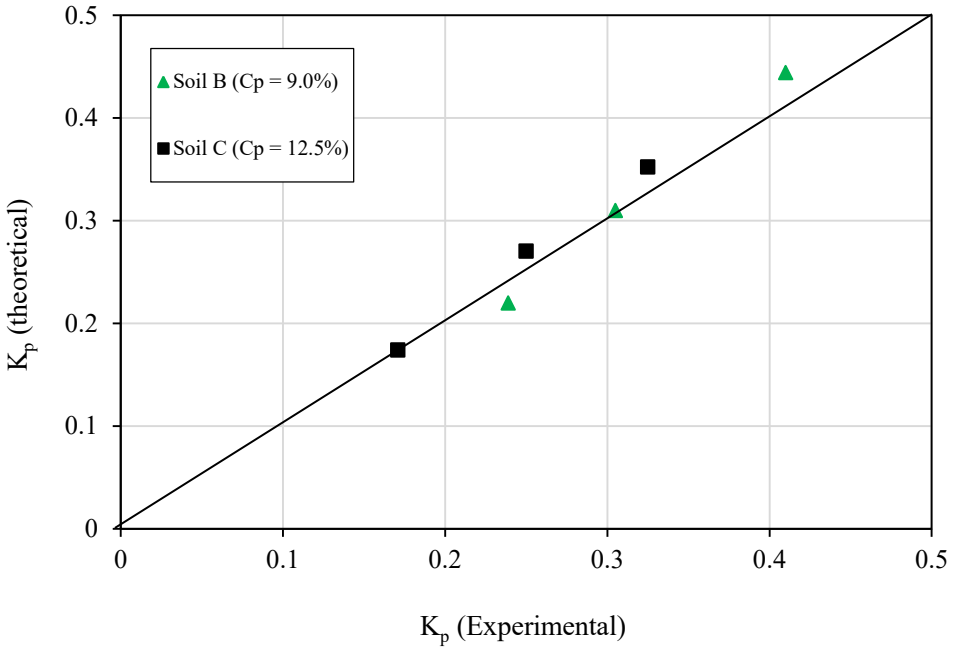

Fig. 5.43. Comparison between experimental results and those obtained from the proposed empirical formula [Eq. (5.14)]

5.5. Proposed design charts for predicting coefficient of passive earth pressure K_p for unsaturated collapsible soil at different degree of saturation

Furthermore, in this investigation, with the assumption that the coefficient of passive earth pressure K_p decreases linearly with the increase of the degree of saturation (S), design charts were developed and presented in Figures 5.44 to 5.47 to predict the coefficient of passive earth pressure K_p of unsaturated collapsible soils as function of the overconsolidation ratio OCR, the collapse potential C_p and the degree of saturation S of the soil.

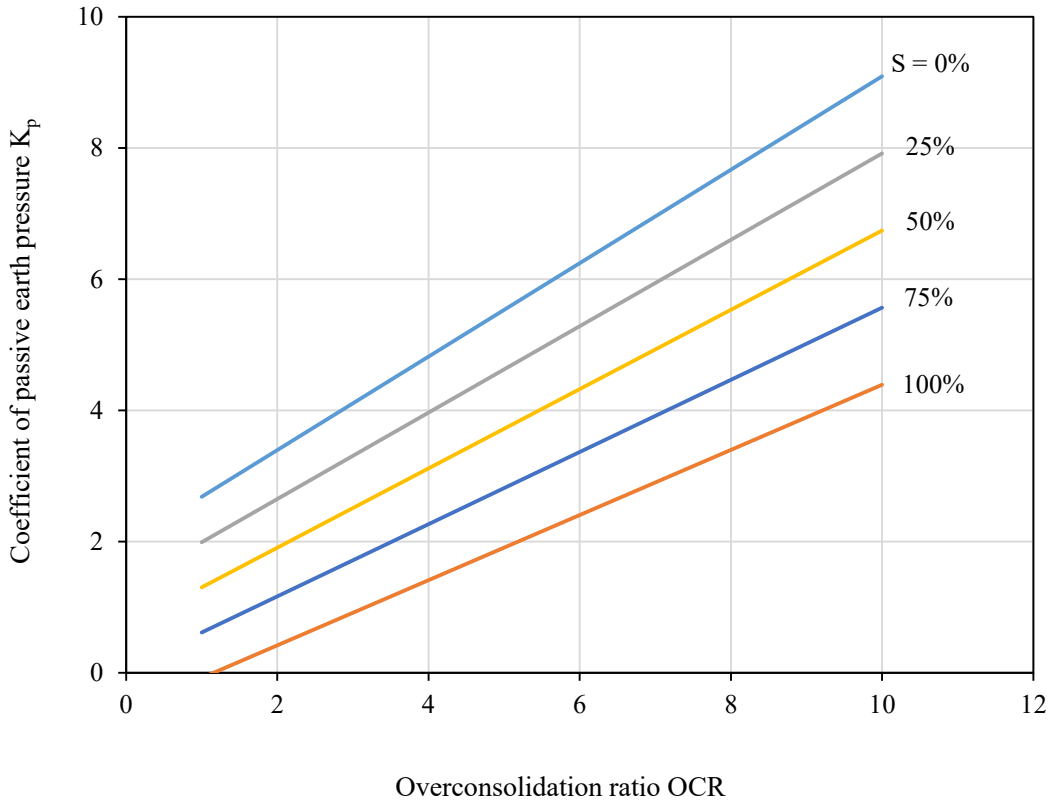

Fig. 5.44. Design charts: Values of K_p for collapsible soils at different degree of saturation "S" (C_p = 4.2%).

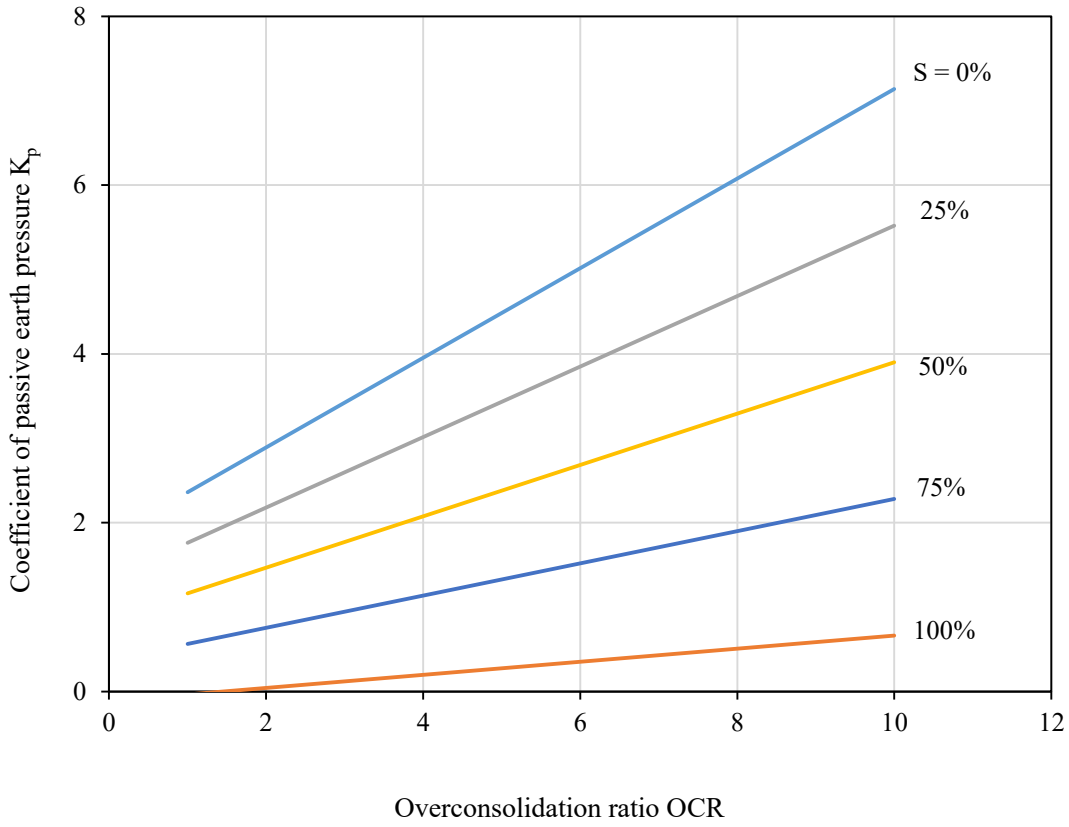

Fig. 5.45. Design charts: Values of K_p for collapsible soils at different degree of saturation "S" (C_p = 9.0%).

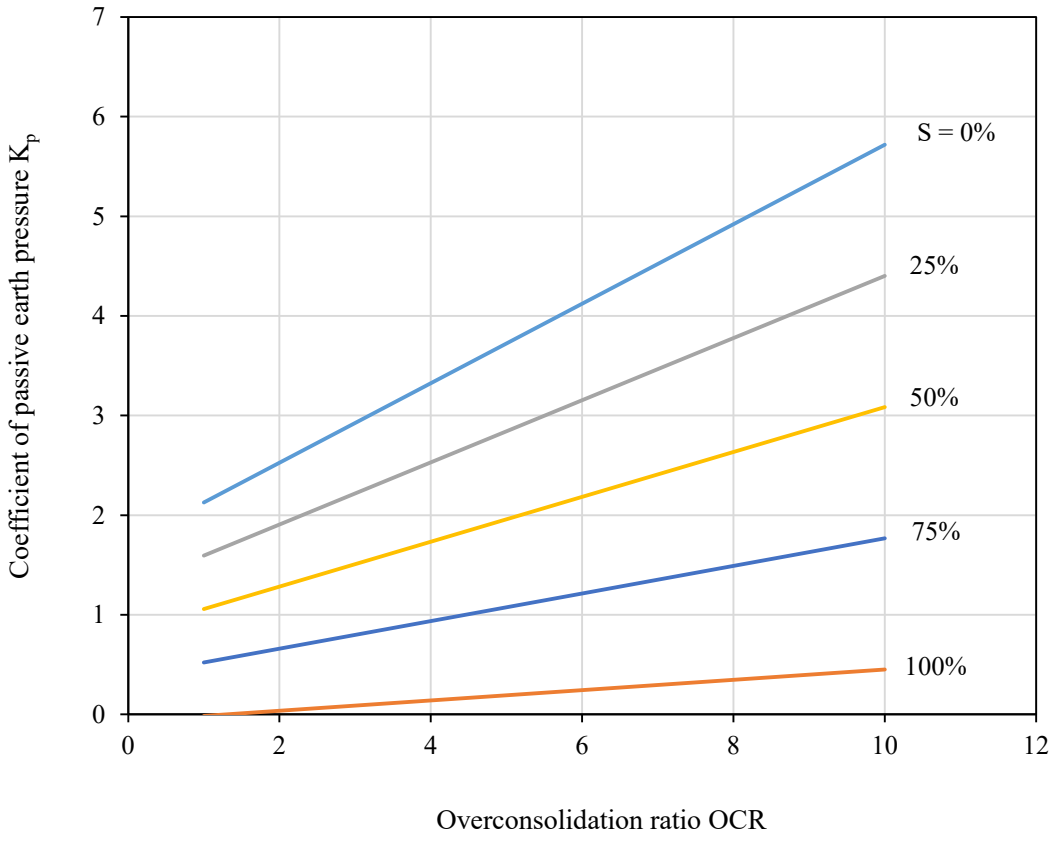

Fig. 5.46. Design charts: Values of K_p for collapsible soils at different degree of saturation "S" (C_p = 12.5%).

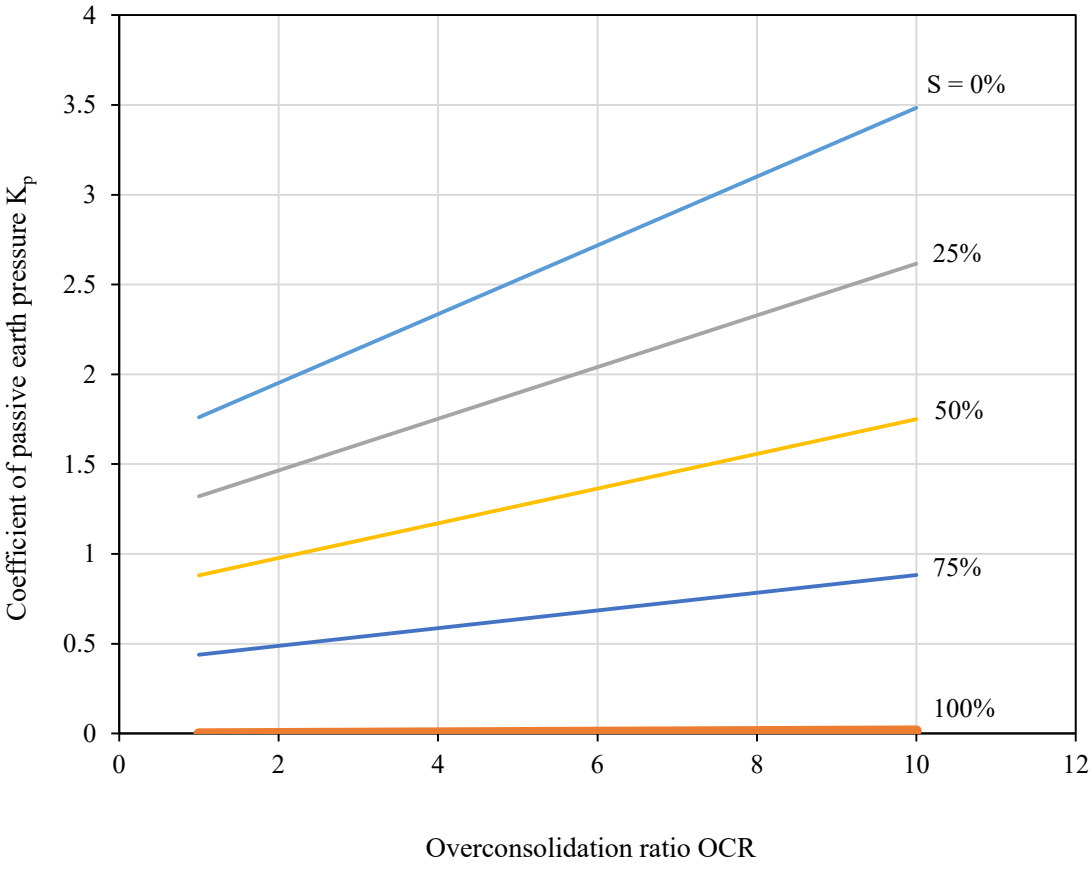

Fig. 5.47. Design charts: Values of K_p for collapsible soils at different degree of saturation "S" (C_p = 18%).

CHAPTER 6
CONCLUSIONS AND RECOMMENDATIONS

6.1. Conclusions

An experimental investigation on at-rest and passive earth pressures of overconsolidated collapsible soil at the dry and at full saturation was conducted. The principal objective of the investigation was to provide methods/theories to predict the at-rest and passive earth pressures of overconsolidated collapsible soil at the dry and saturated states. It was also to establish the effect of soil collapse potential C_p and the overconcolidation ratio OCR on the at-rest and passive earth pressures acting on retaining walls. The following can be concluded:

1. The behavior of collapsible soil was governed by its collapse potential C_p. The collapse potential C_p of the soil increased with the increase of the clay content in the soil.
2. Collapse settlement increased due to an increase of the soil collapse potential C_p. However, the collapse settlement decreased with increasing the overconsolidation ratio OCR of the soil. The collapse settlement increased rapidly after introducing the water up to about 80 % saturation, then continued at a lower rate. Furthermore, collapse settlement took place in relatively short period for higher values of the collapse potential C_p, while it took longer period for higher overconsolidation ratio OCR. The collapse settlement did not end at 100% satuartion but rather continued at a lower rate after, up to 20-40% of the collapse settlement at 100% saturation.
3. The overconsolidation ratio OCR of collapsible soil increased due to the increase of the clay content, which is represented by the collapse potential (C_p) in the soils. The overconsolidation ratio OCR also increased when increasing the surcharge “Ps” on the

soil mass. However, the overconsolidation ratio OCR decreased considerably during the inundation of the soil. At full saturation, the soil with higher collapse potential C_p values experienced significant decrease in the overconsolidation ratio OCR value.

4. The earth pressures on retaining walls (both at-rest and passive cases) are function of the soil collapse potential C_p, the overconsolidation ratio OCR, and the degree of saturation S of the soil.
5. The following conclusions can be noted for the case of at-rest earth pressure:
    a. For the case of dry soils: The at-rest earth pressure increased moderately by increasing the clay content in the soil, accordingly with increasing the collapse potential C_p of the soil.
    b. For the case of saturated soils: the at-rest earth pressure decreased considerably with the increase of the collapse potential C_p of the soil.
    c. At-rest earth pressure increased remarkably with the increase of the overconsolidation ratio OCR for both dry and saturated soils.
    d. Empirical formulae were developed to estimate the coefficient of at-rest earth pressure of overconsolidated collapsible soils at the dry and saturated states. The proposed formulae compared well with the experimental results for the range of collapse potential C_p from 4.2% to 18%.
    e. With the assumption that the coefficient of at-rest earth pressure decreased linearly with the increase of the degree of saturation between the two extreme values for dry and saturated soils, design charts were developed for predicting the coefficient of at-rest earth pressure as function of the collapse potential C_p, the overconsolidation ratio OCR, and the degree of saturation S of the soil.

6. The following conclusions can be drawn for the case of passive earth pressure:
    a. For the case of dry soils: the passive earth force and the wall displacement at failure increased with the increase of the clay content, accordingly with the increase of the collapse potential C_p of the soil. Generally, increasing the clay content in the soil can result in the increase of passive resistance of the soil.
    b. For the case of saturated soils: the passive earth force and the wall displacement at failure decreased significantly with the increase of the collapse potential C_p of the soil.
    c. For the soil having higher values of the collapse potential ($C_p \geq 12.5\%$) the passive earth force of the dry soil was dropped by more than 80% after inundation. Similar observations were noted for the wall displacement.
    d. Passive earth pressure increased remarkably with an increase of the overconsolidation ratio OCR for both dry and saturated soils.
    e. Design theory was presented to estimate the coefficient of passive earth pressure of overconsolidated collapsible soils at the dry and saturated conditions. The design theory compared well with the experimental results for the range of collapse potential C_p from 4.2% to 18%.
    f. With the assumption that the coefficient of passive earth pressure decreased linearly with the increase of the degree of saturation of the soil, design charts were developed for prediction of the coefficient of passive earth pressure of unsaturated collapsible soil at different degree of saturation.

6.2. Recommendations for future work

The recommendations for future investigations are as follows:

1. Conduct field tests on full-scale retaining wall.
2. Conduct tests on partially saturated collapsible soils.
3. Extend the experimental setup to include inclined walls, sloping backfills.
4. Extend the study to investigate the variation of earth pressure induced by different types of wall movements such as rotation about a point above the top of the wall and rotation about a point below the base of the wall.

REFERENCES

Abbeche, K., Bahloul, O., Ayadat, T., and Bahloul, A. "Treatment of Collapsible Soils by Salts using the Double Consolidation Method." *GeoShanghai International Conference. Experimental and Applied Modeling of Unsaturated Soils. Shanghai, China*. 2010

Ali, N.A. "Performance of Partially Replaced Collapsible Soil–Field Study." *Alexandria Engineering Journal* 54.3 (2015): 527-532.

Alpan, I. "The Empirical Evaluation of the Coefficient K_0 and K_{0R}." *Soils and Foundations* 7.1 (1967): 31-40.

ASTM D 5333-03, 2003. Standard Test Method for the Measurement of Collapse Potential of Soils, ASTM International, West Conshohocken

Awn, S. H. A., and Zakaria, W. A. "Behavior of Retaining Wall Founded on Collapsible Soil –A Prototype Laboratory Study." *Diyala Journal of Engineering Sciences* 07.03 (2014): 01-24.

Ayadat, T. and Hanna, A. M. "Design of Foundations Built on a Shallow Depth (Less than 4 m) of Egyptian Macro-Porous Collapsible Soils." *Open Journal of Geology* 3.03 (2013): 209.

Ayadat, T., and A. M. Hanna. "Assessment of Soil Collapse Prediction Methods." *International Journal of Engineering* 25.1 (2012): 19-26.

Ayadat, T., and Hanna, A. M. "Encapsulated Stone Columns as a Soil Improvement Technique for Collapsible Soil." *Proceedings of the ICE-Ground Improvement* 9.4 (2005): 137-147.

Barnes, G. *Soil Mechanics*. Palgrave Macmillan, 2010

Beckwith, G. H. *Experiences with Collapsing Soils in the Southwest*. Sergent, Hauskins & Beckwith, 1979.

Bishop, A. W. (1955). "The Use of the Slip Circle in the Stability Analysis of Slopes." *Geotechnique* 5.1 (1955): 7-18.

Bowles, J. *Foundation Analysis and Design*. McGraw-Hill Book Company, 1968.

Brooker, E.W., and Ireland, H.O. "Earth Pressures At Rest Related to Stress History." *Canadian Geotechnical Journal* 2.1 (1965): 1-15.

Budhu, M. *Foundations and Earth Retaining Structures*. John Wiley & Sons, 2008.

Cai, Y., Chen, Q., Zhou, Y., Nimbalkar, S, and Yu, J. "Estimation of Passive Earth Pressure against Rigid Retaining Wall Considering Arching Effect in Cohesive-Frictional Backfill under Translation mode." *International Journal of Geomechanics* (2016): 04016093.

Cai, G., Liu, S., and Puppala, A. "Assessment of the Coefficient of Lateral Earth Pressure at Rest (K_0) from Seismic Piezocone Tests (SCPTU)." *Geo-Frontiers 2011@ Advances in Geotechnical Engineering*. ASCE

Catt, J. A. *Soils and Quaternary Geology: A Handbook for Field Scientists*. Oxford University Press, 1986.

Clemence, S. P., and Finbarr, A. O. "Design Considerations for Collapsible Soils." *Journal of Geotechnical and Geoenvironmental Engineering* 107.ASCE 16106 (1981).

Clevenger, A. "Experiences with Loess as Foundation Material". *Transactions of the American Society of Civil Engineers* 123.1 (1958): 151-169.

Clough, G. W., and Duncan, J.M. "Earth pressures." *Foundation Engineering Handbook*. Springer US, 1991. 223-235.

Das, B. M. *Principles of Geotechnical Engineering*. Thomson, 2009.

Denisov, N. Y. "The Engineering Properties of Loess and Loess Loams."*Gosstroilzdat, Moscow* 3 (1951): 18-19.

Duncan, J. M., and Robert L. M. "Passive Earth Pressures: Theories and Tests." *Journal of Geotechnical and Geoenvironmental Engineering* 127.3 (2001): 248-257.

Duncan, J. M.,Williams, G. W., Sehn, A. L. and Seed, R. B. "Estimation Earth Pressures due to Compaction." *Journal of Geotechnical Engineering* 117.12 (1991): 1833-1847.

El-Emam, M. "Experimental and Numerical Study of At-rest Lateral Earth Pressure of Overconsolidated Sand." *Advances in Civil Engineering* 2011 (2011).

Fang, Y. S., Ho, Y. C., and Chen, T. J. "Passive Earth Pressure with Critical State Concept." *Journal of Geotechnical and Geoenvironmental Engineering* 128.8 (2002): 651-659.

Fang, Y. S., Chen, J. M. and Chen, C. Y. "Earth Pressures with Sloping Backfill." *Journal of Geotechnical and Geoenvironmental Engineering* 123.3 (1997): 250-259.

Fang, Y. S., Chen, T. J. and Wu, B. F. "Passive Earth Pressures with Various Wall Movements." *Journal of Geotechnical Engineering* 120.8 (1994): 1307-1323.

Feda, J. "Colloidal Activity, Shrinking and Swelling of Some Clays." *Proc. Soil Mech. Seminar, Lodz˙*. 1964.

Garakani, A. A., Haeri, S. M., Khosravi, A., and Habibagahi, G. "Hydro-Mechanical Behavior of Undisturbed Collapsible Loessial Soils under Different Stress State Conditions." *Engineering Geology* 195 (2015): 28-41.

Haeri, S. M., Khosravi, A., Ghaizadeh, S., Garakani, A. A. and Meehan, C. L. "Characterization of the Effect of Disturbance on the Hydro-Mechanical Behavior of a highly Collapsible Loessial Soil." *Unsaturated Soils: Research & Applications* (2014): 261.

Haeri, S. M., Garakani, A. A., Khosravi, A. and Meehan, C. L. "Assessing the Hydro-Mechanical Behavior of Collapsible Soils Using a Modified Triaxial Test Device." *Geotechnical Testing Journal*, Vol. 37, No. 2, 2014, pp. 1-15

Haeri, S. M. "Hydro-Mechanical Behavior of Collapsible Soils in Unsaturated Soil Mechanics Context." *Japanese Geotechnical Society Special Publication* 2.1 (2016): 25-40.

Haeri, S. M., Khosravi, A., Garakani, A. A., and Ghazizadeh, S. "Effect of Soil Structure and Disturbance on Hydromechanical Behavior of Collapsible Loessial Soils." *International Journal of Geomechanics* (2016): 04016021.

Haeri, S. M., and Garakani, A. A. "Hardening Behavior of a Hydro Collapsible Loessial Soil." *Japanese Geotechnical Society Special Publication* 2.4 (2016): 253-257.

Handy, R. L. "Collapsible Loess in Iowa." *Soil Science Society of America Journal* 37.2 (1973): 281-284.

Hanna, A., and Diab, R. "Passive Earth Pressure of Normally and Overconsolidated Cohesionless Soil in Terms of Critical-State Soil Mechanics Parameters." *International Journal of Geomechanics* 17.1 (2016): 04016028.

Hanna, A., and Al-Romhein, R. "At-rest Earth Pressure of Overconsolidated Cohesionless Soil." *Journal of Geotechnical and Geoenvironmental Engineering*134.3 (2008): 408-412.

Hanna, A. and Khoury, I. A. "Passive Earth Pressure of Overconsolidated Cohesionless Backfill." *Journal of Geotechnical and Geoenvironmental Engineering* 131.8 (2005): 978-986.

Hanna, A., Rahman, F., and Ayadat, T. "Passive Earth Pressure on Embedded Vertical Plate Anchors in Sand." *Acta Geotechnica* 6.1 (2011): 21-29.

Hamouche, K. K., Leroueil, S., Roy, M., and Lutenegger, A. J. "In Situ Evaluation of K_0 in Eastern Canada Clays." *Canadian Geotechnical Journal* 32.4 (1995): 677-688.

Houston, S. L., Houston, W. N., Zapata, C. E., and Lawrence, C. "Geotechnical Engineering Practice for Collapsible Soils." *Unsaturated Soil Concepts and Their Application in Geotechnical Practice*. Springer Netherlands, 2001. 333-355.

Howayek, A., Huang, P. T, Bisnett, R., and Santagata, M. C. *Identification and Behavior of Collapsible Soils*. No. FHWA/IN/JTRP-2011/12. 2011.

Iranpour, B., and Haddad, A. "The Influence of Nanomaterials on Collapsible Soil Treatment." *Engineering Geology* 205 (2016): 40-53.

Jaky, J. "The Coefficient of Earth Pressure At Rest." *Journal of the Society of Hungarian Architects and Engineers* 78.22 (1944): 355-358.

Jefferson, I., Evstatiev, D., and Karastanev, D. "The Treatment of Collapsible Loess Soils using Cement Materials." *ASCE Geo Congress* 2008 (2008): 662-669.

Jennings, J. E., and Knight, K. "A Guide to Construction on or with Materials Exhibiting Additional Settlement due to Collapse of Grain Structure." *Proceedings Sixth Regional Conference for Africa on Soil Mechanics and Foundation Engineering*. 1975.

Jiang, M., Hu, H. and Liu, F. "Summary of Collapsible Behavior of Artificially Structured Loess in Oedometer and Triaxial Wetting Tests." *Canadian Geotechnical Journal* 49.10 (2012): 1147-1157.

Kalman, E. "Determination of the Coefficient of Earth Pressure At Rest in Situ in Overconsolidated Clay." *World Tunnel Congress 2008-Underground Facilities for Better Environment and Safety–India*. 2008.

Khoury, R. *Passive Earth Pressure behind a Retaining Wall for Normally Consolidated and Overconsolidated Cohesionless Soil.* MASc thesis. Concordia University, 1994.

Klukanova, A., and J. Frankovska. "The Slovak Carpathians Loess Sediments, Their Fabric and Properties." *Genesis and Properties of Collapsible Soils*. Springer Netherlands, 1995. 129-147.

Knight, K. "The Origin and Occurrence of Collapsing Soils." *Proc. 3rd Reg. African CSMFE (1)* (1963): 127-130.

Kumar, J. and Rao, K. S. S. "Passive Pressure Determination by Method of Slices." *International Journal for Numerical and Analytical Methods in Geomechanics* 21.5 (1997): 337-345.

Landva, A. O., Valsangkar, A. J. and Pelkey, S. G. "Lateral Earth Pressure at Rest and Compressibility of Municipal Solid Waste." *Canadian Geotechnical Journal* 37.6 (2000): 1157-1165.

Liu, C. and Evett, J. B. *Soils and Foundations*. Pearson Prentice Hall, 2008.

Mackey, R. D., and Kirk, D. P. *At Rest, Active and Passive Earth Pressures*. Asian Institute of Technology, 1967.

Li, P., Vanapalli, S., and Li, T. "Review of Collapse Triggering Mechanism of Collapsible Soils due to Wetting." *Journal of Rock Mechanics and Geotechnical Engineering* 8.2 (2016): 256-274.

Massarsch, K. R. "New Method for Measurement of Lateral Earth Pressure in Cohesive Soils." *Canadian Geotechnical Journal* 12.1 (1975): 142-146.

Massarsch, K. R. "Lateral Earth Pressure in Normally Consolidated Clay." *Proceedings of the Seventh European Conference on Soil Mechanics and Foundation Engineering, Brighton, England*. Vol. 2. (1979): 245-250.

Mazindrani, Z. H. and Ganjali, M. H. "Lateral Earth Pressure Problem of Cohesive Backfill with Inclined Surface." *Journal of Geotechnical and Geoenvironmental Engineering* 123.2 (1997): 110-112.

Mayne, P. W., and Kulhawy, F. H. "K_0-OCR Relationships in Soil." *Journal of the Geotechnical Engineering Division* 108.6 (1982): 851-872.

Mayerhof, G. G. "Bearing Capacity and Settlement of Pile Foundations." *Journal of Geotechnical and Geoenvironmental Engineering* 102.ASCE# 11962 (1976).

Mesri, G. and Hayat T. M. "The Coefficient of Earth Pressure at Rest." *Canadian Geotechnical Journal* 30.4 (1993): 647-666.

Michalowski, R. L. "Coefficient of Earth Pressure at Rest." *Journal of Geotechnical and Geoenvironmental Engineering* 131.11 (2005): 1429-1433.

Mohamedzein, Y. E., and Al-Rawas, A. "Cement-Stabilization of Sabkha Soils from Al-Auzayba, Sultanate of Oman." *Geotechnical and Geological Engineering* 29.6 (2011): 999-1008.

Mohamed, A. O., and Gamal, M. M. "Treatment of Collapsible Soils Using Sulfur Cement." *International Journal of Geotechnical Engineering* 6.1 (2012): 65-77.

Mossaad, M. E, Moddather, A. H., and Galaa, A. M. *A Study on Collapsing Soils in Egypt*. Cairo University – National Academy for Scientific Research and Technology, 2006.

Narain, J., Saran, S., and Nandakumaran, P. "Model Study of Passive Pressure in Sand." *Journal of Soil Mechanics & Foundations Div* (1969).

Poterasu, A. M. *Experimental Investigation on Passive Earth Pressure on Walls Retaining Collapsible Soil*. MASc thesis. Concordia University, 2013

Rogers, C. D. F. "Types and Distribution of Collapsible Soils." *Genesis and Properties of Collapsible Soils*. Springer Netherlands, 1995. 1-17.

Sakr, M., Mashhour, M., and Hanna, A. M. "Egyptian Collapsible Soils and Their Improvement." *GeoCongress 2008@ Geosustainability and Geohazard Mitigation*. ASCE, 2008.

Sherif, M.A., Fang, Y.S., and Sherif, R.I. "K_A and K_0 behind Rotating and Non-Yielding Walls." *Journal of Geotechnical Engineering* 110.1 (1984): 41-56.

Soliman, S., and Hanna, A. M. "Performance of Reinforced Collapsible Soil." *Proceedings of GeoFlorida 2010: Advances in Analysis, Modeling and Design, West Palm Beach, Florida, USA, 20-24 February 2010.* American Society of Civil Engineers (ASCE), 2010.

Teerachaikulpanich, N., Okumura, S., Matsunaga, K., and Ohta, H. "Estimation of Coefficient of Earth Pressure at Rest Using Modified Oedometer Test." *Soils and Foundations*, *47*.2 (2007), 349-360.

Vakili, A. "Evaluation of the Lime and Cement Effect on the Mechanical and Physical Characteristics of the Collapsible Soils." *Journal of Basic and Applied Scientific Research*, 2013. 3(8)691-696

Vrecl-Kojc, H., and Skrabl, S. "Determination of Passive Earth Pressure using Three-Dimensional Failure Mechanism." *Acta Geotechnica Slovenica* 4.1 (2007): 11-23.

Weng, M. C., Cheng, C. C., and Chiou, J. S. "Exploring the Evolution of Lateral Earth Pressure using the Distinct Element Method." *Journal of Mechanics* 30.01 (2014): 77-86.

Wroth, C. P. "General Theories of Earth Pressure and Deformation." *Proceedings of the fifth European Conference on Soil Mechanics and Foundation Engineering, Madrid, Spain*. Vol. 2 (1973): 33-52.

Zhou, Y. F., Tham, L. G., Yan, W. M., Dai, F. C., and Xu, L. "Laboratory Study on Soil Behavior in Loess Slope subjected to Infiltration." *Engineering Geology*, *183* (2014): 31-38.

Zhu, D. Y, and Qian, Q. "Determination of Passive Earth Pressure Coefficients by the Method of Triangular Slices." *Canadian Geotechnical Journal* 37.2 (2000): 485-491.